Abrogating GRP78 function as a strategy to increase apoptosis of tumour cells

Shaun Martin

Thesis Submitted in partial fulfilment of the requirements of the regulations for the degree of Doctor of Philosophy

Newcastle University

Faculty of Medical Sciences

Institute of Cellular Medicine

September 2012

This work was funded by Cancer Research UK

Abrogating GRP78 function as a strategy to increase apoptosis of tumour cells

Abstract.

The endoplasmic reticulum (ER) is the major site for protein synthesis, folding and trafficking, as well as lipid synthesis and Ca^{2+} storage. To maintain ER integrity, homeostatic response mechanisms to stimuli which perturb ER function, known as the unfolded protein response (UPR) have evolved. Cancer cells can be exposed to extremes of environmental conditions as a direct consequence of their mechanisms of origin, and may have increased cellular proliferation, coupled with poor vascularisation leading to deficiencies in glucose, oxygen and metabolite requirements for efficient cell growth and survival. When ER function is disrupted, the UPR activates pro-survival mechanisms, such as the induction of chaperones and other folding machinery. However, the UPR also activates pro-death stimuli, to remove cells where the stress is to severe or persists for too long. Glucose regulated protein 78 (GRP78) is the major stress regulator and central hub of the UPR, as well as a key chaperone of the ER. GRP78 bind to and inhibits the activation of; protein kinase-like ER kinase (PERK), inositol requiring element 1 (IRE1) and activating transcription factor 6 (ATF6), known as the UPR activators. Solid tumours, such as melanoma and glioblastoma, may have increased expression of GRP78 correlating with disease stage and resistance to chemotherapy. Conversely, increased GRP78 expression in neuroblastoma has been associated with improved prognosis.

To test the hypotheses that abrogating GRP78 function increases apoptosis of tumour cells and that GRP78 is a biomarker for the outcome of ER-stress in differing cancer types, neural-crest derived cancers were compared by stoichiometric analysis of GRP78 and the UPR activators, and the downstream components of the UPR, activating transcription factor 4 (ATF4) and X-box binding protein 1 (XBP-1). To determine the importance of GRP78 across cancer types, changes in sensitivity to the ER stress inducers fenretinide or bortezomib with respect to cell death (propidium iodide stained flow cytometry) or inhibition of cell viability (MTS assay) were assessed in response to siRNA mediated knock-down, GRP78 over-expression and GRP78 inhibition.

There were differences in cellular concentrations of GRP78 between cell lines representing different cancer types; however the expression of UPR activators did not correlate with GRP78 levels. Stoichiometric analysis of the ratio between GRP78 and the UPR activators demonstrated a significant difference between melanoma and glioblastoma, to that of neuroblastoma. Mapping the activation of the UPR by either fenretinide or bortezomib showed cancer-specific and stress-inducer-dependent responses. Importantly, melanoma and glioblastoma demonstrated significantly greater ATF4 induction whereas neuroblastoma showed prolonged XBP-1 splicing. Testing the effect of altering GRP78 expression on sensitivity to ER-stress-induced cell death demonstrated that high expression of GRP78 in melanoma and glioblastoma correlated with resistance and with neuroblastoma GRP78 over-expression enhanced sensitivity. Investigating the effect of inhibiting GRP78 activity on fenretinide- and bortezomib-induced cell death demonstrated enhanced sensitivity in melanoma and glioblastoma, but no significant enhancement in neuroblastoma.

Thus, down-regulating GRP78 or its function increased the death of melanoma and glioblastoma cells in response to ER stress; however there are differences in UPR signalling between cancer types, which ultimately results in contrasting prognosis as demonstrated in neuroblastoma. Although all three cancer types responded to ER-stress induced death, interpretation of the relationship between GRP78 and the UPR activators is essential for determining dependence on GRP78. The data suggest that melanoma and glioblastoma demonstrate increased sensitivity when GRP78 is inhibited due to a shift in the dynamic equilibrium of the UPR, promoting activation and downstream cell death. However cancer types expressing higher UPR activator concentrations compared to that of GRP78 do not respond positively to the inhibition of GRP78.

Acknowledgements

I would like to thank my supervisors, Dr Chris Redfern and Dr Penny Lovat for the opportunity to learn in a supported and loving atmosphere. I would also like to thank both of you for always being there for me, to give guidance and advice during the last four years. I could have not done this without you both. I would also like to thank you both from the bottom of my heart for working so hard to be awarded this studentship. I thank you for allowing me the opportunity to do what so few people ever get the chance to do, you have changed my life.

I would like to express my thanks to Dr David Hill, Dr Jane Armstrong and Dr Emma Bell for all their help and support throughout my time here at Newcastle University, teaching me techniques and giving insight into my research, you will be greatly missed. I would also like to show my gratitude to Miss Monika Loeher for her help and training, my real-time PCR data is a consequence of your guidance, patience and support. I would like to thank my best friend Ian Jarvis, who until the end of this project was there by my side, giving technical assistance, research advice and a distraction where needed, who introduced me to the institute and has looked after me for so many years now. I would also like to thank Dr Gail Halliday, Dr Lindi Chen and Miss Laura Evans, when times were hard you took me in and gave me the support I need to carry on.

I have been very fortunate to have studied with such a friendly bunch!!!! And I am grateful to everyone I have had the opportunity to get to know both within the NICR and Dermatology.

I would also like to thank my family for their constant love, support and faith over the past 28 years, making me into the person I am today. I am so very lucky.

Finally, I would like to acknowledge Monika, the love of my life; for letting me know day and night how much she loves me. I cannot wait to marry you and knowing you are there by my side makes me the happiest man in the world.

Declaration

I certify that no part of the material documented in this thesis has previously submitted for a degree or other qualification in this or any other university. I declare that this thesis represents my own unaided work, carried out by myself, except where it is acknowledged otherwise in the thesis text.

Shaun Martin

List of Contents

List of Figures.

List of Tables

List of Abbreviations

Abbreviation	Name
2cda	2-chlorodeoxyadenosine
4-HPR	N-(4-hydroxylphenyl)retinamide / Fenretinide
ACTH	Adrenocorticotrophic Hormone
ADP	Adenosine Diphosphate
AIF	Apoptosis Inducing Factor
AJCC	American Joint Committee of Cancer
ANOVA	Analysis of Variance
ANS	Autonomic Nervous System
ANT	Adenine Nucleotide Translocator
APAF1	Apoptotic protease activating factor 1
APH	Aminoglycoside 3' phosphor-transferase
ARE	Anitoxidant Response Element
ASK1	Apoptosis Signal Regulating Kinase 1
ATCC	American Type Culture Collection
ATF4	Activating Transcription Factor 4
ATF6	Activating Transcription Factor 6
ATF6f	Activating Transcription Factor – Full length
ATF6N	Activating Transcription Factor – nucleur fragment
ATG	Autophagy Gene
ATM	Ataxia-telangiectasia mutated
ATP	Adenosine Triphosphate
ATPase	ATP metabolising Activity
Bad	BCL-2 Antagonist of cell Death
BAK	BCL-2 antagonist Killer
BAX	BCL-2 associated X protein
BCL-2	B-Cell Lymphoma 2
BCL-XL	B-cell lymphoma-extra large
BH(1-4)	Bcl-2 homology domain 1- 4
Bid	BH3-interacting Death Domain agonist
BiP	Binding Protein

Bort	Bortezomib
BSA	Bovine Serum Albumin
bZIP	Basic Leucine Zipper domain
Ca2+	Calcium
cAMP	Cyclic Adenosine Monophosphate
CD95	Fas Ligand
cDNA	Copy DNA
C/EBP	CCAAT-enhancer binding protein
CEBPB	CCAAT-enhancer binding protein Beta
CHOP	C/EBP homology protein
CI	Confidence Intervals
ci	Combination Indices
Con	Control
CNS	Central Nervous System
CNX	Calnexin
CRE	cAMP Responsive Element
CREB	cAMP Responsive Element Binding Protein
CRT	Calreticulin
Ct	Cycle Threshold
Cyt C	Cytochrome C
DAPI	4',6-diamidino-2-phenylindole
DAPK1	Death Associated Protein Kinase 1
DCFDA	2',7' –dichlorofluorescein diacetate
DISC	Death Inducing Signalling Complex
DMEM	Dulbecco's Modified Eagles Medium
DMSO	Dimethyl Sulfoxide
DNA	Deoxyribonucleic Acid
DNase	Deoxyribonucleic Acid digesting activity
dNTP	Deoxynucleotide Triphosphates
E1	Ubiquitin Activating Enzyme
E2	Ubiquitin Conjugating Enzyme
E2AK3	eukaryotic translation initiation factor 2-alpha kinase 3
E3	Ubiquitin Ligase
E.Coli	Escherichia coli

EDEM	ER Degradation Enhancing alpha-Mannosidase-like Protein
EDTA	EthaleneDiamineTetraacetic Acid
EGCG	Epigallocatechin Gallate
EGF	Epidermal Growth Factor
EGFR	Epidermal Growth Factor Receptor
eIF	Eukaryotic Initiation factor
eIF2α	Eukaryotic Initiation factor 2 alpha
ER	Endoplasmic Reticulum
ERAD	ER-associated degradation
ERK	Extracellular Regulated Kinase
ERN1	Endoplasmic Reticulum to Nucleus Signalling 1
ERSE	ER stress Element
FADD	Fas-Associated protein with Death Domain
FAK	Focal adhesion kinase
Fas	Fatty Acid Synthase
FasL	Fas Ligand
FCS	Foetal Calf Serum
FenR	Fenretinide
FITC	Flourescien Isothiocyanate
FLIP	FLICE-like inhibitory protein
g	G-Force
G418	Geneticin
Gadd153	Growth arrest and DNA damage inducible 153 (CHOP)
GADD34	Growth arrest and DNA damage inducible 34
GCN2	general control nonrepressed 2
GDP	Guanine Diphosphate
GRP78	Glucose Regulated Protein 78
GRP94	Glucose Regulated Protein 94
GTP	Guanine Triphosphate
h	Hour
H_2O_2	Hydrogen Peroxide
Hac1	Yeast homologue of XBP-1
HCl	Hydrogen Chloride

HDAC1	Histone deacetylase 1
HIF1	Hypoxia Initiation Factor 1
HNK	Honokiol
HOX	Homeobox
HRI	Heme-Regulated Inhibitor
HSP	Heat Shock Protein
HSPA5	Heat Shock Protein A 5
IAP	Inhibitor of Apoptosis Protein
ICP	Intra Cranial Pressure
IFNG	Interferon gamma
IkB	Inhibitor of Kappa B
IMM	Inner Mitochondrial Membrane
INSS	Internationsal Neuroblastoma Staging System
IRE1	Inostitol Requiring Element 1
IRE1p	Inostitol Requiring Element 1 protein
IRES	Internal Ribosomal Entry Site
ITAF	IRES Transacting Factors
JNK	c-Jun N-Terminal Kinase
k+	Potassium
kDa	Kilodalton
KEAP1	Kelch-like ECH-associated protein 1
LB	Lysogeny Broth
MAPK	Mitogen Activated Protein Kinase
MC1R	Melanocortin 1 Receptor
MCL-1	Myeloid Cell leukaemia Sequence 1
Mg+	Magnesium
min	Minute
MITF	Microphthalmia-associated transcription factor
µl	Microlitre
µM	MicroMolar
ml	Millilitre
mM	MilliMolar
mRNA	Messenger RNA
Mt Htt	Mutant Huntingtin

mTOR	Mammalian Target of Rapamycin
MTS	(3-(4,5-dimethylthiazol-2-yl)-5-(3-carboxymethoxyphenyl)-2-(4-sulfophenyl)-2H-tetrazolium
MYCN	v-myc myelocytomatosis viral related oncogene, neuroblastoma derived (avian)
NADH	Nicotinamide adenine dinucleotide
NFAT	Nuclear factor of activated T-Cells
NF-kB	Nuclear Factor Kappa-light chain enhancer of activated B cells
nl	Nanolitre
nM	NanoMolar
NOXA	Pro-Apoptotic member of The BCL-2 Family
Nrf2	Nuclear Factor Erythroid 2
NS	Nervous System
OMM	Outer Mitochondrial Membrane
p53	Protein 53
$P58^{INK}$	58 kDA inhibitor of PKR
P62	Protein 62 or Nucleoporin
p97	Velosine Containing Protein (Protein 97)
PAR2	Protease Activated Receptor 2
PBS	Phosphate Buffered Saline
PBS/T	Phosphate Buffered Saline/Tween
PDI	Protein Disulphide Isomerase
PERK	Protein Kinase-like ER kinase
PFA	Paraformaldehyde
pH	Per Hydrogen
PI	Propidium Iodide
PI3K	Phosphotidylinositol-3-Kinase
PKB	Protein Kinase B
PKR	Protein Kinase
PNS	Parasympathetic Nervous System
PP1	Protein Phosphatase 1
PUMA	Pro-Apoptotic member of The BCL-2 Family
PVDF	Polyvinlylidene Flouride
RAR	Retinoic Acid Receptor

RNA	Ribonucleic Acid
RNase	Ribonucleic Acid digesting activity
ROS	Reactive Oxygen Species
RPM	Revalutions Per Minute
RPMI	Roswell Park Memorial Institute
s	Second
S1P	Site 1 Protease
S2P	Site 2 Protease
SDS	Sodium Dodecyl Sulphate
SiRNA	Silencing RNA
SNP	Small Nucleotide Polymorphism
SNS	Sympathetic Nervous System
SOD1	Superoxide Dismutase 1
SODD	Silencer of Death Domians
SRB	Sulforhodamine B
SREBP2	Sterol Regulatory Element-Binding Protein 2
$SubAB_5$	Subtilase AB_5 Cytotoxin
$SubA_{A272}B_5$	Mutant Subtilase AB_5 Cytotoxin
TBE	Tris/Borate/EDTA
tBid	Truncated Bid
TBS	Tris Buffered Saline
TBS/T	Tris Buffered Saline/Tween
TCA	Trichloroacetic Acid
Tg	Thapsigargin
TNF	Tumour Necrosis Factor
TNFR1	Tumour Necrosis Factor Receptor 1
Tox	GRP78 specific toxin
TP53	Tumour Protein 53
TRAF2	TNF Receptor Associated Factor 2
TRB3	Tribbles Homologue 3
tRNA	Transfer RNA
UFP	UnFolded Proteins
UPR	Unfolded Protein Response
UPRE	Unfolded Protein Response Element

UPS	Ubiquitin Proteasome System
UV	Ultraviolet Light
VCP	Velosine Containing Protein (p97)
VDAC	Voltage Dependent Anion Channel
VMA	
WHO	World Health Organisation
WinMDI	Windows Multiple Document Interface
wt	Wild Type
XBP-1	X-Box Binding Protein 1
XBP-1s	X-Box Binding Protein 1 Spliced varient
αMSH	Alpha-Melanocyte Stimulating Hormone

Chapter 1:

Introduction

Due to the notorious resistance of cancer cells to cell death, cancer research has shifted to focus on interpreting the mechanisms of specific cell signalling pathways that are responsible for either protecting against or inducing death stimuli. Cancer cells have robust signalling mechanisms to adapt and cope with sub-optimal conditions within their microenvironment. In this context, triggering cancer cell death by inducing cytoplasmic stress through targeting the functionality of the endoplasmic reticulum (ER stress) represents a novel mechanism to enhance death of cancer cells resistant to conventional death-receptor- or mitochondrial-mediated apoptosis.

One consequence of ER stress is the activation of the homeostatic response mechanism known as the unfolded protein response, which is based around the key chaperone GRP78. The unfolded protein response characteristically induces pro-survival chaperones and protein folding machinery, however, also induces factors capable of activating cell death. Glucose regulated protein 78 is the sensory hub of the unfolded protein response, and therefore gaining a better understanding of the function and regulation of this protein, as well as the pathway in cancer cells may harness ER stress as a novel therapeutic strategy. Additional target identification will also define the most appropriate use of ER stress-inducing agents that to date have no beneficial effect as single agent therapeutics.

The poor survival rates of patients suffering from metastatic melanoma and glioblastoma are a direct result of a lack of successful treatments. Interestingly, both of these cancer types demonstrate an increase in GRP78 expression with disease stage and therefore may rely on the prevention of the UPR or an increase in UPR signalling capability for survival. However, neuroblastoma also demonstrates an increase in GRP78 in the later disease stages, yet these patients demonstrate an increase in cell death and a more favourable prognosis. Therefore, a comparison of these neural-crest-derived cancer types may allow for differences in signalling to be determined, to help manipulate the unfolded protein response to increase the effect of ER stress for cancer therapy.

1.1: Neurulation and the neural-crest.

1.1.1: Neurulation.

Gastrulation within vertebrates generates an embryo that consists of an internal endodermal layer, intermediate mesodermal layer and an external ectoderm. A key event in human development is the interaction between the dorsal mesoderm and the overlying ectoderm, as this initiates organogenesis. This interaction results in the ectoderm forming a hollow neural tube. Cells of the neural tube begin to develop into neural-crest cells, which eventually will differentiate to form the brain and spinal cord. The process that results in the formation of a neural tube from the flat ectoderm is termed "neurulation" [1]. Neurulation can be sub-divided into four key events: neural plate formation, shaping of the neural plate, bending of the neural plate and closure of the neural groove to form a tube. The neural tube separates from the ectoderm by a shift in the relative expression of adhesion proteins, such as E-cadherin and N-cadherin [2].

The progression of the neural tube into the central nervous system (CNS) occurs by the constriction of the neural tube to form an anatomically distinct brain and spinal cord, along with a rearrangement of cells within the wall of the neural tube, giving rise to multifunctional regions of the CNS [1]. Within the neural tube, neuro-epithelial cells differentiate into the numerous types of neurons and supportive cells present within the body [3]. Different regions of the neural-crest give rise to different cell types. Research using avian models has described neural-crest cells as pluripotent, differentiating to a diverse number of cell types often depending on their starting location in the neural tube [4]. Neural-crest cells will also begin to migrate underneath the ectoderm to form pigment cells or migrate ventrally to give rise to the autonomic nervous system [5]. Despite this migration, all regions of the neural-crest give rise to supportive cells, such as glial and pigment secreting melanocytes [6]. However, the pluripotent phenotype of neural-crest cells diminishes with migration.

1.1.2: Neural-crest development.

The neural-crest is a transient embryonic structure derived from the ectoderm during the process of neurulation. Neural-crest cells are formed from the border between the neural plate and the epidermal ectoderm [7]. During neural tube closure the multi-potent neural-crest cells that leave the dorsal neural tube and migrate, as well as differentiate, give rise to a variety of different cell lineages such as: melanocytes, glia, sensory and sympathetic neurons, endocrine cells, enteric ganglion and cartilage [8].

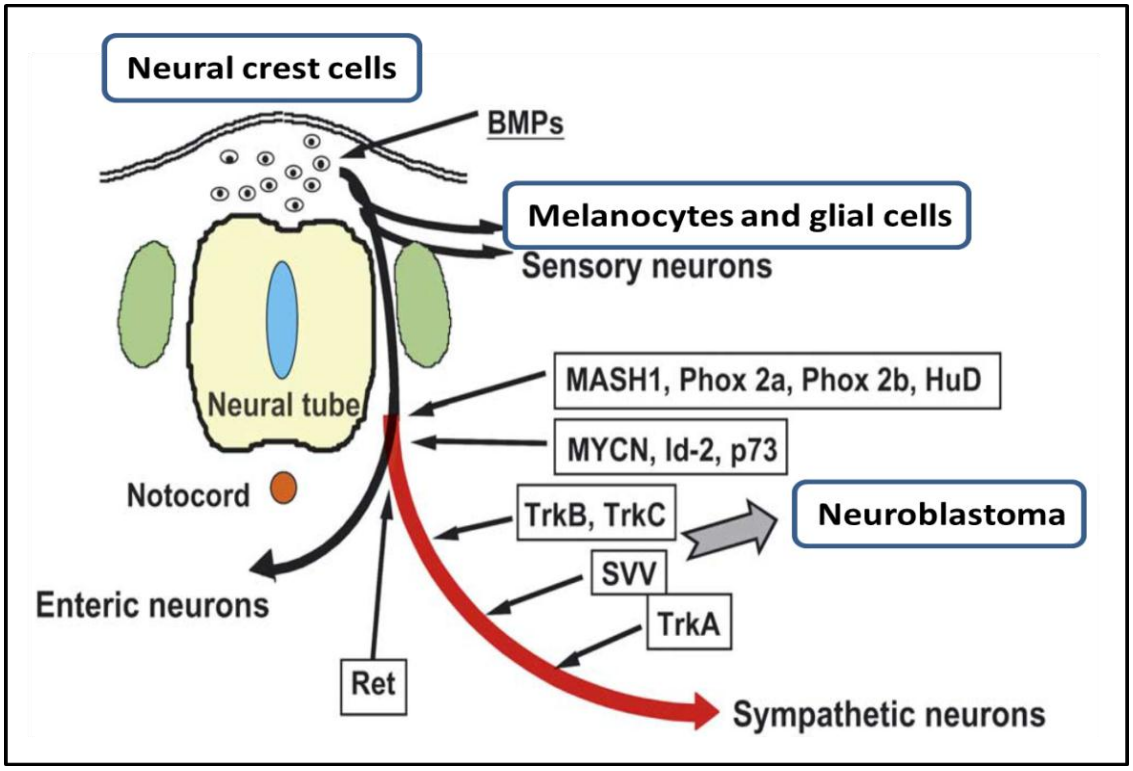

Figure 1.1: *Developmental lineages derived from the neural-crest, including melanocytes and glia cells, as well as the genesis of neuroblastoma. Diagram adapted from Nakagawara and O'Hira (2004).*

Neural-crest cells originate from the dorsal end of the neural tube, migrating and differentiating to form vital components of the nervous system, including the medulla and adrenal glands [9]. Due to the vast importance and number of varying cell types that neural-crest cells can differentiate into, the fate of a neural-crest cell depends ultimately on where it resides and this may explain, for example, why the symptoms of neuroblastoma are so diverse.

With such importance, comes extensive regulation. Neural-crest cells are regulated by a set of transcription factors known as the homeobox (Hox) genes [10]. Found in most eukaryotes, this family is highly expressed during neurulation, with distinct regions showing expression of different dominant family members, influencing not only the development of different neural specific chambers but also the fate of cells [11].

1.2: Cancers of the neural-crest.

Although derived from the ectoderm, the neural-crest has been called the fourth germ layer, due to the high number of differing cell types it differentiates into. A number of cancers originate either by direct dysfunction of neurulation or downstream due to mutations and adaptations in the differentiated cell types. Three well-documented cancer types include melanoma, glioma and neuroblastoma (Figure 1.1).

1.2.1: Melanogenesis and melanoma.

Ultraviolet (UV) radiation can cause acute damage to the skin in the form of sun burn but can also cause long term accumulative DNA damage within the skin, resulting in early aging [12]. To help prevent this, the skin stimulated by UV light produces pigmentation, known as melanin [12]. Melanin, the pigment produced by melanocytes, upon stimulation by keratinocytes in the basal epidermis of the skin comes in the form of black/brown eumelanin or red/yellow pheomelanin [13]. This polymorphous, multifunctional biopolymer with photo-stabling properties confers a protective effect to the cell by shielding nuclear DNA during times of UV exposure [12].

Melanocytes are found predominantly in the basal layer of the skin but are not fixed in their location and migrate within the epidermis [14]. Stimulation by keratinocytes renders the melanocyte into a highly dendritic cell type, capable of interacting with numerous keratinocytes at any one time, increasing the export routes for melanosomes (granules containing melanin) [15]. The extraordinary properties of melanocytes stems from their lineage as neural-crest cells [13]. Melanoblasts have been discovered as early as the second month of embryogenesis [16]. These melanocyte precursors migrate and differentiate throughout the mesenchyme of a developing embryo, residing in the basal epidermis and hair follicles [17]. Once established at the dermal-epidermal

boarder melanoblasts are stimulated into their final step of differentiation, resulting in the formation of melanocytes.

Pigmentation is the outcome of two important cellular events, synthesis of melanin by melanocytes and the trafficking of melanosomes to surrounding keratinocytes [18]. The obligatory step in the synthesis of melanin is the hydroxylation of tyrosine to dopaquinone by tyrosinase. It is this point within melanin production that eumelanin and pheomelanin pathways differ. In stimulated melanocytes, nascent melanosomes receive all their required proteins; both structural and enzymatic, from the golgi before undergoing four maturation stages resulting in a competent melanosome before export [13]. Upon transport, the melanosome requires active uptake into keratinocytes. This is predominantly carried out by protease-activated receptor 2 (PAR2) before the melanosomes are positioned on the sun exposed side of the nucleus, to provide relief [19].

Under periods of UV radiation, melanogenesis becomes hyper-activated due to an increase in melanocyte stimulating hormone (αMSH) and adrenocorticotrophic hormone (ACTH) by the surrounding keratinocytes. These hormones bind and agonise the melanocortin 1 receptor (MC1R) of melanocytes [20]. MC1R receptor is a G-protein coupled receptor that activates adenylyl cyclase, inducing the production of cyclic adenosine monophosphate (cAMP), which results in the phosphorylation of cAMP responsive element binding protein (CREB) and the transcription of the microphthalmia transcription factor (MITF) [21]. MITF is essential for the expression of pigment enzymes required in the production of melanin [22]. Variants of the MC1R receptor have been identified in humans and are associated with a red hair and fair skin phenotype, stemming from the reduced binding capacity present within these variants which results in an individual who is somewhat impaired in their ability to tan and therefore at a greater risk of DNA damage and developing melanoma [23].

In normal skin, melanocytes exist in an even distribution within the basal epidermis and hence differences in pigmentation are due to the expression of melanosomes present in keratinocytes encompassing the melanocytes with variable eumelanin and pheomelanin [24]. Tanned or pigmented skin has been shown to protect the skin against carcinogenesis by an approximate 500 to 1000 fold [25]. Occasionally mutations arise, allowing melanocytes to escape the control of keratinocytes and they proliferate uncontrollably, producing clusters within the basal epidermis. These clusters are the

formation of benign neavus, more commonly known as moles. Further mutations within these benign nevi can result in melanoma [26].

Melanoma is a malignant neoplasm of the melanocytes. As the most aggressive form of skin cancer, the incidence has increased faster than any other malignancy in the last 40 years [27]. According to the world health organisation (WHO), more than 160 000 new cases of melanoma are diagnosed each year worldwide with a colossal 48 000 deaths per annum [27]. Data retrieved from the Surveillance, Epidemiology and End Results program of the National Cancer Institute shows the incidence of melanoma at 20 persons per 100 000 among white populations, where a greater incidence is seen in males. Incidence rates of 24.4 and 16.8 per 100 000 are seen in men and women respectively [28, 29]. Alarmingly, melanoma is the most common form of cancer in the 15 – 34 age groups, demonstrating a disproportionate mortality rate in younger aged individuals and emphasising the acute need for novel therapeutic strategies.

1) Normal mole or neavi *2) Malignant change* *3) Local metastatic disease*

Figure 1.2: *Malignant transformation of a normal mole or lesion. Photomicrographs representing: a normal mole (1), a mole displaying malignant change (2) and a malignant mole (3).*

Risk factors for the development of malignant melanoma include skin pigmentation; pale skin colour and freckling all of which predispose to a higher risk [28, 30], but also include, sunlight sensitivity, exposure to ultraviolet light and genetic mutations [28]. Like all neoplasms, melanoma arises from the accumulation of mutations in the cell cycle regulatory system, acquiring both mutations in proto-oncogenes and tumour suppressor genes [31]. The most well-defined mutation in melanocytes is a single point mutation in the B-RAF gene occurring in 50-70% of all melanomas, which results in the constitutive activation of extracellular regulated kinase (ERK) contributing to cell

proliferation, survival and resistance to apoptosis [32]. However, benign nevi also frequently harbour mutations in the BRAF gene [33], suggesting additional events are required for transformation.

Stage	Definition	5-year survival (%)
I	primary tumour <1mm	93
II	primary tumour >1mm	68
III	regional metastasis	45
IV	systemic metastasis	11

Table 1.1: *The AJCC staging system for melanoma, indicating estimated survival rates for the differing stage melanomas [34].*

The prognosis for melanoma differs dramatically according to disease stage. Malignant change is linked with a change in shape and/or colour of a mole or nevus (*Figure 1.2*). Disease progression is associated with metastasis, initially to regional lymph nodes [35] and in late stage disease with systemic metastasis, frequently to the lungs and/or liver. This progression results in the poor survival rates for patients with advanced stage melanoma (*Table 1.1*). According to the American Joint Committee on Cancer (AJCC) staging system the prognosis for stage I melanoma is a promising 93% survival rate after 5 years, compared to a mere 11% for those patients diagnosed with stage IV systemic disease [34].

1.2.2: Neuroblastoma.

Neuroblastoma arises early in neuro-embryogenesis when neural-crest cells which normally form into sympathetic ganglia or adrenal glands are blocked from entry into a terminal differentiate state. Neuroblastoma is the most common extra cranial solid cancer in childhood and the most common cancer in infants, with an annual incidence of about 7 - 12 per million [36]. As a neuroendocrine tumour, arising from any neural-crest element of the sympathetic nervous system (SNS), close to 50% of neuroblastoma cases occur in children younger than two years of age. A branch of the autonomic nervous

system (ANS), the SNS is a nerve network that carries messages from the brain throughout the body and is responsible for the fight-or-flight response and production of adrenaline. Solid tumours commonly begin in the adrenal glands, though they can also develop in nerve tissues in the neck, chest, abdomen, or pelvis.

Symptoms of neuroblastoma are often subtle and may include fatigue, loss of appetite or fever [37]. Later symptoms are dependent on the location of the tumour:

- In the abdomen, a tumour may cause a swollen stomach, resulting in constipation.
- A tumour in the chest may cause breathing difficulties.
- Mass on the spinal cord cause a feeling of weakness.
- Bone lesions in the legs and hips often cause pain and limping.
- A tumour in the head may cause the eyes to start to bulge outwards and turn black due to the pressure exerted from behind.

Often because symptoms are so diverse and unclear, 50 to 60% of all neuroblastoma have already metastasised by the time a diagnosis has been made [38]. Like melanoma, the prognosis for neuroblastoma is related to the stage of the disease, with patients suffering from early stage disease having a greater chance of survival compared to individuals with late stage disease. The "International Neuroblastoma Staging System" (INSS) established in 1986 and revised in 1988 classifies neuroblastoma depending on its anatomical presence at diagnosis [39].

Stage	Diagnosis	5-year survival (%)
1	Localised disease	90 - 95
2A	Localised disease that cannot be completely removed	
2B	Localised disease that may or may not be completely removed	
3	Tumour cannot be removed and has spread to local lymph nodes	70 - 80
4	Tumour has spread to distant lymph nodes	30 - 40
4S	Tumour has spread to skin, liver and bone marrow in infants less than 1 year	

Table 1.2: *The International Neuroblastoma Staging System and estimated survival rates for the differing stage neuroblastoma*

When a lesion is localized, it is generally curable, however despite aggressive multimodal therapy, long-term survival for children with advanced disease older than 18 months is poor [39]. Biological and genetic characteristics have been identified, which, when added to classic clinical staging, has allowed patient assignment into risk groups for treatment intensity [40]. These criteria include the age of the patient, extent of disease spread, microscopic appearance, and several other biological features, most importantly MYCN oncogene amplification [41]. Taking all criteria into consideration patients are grouped into low, intermediate, and high risk disease states [42]. With current treatments, patients with low and intermediate risk disease have an excellent prognosis with cure rates above 90% for low risk and 70%-80% for intermediate risk. In contrast, therapy for high-risk neuroblastoma results in a survival rate of approximately 30% (Table 1.2) [43].

1.2.3: Glia and glioma.

Glial cells are non-neuronal cells that provide support and nutrition, maintain homeostasis, form myelin, and participate in signal transmission in the nervous system [44]. In the human brain, glial cells are estimated to outnumber neurons by approximately 10 to 1 [44]. Some glial cells do function as the physical support for neurons [44]. Others regulate the internal environment of the brain, especially the fluid surrounding neurons and their synapses, and provide nutrition to nerve cells [44]. Glial cells have important developmental roles, guiding migration of neurons in early development, and producing molecules that modify the growth of axons and dendrites [44]. Recent findings in the hippocampus and cerebellum have indicated that glia are also active participants in synaptic transmission, regulating clearance of neurotransmitters from the synaptic cleft [45], releasing factors such as ATP which modulate presynaptic function [46], and even releasing neurotransmitters themselves [47]. Glia also forms the insulating myelin sheath that coats neurons to aid conductivity [44]. Unlike the neuron, which is generally considered permanently post-mitotic, glial cells are capable of mitosis [48].

Traditionally glia had been thought to lack certain features of neurons. For example, glia cells were not believed to have chemical synapses or to release neurotransmitters [44]. They were considered to be the passive bystanders of neural transmission. However, recent studies contradict these findings. For example, astrocytes are crucial in clearance of neurotransmitter from within the synaptic cleft, which provides distinction between the arrival of an action potentials and prevents toxic build-up of neurotransmitters, such as glutamate (excitotoxicity)[44, 47]. Furthermore, at least in vitro, astrocytes can release the neurotransmitter glutamate in response to certain stimulation. Another unique type of glia, the oligodendrocyte precursor cells, have very well defined and functional synapses from at least two major groups of neurons [44]. The only notable differences between neurons and glia, by modern scrutiny, are the ability to generate action potentials and the polarity of neurons, namely the axons and dendrites which glia lack.

Therefore, it is inaccurate to consider glia as 'glue' in the nervous system as the name implies; rather, they should be considered more as the partner of the neuron. They are also crucial in the development of the nervous system and in processes such as synaptic

plasticity and synaptogenesis [49]. Glia cells have a role in the regulation of repair of neurons after injury [50]. In the CNS glia suppress repair. Astrocytes enlarge and proliferate to form a scar and produce inhibitory molecules that inhibit regrowth of a damaged or severed axon [50]. In the parasympathetic nervous system (PNS) Schwann cells promote repair. After axon injury Schwann cells regress to an earlier developmental state to encourage regrowth of the axon [51]. This difference between PNS and CNS raises hopes for the regeneration of nervous tissues within the CNS.

Arising from glial cells of the central nervous system, glioma is the most common form of brain cancer, with Astrocytes and oligodendrocytes being most noted cell types in glioma development [52]. To date glioma is responsible for 60% of all brain cancers, which themselves make up 1.4% of all cancers diagnosed.

The clinical manifestation of glioma can be appreciated in terms of tumour location, growth rate and size. There are three issues to consider in terms of symptomatology. First, tumour location plays a significant role in the focal neurological symptoms exhibited by patients. For example, if the tumour is located in the frontal lobe, presentation may be related to motor, mood or personality changes. Similarly, tumours located in the dominant temporal region may be associated with speech or memory disturbances. Fast growing glioma often results in increased intra cranial pressure (ICP). Elevated ICP can be the result of obstructive hydrocephalus or oedema, in addition to tumour burden and failure of cerebral compensatory mechanisms to accommodate the volume. Increased pressure will often result in complaints of headache, visual changes, vomiting, and nausea. Lastly, patients often present with seizures, especially in the case of oligodendroglioma. Again, the anatomical location of the mass would determine the type of seizure (e.g., motor based seizures with fronto-temporal tumours and visual based seizures with occipital). In many instances, tumours are discovered by cranial imaging studies when a patient is seeking treatment for an unrelated health issue or following a head injury (benign, slow growing tumours).

Stage	Diagnosis	Example tumour types	5 year Survival (%)
I	Lowest grade tumours	Pilocytic astrocytoma, Subependymal giant cell astrocytoma, Protoplasmic astrocytoma, Ganglioglioma, Xanthomatous astrocytoma, Subependymoma .	60 -80
II	Lower grade malignancies	Fibrillary (gemistocytic, protoplasmic) astrocytoma Ependymoma Oligodendroglioma Mixed oligo-astrocytoma Optic nerve glioma	50 - 60
III	Higher grade malignancies	Anaplastic astrocytoma Anaplastic oligodendroglioma Anaplastic mixed glioma	20 – 40
IV	Highest grade malignancies	Glioblastoma multiforme Gliosarcoma Gliomatosis cerebri	5 -15

Table 1.3: *The American association of surgeons grading system for glioma tumours and estimated survival rates for the differing stages. Glioma is a general term for any tumour that arises from tissues of the brain other than nerve cells and blood vessels. Due to the diversity and location of glioma, a more physical interpretation of cancer type is required. The table also indicates the estimated survival rates for the differing stage glioma.*

Glioma like other neuro-ectodermal derived tumours has a prognosis dependent upon the disease stage. Glioma is an incurable disease, with individuals suffering from stage one and two having a life expectancy of five to ten years, stage three brings a solemn three years and for those individuals with stage 4 disease, such as glioblastoma multiforme a mere one year survival (Table 1.3) [53]. Further complications to the prognosis arise with factors such as age and primary tumour location.

1.3: Chemotherapy.

1.3.1: Current treatment strategies.

Currently, the most common therapeutic agents used for metastatic melanoma include dacarbazine, temozolamide and fotemustine [54, 55]. These drugs have been tried alone or in combination with each other and/or with adjuvant immunotherapy (interferon and interleukin-2) [56]. However, to date no combination has proved more beneficial than single agent dacarbazine which remains limited by a poor response rate of 16%, rarely affective after 6 months [34]. Due to the diverse nature of neuroblastoma, intensive chemotherapy, surgery, radiation therapy, stem cell transplant, differentiation agent isotretinoin also called 13-*cis*-retinoic acid, and frequent immunotherapy with an anti-GD2 monoclonal antibody therapy, as well as therapy with platinum compounds (cisplatin, carboplatin), alkylating agents (cyclophosphamide, ifosfamide, melphalan), topoisomerase II inhibitor (etoposide), anthracycline antibiotics (doxorubicin) and vinca alkaloids (vincristine) are commonly used. Newer regimens include topoisomerase I inhibitors (topotecan and irinotecan) which have been found to be effective against recurrent disease. However, regardless of the chemotherapeutic regime used, only 30% of patients with late stage survive [39].

Glioma therapy encompasses an intensive combination of surgery, radiotherapy and chemotherapy. Surgical removal is the primary goal, to allow for histological analysis of the mass, identifying tumour origin and stage as well as to remove the mass, decreasing any adverse side effects of the tumour. For post-surgical therapy to have any effect on the outcome of treatment, 95% of the tumour mass must be removed. Normally fractionated radiation therapy is used with a specific margin around the resected tumour area to treat any remaining neoplastic cells. More recently, intensity modulated radiation therapy which allows for more homogeneous field coverage of an irregular tumour region. Radiotherapy is combined with chemotherapeutics to accentuate their chance of success, but agents must be able to cross the blood brain barrier. Temozolomide is one agent used in glioma therapy, with little to no success [57]. With the lack of a treatment which works, chemotherapy has moved towards prevention of growth, invasion and metastasis by combining the already existing drugs with agents to prevent vascularisation and angiogenesis. Combination therapies have

shown some success in clinical trials, but still this approach does not represent a successful clinical treatment for glioma. Novel combinational therapies combining the ER stress-inducing agent tetrahydrocannabinol (THC), an active cannabinoid with temozolamide have shown promising effects in animal studies with phase 1 trials now underway [58].

Considering the poor outcomes for melanoma, neuroblastoma and glioma, clearly novel therapeutic approaches are urgently required. These cancers all differ in symptoms and mass localization, but share a poor prognosis and have origins tied to the neuro-ectodermal stem cell. For all three tumour types no treatment exists which shows a significant effect on tumour progression or late stage disease. Further understanding of the apoptotic pathways of these cancers and their homeostatic survival mechanisms may thus give further insight into how more successful treatment strategies may be developed.

1.3.2: Targeting cellular components of a cell.

The poor response of melanoma, glioblastoma and neuroblastoma to current chemotherapeutic intervention likely arises from the notorious resistance of such tumours to apoptosis [34]. For example, advanced metastatic melanoma is highly invasive and has developed many different molecular mechanisms to aid its survival against both immunological and cytotoxic regulation.

Classically, agents capable of targeting and damaging DNA have been used to induce cancer cell death, and as such DNA damage remains the focus of most common chemotherapeutics, as a mechanism to disrupt cellular homeostasis and activate death pathways. Consequently, there is a lack in diversity, with regards to targets, and many cancer types are able to make adaptations within classical cell death pathways which result in their poor response to such therapies.

1.3.2.1: Apoptosis and cellular development of resistance.

Apoptosis is a recognised form of programmed cell death and involves a diverse range of cell signals which may originate from outside (extrinsic) or within (intrinsic) the cell (Figure 1.3) [59]. Extrinsic inducers of apoptosis include; hormones and growth factors,

as well as nitric oxide and cytokines [59]. To induce apoptosis via an external signal, the signalling molecule must either be capable of crossing the cell membrane or be able to transduce the response via an intermediate, for example by activating a member of the death-receptor family [60]. Intrinsically, apoptosis can be activated as a result of direct stress or damage to the mitochondria or the endoplasmic reticulum (ER) or indirectly from stimuli originating from damage to DNA content that activates downstream mitochondrial induced apoptosis [61].

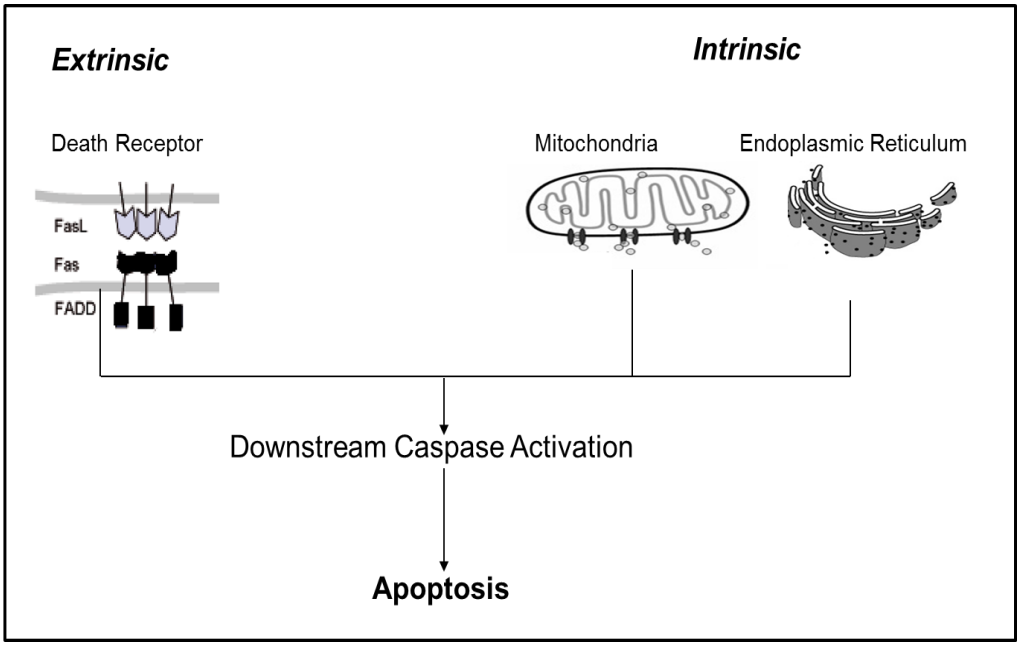

Figure 1.3: *Extrinsic and intrinsic pathways of apoptosis. Apoptosis mediated through the ligation of death receptors or via mitochondria or endoplasmic reticulum converge at the activation of caspases to induce apoptosis.*

1.3.2.2: Death-Receptor-induced apoptosis.

Apoptosis can be induced through the activation of death receptors including: Fas (CD95), TNFαR, DR3, DR4, and DR5 by their respective ligands [60]. Death receptor ligands characteristically initiate signalling via receptor oligomerization, which in turn results in the recruitment of specialized adaptor proteins and activation of caspase cascades [62]. Binding of Fas ligand (FasL) induces Fas trimerization, which recruits initiator procaspase-8 via the adaptor protein FADD [63]. Procaspase-8 then oligomerizes and is activated via autocatalysis. Activated caspase-8 stimulates apoptosis

via two parallel cascades: it can directly cleave and activate caspase-3, or alternatively, it can cleave Bid, a pro-apoptotic Bcl-2 family protein [64]. Truncated Bid (tBid) translocates to the mitochondria, inducing cytochrome c release, which sequentially activates caspase-9 and -3 [64].

Death receptor regulation can occur through a variety of different mechanisms, at differing stages of formation of the death-inducing-signalling-complex (DISC). Firstly, death receptors can be regulated by preventing procaspase 8 from binding to the death effector domain of Fas- associated death domain protein (FADD), decreasing levels of active caspase 8 produced [65]. For example, FADD – like ice inhibitory proteins (FLIP) which contain 2 death effector domains competes directly with procaspase 8 for FADD interaction and therefore represents a natural regulator of caspase activation.

The mammalian form of FLIP known as cFLIP not only competes for the FADD binding, but can also directly interact with procaspase 8 via its death effector domain [66]. Therefore cFLIP can inhibit both components required for caspase activation; enzyme and substrate. Also death receptor activation can be inhibited by a mechanism that is dependent upon the binding of the death receptor ligand. Decoy receptors closely resembling death receptors exist to sequester death ligands, preventing them binding to and activating death receptors [67]. Finally, death-receptor-induced apoptosis can be regulated by inhibiting the activation of procaspase 8 [65]. The silencer of death domain (SODD) protein, a 60 kDa inhibitor of procaspases, inhibits the proteolytical activation of procaspases directly [68].

1.3.2.3: Mitochondrial-induced apoptosis.

The mitochondria are sometimes described as the cellular power plant of the cell because they generate most of a cell's supply of adenosine triphosphate (ATP), used as a source of chemical energy [69]. In addition to supplying cellular energy, mitochondria are involved in a range of other processes, such as signalling, cellular differentiation, cell death, as well as the control of cell cycle and growth [70].

Mitochondrial-induced apoptosis is regulated by the B-cell lymphoma 2 (BCL-2) family [71]. BCL-2 family members can be either pro or anti apoptotic, with the pro apoptotic group being sub divided further into inhibitors of anti-apoptotic BCL-2 members or

initiators of apoptosis (Figure 1.4). The crucial factor for mitochondrial-induced apoptosis is membrane permeability. Mitochondria have two membranes: an outer (outer mitochondrial membrane (OMM)) and an inner (inner mitochondrial membrane (IMM)) mitochondrial membrane [72]. BCL-2 family members such as BCL-2, BCl-x_L and MCL-1 reside within the mitochondria due to their hydrophobic C terminals, stabilising the barrier function of the mitochondrial membranes, preventing apoptogenic factors from being released [72, 73]. Pro-apoptotic BCL-2 family members such as Bad, Bid, NOXA and can shuttle between mitochondrial localisation. When apoptosis is induced these pro-apoptotic proteins localise in the mitochondria, binding and inhibiting the function of the anti-apoptotic members [73] which allows for the activation, by conformational change, of apoptotic initiator members Bax and Bak. When activated, Bax and Bak enter the mitochondrial membranes resulting in membrane disruption and the release of cytochrome c and other pro apoptotic stimuli [74].

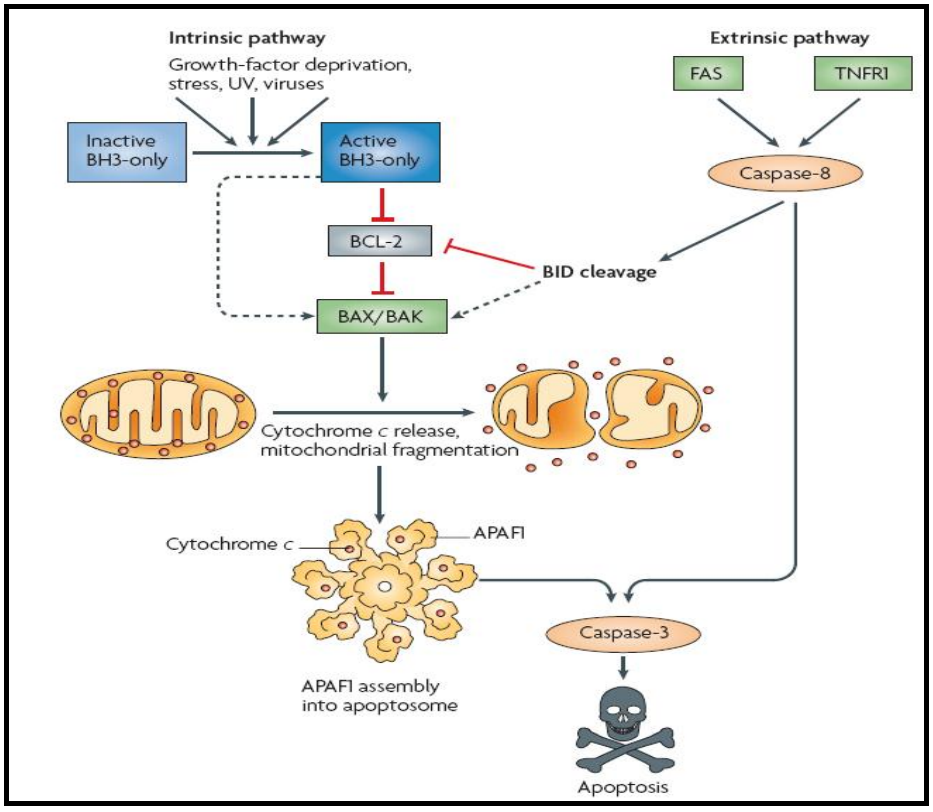

Figure 1.4: *Interactions of the opposing BCL-2 family members in the initiation of apoptosis. Binding of pro apoptotic members of the BCL-2 family to the opposing anti apoptotic members inhibiting their effect on mitochondrial membrane stability and their inhibitory effect on apoptosis initiating family members Bax and Bak [75].Image adapted from Youle and Strasser et al (2008).*

There are conflicting theories explaining the role by which the apoptotic initiator members of the BCL-2 family Bax and Bak induce of apoptosis; from homo-oligomerisation following cleavage by caspases and channel formation [74], to the interaction with already present channels, such as the adenine nucleotide translocator (ANT) or the voltage-dependant anion channel (VDAC) altering their function, resulting in the permeabilisation of mitochondrial membranes [73, 76]. Although the mechanism of these members is not yet fully understood, their consequence within the mitochondrial membranes has been a well-known characteristic of mitochondrial-induced apoptosis for many years [77].

A well-accepted model to date is the formation of a four Bax pore within the OMM allowing the release of pro apoptotic factors such as Cytochrome c, Apaf1 and SMAC DIABLO (an inhibitor of the inhibitor of apoptosis protein family (IAP's)) by simple diffusion. Upon release Cytochrome c binds to apoptotic protease activating factor 1 (Apaf 1) forming the apoptosome which can now bind and process procaspase 9 due to allosteric changes that occur during apoptosome formation. This results in an increase in active caspase 9 levels [78] which activates executioner caspases increasing proteolysis and free DNase to digest chromatin [79].

1.3.2.4. Targeting cytoplasmic stress.

As for the deoxyribonucleic acid (DNA)-containing nucleus, cytoplasmic components on the cell are also vital for survival. The importance of DNA in cell survival has resulted in a number of control mechanisms to identify and repair damage to DNA [80]. If the damage cannot be rectified, signalling cascades are activated and death stimuli induced to remove the cell and save the integrity of the surrounding tissues (Figure 1.5) [81]. This concept also applies to a number of differing cell components, including organelles and the cell membrane, where damage results in the activation of homeostatic mechanisms to repair the functionality of the cellular component, however if the damage is too severe, actively remove the cell [82, 83].

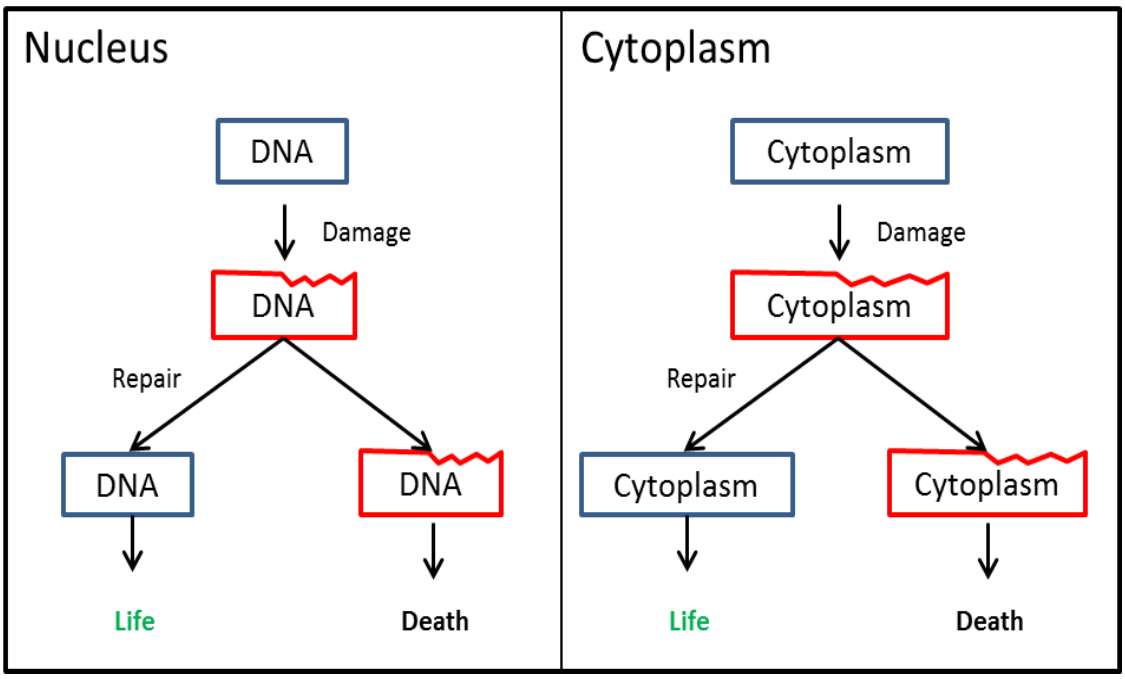

Figure 1.5: *Comparing nuclear to cytoplasmic induced stress as targets for cancer treatment. Stress or damage to the nucleus or components of the cytoplasm results in the induction of homeostatic repair mechanisms, capable of inducing cell death in cells where the damage is too severe or persists for too long.*

Although, in a high number of cancer types, DNA damaging agents have shown success, these agents often result in collateral damage to normal cells which results in severe adverse side effects from therapy, as well as a high risk of developing a secondary cancer. Characteristics of cancer cells, such as high proliferation rate, coupled with poor environmental conditions increases the load present upon organelle productivity [84, 85]. This sensitizes cancer cells to stress. Therefore, using agents capable of targeting cytoplasmic stress rather than nuclear stress or combining agents to target both cellular regions, may allow for a reduction in the dose of DNA damaging agents and therefore a reduction in the side effects and an increase in therapeutic success. Due to the importance of the endoplasmic reticulum (ER) in protein production, coupled with success of the current chemotherapeutic bortezomib in multiple myeloma [86], this study will focus on targeting the ER to induce cytoplasmic stress.

1.4. The Endoplasmic reticulum and the regulation of homeostatic stress.

The ER is a eukaryotic organelle that forms an interconnected network of tubules, vesicles and cisternae within cells, making up approximately 10% of a cells inner mass [87]. These complex structures are responsible for several specialized functions such as: protein translation and folding, as well as the transport of proteins that are to be used both within the cellular membrane (transmembrane receptors and other integral membrane proteins), or secreted (exocytosed) from the cell (e.g. digestive enzymes) [88]. The ER is also responsible for sequestration of Ca^{2+}; and the production and synthesis of glycogen, steroids and other macromolecules [89]. Ribosomes that are present upon the cytosolic surface of the ER membrane are responsible for the monopoly of protein translation within eukaryotic cells [90]. Regulation of protein translation is a key step in ER stress homeostasis [91].

1.4.1: Protein translation

Translation, the decoding of messenger ribonucleic acid (mRNA) by ribosomes to produce an amino acid chain known as a polypeptide, is comprised of four stages; activation, initiation, elongation and termination [92]. Translation begins after the formation of a complex structure, where eukaryotic initiation factor (eIF) 2 bound to guanidine triphosphate (GTP) and Met-tRNAimet associates with the 40S ribosomal subunit (in complex with eIF1A and eIF3), this interaction forms the 43S pre-initiation complex [92]. When a transfer RNA (tRNA) carrying a methionine and the pre-initiation complex bind to messenger (m)RNA, close to the start codon (a series of three adjacent bases in one polynucleotide chain of a DNA or RNA molecule, which codes for a specific amino acid) the initiation complex is complete [92]. Upon activation of the initiation complex, the large 60s subunit of the ribosome binds to the complex, aided by eIF5 and eIF2-guanadine diphosphate (GDP), resulting in the formation of the 80S subunit [93, 94]. The formation of the 80S results in the release of the initiation factors from the complex [92].

The large subunit of the ribosome has three sites where interaction with tRNA occurs, known as site A, site P and site E. Site A is the location where aminoacyl-tRNA anticodon pairs up with mRNA, to ensure that only the correct amino acid is inserted

into the growing polypeptide chain. Site P is where the amino acid is added to the growing polypeptide chain and finally site E is the location where the empty tRNA resides before release [92].

To translate the mRNA fully into the amino acids that form the polypeptide chain, the ribosomal based initiation complex must be exposed to the complete mRNA sequence and therefore a physical movement is required to shift the complex to the next codon, in a 5' to 3' direction [92]. This process is known as the elongation stage, where the full mRNA sequence is processed by the active ribosome. For movement of the ribosome (translocation), elongation factor G is required. After translocation the next tRNA can interact with site A within the ribosome. This process requires elongation factors (EG-Tu and EG-Ts) as well as GTP [62]. Upon binding of the tRNA amino acid complex in site A of the ribosome, GTP is cleaved to form GDP generating the energy required for elongation [95]. Elongation persists until the ribosomal based initiation complex reaches a stop codon; one of three specific sequences which have no tRNA based anti-codon sequence [95]. In place of tRNA, a release factor can bind and facilitate the release of the polypeptide.

1.4.1.1: Cap dependent or independent translation initiation.

During protein synthesis, the cap serves as a tag, highlighting where the 40s ribosomal subunit interacts. Important in this process is the eIF4F complex, formed from eIF4A, eIF4E, eIF4G [96, 97]. The formation of the eIF4F complex enhances the activity of each component. Initiation factor eIF4A is a helicase, which couples ATP hydrolysis with RNA binding and duplex separation, unwinding any secondary structures that may have formed [97]. EIF4E is the cap binding protein and is therefore essential for cap dependent translation. Finally eIF4G acts as scaffolding, aiding the assembly of the initiation complex, which leads to the recruitment of the template mRNA to the translation machinery [97, 98].

Translation of the uncapped mRNA is also achievable, mediated by an RNA structure which allows assembly of the translational machinery close to or directly at the start codon [99]. This is known as the internal ribosome entry segment (IRES). IRES mediated translation has been shown to be independent of 5' end of RNA and does not require a cap, however IRES allows for the recruitment of the 40s ribosomal subunit,

independently of the 5’ and 3’ ends of the RNA [97]. IRES elements are not yet fully understood, but are believed to contain a Y-shaped, double hairpin structure which is followed by a smaller hairpin, forming a RNA motif [100]. These have been found upstream of the start codon in a variety of IRESs. To be functional, IRES requires IRES trans acting factors (ITAFs) [97]. IRES have been found in a number of cellular mRNAs, and although often capped, some mRNAs which encode important initiation factors, transcription factors, survival proteins, as well as oncogenes, growth factors and homeotic genes contain IRES elements [98]. This adaptation in translation may allow for the induction of vital cellular components, when protein synthesis is impaired.

IRES mediated translation has been shown in some models to require the eIF4F complex, as well as ATP. However, eIF4E is not essential within the complex [98]. The involvement of the 48s is not found for all IRESs. The generally accepted theory is that the ribosomal P site is orientated into the proximity of the initiation codon and then eIF2-GTP/Met-tRNAi complex is recruited to the 40S/IRES complexes, forming the 48s ribosomal subunit [98].

1.4.1.2: Protein folding and misfolding.

Protein folding is the process by which a polypeptide assumes its functional conformation. Protein folding is a physical mechanism were a polypeptide folds into a complex three-dimensional structure from a random coil. Once the protein has taken its nascent polypeptide form a signal sequence within its amino acid sequence is detected by signal recognition particles in the cytosol, trafficking of the polypeptide to the sec61 aqueous pore complex within the ER membrane [101]. Polypeptides reach protein secondary structural status due to the presence of the unique intrinsic properties held within each amino acid in the polypeptide sequence. This can start to interact and fold up, while the remaining polypeptide chain is still being synthesised. This is then followed by active bond addition and fragment amalgamation to form fully synthesised and functioning protein [102].

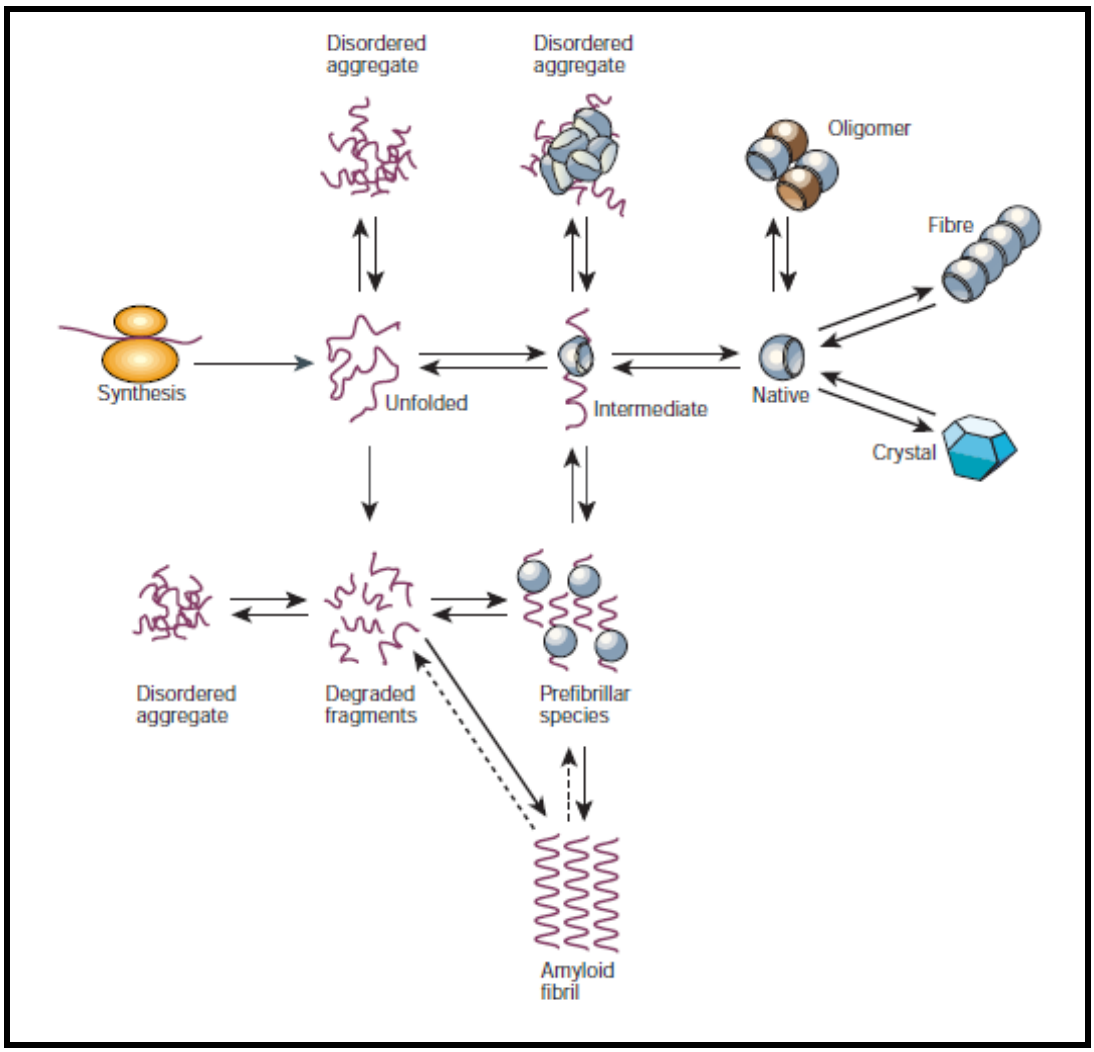

Figure 1.6: *Protein folding and the structures that can be formed by polypeptide chains on route to functionality. An unstructured chain, for example newly synthesized on a ribosome, can fold to a monomeric native structure, often through one or more partly folded intermediates. It can, however, experience other fates such as degradation or aggregation. An amyloid fibril is just one form of aggregate, but it is unique in having a highly organized 'misfolded' structure. Other assemblies, including functional oligomers, macromolecular complexes and natural protein fibres, contain natively folded molecules. The populations and inter-conversions of the various states are determined by their relative thermodynamic and kinetic stabilities under any given conditions. In living systems, however, transitions between the different states are highly regulated by the environment and by the presence of molecular chaperones, proteolytic enzymes and other factors. Failure of such regulatory mechanisms is likely to be a major factor in the onset and development of misfolding diseases. Image adapted from Dobson et al (2004) [103]*

Due to the complexity and number of possible interactions present within a polypeptide a number of different structures can be generated from a single polypeptide and therefore tight regulation of protein folding is essential to ensure the outcome of functional proteins (Figure 1.6) [104]. Approximately 90% of all proteins are of sufficient size (> 100 amino acids) to collapse in aqueous solutions to non-native conformations [105]. These confirmations may be a required intermediate state, a "stepping stone" to the correct conformation, or a kinetically stable misfolded state [105]. Recent research has shown that even for small polypeptides, that ultimately reach their folded state on a sub-second timescale, pass through structural intermediates [105].

Partially folded or misfolded proteins tend to aggregate, as a direct consequence of exposed hydrophobic amino acid residues, as well as regions of unstructured polypeptide backbones. These regions are buried in a correctly folded protein [106]. Aggregation of protein intermediates and misfolded proteins primarily results in amorphous structures [107], due to the non-specific interactions required to bury exposed hydrophobic regions, but larger organised fibrillar aggregates called amyloid are also known to occur [105]. Somatic mutations in the gene sequence of a protein or errors in transcription/translation can lead to the translation of a mutant protein unable of adopting the native state [107]. Studies have indicated that protein intermediates are more likely to aggregate in the crowded environment (300 – 400 g/l of protein and other macromolecules), found in a cell. This increased likelihood may explain the requirement of chaperones [92].

1.4.1.3: Endoplasmic reticulum stress, quality control and homeostasis.

The protein folding process has been shown not to involve a fixed series of steps between specific partly folded states, but is comprised of a random search of the many possible conformations accessible to the individual polypeptide chain, depending on the charges and their distributions [32]. Therefore, incompletely folded proteins must expose to the surroundings at least some regions of the structure which would normally be buried in their native state, in the quest for the correct confirmation, leaving them prone to inappropriate interactions within their own peptide structure or with other molecules within the crowded environment of a cell [92]. The most frequent outcome for misfolded proteins is aggregation [92]. This unwanted outcome is known as ER stress and can be enhanced by cellular insults that disrupt the balance between protein

synthesis, folding and trafficking within the lumen of the ER [107]. For example, reduction in glucose or oxygen can affect the ability of cells to produce functional proteins [108].

Due to the toxic effect of ER stress, a range of strategies have evolved to help prevent unwanted interactions and improve the efficiency of protein folding. Folding catalysts such as peptidylproylyl isomerases and protein disulphide isomerases (PDI) are enzymes that increase the rate of folding, as they physically implant bonds within a peptide structure to form the tertiary state. Molecular chaperones are present in all types of cells and in all compartments, play important roles within protein folding and as an adaptive response under times of ER stress [109]. Molecular chaperones do not themselves increase the rate of protein folding, but increase the efficiency by which a protein is folded by interacting with exposed residues, helping to orientate the peptide structure in the optimal way for processing by foldases [110]. Molecular chaperones also aid protein folding by reducing the probability that the immature protein intermediates interact, forming aggregates and therefore reduce the chance of a toxic insult damaging the functionality of the cell. Evidence for the importance of molecular chaperones for homeostasis has demonstrated a significant increase in their expression during periods of stress or damage. In particular, the heat shock protein family (HSP) has been well documented to play a key role under both periods of normal physiology and stress [110]. One important member of The HSP family is HSPA5, also known as glucose regulated protein 78 (GRP78), which is the central sensory hub of a cell based homeostatic response mechanism to ER stress known as the unfolded protein response (UPR) [91, 111]. Neural-crest-derived melanoma, glioblastoma and neuroblastoma have all previously been shown to respond to ER stress [82, 112, 113] however studies suggest that differences exist between these cancer types, in the context of GRP78 regulation [113-116].

1.5: Unfolded protein response.

The UPR is activated in response to an accumulation of unfolded or misfolded proteins within the ER. This homeostatic response is made up of three cascades, stemming from the central stress sensor protein: GRP78 [87]. The desired effect of the UPR is to govern the survival response of the ER by reducing the load upon it, yet at the same time hold in place routes through which to remove the cell and minimize the damage to the tissue as a whole. There are many consequences of the pro-survival response of the UPR, such as cell cycle and protein synthesis arrest, reducing the requirement/production of proteins and allow ER folding machinery time to recover. Also ER resident chaperones are activated, aiding the ER folding machinery and buffering unfolded or misfolded protein levels. Finally, the activation of ER-associated degradation (ERAD) eliminates unwanted proteins to aid the ER under times of stress [117, 118]. The ability of PERK, IRE1 and ATF6 to fight against stress, stems from the activation of these three proteins by GRP78 (Figure 1.7) [119].

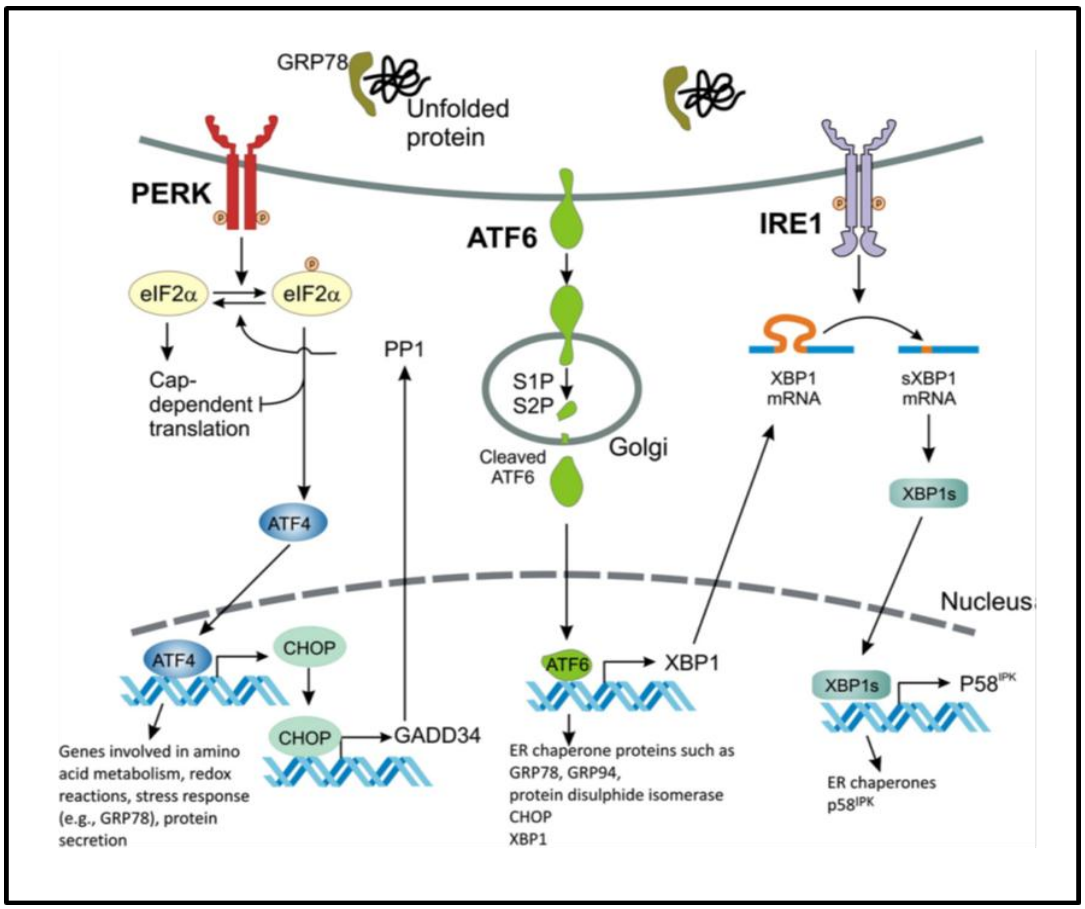

Figure 1.7: *The role of GRP78 as the central regulatory force of the UPR. When there is an increase in unfolded proteins in the ER, GRP78 dissociates from; IRE1, PERK and ATF6, allowing for their activation. IRE1 homodimerises forming a competent RNase domain allowing for the processing of X-box binding protein 1 (XBP-1) mRNA to make an active splice variant sXBP-1. sXBP-1 is the active transcription factor and translocates into the nucleus where it induces the expression of chaperones by binding to ER response elements within appropriate promoter sites. PERK, like IRE1, is activated under stress by autophosphorylation and homodimerisation to form an active kinase. PERK phosphorylates eukaryotic initiation factor 2α (eIF2α), this phosphorylation blocks the translation of normal protein synthesis but allows activating transcription factor 4 (ATF4) and other essential mediators of the stress response to be translated. ATF4 translocates to the nucleus and induces genes involved in homeostasis and apoptosis. Upon release, AFT6 translocates to the Golgi apparatus where it is processed by site 1 and site 2 proteases (S1P, S1P), into an active transcription factor ATF6f, which is a fragment of the cytosolic domain. ATF6f can up regulate the expression of chaperone proteins, ERAD, XBP1 and P58IPK (an inhibitor of PERK). Image adapted from Stankiewicz et al [120].*

1.5.1: Glucose regulated protein 78.

Glucose regulated protein 78 (GRP78), also known as immunoglobulin heavy chain binding protein (BiP), is encoded by the HSPA5 gene (chromosome 19q33.3). GRP78 is a 78 kDa member of the glucose regulated protein (GRP) family, induced when cells are deprived of glucose, and a member of the heat shock protein (HSP) family [121]. GRP78 shares 61% amino acid sequence homology with human HSP70 [122] and consists of an N-terminal containing a single ATPase catalytic site and a substrate binding C-terminus (Figure 1.8) [123]. GRP78 is translated in a cap-independent manner and exists within the cell in multiple forms. Post-translational modification by phosphorylation or ADP ribosylation results in inactivation of GRP78 by oligomerisation into chains in the ER [124]. This inactive form, representing a neutral reservoir within the ER which can be re-activated, allows fast action upon realization of ER stress, this increases a cells chance of survival [124].

GRP78va, a novel isoform of GRP78 has been described. GRP78va is induced during ER stress, when GRP78 enhances the retention of intron 1 of the GRP78 transcript, resulting in a GRP78 molecule without an ER localisation sequence (signal peptide sequence) [125]. GRP78va exhibits a more cyto-protective role, but still regulates the UPR from the cytosol. Evidence is rapidly accumulating for the existence of cell surface GRP78 [126]. Research demonstrated this sub-population in pathological tissues, such as cancer or in cells under stress [125]. This surface-localised GRP78 is too distant to regulate ER-based UPR activators PERK, IRE1 and ATF6 and has been implicated in oncogenic signalling and metastasis [127].

Populations of GRP78 have also been discovered in the nucleus, following over-expression or ER stress, as well as in the mitochondria. These populations, although expressed at a much lower level than the ER localised GRP78 have been implicated in prevention of DNA-damage-induced cell death signalling and regulation of energy within the mitochondria during periods of ER stress [125].

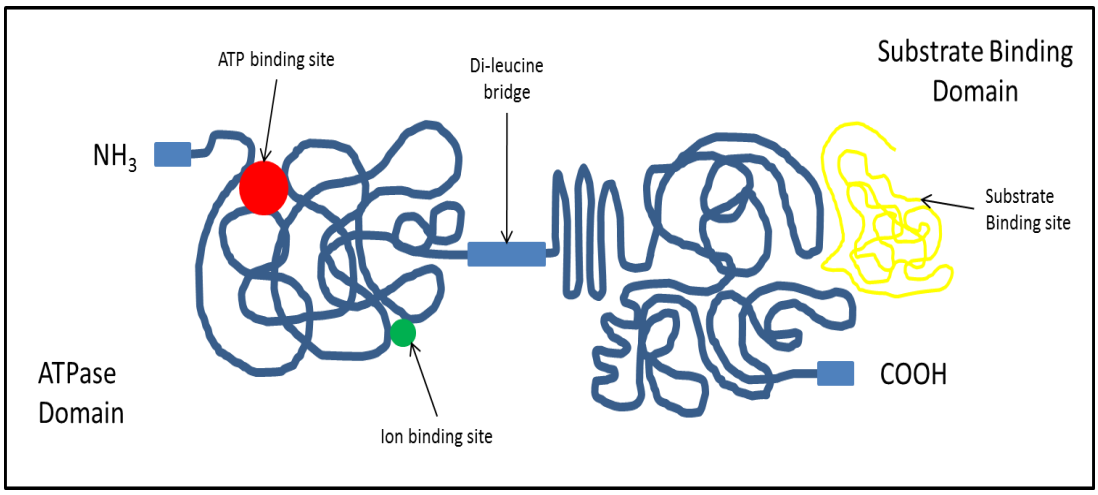

Figure 1.8: *Depiction of GRP78 structure and binding sites. This figure shows the ATPase and substrate binding domains of GRP78 connected together by a di-leucine bridge. The Ion binding domain present within the ATPase N-terminal region of GRP78 is also indicated.*

Evidence for the importance of GRP78 can be seen by its sequence conservation between species. From yeast (Saccharomyces cerevisiae) to humans, GRP78 sequence homology is highly conserved [128]. For example sequence analysis of GRP78 in rats and hamsters has shown 99.4% identity [129]. This therefore demonstrates the vital role to which GRP78 plays in the survival of life, for it to be so highly conserved from more basic life forms such as Porifera [128], to the more complicated life of multi-cellular organisms. Further evidence for the vital role of GRP78 on life, is its expression in early embryonic development. Expression of the UPR master regulator and ER stress sensor GRP78 has been detected at the two-cell stage of embryonic development, with high concentrations present at the blastocyte stage [130]. GRP78 is believed to be important in proliferation and survival of the inner cell mass [131, 132], which is the precursor of the pluripotent stem cell. More-recent studies have discovered the presence of glucose regulated proteins in cardiac tissue and their involvement in the development and differentiation of these tissues, along with the alleviation of cardiac cell metabolic stress due to hypoglycaemia [133].

In healthy unstressed cells, GRP78 exists bound to the luminal domain of protein kinase-like ER kinase (PERK), inositol-requiring element 1 (Ire1) and activating transcription factor 6 (ATF6) [131]. When ADP is bound to GRP78 it has higher affinity for protein substrates with slower off rates than with ATP [134]. When bound to

a substrate, not only are they locked in a specific conformation but this interaction with the substrate results in the dissociation of PERK, IRE1 and ATF6. Also the binding of protein substrates to GRP78 stimulates its ATPase activity, resulting in the replacement of ADP with ATP [134]. ATP binding also causes a decrease in GRP78 affinity for protein substrates which in turn results in substrate release [135]. GRP78 processing of ATP occurs in a cycling system, therefore a constant supply of ATP is required [123]. Cycling of ATP/ADP within GRP78 therefore effects the association of both protein substrates and UPR proteins as they are dependent upon this for interaction.

Increased levels of unfolded or misfolded proteins in the ER result in an increased level of GRP78 bound to these substrates, resulting in a greater level of UPR proteins being free within the ER. However, the role of GRP78 with respect to cell survival does not end with the activation of the UPR, although this is seen as a major contributing factor. Binding of substrates to GRP78 is not simply an activator of a stress response mechanism. GRP78 holds a substrate, preventing structural changes and allowing ER folding machinery to work more efficiently to fold or recovery these proteins. E.g. GRP78 holds a protein in an optimal orientation to allow PDI to remodel bonds within misfolded proteins. Finally the interaction of GRP78 with incorrectly folded proteins or nascent polypeptides prevents or decreases their rate of aggregation into insoluble masses within the ER, which would exert extra pressure upon an already stressed system by interfering with transport, as well as associating with newly synthesised proteins.

The C-terminal binding site of GRP78 is also capable of also binding and sequestering calcium (Ca^{2+}). Although this interaction is on a one to one scale, this property could help to stall Ca^{2+} release from the ER, an early indicator of ER stress and also helps preserve Ca^{2+} homeostasis [136]. Buffering Ca^{2+} release from the ER can reduce the chance of apoptosis induction, increasing the time the ER has to recover before the cell is condemned to death [79]. With only a single binding site, GRP78 ion binding potential is low but with a sufficiently high expression within the cell, coupled with other chaperone family members, along with the cycling of binding potential, to significantly prevent or slow the flow of Ca^{2+} stores from the ER.

GRP78 has been shown as a diverse protein capable of preventing the induction of apoptosis by buffering characteristic attributes which would normally result in apoptosis. Within the UPR, growth arrest and DNA damage 153 (GADD153 or CHOP) is a critical

component of the pro-apoptotic arm. Induction of GADD153 signals that a level of stress beyond repair has existed for too long. Induction of GADD153 indicates initiation of a cell to apoptosis [137]. Studies in glioma indicate that GRP78 was a crucial factor in GADD153 induction [138]. This research demonstrated that in the presence of GRP78 knockdown a clear up regulation of GADD153 was present, demonstrating an inhibitory relationship that exists between GRP78 and UPR-stimulated GADD153 induction and the eventual activation of apoptosis [138].

Like GADD153, the fate of the executioner caspase 7 is also coupled to GRP78 activity [139]. GRP78 present within the ER membrane forms a complex with procaspase 7 preventing it from being activated or released into the cytoplasm [140]. This area is not yet understood fully but it is known that GRP78 can only halt the release of caspase 7 for approximately 24 hours [141]. The reasoning behind this reversible inhibition is still under debate with conflicting ideas arising, from correlation to the half-life of GRP78 (which is approximately 24 hours) to the proteolytic cleavage of GRP78 by caspase 7 [139] or simply the as a consequence of the cycling kinetics of GRP78, which ensures GRP78 itself is never irreversibly inhibited. During periods of ER stress, GRP78 has been shown to localize to different areas of the ER and cell including the ER membrane, cytoplasm, nucleus and cell membrane [125]. Conflicting explanations exist for this observation, suggesting that there is a planned redistribution of GRP78 to help the cell under stress, another theory is that GRP78 increased presence around the ER and other regions of a cell is a consequence of protein up-regulation [139].

1.5.2: Protein kinase-like endoplasmic reticulum kinase

Double-stranded RNA-activated protein-kinase-like ER kinase (PERK) also known as eukaryotic initiation factor 2 alpha kinase 3 (E2AK3) and is located on chromosome 2p12. PERK is a type I transmembrane protein and one of the unfolded protein response stress sensors or activators that exerts a key role within cell survival. Dissociation from GRP78 allows activation of PERK by homodimerization and autophosphorylation [142] creating an active cytosolic Serine/threonine-kinase domain. PERK kinase activity is involved in the prevention of global protein synthesis [143, 144], while allowing selective mRNA translation to commence [145] resulting in up-regulation of stress response proteins. The inhibition of cap-dependent translation (global protein synthesis) decreases the load placed upon the ER by reducing protein translation, as well as halting

proliferation. For example inhibition of protein production can cause cell cycle arrest due to the reduction of integral proteins such as Cyclin D1 [146]. Active PERK is a major contributing force along with haem regulated inhibitor (HRI), double stranded RNA activated protein kinase (PKR) and "general control non-repressed 2" (GCN2) that determine the phosphorylation state of eukaryotic initiation factor 2 alpha (eIF2α), as well as phospho-regulation the bZIP cap and collar transcription factor NF-E2 p45-related factor 2 (Nrf2) [147].

Phosphorylated eIF2α at serine 51 interferes with the formation of a 43S translation-initiation complex by inhibiting the guanidine nucleotide exchange factor for the eIF2 complex (eIF2B), reducing global mRNA translation [148]. Therefore PERK is responsible for the up-regulation in translation of ER stress response genes to help the ER recover. Activating transcription factor 4 (ATF4), is one key protein under uORF translation, which when translated becomes an important bZIP transcription factor that can influence both pro –survival and -death signalling [149]. EIF2α activation results in the incomplete formation of the 43S translation-initiation complex which is capable of binding and scanning ATF4 mRNA at a differing 5' open reading frame site [150]. ATF4 can bind to and activate ER stress response elements (ERSE I + II) and unfolded protein response elements (UPRE). Genes incorporating these response elements encode an array of proteins required to aid a cell under times of ER stress. ATF4 stimulates the synthesis of chaperones such as GRP78 and GRP94, as well as other proteins that are involved in amino acid production/recovery and the regulation of homeostasis [151]. GADD153, the bZIP transcription factor associated with pro-apoptotic aspects of the UPR is also up regulated by the PERK/ eIF2α/ ATF4 pathway under times of severe or prolonged stress [152]. The level of GADD153 mRNA within a normal cell is relatively low. ER stress-induced transcription to translation of GADD153 therefore takes longer, than the IRES translation of GRP78 and other key components of the pro-survival response. This represents a time delay in the stimulation of pro-apoptotic stimuli, providing a cell with the chance to recover from a perturbation in function.

Nrf2 in non-stressed cells is anchored to the cytoskeletal protein Kelch-like ECH-associated protein 1 (Keap1) in a cytoplasmic complex [147]. PERK phosphorylates Nrf2 allowing it to dissociate from Keap1 and migrate to the nucleus where this transcription factor activates the antioxidant response element (ARE) [153], a characteristically pro-survival response. With PERK holding great influence upon the

rate of protein synthesis, PERK itself is negatively regulated by HSP40 to ensure protein synthesis can be restored, once stress has diminished. HSP40, also known as $P58^{IPK}$, is induced late within the UPR and binds to and inhibits the kinase domain of PERK, relieving UPR based inhibition of protein translation [154]. EIF2α is also regulated to prevent an irreversible inhibition of translation, which would be as fatal to a cell as the stress to which it was induced from. Nck-1, a phosphatase results in eIF2α de-phosphorylation, restoring global protein synthesis [155].

1.5.3: Inositol requiring element 1

ER stress sensor inositol requiring element 1 (IRE1) is the oldest component of the UPR and is present within all eukaryotic cells. IRE1 is encoded by the ER to nucleus signalling 1 (ERN1) gene on chromosome 17q24.2. GRP78 holds IRE1 inactive by masking the required motifs for homo-dimerization. Once released, sequences within its alpha domain are exposed allowing phosphorylation and oligomerization to an active state [123]. IRE1 encodes a type 1 transmembrane protein kinase endoribonuclease (IRE1p) [156]. There are two forms of IRE1: α and β. IRE1α is the primary copy of IRE1, expressed throughout the organism and has been implicated in embryonic development [157]. Whereas expression of IRE β on the other hand is localized to the gut and has not yet been linked with cell development but has been implicated in resistance of the gut to stress induced by xenobiotics [158]. IRE1 has also been implicated in chaperone and ER activated degradation (ERAD) induction, as well as the activation of cell death via GADD153 and JNK activation [159].

A luminal dimerization domain, kinase domain, ATP binding domain and finally an RNase domain are the main components of IRE1 transmembrane protein [123]. IRE1 can undergo oligomerization and autophosphorylation to activate its RNase domain [160]. Active IRE1 results in splicing of the bZIP transcription factor XBP-1. Splicing of XBP-1 (XBP-1s) causes a frame shift and the formation of an alternative C-terminus, holding greater transcriptional activation potential [123], within a transcription factor now capable of entering the nucleus [161]. XBP-1s regulates a selection of ER-resident chaperones involved in protein folding and importantly the tagging of terminally-mutated proteins for degradation.

IRE1 kinase activity results in the phosphorylation of tumour necrosis factor receptor 2 (TRAF2) [162]. The TRAF family have no known enzymatic activity and are known as signal adapters [163]. When TRAF2 is in complex with IRE1, c-Jun N-terminal kinase (JNK) is recruited and phosphorylated to an active state. TRAF2 appears to be specifically important in this regard, as deletion of the gene abolishes JNK activation [159]. TRAF2 can also complex with nuclear factor-Kappa B (NF-kB), activating anti-apoptotic signalling [164]. Active JNK can induce cell death, as well as tumourgenesis, cell migration and inflammation. JNK inhibition of BCL-2, by phosphorylation, results in BAX activation as a result of a decrease in BCL-2 regulation, allowing BAX translocation and dimerization/oligimerization into mitochondrial membranes and the release of pro-apoptotic factors, such as cytochrome c and APAF1 [165]. Activation of JNK also induces caspase 8 independent cleavage of Bid at a distinct site to generate the Bid cleavage product jBid [166]. Translocation of jBid to the mitochondria results in the release of Smac/DIABLO [166]. This release of Smac/DIABLO then disrupts the TRAF2-cIAP1 complex. The JNK pathway is therefore required to relieve the inhibition imposed by TRAF2-cIAP1 on caspase 8 activation and induction of apoptosis [166]. JNK has also been described to activate up-regulation of genes, such as c-jun and nuclear factor of activated T cells (NFATs) [167].

1.5.4: Activating transcription factor 6

Originally activating transcription factor 6 (ATF6) was isolated as a member of the leucine zipper protein family which are capable of forming heterodimers with DNA. Upon ATP binding to GRP78, ATF6 is released, migrating to the golgi apparatus [168]. When ATF6 reaches the golgi it is cleaved by site 1 proteases (S1P) at its luminal domain before it is cleaved by S2P at its N-terminal anchor domain [161]. These modifications to a 670 amino acid molecule result in the release of a basic leucine zipper transcription factor, which was embedded within ATF6's N terminus [169]. ATF6 binds ERSE 1 and 2, as well as binding the ATF/CRE element [123]. ATF6 has regulatory control over a number of important molecules within the UPR such as molecular chaperone GRP78, XBP-1 and GADD153 [170].

Research has revealed the existence of two forms of ATF6: α and β, both individually regulate the translation of molecular chaperones and ER folding machinery positively [123]. ATF6 is encoded by the ATF6 gene on chromosome 1q23.3 or 6p21.33

depending on the form of protein. Complexes of combined α and β forms result in repression of GRP78 by binding its promoter, preventing the required complex formation for transcription. ATF6 has a variety of functions that are also present within the other two UPR cascades. This overlap in activities could be present as an evolutionary backup within the UPR, preventing any of the important functions from being lost by having more than one route to their activation. For example, molecular chaperones and/or GADD153 have been shown to be regulated by PERK, IRE1 and ATF6. ATF6 activation results in the induction of XBP-1 mRNA synthesis helping to up regulate XBP-1, providing ample substrate for the IRE-1 cascade [120]. On the other hand, the overlap in response outcomes may allow for changes in response strength, as well as diversity in response type, depending on the type of stress.

One function within the UPR which ATF6 holds alone, is the inhibition of lipogenesis [123]. Forming a heterodimer with the basic helix-loop-helix transcription factor sterol response element binding protein 2 (SREBP2), ATF6 inhibits the lipogenic activity of SREBP2 by recruiting histone deacetylase complex 1 (HDAC1) [171].

1.5.5: Feedback mechanisms of the unfolded protein response.

The UPR holds great responsibility for the fate of a cell and its surrounding tissues during times of ER stress. Being capable of defending the integrity of a cell under times of stress makes the UPR a vital process in the physiology of living organisms.

One of the most important components of the UPR is the induction of key transmitter proteins XBP-1 and ATF6. A consequence of UPR activation is the downstream processing of XBP-1 and ATF6 to active transcription factors, thus the regeneration of cellular expression is essential to reset the dynamic equilibrium of the UPR during periods of prolonged stress or after homeostasis has be restored. Without this replenishment the dynamic equilibrium present between GRP78 and the UPR transmembrane proteins would be skewed in favour of activation, ultimately pushing the cell towards death. Therefore, evolution of mechanisms within the UPR, to reduce the activity of the cascades, is also essential for life. Endogenous expression of XBP-1 is regulated by both positive and negative feedback mechanisms. XBP-1s can itself activate XBP-1 mRNA transcription, amplifying the response to the stress signal from

IRE1. On the other hand, this response is quickly inhibited as newly synthesized XBP-1 protein acts to mediate the degradation of XBP-1s.

Research into the field of viral infection has identified $P58^{IPK}$ as an inhibitor of PERK [172]. Primarily, data has shown that the activation of $P58^{IPK}$ inhibits PKR-mediated translational arrest by binding to and inactivating the kinase domain of PKR, thereby ensuring that cellular protein-synthesis machinery remains available to synthesize viral proteins. Following on from this work, studies have demonstrated that $P58^{IPK}$ inhibited PERK phosphorylation of eIF2α, a key step in the activation of the UPR and inhibition of global protein synthesis [172]. This research has highlighted the presence of a key regulatory step within the UPR that ensures that global protein synthesis can re-commence following the stabilisation of the ER, as a downstream consequence of UPR activation.

The importance of re-establishment of protein synthesis again highlights the negative feedback loop present within the PERK arm of the UPR. GADD34 demonstrates the ability to influence the phosphorylation state of eIF2α by binding to and activating phosphprotein phosphatase 1 (PP1). Insights into the function of GADD34 were highlighted through the use of ATF4 deficient mice embryonic fibroblasts [173], demonstrating prolonged eIF2α phosphorylation when ATF4 was knocked out. Researching the role that ATF4 plays in GADD34 mediated eIF2α de-phosphorylation showed that ATF4 was capable of regulating GADD34 transcription by directly binding to the conserved ATF site within the GADD34 promoter and inducing GADD34 expression under periods of ER stress or amino acid deprivation [173]. Therefore, within the UPR there have been various adaptations to ensure the replenishment of the UPR, as well as the mechanisms to help the cell recover from the consequences of UPR activation. The complexity of the UPR demonstrates the importance of this homeostatic response.

One major problem with this widely adapted process is that it cannot distinguish between normal and cancerous cells. One of the many factors that aid a cancer cell under periods of therapy is the up-regulation of vital components of the UPR such as GRP78 or PDI. Therefore translational research has now shifted; focusing on combination therapies of novel UPR inhibitors with already established chemotherapeutic agents to induce an imbalance within the UPR cascades, resulting in an insufficient homeostatic response and an increase in ER stress-induced cell death.

1.5.6. Endoplasmic reticulum-induced protein degradation

The recognition of misfolded or mutated proteins depends on the detection of substructures within proteins, such as hydrophobic regions, unpaired cysteine residues and immature glycans [174]. In mammalian cells for example, there exists a mechanism called glycan processing [175], whereby the lectin-type chaperones calnexin/calreticulin (CNX/CRT) provide immature glycoproteins the opportunity to reach their native conformation [176]. They can do this by way of re-glycosylating glycoproteins by an enzyme called UDP-glucose-glycoprotein glucosyltransferase [176]. Terminally misfolded proteins, however, must be extracted preventing their accumulation in the ER, to decrease ER load and stress levels. This is carried out by ER Degradation Enhancing alpha-Mannosidase-like Protein (EDEM) and ER mannosidase I [177]. This mannosidase removes one mannose residue from the glycoprotein and this is recognized by EDEM, which targets these misfolded glycoproteins for degradation [178]. Because the ubiquitin-proteasome system (UPS) is located at the cytoplasm, terminally misfolded proteins have to be transported from the ER back into the cytoplasm. It seems that a protein complex, called Sec61, an ER membrane translocator containing the channel necessary for the transport of misfolded proteins to the cytoplasm is important in the removal of ubiquitin-tagged proteins for degradation [178, 179]. Furthermore, due to the involvement of this transporter in importing polypeptides to the ER, this translocation of misfolded proteins requires a driving force to determine the direction of transport. Since poly-ubiquitination is essential for the export of substrates, it is likely that this is the driving force. One of these ubiquitin-binding factors is the Cdc48p-Npl4p-Ufd1p complex [180]. Cdc48 (which is also known as valosine-containing protein (VCP) or p97) recognises ubiquitin tails and transports substrates from the ER to the cytoplasm with its ATPase activity to aid degradation of substrates by the 26S proteasome [178].

The ubiquitination of terminally misfolded proteins is caused by a cascade of enzymatic reactions. The first of these reactions takes place when ubiquitin-activating enzyme E1 hydrolyses ATP and forms a high-energy thioester linkage between a cysteine residue in its active site and the C-terminus of ubiquitin. The resulting activated ubiquitin is then passed on to E2, which is a ubiquitin-conjugating enzyme. Another group of enzymes, more specifically ubiquitin protein ligases called E3, bind to the misfolded protein [178]. Next they align the protein and E2, thus facilitating the attachment of ubiquitin to

lysine residues of the misfolded protein. Following successive addition of ubiquitin molecules to lysine residues of the previously attached ubiquitin, a poly-ubiquitin chain is created. A poly-ubiquitin tagged protein is produced and this is recognized by specific subunits in the 19S capping complexes of the 26S proteasome. Hereafter, the polypeptide chain is fed into the central chamber of the 20S core region that contains the proteolytically active sites. Ubiquitin is cleaved before terminal digestion by de-ubiquitinating enzymes. This third step is very closely associated with the second one, since ubiquitination takes place during the translocation event [178, 181].

1.6: Endoplasmic reticulum stress-induced apoptosis.

There are many factors that can result in perturbation of ER function such as hypoxia, decreased glycosylation or glucose availability, disruption in calcium (Ca^{2+}) homeostasis and primarily a disruption in the equilibrium of protein synthesis to folding and trafficking. ER stress occurs when the balance between protein synthesis and the folding capacity of the ER is disrupted, resulting in an accumulation of unfolded or misfolded proteins in the lumen of the ER [119]. Failure of the ER to maintain this balance can be critical, not only to the cell in which the defect has occurred but the surrounding tissues. If the folding capacity of the ER cannot match the rate of translation it leads to a build-up of unfolded and misfolded proteins within the ER lumen. Proteins that have not been folded or misfolding of proteins leaves vacant charges within the protein structure giving it the capability to interact with structures outside its theoretical function, which can interfere with other cellular processes or aggregate together forming insoluble structures, jeopardising the integrity and survival state of the tissue [182]. Therefore mechanisms have evolved to provide an ER quality control mechanism that helps buffer out minor changes or insults to ER function or push the cell towards cell death when the integrity of the ER can no longer be recovered. This UPR homeostatic response mechanism is responsible for aiding the cell under times of mild to moderate stress and for pushing the cell towards apoptosis when severe stress prevents full recovery of the ER function [87].

To date there is major controversy about how ER stress activates cell death. Research occurring in mice has identified the activation of Caspase 12 under periods of high stress [87] indicating apoptosis as the primary mechanism. The human homologue of caspase 12, caspase 4, has not yet been linked with ER stress; however research has

suggested a role for caspase 8 [183]. The accepted route of ER stress-induced apoptosis requires cross talk between the ER and the mitochondria. Studies have shown that members of the pro apoptotic arm of the BCL-2 family reside within the ER membrane (e.g. NOXA and Bim) [184]. Upon ER stress, NOXA induction and translocation to the mitochondria occurs, setting in motion the downstream mitochondrial-induced apoptotic cascade [185, 186]. Currently the full mechanism and role of the BCL-2 family in ER stress-induced apoptosis is not fully understood but research over-expressing anti apoptotic members (e.g. BCL-2, BCL-$_{XL}$) abrogates the effect of ER stress-inducing stimuli [186]. Further studies have shown that expression of the homologous transcription factor GADD153 induced by the UPR results in the down regulation of BCL-2 under periods of severe stress [120].

1.6.1: Endoplasmic reticulum stress-inducing agents.

ER stress can be induced by any stimulus that perturbs ER function. A number of modern day chemotherapeutics induce ER stress. Two examples are fenretinide and bortezomib (Figure 1.9). Inducing cell death via cytoplasmic stress may not have the same long-term repercussions to that of targeting DNA damage to induce cell death, as components of the cytoplasm are produced from the DNA blueprint rather than copied from the existing components, as for DNA. Therefore damage to cytoplasmic components will not be passed on during replication. This factor will reduce the risk of secondary cancers as a consequence of treatment. Both agents induce ER stress by very different mechanisms of action, therefore allowing for a more thorough interpretation of the effect of ER stress.

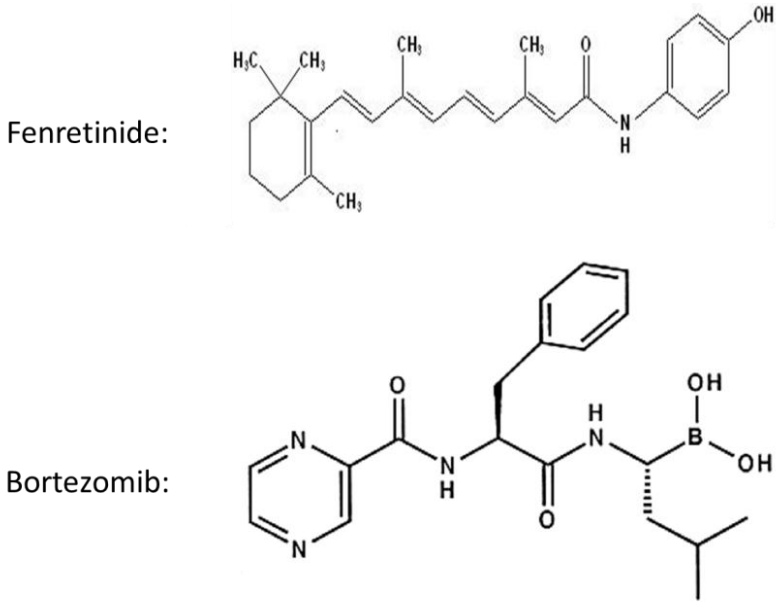

Figure 1.9: *Structural depiction of ER stress-inducing agents fenretinide and bortezomib.*

Fenretinide or 4-hydroxy (phenyl) retinamide (4-HPR) is a synthetic derivative of retinoic acid. Retinoids are substances related to vitamin A [82]. It has been investigated for potential use in the treatment of cancer, as well as in the treatment of cystic fibrosis, rheumatoid arthritis, acne, psoriasis [187]. Phase III clinical trial data have suggested that fenretinide reduces breast cancer relapse in pre-menopausal women. Common side effects associated with fenretinide treatment include skin dryness and night-blindness, which is reversible upon cessation of treatment [188]. Current chemotherapy for the treatment of neuroblastoma includes the use of 13-cis retinoic acid [189]. However tumours are often resistant or become resistant to 13-cis retinoic acid. Fenretinide has the capability to induce cell death in these resistant tumours [189]. Currently fenretinide has shown success for the treatment of minimal residual disease in neuroblastoma patients [190].

In cancer studies, Fenretinide shows weak activation of nuclear retinoic acid receptors (RARs) and treatment may cause ceramide (a wax-like substance) to build-up in tumor cells and is associated with the accumulation of reactive oxygen species (ROS), resulting in cell death through apoptosis and/or necrosis [189]. Fenretinide accumulates preferentially in fatty tissue such as the breast, which may contribute to the effectiveness of fenretinide against breast cancer [188]. Specific types of cancer under

investigation include or have included ovarian, prostate, cervical, lung, renal, bladder, breast, glioma, skin, head and neck carcinoma, non-Hodgkin's lymphoma, neuroblastoma, and Ewing's sarcoma.

Bortezomib (VELCADE®) is a dipeptydl, water soluble, boronic acid derivative that can reversibly and selectively binds the threonine residue and inhibits the 26S proteasome [191]. The 26S proteasome is important in protein degradation and vital for cancer cell survival. In particular bortezomib has been shown to have anti-tumour activity in B cell malignancies [192]. One central mechanism by which bortezomib functions in multiple myeloma is to inhibit the breakdown of inhibitory kappa B (IκB) and consequently the stabilization of the nuclear factor kappa B (NFκB) complex [193-195]. This prevents NFκB translocation to the nucleus preventing the activation of multiple downstream pathways known to be important in myeloma cell signaling [194]. However, the inhibition of the 26S proteasome also results in an accumulation of unfolded or misfolded proteins in the ER that have been tagged for degradation. This build-up results in ER stress responses that can help aid a cell or sensitize it to death stimuli.

1.7: Aims.

The central aim of the current study was to determine the relationship between GRP78 and the UPR activators PERK, IRE1 and ATF6 across neural-crest-derived cancer types and to gain a better understanding of the influence of GRP78 on ER stress-induced apoptosis. To achieve this aim, specific objectives were to:

1. Assess the basal expression of GRP78 to that of key regulators of the unfolded protein response PERK, IRE1 and ATF6 in neural-crest-derived cancer models and whether these are related to the dynamics of ER stress progression across the panel of cell lines used as cancer models.

2. Investigate the role of GRP78 as a key regulator of the unfolded protein response and the role it has in the ER stress response of neural-crest-derived tumours.

3. Assess the effect of a panel of GRP78 inhibitors for their effect on ER stress as well as the ability to enhance the efficacy of fenretinide or bortezomib.

Chapter 2:

Materials and Methods

2.1: Growth and maintenance of cancer cell lines.

CHL-1 and WM266-4 (ATCC #; CRL-9446, CRL-1676) human metastatic melanoma cells and U251 and MO59J human glioblastoma cell lines (a kind gift from Dr Gareth Veal and Prof Nicola Curtin, respectively) were cultured in high glucose (4.5 g/L) Dulbecco's Modified Eagle's Medium (DMEM; Sigma-Aldrich Co; Poole, UK) supplemented with 10% foetal calf serum (FCS; F7524, Sigma-Aldrich) (culture medium). SH-SY5Y and NGP human neuroblastoma cell lines (a kind gift from Dr June Biedler and Prof Debbie Tweddle, respectively) were cultured in Roswell Park Memorial Institute 1640 medium (RPMI-1640, Sigma-Aldrich) supplemented with 10% foetal calf serum (FCS, Sigma-Aldrich).

Melanoma cell lines were validated for B-RAF mutational status by single nucleotide polymorphism (SNP) genotyping assays for the presence of B-RAF^{V600E} or B-RAF^{V600D} genotypes. Validation of glioblastoma and neuroblastoma cancer cell lines was carried out by previous groups, before aliquots were stored in liquid nitrogen. Glioblastoma cell lines were validated by assessing the p53 mutational status and DNA-dependant protein kinase status of each cell line. Neuroblastoma cancer cell lines were validated by assessing MYCN, p53, MDM2 amplification and p14ARF deletion and methylation status of each cell line.

Normal human melanocytes were obtained from human foreskin by selective trypsinisation, confirmed by immunohistochemical staining for the melanocyte differentiation antigen Melan-A (Abcam, Cambridge, UK) and cultured in medium 254 supplemented with human melanocyte growth supplement-2 (Invitrogen Ltd; Paisley, UK).

All cells were maintained at 37°C, in a humidified atmosphere of 5% CO_2 in air. All cell lines were cultured continuously up to a maximum of 50 passages, at which point fresh cells were taken from frozen stocks in 90% FCS and 10% DMSO stored in liquid nitrogen. All immortalised cell lines were subjected to regular mycoplasma testing and were not infected.

2.2: Drug preparation and treatment regimes.

ER stress-inducing agents fenretinide (Janssen-Cilag Ltd; Switzerland) and bortezomib (Velcade; Millenium, Janssen Cilag Ltd; High Wycombe, UK) were dissolved in ethanol (for fenretinide) or dimethyl sulfoxide (DMSO, for bortezomib) and added to experimental cell cultures, along with an equal volume of vehicle used to treat control cells. In all cases the volume of vehicle control did not exceed 0.01% of the total culture volume. Bortezomib was stored at a stock concentration of 1 mM at -80^{o}C for up to 12 months; fenretinide was stored at a stock of 10 mM at -20^{o}C for up to 1 month. Concentrations of fenretinide and bortezomib used in all experiments were within the clinically achievable range or fluctuated around a central clinically-achievable dose [196, 197].

GRP78 inhibitors: Epigallocatacin gallate (EGCG, Sigma-Aldrich) and $SubAB_5$ subtilase cytotoxin were dissolved in phosphate buffered saline (PBS) or PBS containing 0.1% sodium azide). Research incorporating $SubAB_5$ was carried out in comparison to the control, proteolytic inactive, mutant of $SubAB_5$, known as $SubA_{A272}B_5$. $SubA_{A272}B_5$ contains a seine to alanine mutation within the active site at position 272. Honokiol (Sigma-Aldrich) was dissolved in DMSO (Sigma-Aldrich). All agents were added to final cultures alone or in combination with ER stress-inducing agents, with an equal volume of vehicle added to control cells. EGCG at a stock concentration of 1 mM was stored for up to 1 month at 4^{o}C prior to use. $SubAB_5$ and $SubA_{A272}B_5$ was a kind gift from James Paton [198-200]. $SubAB_5$ was stored at a stock concentration of 2 mg/ml at -20^{o}C and diluted to an intermediate 5 µg/ml stock prior to experimental use. Honokiol was dissolved to a stock concentration of 20 mM and stored at -20 ^{o}C for up to 6 months prior to use.

Standard experimental procedure for the treatment of cancer cell lines within this study was to expose cells to ER stress-inducing agents and GRP78 inhibitors for 24 hours (h) alone or in combination, before experiments were either stopped by fixation or dye added. To investigate the induction of ER stress over time, time-course experiments were carried out at 0, 1, 2, 4, 8 and 24 h time points. For experiments investigating the induction of reactive oxygen species, analyses were carried out over 0, 0.5, 1, 2, 3, 4, 5 and 6 h. For the accumulation of ubiquitin-tagged proteins, experiments were carried

out at 0, 1, 2, 4, 6, 8 and 24 h time points. The effect of combining a GRP78 inhibitor on cell line susceptibility to ER stress-induced cell death was evaluated at 6 and 12 h.

2.3: Cell viability assays.

2.3.1: MTS assay.

Cell viability was measured using a commercially-available colorimetric based metabolic assay (referred to subsequently as an MTS assay) relying on the reduction of a tetrazolium salt to a soluble formazan compound which absorbs at 490 nm. Cells were cultured in flat-bottomed 96-well tissue culture plates (Helena Biosciences; Gateshead, UK) at a density of 5000 cells per well in a final volume of 100 µl of tissue culture medium and allowed to attach overnight at 37°C, 5% CO_2 prior to treatment. Cells were subsequently treated for 24 h with drugs either as single agents or in combination with other agents at given final concentrations, in a final volume of 100 µl per well. Cell viability was assessed by the addition of 20 µl of CellTiter 96 Aqueous One Solution reagent (Promega, Southampton, UK) to each well followed by incubation at 37°C for a further 4 – 6 h prior to the measurement of absorbance at 490 nm using a FLUOstar Omega (BMG labtech, Aylesbury, UK) plate reader. In viable cells, MTS is bioreduced by dehydrogenases, resulting in the conversion of the tetrazolium compound present to a coloured formazan product.

2.3.2: Sulphorodamine B colorimetric cytotoxicity assay.

An SRB assay was used for all experiments containing EGCG as this compound is auto-fluorescent at 490 nm and interferes with the MTS assay.

Cells were cultured on flat bottomed 96-well plates (Helena Biosciences) at a density of 5000 cells per well in 100 µl of culture medium and allowed to attach overnight prior to treatment. Cells were subsequently treated for 24 h with drug or combination of drugs at given final concentrations. Cells were fixed by initially aspirating all media from the plates, followed by addition of 200 µl of cold PBS and 50 µl of cold 50% trichloroacetic acid (TCA, Sigma-Aldrich). After incubation at 4°C for 1 h, plates were washed and stored at 4°C prior to staining. 100 µl of SRB stain was added to each well followed by

incubation room temperature for 30 minutes (min). Excess dye was removed by rinsing 5 times with 1% acetic acid (VWR; Lutterworth, UK). Rinsing was performed quickly but gently to avoid dislodging cells and prevent desorption of the protein-bound dye. Stained plates were air-dried overnight before addition of 10 mM Tris to solubilise the dye. Absorbance at 520 nm was measured using a FLUOstar Omega (BMG labtech) plate reader.

2.4: Flow cytometry

2.4.1: Flow cytometry of propidium iodide stained cells

After confirmation of apoptosis in response to fenretinide, bortezomib by flow cytometry of annexin V stained cells, all subsequent experiments to measure apoptosis were performed by flow cytometry of fixed, propidium iodide-stained cells [201]. Cancer cells were seeded in flat bottomed 6-well plates (Corning, Sigma-Aldrich) at 1.5 x 10^5 cells per well for CHL-1 cells, or 2.0 x 10^5 cells per well for U251, MO59J, SH-SY5Y and NGP cells or 2.5 x 10^5 cells per well for WM266-4 cells in a final volume of 3 ml of relevant culture medium and allowed to attach overnight at 37^{o}C. Cells were then treated with ER stress-inducing agents or GRP78 inhibitors alone or in combination for 24 h or a time course ranging over 24 h. After treatment, both cells and supernatant were harvested by trypsinization as previously described [202, 203]. Cells were pelleted by centrifugation at 330 x g (1200 revolutions per minute (RPM), mistral 3000i centrifuge, MSE, London, UK) for 5 min at 4^{o}C and washed twice in PBS. The pellet was then resuspended in 500 µl PBS and transferred to a 5 ml round-bottom test tube (Becton Dickenson (BD) Biosciences, Oxford, UK) before being fixed with an equal volume of cold methanol: acetone (4:1) solution, before storage at 4^{o}C for up to 1 week prior to analysis.

To prepare samples for flow cytometry, cells were washed once with PBS and cells pelleted by centrifugation. Supernatant was aspirated before treatment with 100 µl RNase A (0.155 µg/ml in PBS; Sigma-Aldrich) for 20 min at 37^{o}C. Finally, cells were stained by the addition of 300 µl of propidium iodide (PI; 100 µg/ml in PBS; Sigma-Aldrich) and incubation continued for a further 25 min. Data were collected, using CellQuest version 3.3 software, with either a FACScan or FACScalibur flow cytometer

(BD immunocytometry systems, Oxford, UK) by recording the percentage of cells with hypodiploid DNA (sub-G1 peak) as a measure of cell death. Events were collected using a gated amplifier for FL2 (wavelength (λ) 625 nm), corresponding to emissions from PI and a signal threshold was applied for forward and side scatter to exclude debris. Double nuclei and aggregates were excluded by gating a plot of FL2-A (area) against FL2-W (width). Data were analysed using either WinMDI 2.8 for flow cytometry (Bio-soft.net) or Cyflogic 1.2.1 (Cyflogic, Turku, Finland).

2.4.2: Flow cytometry for the induction of Reactive Oxygen Species.

Cancer cells were seeded in flat bottomed 6-well plates at 1.5 x 10^5 cells per well for CHL-1, cells or 2.0 x 10^5 cells per well for U251, MO59J, SH-SY5Y and NGP cells or 2.5 x 10^5 cells per well for WM266-4 cells in a final volume of 3 ml of preferred culture medium and allowed to attach overnight at 37^{o}C. Cells were then treated with ER stress-inducing agents over a time course of 6 h. Experiments were designed in such a way that the drug was added at differing times during the experiment, to allow all samples to reach their designated time point at the same time. After treatment the supernatant was removed and cells were washed twice in PBS before the cells were harvested by trypsinisation. Samples were pelleted by centrifugation at 330 x g for 5 min prior to resuspension in 500 µl of 5 µM of 5-(and-6)-Carboxy-2',7'-Dichlorofluorescein Diacetate (DCFDA, Sigma-Aldrich) and samples incubated at 37°C for 15 min. Samples were then washed twice in ice cold PBS by centrifugation at 330 x g to pellet cells and stored on ice prior to analysis by flow cytometry. All experiments were carried out with negative controls of unstained cells and working dye solution alone, as well as positive controls of cells treated with hydrogen peroxide at 25 µM and 50 µM for 6 h (H_2O_2, Sigma-Aldrich).

Data were collected, using CellQuest version 3.3 software, with either a FACScan or FACScalibor flow cytometer (BD Immunocytometry systems). Events were collected using a gated amplifier for FL1 (λ 530/30 nm), corresponding to emissions from fluorescein and a signal threshold was applied for forward and side scatter to exclude debris. Data were analysed using Cyflogic 1.2.1 (Cyflogic) for FL-1 peak area.

2.5: Western blotting

2.5.1: Western blot analysis for relative protein expressions.

Proteins from cultured cells were extracted from cell pellets using 200 µl of cell lysis buffer (0.1 M Tris-Hcl, pH 7.4, 0.1 M NaCl, 25 mM NaF, 1 mM benzamidine, 2 mM EDTA, 0.1 mM sodium orthovanadate, 0.1% Triton-X100, EDTA-free protease inhibitor cocktail) per well of a 6-well plate [184]. Cell lysates were incubated on ice for 30 min and then probe sonicated for 2 pulses, each for 5 seconds with a sonicator (Soniprep150, MSE, UK) set to 7 microns amplitude. Quantification of protein concentration was performed using Bradford assay reagent (Pierce Biotech., Rockford, IL, USA) in a 96-well plate (Helena Biosciences) in comparison to a bovine serum albumin (BSA) standard curve of 0 – 6 mg/ml and absorbance measured at 595 nm using a FLUOstar Omega plate reader (BMG labtech).

The mini-Protean tetra electrophoresis system (Bio-Rad laboratories; Hemel Hempstead, UK) was used to separate proteins by electrophoresis through a 4-20% mini-Protean Tris-glycine gel (Bio-Rad laboratories) with Tris-glycine running buffer (250 mM Tris base and 1.9 M glycine (Sigma-Aldrich) containing 1% SDS (Fisher Scientific; Loughborough, UK)). The gels were subsequently blotted onto immune-Blot polyvinylidene fluoride (PVDF) transfer membrane (Bio-Rad laboratories) using Tris-glycine buffer containing 20% methanol (Fisher Scientific; Loughborough, UK) and 0.1% SDS (Fisher Scientific). Blots were then washed in 5% non-fat milk for 1 h to block exposed hydrophobic sites and then subsequently probed with antibodies, diluted in 5% non-fat milk (TBS/T) to relevant concentration (Table 2.1), for either 1 h at room temperature or 4 ^{o}C overnight. Membranes to be probed with antibodies for phosphorylated proteins were blocked and antibodies diluted in 5% BSA (TBS/T).

Antibody	Band size (~kDa)	Company	Dilution
GRP78 C-Terminus	78	Santa Cruz	1:1000
GRP78 N-Terminus	78	Santa Cruz	1:1000
PERK	125	Santa Cruz	1:2000
IRE-1 α	110	Santa Cruz	1:2000
ATF6 α	90	Santa Cruz	1:500
ATF4	39	Santa Cruz	1:500
Gadd153	30	Santa Cruz	1:1000
NOXA	11	Cell Signalling	1:500
Phospho-eIF2 α	36	Cell Signalling	1:1000
Cleaved Caspase 3	17, 19	Cell Signalling	1:500
Ubiquitin	8.5*	Cell Signalling	1:1000
Actin	42	Sigma-Aldrich	1:5000

Table 2.1: *Primary antibody information for western blot analysis. List of all primary antibodies used and the relevant company and experimental information required. (* - In the case of ubiquitin, a band was detected at approximately 8.5 kDa but also a smear of ubiquitin-tagged proteins was detected across the gel with increased ER stress).*

To detect primary antibody binding, blots were incubated with horseradish peroxidase-conjugated secondary antibodies (Upstate Biotechnology, Boston, USA; diluted 1:2000) and visualized using the ECL-plus system (Amersham Biosciences, Little Chalfont, UK) and imaged using a Fujifilm FLA-3000 fluorescence imager (Raytek Scientific Ltd, Sheffield, UK). Densitometric quantification of signal intensity was performed using Aida Image Analyser version 3.28 software and quantified relative to a loading control to correct for loading error.

2.5.2: Western blot analysis for cellular protein expression.

Cellular lysates were formed using a Vi-Cell counter (Beckman Coulter, Dunstable, UK) to determine cell counts and allow for lysates to be generated containing 100 000 cells per 10 µl of lysis buffer (buffer same as previously described). Proteins were then separated using the same protocol as for relative protein expression, except for the addition of a purified protein standard curve present on all gels for the protein of interest. Protein standards were as follows: Full length GRP78 (His-tagged protein, a kind gift from Prof AR Hawkins (Newcastle University, UK). Purified protein fragments for PERK (Myc-tagged protein fragment corresponding to amino acids 1-581, 66.1 kDa, a kind gift from Prof AR Hawkins, Newcastle University, UK), IRE1 (proprietary-tagged protein fragment corresponding to amino acids 401-500, 36.6 kDa; Abcam), ATF6 (His-tagged protein that corresponds to amino acids 567-670, 25 kDa; Abcam) and ATF4 (His-tagged protein corresponds to amino acids 123-351, 26 kDa; Abcam) were all used at the range of 10 µM – 1 nM.

For detection, all antibodies were used as previously described and detected using the ECL plus system and imaged using a Fujifilm FLA-3000 fluorescence imager to ensure linear absorption (Raytek Scientific Ltd). Densitometry quantification of signal intensity was performed using Aida Image Analyser version 3.28 software and analysed by reverse prediction modelling using ChemCal, a statistical computer package for R 2.14.1. Cell and nuclear diameters were determined using a micrometer stage for comparison to light microscopy (cell) or 4',6-diamidino-2-phenylindole (DAPI) stained (nuclear) confocal microscopy images of detached spherical cells. Volumes were determined accordingly and the nuclear volume subtracted.

2.6: Small interfering RNA (SiRNA)-mediated knockdown of GRP78 expression using oligonucleotides.

Silencing-mediated knockdown of target genes was performed using transfection of siRNA purchased from Qiagen (Crawley, UK). Occasionally non-specific effects will be triggered by experimental introduction of siRNA, however, all experiments looking for the effect of siRNAs on GRP78 expression were carried out alongside control

transfections with a scrambled siRNA as control. The control scrambled used in all experiments was also from Qiagen.

Qiagen siRNA oligomers were supplied as annealed, lyophilised powders requiring re-suspension in the supplied buffer. Each siRNA was pre-designed and validated to target a specific 21 nucleotide sequence (Table 2.2; Qiagen, Crawley, UK). Prior to use, siRNA from either source was heated to 90^{o}C for 1 min followed by incubation at 37^{o}C for 60 min to disrupt higher aggregates and maximise silencing potential.

Human cancer cells were seeded overnight in a volume of 3 ml of appropriate culture medium in 6 well plates to achieve a desired cell density of 70-90%, corresponding approximately to 0.25 x 10^6 cells per well for CHL-1, WM266-4, MO59J cells and 0.3 x 10^6 cells per well for NGP and SH-SY5Y neuroblastoma cell lines. Cells were gently washed in PBS and siRNA was transiently transfected using lipofectamine 2000 according to the manufacturers' specification for 8 h in 2.0 ml serum-free Opti-MEM growth medium (Invitrogen Ltd) to given final concentrations of 40 nM. Opti-MEM was replaced with 3.0 ml complete culture medium and incubation was continued overnight before transfection was repeated. Knockdown of the target gene was verified by Western blot analysis 24 h after the second transfection had ceased or subsequent cell viability and death assays were performed.

Qiagen	Sense Sequence	Antisense Sequence
Control	UUCUCCGAACGUGUCACGUdTdT	ACGUGACACGUUCGGAGAAdTdT
GRP78	GGGUGUGUGUUCACCUUCAdTdT	UGAAGGUGAACACACACCCdTdA

Table 2.2: *Target sequences for siRNA to GRP78 as well as the scrambled control (Qiagen). Annealed double-stranded siRNA was introduced into cells using lipofectamine 2000-mediated transfection.*

2.7: Reverse transcriptase Polymerase chain reaction

2.7.1: RNA extraction and purification.

Total RNA was extracted from cells using RNeasy Kit (Qiagen). Cells were washed with PBS and treated with 1 x Trypsin-EDTA (Sigma-Aldrich) to detach them from culture plate. Cells were then pelleted by centrifugation at 330 x g for 5 min. Supernatant was aspirated from pellets prior to washing with PBS and again pelleted by additional centrifugation. Supernatant was removed and 500 µl RLT cell lysis buffer (part of RNeasy kit), containing 10% β-mercaptoethanol, was added to the pellet and the suspension was and samples transferred to a microfuge tubes. Samples were sonicated for 30 seconds (s) and before addition of an equal volume of 70 % ethanol was added (diluted to 70% in RNase free water) and vigorous mixing by vortex. The sample was added to a mini-column (provided within RNeasy kit), placed within a mini collection tube (also provided) and centrifuged at 900 x g (10 000 rpm) for 15 s to collect the eluate. The eluate was discarded and column transferred to a new mini collection tube. 500 µl of RPE wash buffer wash containing 80% ethanol (part of RNeasy kit) wash added to the column and centrifuged at 900 x g for 15 s. The eluate was again discarded and another 500 µl RPE wash buffer to the column prior to centrifugation at 900 x g for 2 min. Again the eluate was discarded and 50 µl of RNase free water was added to the column. Finally the column was placed in a fresh eppendorf tube and centrifuged at 900 x g for 1 min.

Total RNA was collected and stored at -80°C for up to 1 year. The RNA concentration was determined using the NanoDrop ND-1000 spectrophotometer (NanoDrop Technologies, Wilmington, USA). RNA concentration for 1 µl of each sample was determined from an absorbance reading at 260 nm. RNA quality was determined by the ratio of 260:280 nm readings and should be between 0.9 and 2.1.

2.7.2: Generation of cDNA.

RNA was reverse transcribed to cDNA using the superscript reverse transcripase method. 0.5 µg RNA was combined with 0.5 µg random oligo DT primers (Fermentas, St. Leon-Rot, Germany), 0.5 mM mixed of Deoxynucleotides (dNTPs; Fermentas), and RNase free water (Fermentas) to a final volume of 20 µl. The solution was incubated at 65°C for 5 min followed by 1 min on ice. To the solution add 4 µl first strand buffer (Fermentas), 1 µl 0.1 M DTT (Fermentas), 1 µl RNase Inhibitor (Fermentas) and 1 µl Superscript Reverse Transcriptase (Fermentas) and the solution incubated at 55°C for 60 min prior to 70°C for 15 min to inactivate the reaction. To the solution, 0.5 µl RNase H (of 5U/µl stock; Fermentas) was then added before further incubation for 20 min at 37°C. The sample reaction was then inactivated by a further incubation of 10 min at 65°C and cDNA stored at -20°C for up to 1 month.

2.7.3: Quantitative Polymerase chain reaction.

The cDNA from the reverse transcription was used in a real-time PCR reaction. Real-time PCR reactions were carried out in 96 well plates in a final volume of 20 µl final per well. Primer probe sets for GRP78, XBP-1, XBP-1 spliced form (XBP-1 (S)) and β-Actin (control) were all purchased from Sigma-Aldrich Co consisting of two unlabelled PCR primers per target (Table 2.3). A 2 x concentration of fast SYBR green master mix containing AmpliTaq fast DNA polymerase, SYBR Green-1 dye and deoxyneucleotide triphosphate (dNTPs) were purchased from Applied Biosystems (Carlsbad, California, USA). Master mixes containing diluted primer-probes and the SYBR Green master mix were produced for the number of reactions/well and this primer probe master mix was aliquoted into each well individually. The 2 x fast SYBR green master mix was diluted to a final 1 x concentration in each well. The real-time PCR plate was set-up in such a way that each sample was used in triplicate reactions for all primer sets. The plate was loaded into a 7500 fast real-time PCR machine with SDS software (Applied Biosystems) and subjected to specific thermocycling programs (Table 2.4). The PCR machine consisted of an argon laser that distributes light to the plate and CCD camera to detect emitted fluorescence between 500 and 600 nm wavelengths. Because SYBR Green can bind to any double stranded DNA, to confirm that only the desired PCR product has been amplified, melting curve analysis was performed. Melt curve analysis heats the

PCR reaction and measures a change in fluorescence as double stranded DNA dissociates.

2.7.4: Quantitative Polymerase chain reaction analysis.

Data obtained from the real time PCR machine were analysed using SDS2.2 software (Applied Biosystems). Amplification plots were generated for each well where magnitude was plotted against cycle number. The threshold level of expression was set to a value on the exponential phase of the amplification plot and was kept the same for all related primer-probe experiments. The number of PCR cycles taken to reach the threshold level of expression (Ct) for each sample was generated as mean ± 95% confidence intervals (CI). All mean Ct values for all investigative primer/probes were normalised to the β-Actin control data. Data were then normalised to the vehicle treated control samples. Data were statistically analysed using SPSS 17.0 and graphs plotted in SigmaPlot 11.0 or GraphPad Prism 5.

Target	Forward	Reverse
XBP-1	CCT TGT AGT TGA GAA CCA GG	GGG CTT GGT ATA TAT GTG G
XBP-1 (s)	GGT CTG CTG AGT CCG CAG CAG G	GGGCTTGGTATATATGTGG
GRP78	GTT CTT GCC GTT CAA GGT GG	TGG TAC AGT AAC AAC TGC ATG
β-Actin	AAT CTG GCA CCA CAC CTT CTA CA	CGA CGT AGC ACA GCT TCT CCT TA

Table 2.3: *Primer sequences for XBP-1, XBP-1(s), GRP78 and control β-Actin.*

Gene	Stage 1	Stage 2 (50 cycles)	Stage 3	Stage 4
GRP78	95°C–10 min	95°C – 15 sec 60°C – 1 min	95°C – 30 sec 60°C – 1 min	Melt Curve
XBP-1	95°C – 5 min	95°C – 30 sec 55°C – 30 sec 72°C – 30 sec	95°C – 30 sec 60°C – 1 min	
XBP-1 (s)	95°C – 5 min	95°C – 30 sec 55°C – 30 sec 72°C – 30 sec	95°C – 30 sec 60°C – 1 min	
Actin	95°C – 10 min	95°C – 15 sec 60°C – 45 sec 72°C – 30 sec	95°C – 30 sec 60°C – 1 min	

Table 2.4: *Thermocycling programs for XBP-1, XBP-1(s), GRP78 and control β-Actin.*

2.8: Immunofluorescent staining of cell line cultures.

Cancer cell lines were seeded into flat bottomed 6 well plates containing a sterile glass cover slip (18mm x 18mm, Fischer Scientific). Cells were seeded at 1.5 x 10^5 cells per well for CHL-1, cells or 2.0 x 10^5 cells per well for U251, MO59J, SH-SY5Y and NGP cells or 2.5 x 10^5 cells per well for WM266-4 cells in a final volume of 3 ml of preferred culture medium and allowed to attach overnight at 37^{o}C. For localisation experiments, cells were fixed after 24 h. For the effect of drug treatment on protein expression or localisation, cells were treated with ER stress-inducing agents for 24 h prior to fixation. Cells were fixed in either 100% ice cold methanol (Fisher) for 30 min or 4% paraformaldehyde (PFA; Sigma-Aldrich) for 20 min, before storage at 4 ^{o}C in PBS.

For staining, cells were washed in PBS containing 0.05% Tween 20 (PBS/T; Sigma-Aldrich) and then permeabilised in 0.2% Triton X100 (Sigma-Aldrich, diluted in PBS/T) for 30 min. Cells were then washed 3 times in PBS/T and then blocked by the addition of 2% bovine serum albumin (BSA, dissolved in PBS/T) and incubated for 1 h on a

platform shaker. After blocking, samples were again washed 3 times in PBS/T and then incubated with primary antibody, dissolved in 0.2% BSA-PBS/T for 1 h at room temperature (primary antibody dilutions described in table 2.5). Samples were then washed 3 times in PBS/T, followed by blocking in 10% secondary host-antibody-specific serum (dissolved in PBS/T, Serums described in Table 2.5) for a minimum of 30 min before samples were incubated in fluorescently-labelled secondary antibodies diluted in 1% host-specific serum for 1 h in the dark, at room temperature on a platform shaker (Secondary antibody information described in table 2.5). Again, samples were washed 3 times in PBS/T and then incubated with control nuclear stain DAPI (Sigma-Aldrich, diluted in PBS/T) for 25 min in the dark, at room temperature.

Antibody	Company	Dilution	Fixative	Host	Blocking agent
GRP78	Santa Cruz	1:500	Methanol	Goat	BSA
IRE1	Santa Cruz	1:500	Methanol	Rabbit	BSA
Cleaved Casp 3	Cell Signalling	1:500	4% PFA	Rabbit	BSA
Calnexin	Abcam	1:500	4% PFA	Rabbit	BSA
DAPI	Sigma-Aldrich	1:2000	either	-	-
AlexaFluor 488	Invitrogen	1:1000	-	Donkey	Donkey
Alexa Fluor 594	Invitrogen	1:1000	-	Donkey	Donkey
Alexa Fluor 594	Invitrogen	1:1000	-	Sheep	Sheep

Table 2.5: *Antibody information for the immunostaining of fixed culture cells.*

The cover slip containing stained cells was then carefully removed from each well of a 6 well plate and placed cell side down onto a glass slide (Fischer Scientific) with 5 µl of vector shield mounting medium (Vector Laboratories LTD, Peterborough, UK). Samples were then stored at 4^{o}C in the dark and imaged within 24 h using a Zeiss LSM 700 confocal inverted scanning microscope using Zen 2009 software (Zeiss, Hertfordshire, UK). All images were taken using an x48 objective with averaging of 4 and a frame size of 1024 x 1024 pixels. The microscope consists of a 405, 488 and 530 nm lasers and the appropriate laser was used for each fluorochrome throughout this

study. Each experiment included a negative control of unstained cells, as well as secondary antibody only to investigate non-specific binding. Laser power was optimised on control- stained cells and remained the same throughout each individual experiment.

Colocalisation can be explained as the existence of two or more signals from the same pixel location. Although observation of colocalisation of multiple antigens does not provide direct proof of a functional relationship, it does highlight to researches a structural and function characteristic. Colocalisation is estimated using specifically developed algorithms which calculate a number of representative coefficients, containing different sensitivity and applicability. Data were analysed using the Zeiss software: Zen 2009 (Zeiss).

2.9: Over-expression of GRP78 in a panel of neuroectodermal derived cancer cell lines.

2.9.1: Plasmid amplification and purification.

2.9.1.1: Bacterial transformation.

Plasmid DNA was amplified by transformation into JM109 competent E-coli. JM109 competent cells were thawed on ice prior to use. All DNA plasmids contained an antibiotic resistance gene for ampicillin. 100 ng of pcDNA3.1 (+) GRP78 or the control plasmid pcDNA3.0 were diluted to a volume of 30 µl in Luria Bertani broth (LB broth; 10 g tryptone, 5 g yeast and 5 g NaCl in 1 L distilled water; Sigma-Aldrich) and added to 70 µl of competent JM109 cells. Cells were then incubated on ice for 20 min prior to heat shock at 42°C for 30 s. 400 µl of LB broth was then added and incubation continued at 37°C for 30 min. The cells were then pelleted by centrifugation at 2250 x g (5000 rpm) for 5 min before resuspension in 100 µl of LB broth. To select for transformed bacterial cells that had taken up the desired plasmid DNA and therefore expressed the relevant antibiotic resistance, the transformed samples were plated onto agar plates (10 g tryptone, 5 g yeast, 5 g NaCl and 15 g agar in 1 L distilled water; Sigma-Aldrich) containing 50 µg/ml ampicillin (Sigma-Aldrich) and incubated over night at 37°C. All transformations were carried out alongside a negative control, which consisted of competent bacterial cells alone. Large, isolated colonies were then picked

and amplified in 5 ml LB broth containing the appropriate antibiotics by overnight incubation in an orbital incubator (225 rpm) at 37°C.

2.9.1.2: Plasmid purification from bacteria.

Bacterial cultures were aliquoted into microfuge tubes and pelleted by centrifugation at 15 000 x g (13 000 rpm) for 1 min. The supernatant was removed and 100 µl of ice-cold solution 1 (50 mM glucose, 25 mM Tris-HCL (pH 8.0), 10 mM EDTA (pH 8.0) added and samples vortexed and incubated on ice for 5 min. 200 µl of fresh solution 2 (200 mM NaOH containing 10% SDS; Sigma-Aldrich) was subsequently added and samples mixed by inversion (but not vortexed) prior to incubation on ice for a further 5 min. Finaly, 200 µl of solution 3 (2.5 M potassium acetate containing 10% glacial acetic acid) was added and the samples vortexed prior to centrifugation at 11 000 x g (11 000 rpm) for 30 sec. The plasmid DNA-containing supernatant was transferred to a fresh microfuge tube containing 500 µl phenol : chloroform (1:1; Sigma-Aldrich) and samples again vortexed prior to centrifugation at 11 000 x g at 4°C for 2 min. The supernatant was then transferred to a new tube and 1 ml ethanol was added before incubation for 2 min and centrifugation at 11 000 x g at 4°C for a further 5 min and the supernatant discarded. The plasmid DNA pellet was then washed in 1 ml ice cold 70% ethanol prior to centrifugation at 11 000 x g at 4°C for 5 min. Plasmid DNA was then air dried and finally resuspended in 25 µl sterile distilled water and stored at -20°C.

2.9.2: Plasmid concentration.

The concentration of DNA per sample was determined using a NanoDrop spectrophotometer (The NanoDrop ND-1000 form NanoDrop technologies, Wilmington, USA). The NanoDrop requires 1 µl of sample to be loaded and concentration is calculated. The machine was blanked against sterile distilled water. The concentration of DNA was determined for the absorbance reading of each sample measured at a wavelength of 260 nm.

2.9.3: Plasmid confirmation by restriction digests.

Single and double restriction digests were set up and incubated for either 1 h (final reaction volume 20 µl) or overnight (final reaction volume 50 µl) at 37 °C. Single and double digests used 1-2 µg of DNA, 0.5 Units of restriction enzyme and 1 x restriction digest buffer (restriction enzyme specific or universal buffer). Some restriction enzymes also required 1 x BSA in the restriction digest reaction. All restriction enzymes, 10 x Restriction digest buffers and 10 x BSA were purchased from New England Biolabs (New England Biolab, NEB; Hitchin, UK, Table 2.6).

Enzyme	**NEB Buffer**	**BSA**	**Activity of Enzymes in Selected Buffer**
Hind III	2	-	100% activity
XhoI	2	BSA	100% activity
Hind III + XhoI	2	BSA	100% activity

Table 2.6: *Enzyme information for restriction digests.*

2.9.4: Gel electrophoresis.

Electrophoresis through 1 % agarose was used to visualise and check the size of the DNA and to separate DNA plasmids and fragments after restriction digest. Agarose solutions were prepared by dissolving the electrophoresis-grade agarose (Invitrogen Ltd, Paisley, UK) in 1 x Tris-Borate/EDTA (TBE) solution (10 x TBE stock: 54 g Tris-Base, 27.5 g Boric acid, 20 ml 0.5 M EDTA pH 8.0 made up to 1 litre with double de-ionized water; final pH 8.3). The suspensions were boiled, using an 800 Watt microwave set at high-power, in a 500 ml glass beaker for 3 min or until the agarose had completely dissolved. The liquid was allowed to cool to approximately 60 °C and ethidium bromide added to a final concentration of 0.5 µg/ml. The mixture was poured onto a gel plate containing a well comb and allowed to set at room temp for approximately 20 min. The set gel was placed in an electrophoresis tank and the tank filled with 1 x TBE buffer

until the gel was submerged. An aliquot of each DNA sample was prepared by the addition of 6 x loading buffer (0.25% Bromophenol blue, 0.25% xylene cyanol FF, 30% glycerol in water) so that the total volume did not exceed 25 µl and the loading buffer was diluted to 1 x. Samples were loaded into separate wells. Gene Ruler 1 kb DNA molecular weight marker (Band sizes: 500-10 000 bp; Roche Diagnostics, Burgess Hill, UK) was used as a reference size marker. Electrophoresis was carried out at 100 V for 1 h at room temperature for the 1% agarose gels. DNA bands were visualised using a UV light source.

2.10: Stable over expression of pcDNA3.1 (+) GRP78.

DNA constructs pcDNA3.0 (a kind gift from Professor Olaf Heidenreich) and pcDNA3.1 (+) GRP78 (a kind gift from Dr Randal Kaufman) were transfected into melanoma, glioblastoma and neuroblastoma cell lines. Transfected cells were selected by antibiotic selection and expanded into mixed cell clones. PcDNA3.0 and pcDNA3.1 (+) GRP78 constructs both contain a mammalian resistance gene for neomycin. Neomycin resistance is conferred by utilizing the bacterial gene encoding the enzyme aminoglycoside 3' phosphor-transferase (APH). Two distinct APH enzymes, encoded by the bacterial transposons Tn5 and Tn601, confer resistance to aminoglycoside antibiotics such as Kanamycin, Neomycin and Geneticin (G418), which inhibit protein synthesis in both prokaryotic and eukaryotic cells. For selection of positive constructs geneticin (G418; Invitrogen, Paisley, UK) was used at a final concentration of 1500 - 2000 µg/ml. For experiments, G418 selection was removed from the cells 3 days prior to use.

2.10.1: Transfection of DNA constructs.

Melanoma, glioblastoma and neuroblastoma cancer cell lines were seeded in flat-bottomed 6-well plates at 2.5 x 10^5 cells per well for CHL-1, cells or 3.0 x 10^5 cells per well for U251, MO59J, SH-SY5Y, NGP and WM266-4 cells in a final volume of 3 ml of relevant culture medium and allowed to attach overnight at 37°C. 4 µg of DNA (in approx. 8 µl) and 12 µl of Lipofectamine 2000 transfection reagent (Invitrogen) were mixed in separate tubes with 500 µl serum-free OptiMEM media (Invitrogen Ltd). The contents of both tubes were mixed together at room temperature for 15 min on the roller.

The DNA-Lipofectamine transfection mix was diluted by adding 1.5 ml serum-free OptiMEM media. Culture medium was removed from the cells seeded into the 6 well dishes and they were washed carefully with serum-free OptiMEM media. The 2 ml transfection mix was added to the cells and incubated for 24 h at 37°C. After 24 h the medium on the cells was replaced with 3 ml of preferred culture medium containing 10% FBS and 2mM L-glutamine, and incubated for 48 h at 37°C before commencing antibiotic selection of transfected cells.

2.10.2: Antibiotic selection of transfected cells.

Dose-response experiments were carried out on non-transfected cells to determine the optimal dose of G418 for selection of cells transfected with pcDNA3.0 or pcDNA3.1 (+) GRP78. For the treatment of melanoma and glioblastoma cells, 2000 µg/ml G418 was required while 1500 µg/ml was used to select neuroblastoma cells. Transfected cells were maintained under G418 selection, except during experimentation where cells were placed in normal culture media for a minimum of 3 days prior to the start of each experiment. Over-expression of GRP78 was confirmed by both quantitative real time PCR and Western blot analysis for mRNA and protein expression, respectively.

2.11: Statistics

Results were expressed as the mean of individual experiments +/- the 95% confidence intervals (95% CI) using Prism 5 (GraphPad Software Inc; La Jolla, CA, USA) or Sigma Plot 11 (Systat Software Inc; San Jose, CA, USA) software. The statistical significance of drug responses was compared by one- or two-way ANOVA with either Dunnett's, Bonferroni's or Tukey's post-hoc tests using Prism 5 or SPSS release 17.0 (IBM; Chicago, IL, USA) software. To analyse the synergistic effects of fenretinide and bortezomib alone or in combination with GRP78 inhibitors on induction of cell apoptosis or inhibition of cell viability, combination indices were generated using CalcuSyn software (Biosoft) as previously described [204]. Combination index (or indices (ci)) values obtained for the effect of drug interaction for either cell death or inhibition of cell viability are characterised as: ci > 1 are Inhibitory, ci = 1 are additive and ci < 1 are synergistic. In this study values were characterised as synergistic if the ci < 0.9 and inhibitory if the ci > 1.1.

The combination index data were ranked and these ranked data analysed using R, initially with linear models to test for the effect of drug dose (not significant; $P > 0.05$) and then by nested ANOVA (cell line nested within cell type); pairwise comparisons of mean combination indices by cell line or cell type (depending on the results from the nested ANOVA) were carried out using Tukeys HSD after one-way ANOVA. Q-Q plots were used to assess the fit of residuals from the models

To quantify protein expression in comparison to a specific protein standard curve, ChemCal for inverse prediction was carried out using R 2.14.1 [205]. Interpretation of dose response curves for EC_{50} and asymptote were carried out using R. For cell death work drc package with R was used. However, for viability drc was used to fit curves to data and extract parameters for further analysis by t-test or ANOVA. To determine the correlation between GRP78 expression and ROS, Pearson's correlation was carried out using R.

Chapter 3:

The effect of ER stress on the Unfolded Protein Response

3.1: Introduction.

The ER is the primary site for protein synthesis, folding and trafficking and therefore an essential organelle of all eukaryotic cells [206]. Due to the importance of protein synthesis, the ER has established a complex and diverse homeostatic response mechanism to stimuli that hinder the productivity and quality of the ERs protein synthesis capacity (ER stress). The UPR is an evolutionary conserved and adaptive response mechanism to stress [207]. Mammals have preserved the basic components of the yeast UPR and then greatly developed it to manage the stress of a multi-cellular organism [208]. The mammalian UPR consists of three response activators; PERK, IRE1 and ATF6 that are held inactive by the UPR stress regulator GRP78 [168, 209, 210]. GRP78 is a molecular chaperone which serves as a holdase of newly synthesised or mis-folded proteins within the lumen of the ER, resulting in optimal orientation of substrates for folding machinery [211].

GRP78 possesses high affinity for hydrophobic or hydrophilic regions exposed on the surface of unfolded or mis-folded protein substrates. On interaction with a substrate; PERK, IRE1 and ATF6 dissociate from GRP78 (Figure 3.1) [209, 210]. These free UPR activators no longer have critical sequences masked by their interaction with GRP78 and therefore are capable of activation. For ATF6 the dissociation from GRP78 unmasks Golgi localisation sequences that result in its migration and the eventual processing of ATF6 by S1P and S2P proteases to form an active transcription factor that is capable of translocation to the nucleus. In the case of PERK and IRE1 the dissociation from GRP78 allows both proteins to undergo homo-dimerization and auto-phosphorylation to form active kinases, and in the case of IRE1 the formation of an active endoribonuclease [91, 111, 212].

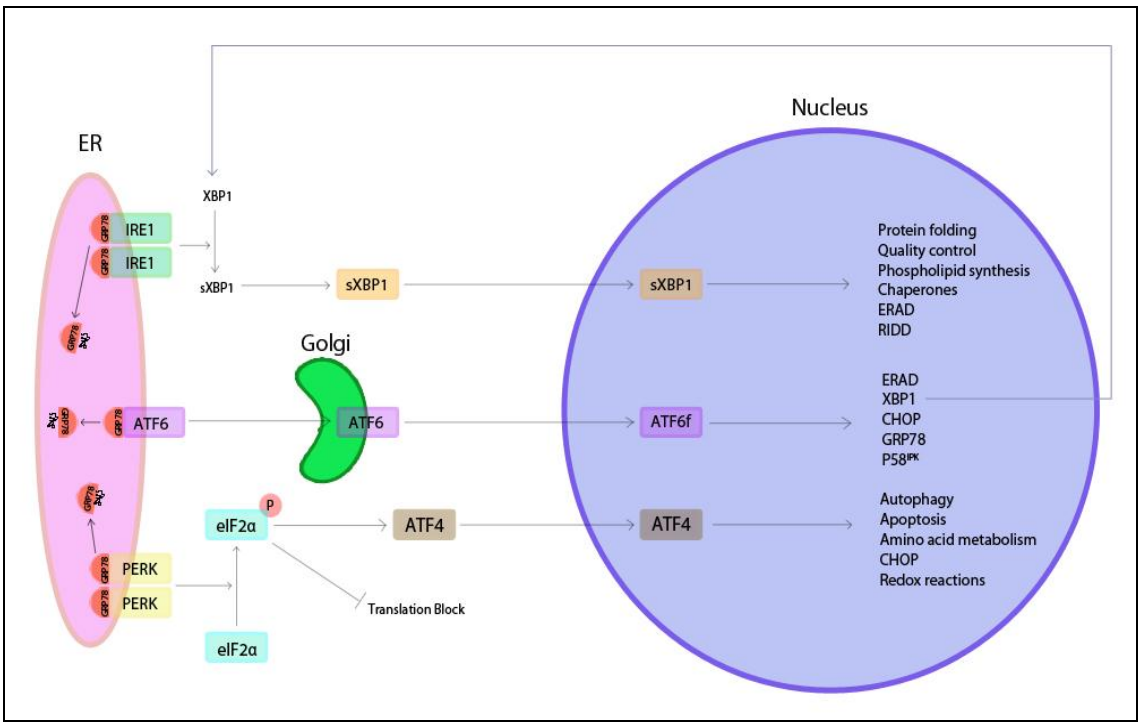

Figure 3.1: *The unfolded protein response. Schematic representation of the ER based homeostatic response mechanism to stress. Under periods of no stress, GRP78 binds to and inactivates PERK, IRE1 and ATF6. When cellular stress disrupts the homeostasis of the ER resulting in an increase in unfolded or mis-folded proteins in the lumen of the ER (ER stress), GRP78 binds to these substrates, simultaneously releasing PERK, IRE1 or ATF6. Upon release these proteins result in the activation of three diverse cascades which alter ER functioning to try to save the cell. However, if the stress is to severe or persists for too long, cell death pathways are activated to remove the cell [213].*

The activation of PERK into a functional kinase results in the phosphorylation of downstream eIF2α [214]. This act results in the inhibition of conventional protein synthesis by preventing the exchange of GTP for GDP, as well as blocking the recruitment of methionine tRNA [215] . However, via a non-conventional open reading frame, known as an internal ribosomal entry site (IRES), proteins capable of aiding a cells recovery from ER stress can still be translated. These proteins include chaperones such as GRP78 and GRP94, as well as the transcription factor ATF4 [91]. The induction of ATF4 translation helps to alleviated stress present upon the ER by two main mechanisms; stimulation of Nrf2 to increase amino acid recovery, and the activation of genes that have ERSE and UPRE response elements within their promoter sequences [216, 217]. These genes include chaperones and folding machinery such as the PDI

superfamily. A protein family important for the addition and removal of disulphide bonds during protein synthesis. The activation of IRE1, results in the formation of a functional endoribonuclease domain that processes XBP-1 substrate to an active splice variant (XBP-1s). XBP-1s is also a transcription factor which can result in the promotion of ER stress response genes [218, 219].

As well as inducing the transcription of genes that can aid the ER under periods of stress, ATF6, ATF4 and XBP-1s signalling also induce the transcription of Gadd153 (also known as CHOP), which itself is a transcription factor that can stimulate pro-apoptotic stimuli, to drive the cell to death, if the stress is too severe or persists for too long [220].

Research into the role of GRP78 and the UPR has demonstrated the importance of this evolutionary conserved homeostatic response pathway for the survival of cancer cells. Neoplastic progression requires genetic alterations that allow a cell to ignore or evade growth controls and disable apoptotic stimuli. These characteristic attributes of cancer cells often result in an increased rate of proliferation and result in an ever expanding mass, which exhibits poor vascularisation [221]. A consequence of this is changes within tumour microenvironment, a harsh and inadequate cellular environment. Tumour cells are often exposed to highly acidic conditions which contain low oxygen, nutrients and glucose conditions and have altered Ca^{2+} levels, all essential for cell survival and growth [222]. This inadequate environment places added pressure upon the ER to maintain the high rate of protein synthesis required for turn-over and cellular division [208].

As a solid tumour grows larger, cells respond by over producing pro-angiogenic factors to stimulate the formation and attraction of blood vessels [223]. Many studies have demonstrated the importance of hypoxia inducible factor 1 (HIF1) for the stabilisation of tumour microenvironments [208]. To date, there are abundant data to demonstrate the activation of the UPR in solid tumour models, indicating that the UPR is an important component of defence against hypoxia, allowing cancer cells to buffer periods of severe stress and deprivation, which would in the case of normal physiology have induced cell death to preserve the integrity of the organism.

Data have demonstrated that within neural-crest-derived cancer cells, melanoma and glioblastoma, there is a direct correlation between expression of GRP78 and cancer

disease state and resistance to therapy [113, 224]. In contrast, however, neuroblastoma shows favourable prognosis for patients with high GRP78 expression [116]. Therefore, research looking at the activation of the UPR and cancer cells response to pharmacologically induced ER stress is required for a better understanding of the UPR with regards to cellular sensitivity to ER stress.

Armstrong *et al.,* investigating early events of ER stress signalling and response pathways induced by fenretinide and bortezomib demonstrated signals mediated by the eIF2α - ATF4 signalling pathway and highlighted differences within drug induction of ATF4 between cell types, as well as demonstrating differences between the ability of ER stress-inducing agents fenretinide and bortezomib to activate the UPR [112].

Previous work has highlighted the ability of ER stress-inducing agents to increase apoptosis of metastatic melanoma [82, 83]. However, the activation of the UPR hinders the ability of pharmacological agents to induce cell death, due to downstream up regulation of chaperones or folding machinery such as GRP78 or PDI respectively, which aid the cell under periods of ER stress [202]. Therefore for treatment of cancer cells with ER stress-inducing agents, the stress achieved must result in the induction of sufficient stress to ensure cell death, rather than the induction of pro-survival stimuli. Strategies to combine ER stress-inducing agents with specific inhibitors to important components of the UPRs pro-survival function (eg. GRP78 or PDI) may also prove successful in overcoming the pro-survival activity of the UPR.

The importance of GRP78 and the UPR during stress has been well documented, as well as a possible role in cancer cell survival to host death stimuli and chemotherapy. However, to date limited data are available to explain the signalling mechanism behind the UPR ability to switch a characteristically pro-survival response, towards a signalling cascade that results in cell death. Previous work by Lin *et al.,* and Hetz *et al.,* has described the importance of time in determining the outcome of the UPR [225, 226]. These publications described a difference between PERK, IRE1 and ATF6 signalling time resulting in the loss of ATF6 pro-survival attributes first. This leaves PERK and IRE1 which are capable of down-stream Gadd153 induction and death signalling. Another time-dependent factor of the UPR is the induction of Gadd153 itself. Unlike the induction of chaperones and other transcription factors, such as ATF4, Gadd153 induction is a secondary cycle of the UPR, requiring the induction and translation of ATF4 or processing of XPB-1 prior to induction. This therefore ensures a standardised

time for a homeostatic response to stabilise the ER prior to committing the cell to death. Research has also indicated that individual arms of the UPR may be activated to different degrees depending upon the type of stress [227]. These findings highlight the possibility of a more selective and sensitive UPR cascade than previously thought [227].

Taking these data into consideration, further research is required to determine if the difference in clinical outcome of neural-crest-derived tumours correlates with GRP78 expression, and is in part a consequence to differences in UPR signalling. Research investigating the balance between pro-survival and pro-death stimuli under pharmacological treatments, is therefore required to gain a better understanding of the threshold required to induce cell death in cancer cells, and the development of novel strategies through which to induce cell death in cancer cells resistant to apoptosis via conventional mechanisms.

The aim of this study was to test the hypothesis that differences within the UPR exist between neural-crest-derived cancer types, resulting in the opposing prognostic outcomes observed for melanoma and neuroblastoma. In order to test this hypothesis experiments were designed to quantify the cellular expression of GRP78 and the UPR activators PERK, IRE1 or ATF6. This would allow for a direct comparison of cellular concentrations that exist not only between proteins, but also across cancer types. To confirm that the cellular localisation of GRP78 may affect a cancers response to stress, co-localisation experiments looking at GRP78 in comparison to the ER marker calnexin were also carried out. To determine cellular localisation, samples were assessed under both normal and pharmacologically-induced stressed conditions allowing for interpretation of any changes within expression and protein localisations as a direct result of stress. To generate a detailed understanding of the UPR, experiments were also undertaken to map the effect of ER stress on the activation of all three arms (through both time and dose response studies) of the UPR for; ATF4 induction, XBP-1 splicing and ATF6 cleavage in the different cancer cell types.

3.2: Results.

3.2.1: Stoichiometry of UPR sensor components.

To test the hypothesis that differences exist within the expression levels of GRP78 and the UPR activators across neural-crest-derived cancer cells, experiments were carried out to quantify the cellular concentration of GRP78 in a panel of neural-crest-derived cancer cells, consisting of metastatic melanoma, glioblastoma and neuroblastoma (Figure 3.2). Western blot analyses for the quantification of GRP78 concentration in CHL-1 and WM266-4 metastatic melanoma or MO59J and U251 glioblastoma or NGP and SH-SY5Y neuroblastoma cell lines against a standard curve of purified full length GRP78 standard (Figure 3.2. i - iii) were carried out with 100 000 cells and expression per cell calculated by measurement from a specific standard curve and adjusted by cell volumes to determine cellular concentrations.

These data showed that for melanoma, glioblastoma and neuroblastoma there was no significant difference in GRP78 concentration between cell lines of the same cancer type ($P > 0.05$). When concentrations of GRP78 were compared between differing cancer types, there was, however, a significant difference in GRP78 concentration (Figure 3.2.B). The expression of GRP78 in metastatic melanoma cells was increased in comparison to normal primary melanocytes (Figure 3.2 C, Two-Way ANOVA, $F_{3, 8} = 87.6$, $P < 0.0001$) and melanoma cells demonstrated significantly greater expression than that observed in either glioblastoma or neuroblastoma (Figure 3.2.B, for the comparison of metastatic melanoma to glioblastoma, One Way ANOVA with contrast coefficients $F_{1, 29} = 19.3$ $P < 0.005$, or neuroblastoma $F_{1, 29} = 38.6$, $P < 0.001$). Data also showed a significant difference in the concentration of GRP78 between glioblastoma and neuroblastoma (Figure 3.2.B, for the comparison of glioblastoma to neuroblastoma $F_{1, 29} = 38.7$, $P < 0.005$). These data thus highlight a significant difference in GRP78 concentration between cancer types.

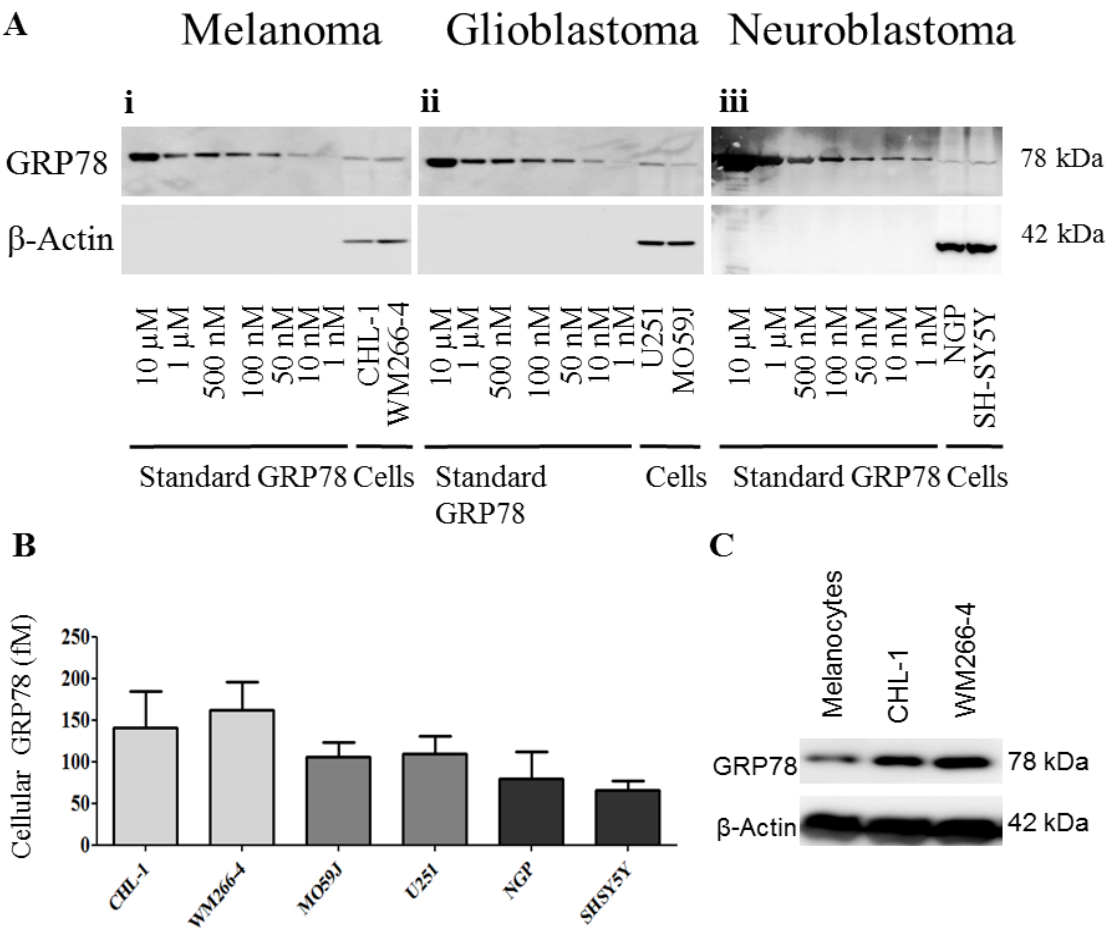

Figure 3.2: *Cellular concentrations of GRP78.* ***(A)*** *Western blot analysis of CHL-1, WM266-4 (metastatic melanoma cells), MO59J, U251 (glioblastoma cells), NGP and SH-SY5Y (neuroblastoma cells) were carried out to determine the cellular concentration of GRP78. Concentration of each cell line were determined per 100 000 cells in comparison to a standard curve of full length purified GRP78 standard, ranging from 10 µM – 1 nM.* ***(B)*** *Comparison of cellular concentrations of GRP78, determined for densitometry analysis of western blots and cell line expression measured from a specific standard curves and the resulting data adjusted for per cell. Cell volumes were derived from confocal images of detached DAPI stained spherical cells, to allow for the volume of the nucleus to be subtracted, and compared to a µm gauge slide.* ***(C)*** *Western blot analysis comparing the expression of GRP78 in metastatic melanoma cell lines to that of primary melanocytes. Western blot data were expressed as the mean ± 95% CI of three independent experiments.*

Since GRP78 is thought to bind PERK, IRE1 and ATF6, experiments were carried out to quantify the cellular concentration of the UPR activators to assess their stoichiometry in relation to GRP78. Western blot analysis for the quantification of PERK, IRE1 and ATF6 expression in CHL-1 and WM266-4 metastatic melanoma or MO59J and U251 glioblastoma or NGP and SH-SY5Y neuroblastoma cell lines against standard curves of purified fragments of each specific protein standard (Figure 3.3) were carried out with 100 000 cells and expression per cell calculated by measurement from protein specific standard curves and adjusted by cell volume for their cellular concentrations.

To determine, if like GRP78, differences in the expression levels of the UPR activators; PERK IRE1 and ATF6 also existed between differing neural-crest-derived cancer types that may alter the UPR capacity to react to stress, stoichiometric analysis were performed to quantify cellular concentrations. Data demonstrated that there was no significant difference in the cellular concentrations of PERK or ATF6 between cell lines of the same cancer type, or between differing cancer cell types ($P > 0.05$). However, for the cellular concentration of IRE1 there was a significant difference between cell lines within melanoma and neuroblastoma (Figure 3.3, analysis by One Way ANOVA for the concentration of IRE1 between metastatic melanoma $F_{1, 18} = 7.6$, $P < 0.01$ and between glioblastoma cell lines $F_{1, 18} = 4.5$, $P < 0.05$), and also between glioblastoma and neuroblastoma (analysis by One Way ANOVA $F_{1, 18} = 5.6$, $P < 0.01$). In summary, these data demonstrate that although there were differences between cell lines in the cellular concentrations of UPR activators, these did not correlate with the differences observed for the cellular concentrations of GRP78. Furthermore, when comparing the cellular expressions of PERK, IRE1 and ATF6 to each other or between cell lines, there was a significant difference in IRE1 expression compared with both PERK and ATF6 across all cell lines (Figure 3.3, comparing the expression of IRE1 to PERK $F_{3, 47} = 67.3$ or ATF6 $F_{3, 47} = 94.2$, $P < 0.001$ for either).

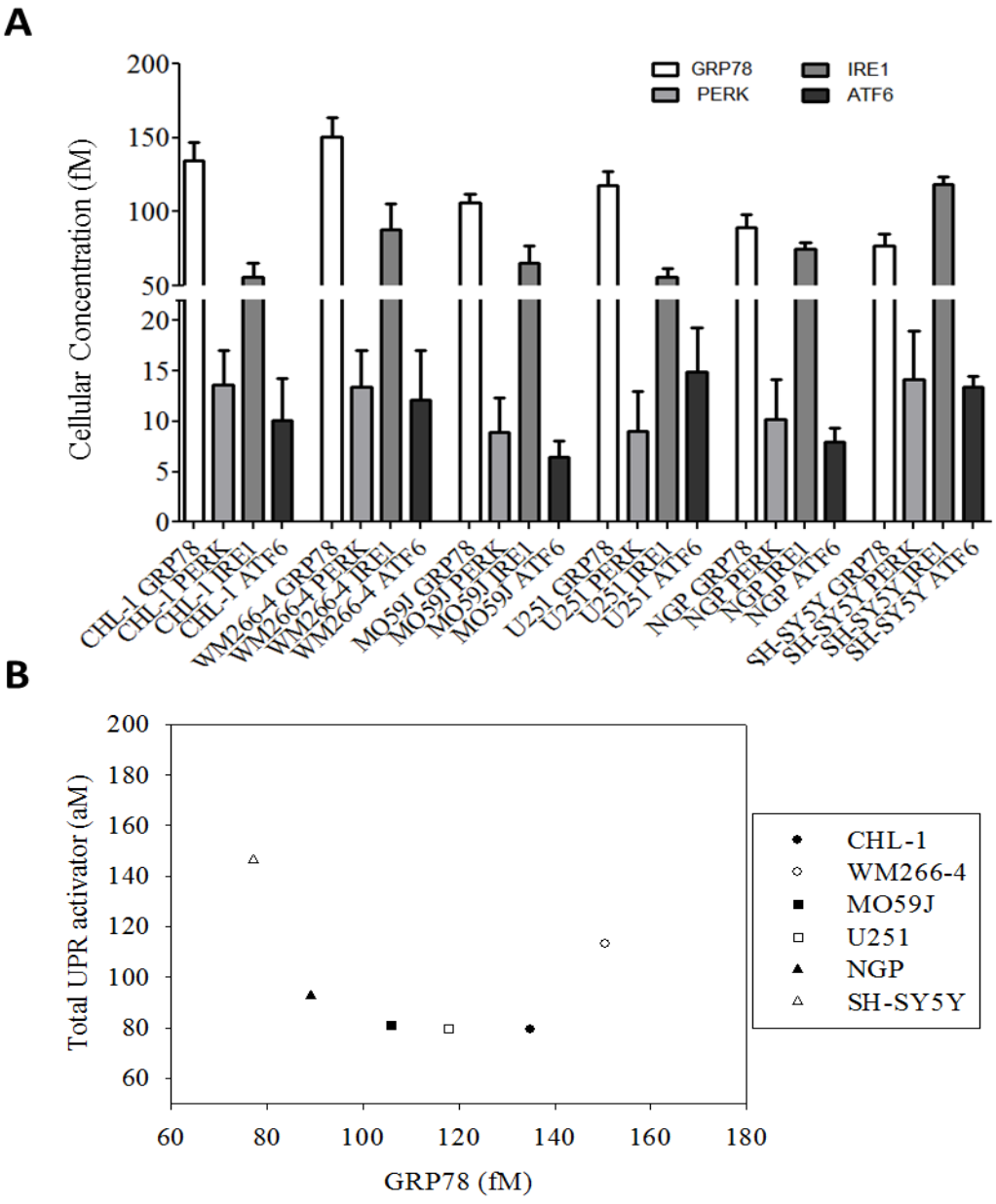

Figure 3.3: Cellular concentration of GRP78 and the UPR activators. **(A)** Western blot analysis of CHL-1, WM266-4 (melanoma cells), MO59J, U251 (glioblastoma cells), NGP and SH-SY5Y (neuroblastoma cells) were carried out to determine the cellular expression of GRP78, PERK, IRE1 and ATF6. Expression of each protein, within each cell line, was determined per 100 000 cells in comparison to a standard curve of either; full length purified GRP78 or fragments of each individual UPR activator, ranging from 500 nM – 1 nM. Cellular concentrations were determined as described previously Western blot data were expressed as the mean ± 95% CI of three independent experiments. **(B)** To illustrate the relationship between GRP78 and the UPR activators, scatter plots analysis for the mean GRP78 and total UPR activator concentrations are shown. Representative western blot images for the detection of PERK, IRE1 and ATF6 are demonstrated in Figure 5.10 (Chapter 5, page 170).

Comparing the expression levels of PERK, IRE1 or ATF6, within cell lines of the same cancer type, showed that for PERK and ATF6 there was no significant difference in expression between cell lines ($P > 0.05$). However, for the expression of IRE1, there was a significant difference between cell lines (Analysis by One Way ANOVA $F_{1, 23} = 13.6$, $P < 0.005$). The expression of IRE1 between metastatic melanoma and neuroblastoma cells showed a significant difference in expression (comparing metastatic melanoma cells, One Way ANOVA; CHL-1 to WM266-4 $F_{1, 21 =} 8.9$, $P < 0.05$ and neuroblastoma cells NGP and SH-SY5Y $F_{1, 21} = 17.3$ $P < 0.01$); however no significant differences between glioblastoma cell lines were evident ($P > 0.05$). Interestingly, the expression of IRE1 did not correlate with GRP78 expression, and demonstrated that SH-SY5Y cells have significantly higher expression compared to all other cells lines (comparing SH-SY5Y expression of IRE1 by One Way ANOVA with Dunnett's post hoc corrections to; CHL-1 = $P < 0.001$, WM266-4 = $P < 0.05$, MO59J = $P < 0.005$, U251 = $P < 0.0001$ and NGP = $P < 0.01$).

Although there was no correlation between GRP78 and the UPR activator concentrations, data were analysed to investigate the relative relationship between GRP78 and the total UPR activator concentration (the sum of PERK, IRE1 and ATF6 concentrations within a given cell line) as a more representative predictor of UPR capacity. Comparing the mean GRP78 expression against the accumulative means of PERK, IRE1 and ATF6 for metastatic melanoma and glioblastoma indicated a significant difference in favour of GRP78 (Comparing GRP78 to UPR activators by One Way ANOVA with Dunnett's post hoc corrections within CHL-1 = $P < 0.0001$, WM266-4 = $P < 0.001$, MO59J = $P < 0.005$ and U251 = $P < 0.001$). In the case of neuroblastoma cell lines, data also demonstrated a significant difference between GRP78 and total UPR activator expression, however for neuroblastoma cell lines the stoichiometry was in favour of UPR activators (Comparing GRP78 to UPR activators, by One way ANOVA with Dunnett's post hoc correction, within neuroblastoma cell lines as for melanoma and glioblastoma, data demonstrated for NGP = $P < 0.05$ and SH-SY5Y = $P < 0.0001$ in favour of excess UPR activators).

In summary this study highlighted a significant difference between cancer types in the stoichiometry of the UPR sensor mechanism. The difference in ratio between GRP78 and UPR activators present for metastatic melanoma and glioblastoma, to that of neuroblastoma demonstrates a difference in UPR activity across cancer types. These results suggest that differences in the dynamic equilibrium across cancer types. The

expression of GRP78 to that of the UPR activators and therefore the ability of GRP78 to negatively regulate the UPR, which in metastatic melanoma and glioblastoma results in the inactivation of the UPR due to an excess in GRP78. Conversely, in neuroblastoma the system may become primed towards an active UPR, due to the high expression of UPR activators to GRP78.

3.2.2: Subcellular localisation of GRP78.

To compare the localisation and distribution of GRP78 in different cell lines, methanol-fixed cells were stained with antibodies to GRP78 and calnexin as an ER-resident marker. Cells were then analysed for their co-localisation coefficient to determine if there were any differences in cellular localisation between cell lines (Figure 3.4) and to determine if treatment of differing cancer cells lines with ER stress-inducing agents altered the distribution (Figure 3.5).

For metastatic melanoma there was a significant difference in co-localisation coefficients between CHL-1 and WM266-4 cells (Analysis by ONE Way ANOVA, $F_{1, 18} = 14.9$ $P < 0.05$), but no difference was observed between glioblastoma or neuroblastoma cell lines ($P > 0.05$). There was also a significant difference in the localisation of GRP78 in relation to calnexin across the differing cancer types (Investigation GRP78 to calnexin localisation by One Way ANOVA $F_{5, 18} = 29.7$ $P < 0.0001$: One Way ANOVA with Dunnetts post hoc correction for the comparison of metastatic melanoma to glioblastoma or neuroblastoma $P < 0\ 001$ and $P < 0.05$ respectively or for glioblastoma to neuroblastoma $P < 0.001$).

To investigate the effect of ER stress on the co-localisation of GRP78 and calnexin (Figure 3.5 and Figure 3.6), cells were treated with either fenretinide or bortezomib for 24 h and fixed in 100% ice cold methanol prior to staining for GRP78 and calnexin. The co-localisation coefficients for the effect of treatment on distribution were not statistically significant (Figure 3.6). Nevertheless, there was an apparent trend for an increase in localisation of GRP78 to calnexin when cells were treated with either ER stress-inducing agent. When assessing the effect of fenretinide or bortezomib, irrespective of cell, data demonstrated a significant increase in co-localisation with either ER stress-inducing agent (One Way ANOVA with Dunnett's post hoc corrections, for fenretinide $P < 0.05$ or bortezomib $P < 0.01$). These data indicate that cellular distribution of GRP78 is influenced by stress and that GRP78 is extensively cytoplasmic in all cancer types tested.

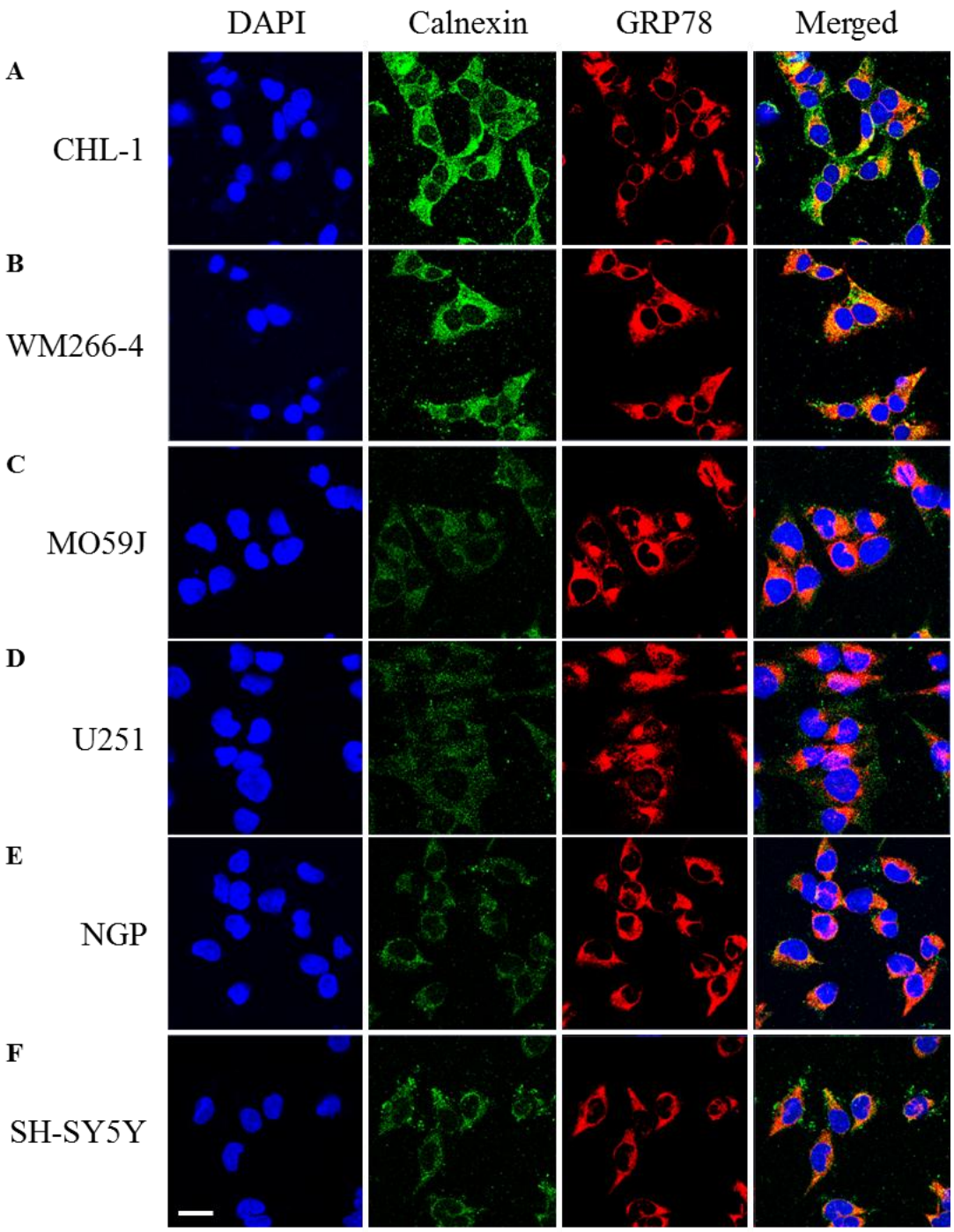

Figure 3.4: *Cellular distribution of GRP78. Cancer cell lines; CHL-1, WM266-4 (melanoma cells), MO59J, U251 (glioblastoma cells), NGP and SH-SY5Y (neuroblastoma cells) were fixed in 100% ice cold methanol and stained for GRP78 in comparison to the ER resident chaperone Calnexin. Images are representation of 3 independent experiments, each experiment a minimum of 4 images were acquired to allow for the collection of co-localisation coefficients for a minimum of 30 cells per condition. Scale bar = 20 µm.*

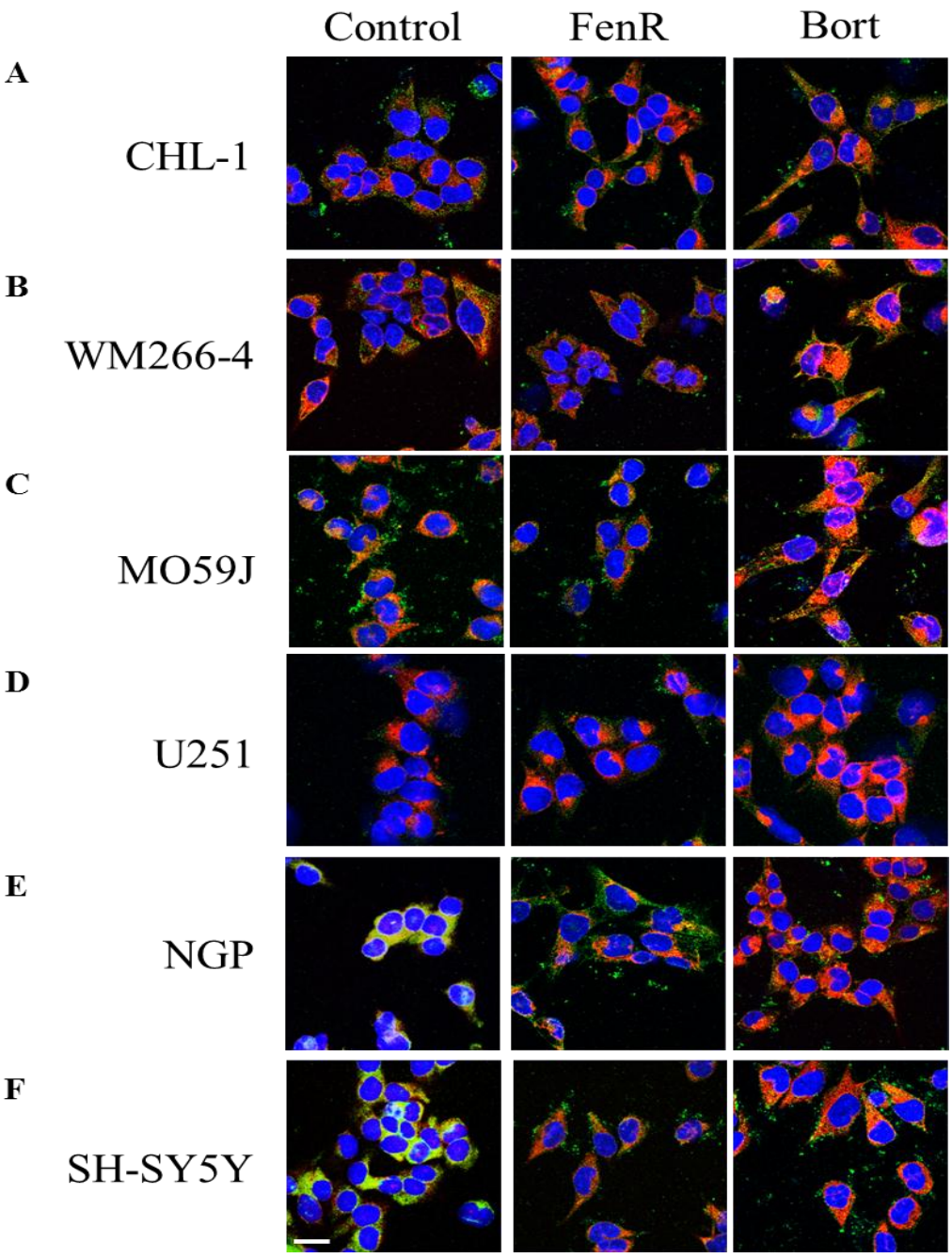

Figure 3.5: *The effect of ER stress on GRP78 distribution. Cancer cell lines; CHL-1, WM266-4 (melanoma), MO59J, U251 (glioblastoma), NGP and SH-SY5Y (neuroblastoma) cell lines were treated with fenretinide (FenR, 10 µM for melanoma or glioblastoma or 5 µM for Neuroblastoma) or bortezomib (Bort, 200 nM for melanoma or glioblastoma or 20 nM for Neuroblastoma) for 24 h prior to being fixed in 100% ice cold methanol and stained for GRP78 in comparison to the ER resident chaperone Calnexin. Images are representation of 3 independent experiments, each experiment a minimum of 4 images were acquired to allow for the collection of co-localisation coefficients for a minimum of 30 cells per condition. Scale bar = 20 µm.*

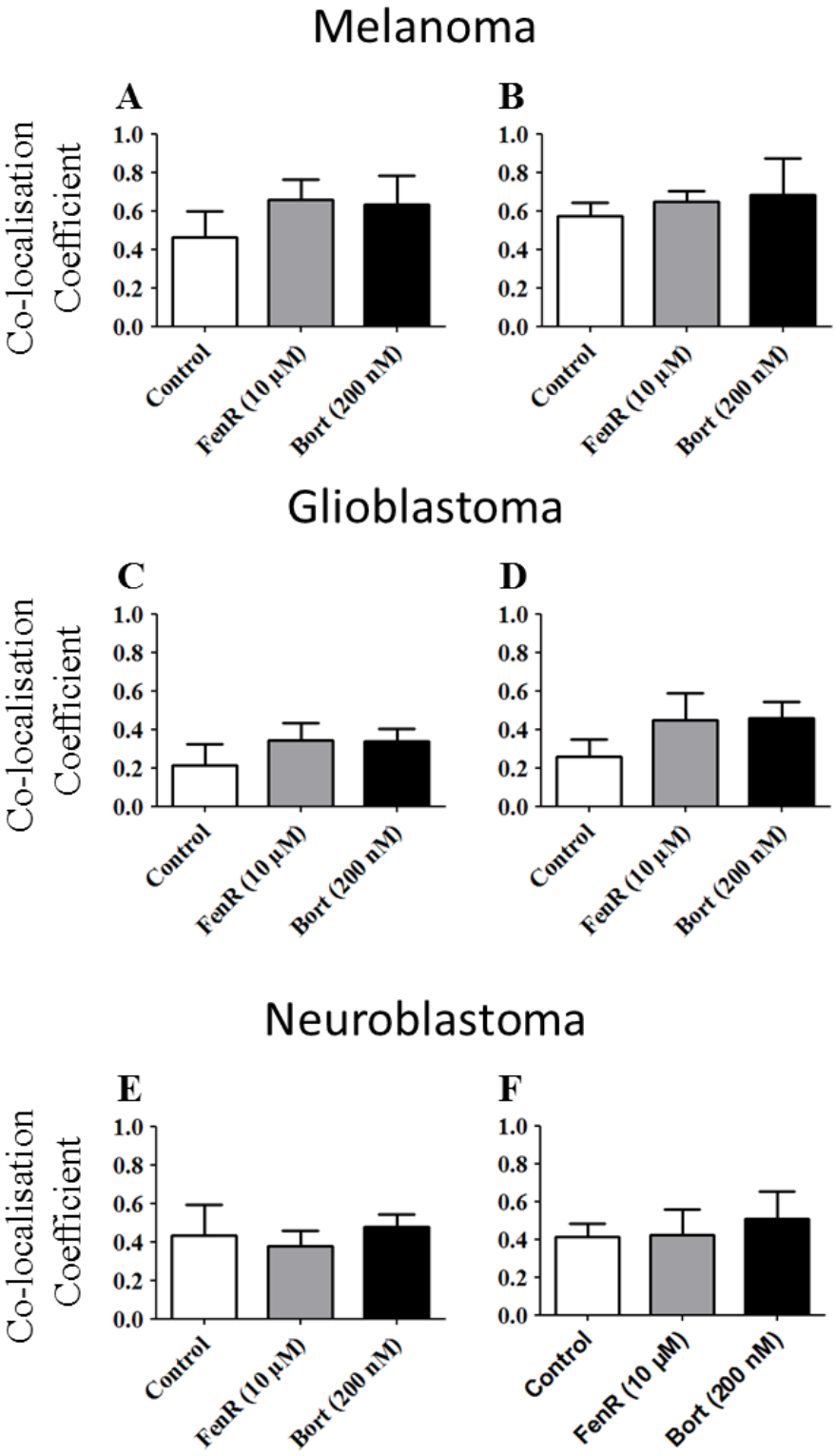

Figure 3.6: *The effect of ER stress on GRP78 cellular distribution. A comparison of coefficients. Coefficients for the effect of fenretinide or bortezomib treatment of GRP78 co-localisation with Calnexin were generated from confocal microscopy data (experimental setup as for Figure 3.5). Data are the average of 3 replicate experiments containing a minimum of 4 images per experiment ± 95% CI.*

3.2.3: Induction of the UPR in response to ER stress.

To investigate the induction of the UPR in metastatic melanoma and glioblastoma in comparison to neuroblastoma, cells were treated with increasing doses of fenretinide and bortezomib (1 – 15 μM fenretinide and 10 – 300 nM bortezomib for melanoma and glioblastoma or 0.5 – 10 μM and 1 – 30 nM bortezomib for neuroblastoma) for 4 h prior to the analysis of ATF4 induction by western blotting. Concentrations of either fenrretinide or botezomib used to treat neuroblastoma cell lines were lower than those used for melanoma and glioblastoma, since neuroblastoma cells are more sensitive to cell death [112], but each agent was employed up to and including the maximum clinically-achievable dose. Western blots were carried out as for GRP78 and the UPR activators to allow for cellular concentrations of ATF4 to be determined.

Results demonstrated that both ER stress-inducing agents activated the UPR in a dose dependent manner. For fenretinide CHL-1, MO59J, U251, NGP amd SH-SY5Y cells; a minimum of 5 μM fenretinide was sufficient to induce the expression of ATF4 ((Figure 3.7 A, C & E) analysis by One Way ANOVA with Dunnetts post hoc corrections for CHL-1, MO59J, U251 cells treated with 5 – 15 μM fenretinide $P < 0.0001$ and for neuroblastoma cell lines NGP and SH-SY5Y 5 - 10 μM fenretinide $P < 0.001$- 0.0001 respecively). WM266-4 cells treatment with fenretinide resulted in a significant induction of ATF4 but required concentrations of 10 μM ((Figure 3.7 A) analysis by One Way ANOVA with Dunnetts post hoc corrections for treatment with 10 μM $P < 0.001$ and 15 μM $P < 0.0001$ fenretinide respectively). Treatment with bortezomib, in all cell lines, resulted in a significant induction of ATF4 (Figure 3.7 B, D & F). In metastatic melanoma and glioblastoma cells ATF4 was significantly induced by concentrations of 100 nM bortezomib (Analysis by One way ANOVA with Dunnetts post hoc corrections, for CHL-1 and WM266-4 metastatic melanoma or MO59J and U251 glioblastoma cell lines treated with bortezomib doses of 100 – 300 nM $P < 0.0001$), while in WM266-4 cells, significant induction was demonstrated in response to 10 nM concentrations ($P < 0.001$).

Bortezomib also significantly induced ATF4 expression in neuroblastoma cell lines, where a significant induction was evident in resposne to a lower dose of 10 nM (Analysis by One way ANOVA with Dunnett's post hoc corrections for NGP and SH-SY5Y cells treated with 10 nM – 30 nM bortezomib $P < 0.0001$, except for NGP with

10 nM bortezomib $P < 0.001$) indicating that both fenretinide and bortezomib are potent inducers of the UPR.

These data indicate a difference in UPR activation strength between melanoma and neuroblastoma cell lines, demonstrating a significant difference between cancer cell type (Comparing cancer types for the effect of fenretinide by One way ANOVA with Dunnetts post hoc corrections $P < 0.01$ and Bortezomib $P < 0.001$). Furthermore these data also highlighted a difference between fenretinide and bortezomib induction of ATF4 within all cell lines except U251 glioblastoma cells (Comparing the effect of fenretinide and bortezomib for CHl-1 $F_{4, 72} = 3.164, 2229.8$, $P < 0.0001$ and WM266-4 154.6 and 2991.2, $P < 0.0001$ respecitvely. For MO59J cells $F_{4, 72 =}$ 226.5, 612.1, $P < 0.05$, neuroblastoma cell lines NGP $F_{4, 72} = 33.7, 52.3$, $P < 0.001$ and SH-SY5Y $F_{4, 72} =$ 19.7 or 106.2, $P < 0.01$ respectively).

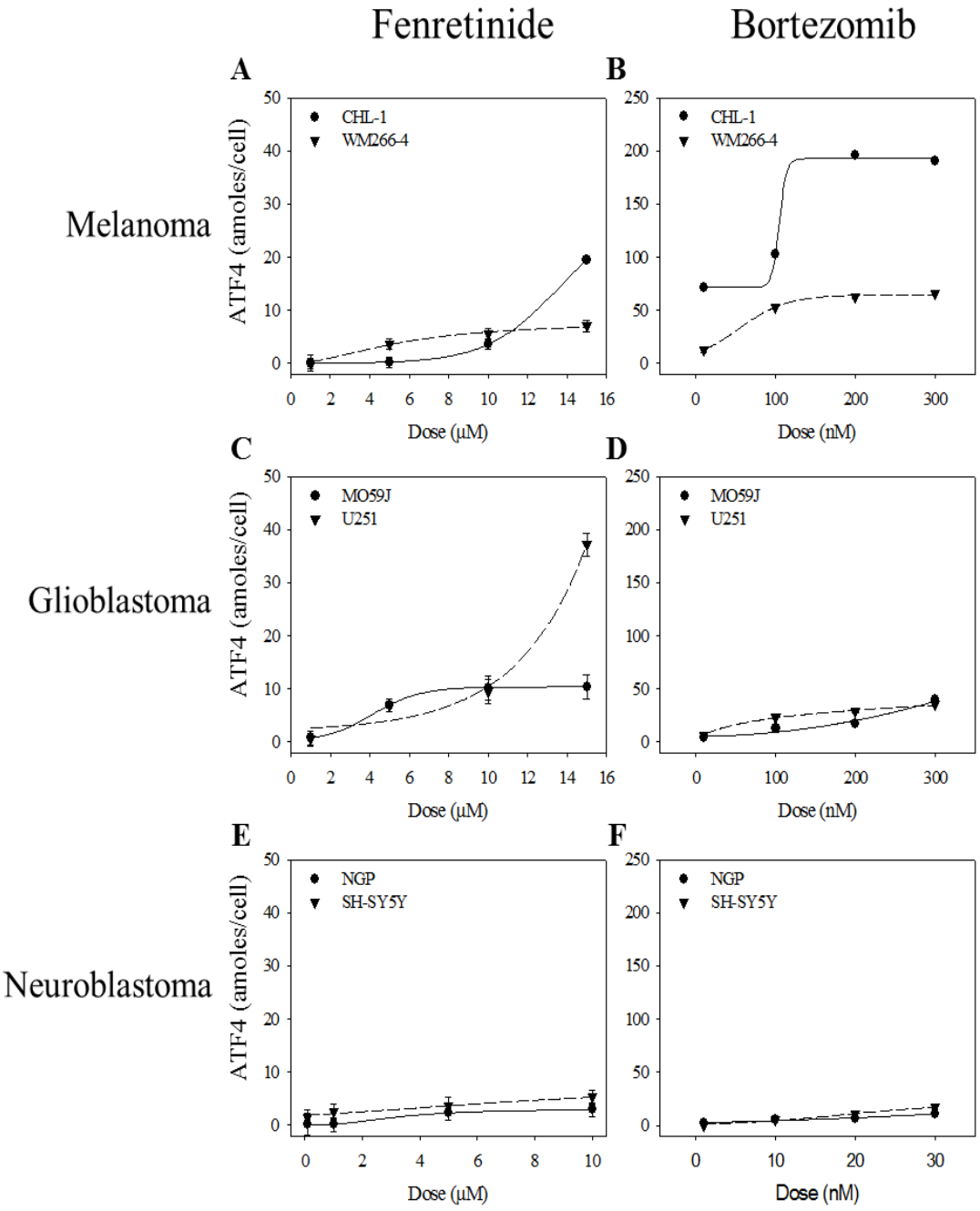

Figure 3.7: *The effect of fenretinide and bortezomib dose on the induction of ATF4 as an indicator of UPR activation.. Assessing ATF4. CHL-1, WM266-4 (melanoma), MO59J, U251 (glioblastoma), NGP and SH-SY5Y (neuroblastoma) cell lines were treated with fenretinide (FenR, 1 - 15 µM for melanoma or glioblastoma or 0.1 - 10 µM for Neuroblastoma) or bortezomib (Bort, 10 - 300 nM for melanoma or glioblastoma or 1 - 30 nM for Neuroblastoma) for 4 h prior to harvesting. Cells were then counted and western blots used to determine cellular concentration (as described for GRP78). Western blot data were expressed as the mean ± 95% CI of three independent experiments.*

To determine the effect of each ER stress-inducing agents over time, cells were treated with fenretinide or bortezomib (10 µM fenretinide and 200 nM bortezomib for metastatic melanoma and glioblastoma cell lines or 5 µM fenretinide and 20 nM bortezomib for neuroblastoma cell lines) and cellular concentrations of ATF4 determined at 0, 1, 2, 4, 8 and 24 h (Figure 3.8). Results showed that fenretinide significantly induced the expression of ATF4; however this effect was not time dependant (Figure 3.8 A, C & E).

Fenretinide induced UPR activation over variable times, with the most significant effect occuring at 4 – 8 h, while ATF4 expression in all cell lines decreased in expression by 24 h. CHL-1, MO59J , U251 and NGP demonstrated a significant induction of ATF4 by 2 h (One way ANOVA with Dunnett's post hoc corrections for CHL-1, U251 and NGP cell lines $P < 0.05$ or MO59J = $P < 0.0001$), where WM266-4 and SH-SY5Y cells showed significant induction by 4 h (One way ANOVA with Dunnett's post hoc corrections for WM266-4 and SH-SY5Y cell lines = $P < 0.0001$ or $P < 0.01$ respectively). Metastatic melanoma and neuroblastoma cells showed maximum induction of ATF4 by 4 h fenretinide treatment (One way ANOVA with Dunnett's post hoc corrections for or CHL-1, WM266-4 and NGP cell lines = $P < 0.0001$ or SH-SY5Y cells = $P < 0.01$) however, glioblastoma showed a slower induction, reaching maximum induction at 8 h (One way ANOVA with Dunnett's post hoc corrections for or both MO59J and U251 = $P < 0.0001$).

ATF4 induction by bortezomib in metastatic melanoma and neuroblastoma cancer types increased in a time dependent manner (Figure 3.8 B, D & F), with a significant response detectable by 2 h for melanoma and 4 or 8 h for NGP and SH-SY5Y neuroblastoma cell lines respectively (One way ANOVA with Dunnett's post hoc corrections for or CHL-1 and WM266-4 = $P < 0.0001$, NGP = $P < 0.05$ and SH-SY5Y = $P < 0.01$) which achieved maximum effect by 24 h.

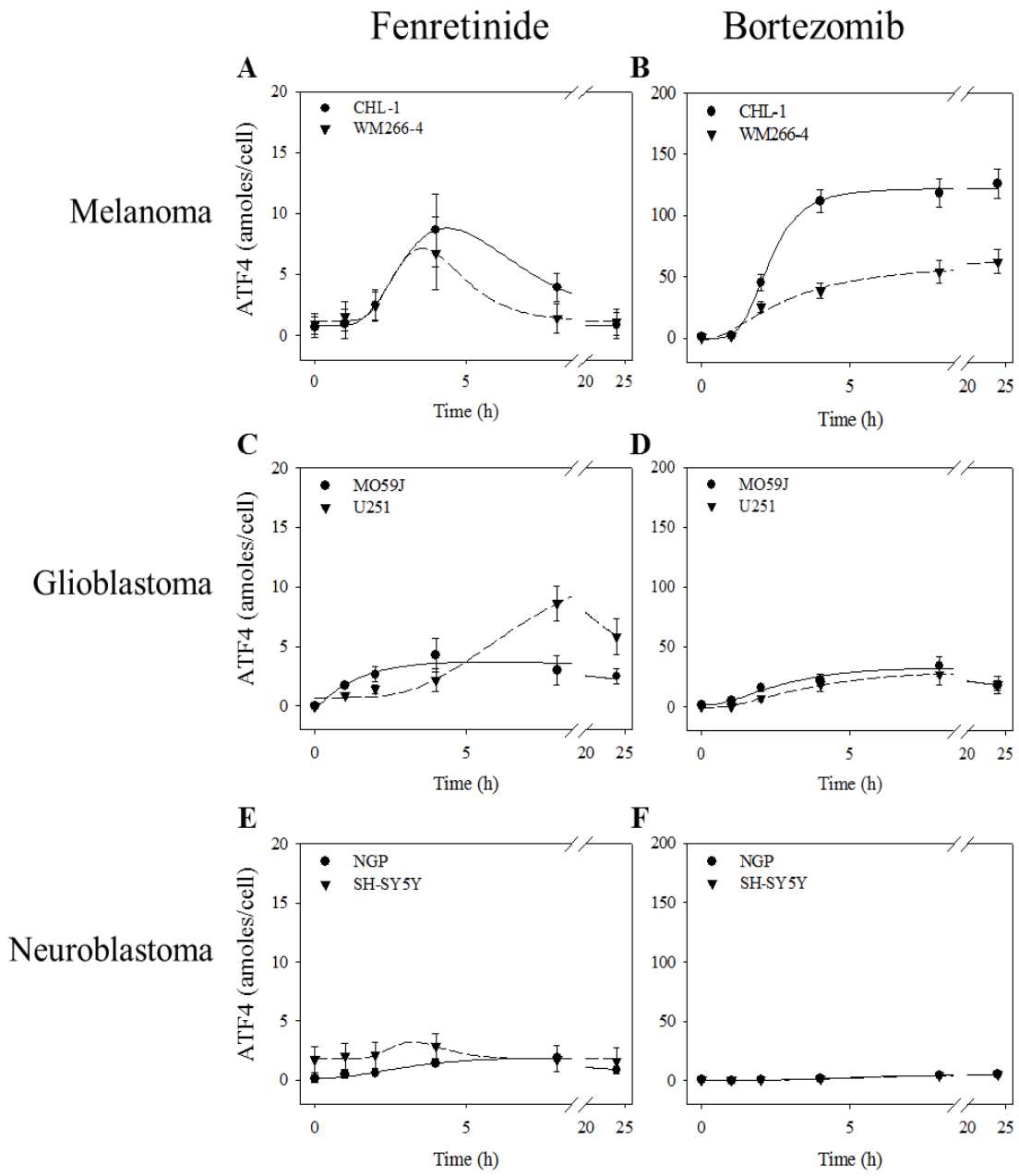

Figure 3.8: *Assessing ATF4 induction over time for the effect of ER stress-inducing agents fenretinide and bortezomib on UPR activation. CHL-1, WM266-4 (melanoma), MO59J, U251 (glioblastoma), NGP and SH-SY5Y (neuroblastoma) cell lines were treated with fenretinide (FenR, 10 µM for melanoma or glioblastoma or 5 µM for Neuroblastoma) or bortezomib (Bort, 200 nM for melanoma or glioblastoma or 20 nM for Neuroblastoma) for 0, 1, 2, 4, 8 and 24 h prior to harvesting. Cells were then counted and western blots ran to determine cellular concentration (as described for GRP78). Western blot data were expressed as the mean ± 95% CI of three independent experiments.*

Glioblastoma cells treated with bortezomib demonstrated a similar trend of ATF4 induction over time to that seen with fenretinide, with cell lines demonstrating reaching a maximal response by 8 h treatment, and with induction detectable by 2 h (One way ANOVA with Dunnett's post hoc corrections for MO59J = $P < 0.0001$ and U251 = $P < 0.05$), reaching maximum response at 8 h ($P < 0.0001$) followed by a reduction in expression by 24 h.

Collectively, these data show a difference between individual cell line response to either fenretinide or bortezomib, demonstrating that UPR activation can differ depending on the type of ER stress (Two-way ANOVA, Comparing the effect of fenretinide over cell lines $F_{6, 108} = 6.2$, $P < 0.01$ or Bortezomib $F_{6, 108} = 35.6$, $P < 0.0001$). These data also confirmed the findings for the effect of dose of ER stress-inducing agent on ATF4 induction, showing both agents are capable of inducing the UPR. However, bortezomib demonstrated a greater effect on inducing the UPR (Two-way ANOVA, Comparing the effect of fenretinide and bortezomib, per cell line induction of ATF4 over time; CHL-1 and WM266-4 melanoma and MO59J or U251 glioblastoma cells $F_{2, 36} = 36.2$, $F_{2, 36} = 37.6$, $F_{2, 36} = 36$ and $F_{2, 36} = 27.2$, $P < 0.0001$ respectively or NGP neuroblastoma cells $F_{2, 36} = 9.4$, $P < 0.01$), as well as activating the UPR for longer.

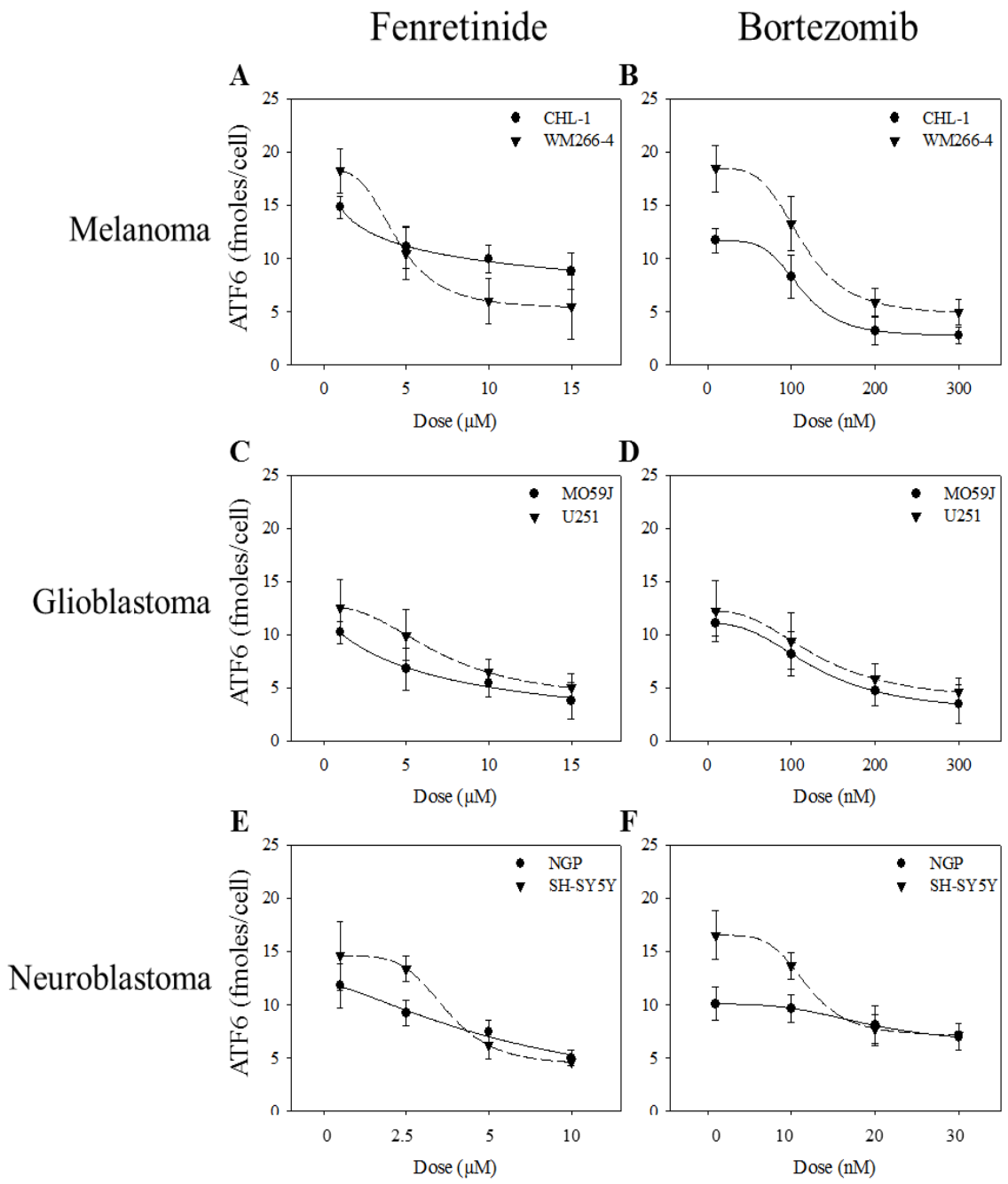

Figure 3.9: *The effect of fenretinide and bortezomib dose on ER stress-induced ATF6 cleavage. CHL-1, WM266-4 (melanoma), MO59J, U251 (glioblastoma), NGP and SH-SY5Y (neuroblastoma) cell lines were treated with fenretinide (FenR, 1 - 15 µM for melanoma or glioblastoma or 0.1 - 10 µM for Neuroblastoma) or bortezomib (Bort, 10 - 300 nM for melanoma or glioblastoma or 1 - 30 nM for Neuroblastoma) for 4 h prior to harvesting. Cells were then counted and western blots used to determine cellular concentration (as described for GRP78). Western blot data were expressed as the mean ± 95% CI of three independent experiments.*

The effect of ER stress on the activation of the ATF6 arm of the UPR in melanoma, glioblastoma and neuroblastoma neural-crest-derived cancer types was also determined in response to fenretinide and bortezomib. Antibodies that would reliably detect the cleaved form of ATF6 were not commercially available; therefore an antibody that detected full length ATF6 was used. The activation of the UPR results in the processing of ATF6 by cleavage, resulting in a decrease in full length products and increase in an active component that was undetectable using the ATF6 antibody employed.

As in previous experiments, cells were treated with increasing doses of fenretinide and bortezomib (1 – 15 μM fenretinide and 10 – 300 nM bortezomib for melanoma and glioblastoma or 0.5 – 10 μM and 1 – 30 nM bortezomib for neuroblastoma) for 4 h prior to western blot analysis for the expression of ATF6 in comparison to a standard curve of purified ATF6 fragment (Figure 3.9). Dose response curves for fenretinide or bortezomib showed that the cellular concentration of ATF6 was reduced in a dose dependant manner. All cancer types demonstrated significant reduction of full length ATF6 when cells were treated with a minimum of 5 μM fenretinide (Figure 3.9 A, C & E, One-way Anova with Dunnett's post hoc corrections for melanoma = $P < 0.05$, glioblastoma = $P < 0.01$ and neuroblastoma = $P < 0.0001$). For all cells, the significance in response (with regards to ATF6 cleavage) increased with the dose of fenretinide (reaching = $P < 0.0001$ in all cell lines by 10 μM). Also for NGP neuroblastoma cells a significant response was detectable at 2.5 μM (One-way Anova with Dunnett's post hoc corrections = $P < 0.05$).

With respect to bortezomib treatment (figure 3.9 B, D & F), except CHL-1 cells, data showed no significant difference to that for fenretinide (One-way Anova with Dunnett's post hoc corrections for CHL-1 = $P < 0.0001$). Analysing the effect of bortezomib dose on ATF6 expression showed a significant effect for melanoma and glioblastoma cells from concentrations of 100 nM (One-way Anova with Dunnett's post hoc corrections, for the effect of bortezomib on ATF6 expression; CHL-1 and WM266-4 cells $P < 0.0001$ or MO59J = $P < 0.01$ and U251 = $P < 0.05$) and expression significantly decreased further with dose (with melanoma and glioblastoma reaching = $P < 0.0001$). For neuroblastoma cell lines a significant effect of bortezomib on ATF6 was achieved by 20 nM (One-way Anova with Dunnett's post hoc corrections, for NGP = $P < 0.05$ and SH-SY5Y = $P < 0.0001$) increasing further with dose ($P < 0.0001$ for both cell lines).

Although there was only a significant difference between CHL-1 response to fenretinide or bortezomib-induced reduction in ATF6 expression, data demonstrated that the effect of both fenretinide and bortezomib did significantly differ between cancer types (For fenretinide and bortezomib $F_{2, 72}$ = 49.2 or 51.5, $P < 0.0001$ respectively). The data for the ability of ER stress-inducing agents fenretinide and bortezomib to activate the induction of ATF4 or processing of ATF6 (reduction in expression) differed, with respect, that fenretinide is a more potent activator of ATF6 cleavage. This may represent a stressor-specific outcome of the UPR as described by DuRose et al [227].

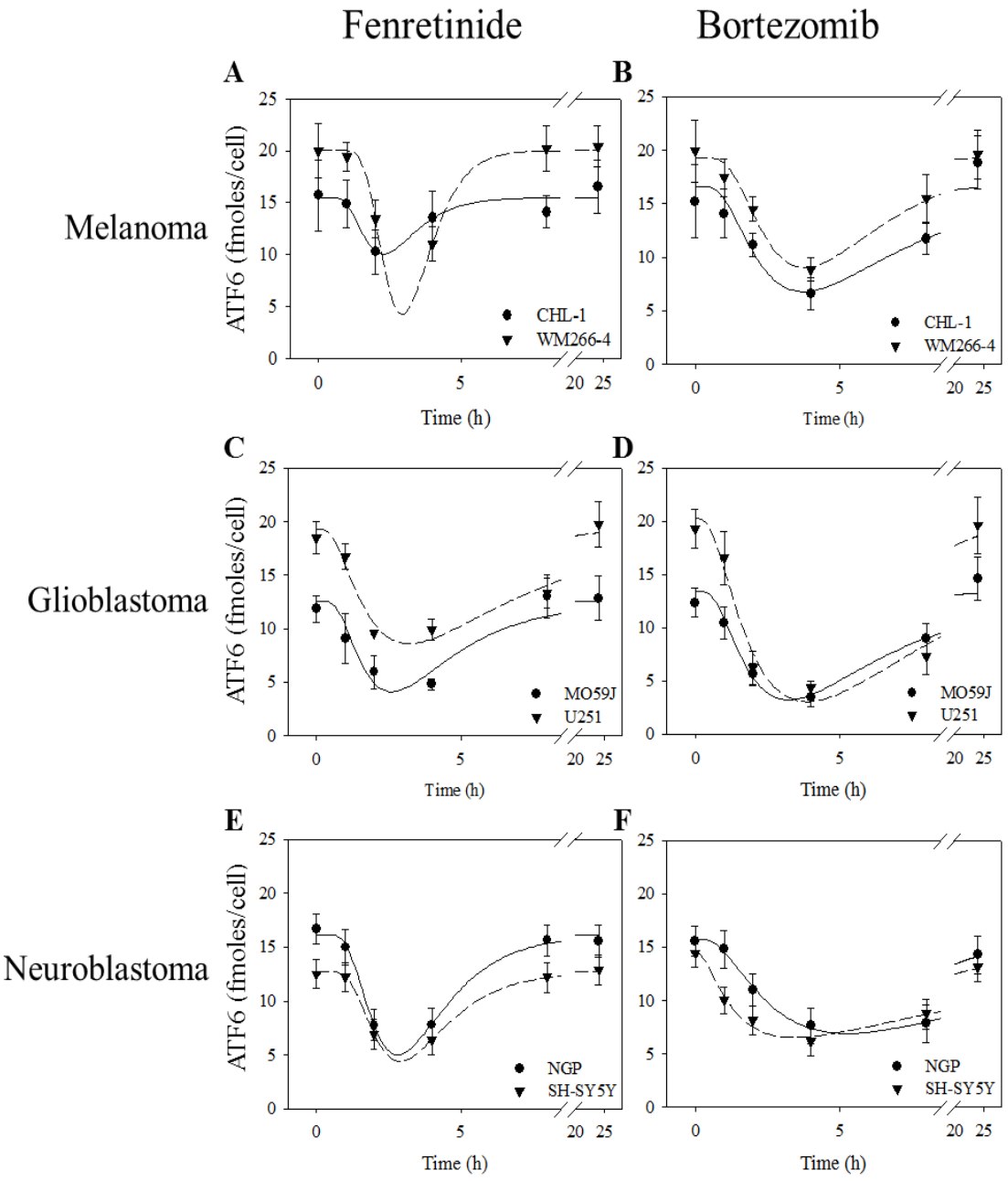

Figure 3.10: *The effect of ER stress-inducing agents fenretinide and bortezomib on ATF6 cleavage over time. CHL-1, WM266-4 (melanoma), MO59J, U251 (glioblastoma), NGP and SH-SY5Y (neuroblastoma) cell lines were treated with fenretinide (FenR, 10 µM for melanoma or glioblastoma or 5 µM for Neuroblastoma) or bortezomib (Bort, 200 nM for melanoma or glioblastoma or 20 nM for Neuroblastoma) for 0, 1, 2, 4, 8 and 24 h prior to harvesting. Cells were then counted and western blots ran to determine cellular concentration (as described for GRP78). Western blot data were expressed as the mean ± 95% CI of three independent experiments.*

To characterise the time course of the UPR, with respect to ATF6, cells were treated with either fenretinide or bortezomib (10 µM fenretinide and 200 nM bortezomib for metastatic melanoma and glioblastoma cell lines or 5 µM fenretinide and 20 nM bortezomib for neuroblastoma cell lines) for 0, 1, 2, 4, 8 and 24 h prior to analysis for ATF6 cellular expression as described previously (Figure 3.10).

Measurements of ATF6 cellular concentration over time allows for the detection of both UPR activation (a decrease in ATF6 concentration) and the eventual downstream induction of ATF6 (an eventual increase in ATF6 concentration), as the system returns to equilibrium. Data for the effect of fenretinide on ATF6 cellular concentration (Figure 3.10 A, C & E) demonstrated a significant reduction in ATF6 concentration within all cell lines. For glioblastoma and NGP neuroblastoma cells, a significant effect was detectable by 1 h exposure to fenretinide (One-way Anova with Dunnett's post hoc corrections = $P < 0.05$ for all), with melanoma and SH-SY5Y neuroblastoma cells showing a significant response by 2 h (One-way Anova with Dunnett's post hoc corrections, $P < 0.0001$). Bortezomib showed a significant effect on WM266-4, MO59J, U251 and SH-SY5Y cells by 1 h (One-way Anova with Dunnett's post hoc corrections, for WM266-4 and MO59J $P < 0.05$, U251 = $P < 0.01$ and SH-SY5Y = $P < 0.0001$) with CHL-1 and NGP cells showing a response at the 2 h time point (For CHl-1 = $P < 0.005$ and NGP = $P < 0.0001$).

All cell lines showed maximum response to either ER stress-inducing agent between 2 and 4 h (all cell lines reaching = $P < 0.0001$ in comparison to control). Although data indicated that the maximum response for bortezomib-treated cells occurred at 4 h, where fenretinide demonstrated maximum responses from 2 h, there were no significant difference between cellular responses within the ATF6 arm of the UPR (Figure 3.10, $P > 0.05$). These data also demonstrated there were no significant differences within the response of individual cell lines to ER stress ($P > 0.05$); although there was a significant detectable difference across cancer type for both fenretinide and bortezomib ($F_{6, 108}$ = 10.1 or 4.8 with $P < 0.0001$ respectively).

Collectively these data demonstrate the cellular response to stress via the ATF6 arm is detectable at early time points (2 h), with the expression of ATF6 beginning to recover by 8 h within all cell lines (indicating the translation of ATF6), and returning to basal levels by 24 h, indicating a reproducible response across all cancer types.

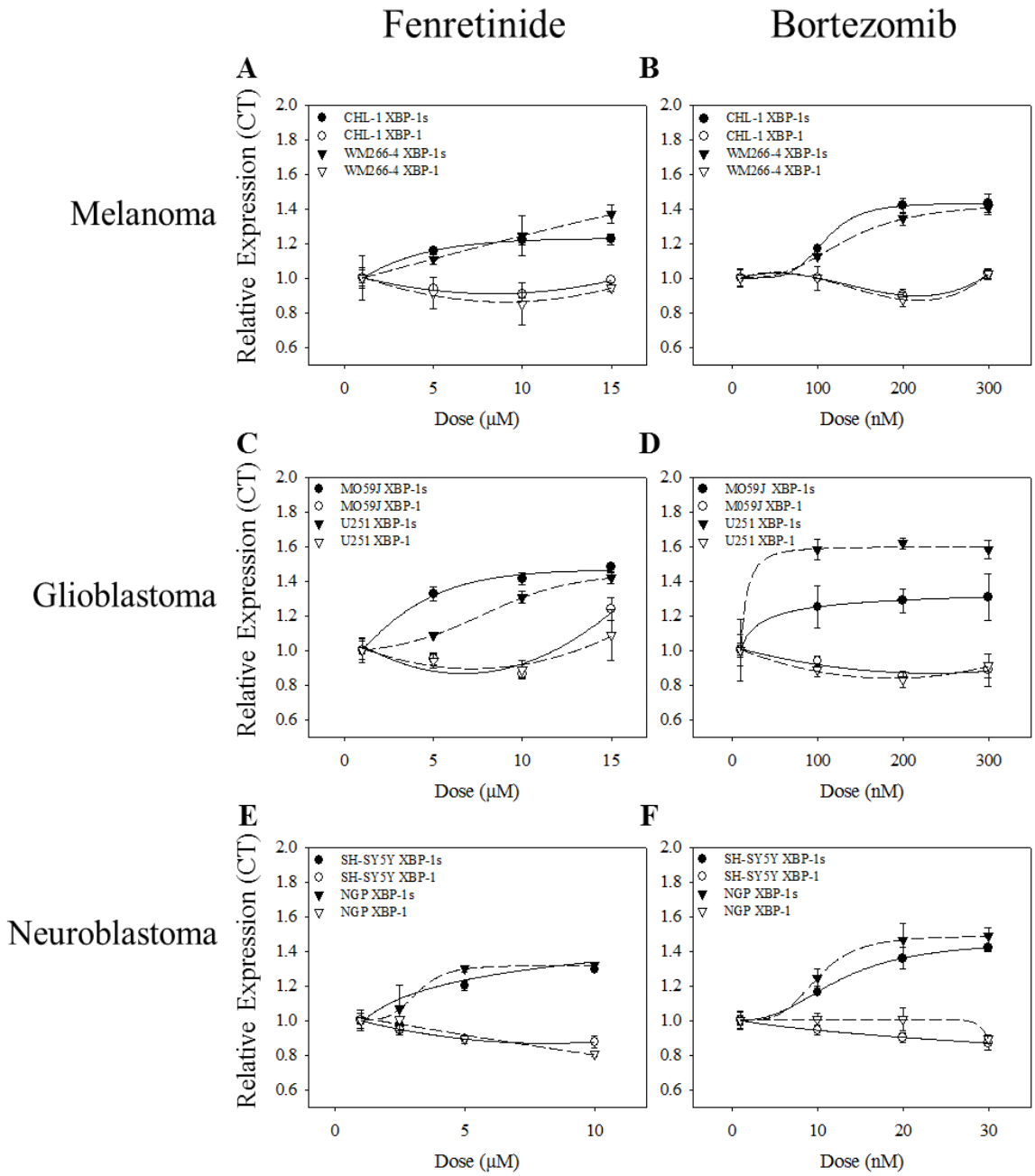

Figure 3.11: *The effect of fenretinide and bortezomib dose on ER stress-induced activation of XBP-1 splicing. CHL-1, WM266-4 (melanoma), MO59J, U251 (glioblastoma), NGP and SH-SY5Y (neuroblastoma) cell lines were treated with fenretinide (FenR, 1 - 15 µM for melanoma or glioblastoma or 0.1 - 10 µM for Neuroblastoma) or bortezomib (Bort, 10 - 300 nM for melanoma or glioblastoma or 1 - 30 nM for Neuroblastoma) for 4 h prior to harvesting. Cells were then counted and assessed by real time PCR for XBP-1 and XBP-1s expression over time, using actin as control. Data were expressed as the mean of 3 independent experiments ± 95% CI.*

To complete the characterisation of the activation of the UPR within neural-crest-derived melanoma, glioblastoma and neuroblastoma cancer cells, the activation of the IRE1 arm of the UPR was assessed by measurement of the product of splicing of XBP-1, a downstream process of active IRE1. As in previous experiments, cells were treated with increasing doses of fenretinide or bortezomib (1 – 15 μM fenretinide and 10 – 300 nM bortezomib for melanoma and glioblastoma or 0.5 – 10 μM and 1 – 30 nM bortezomib for neuroblastoma) for 4 h prior to real time PCR analysis for the expression of UPR components XBP-1 and XBP-1s in comparison to β-Actin (Figure 3.11).

Data demonstrated a significant dose dependent induction of XBP-1s in all cell lines with increasing doses of fenretinide, coupled with a significant reduction in XBP-1 (Figure 3.11 A, C & E). There was a significant induction of XBP-1s for all cell lines after treatment with 5 μM fenretinide (One-way Anova with Dunnett's post hoc corrections, for WM266-4, U251 or SH-SY5Y cell lines = $P < 0.05$, and CHL-1 or NGP = $P < 0.01$ or MO59J = $P < 0.0001$), however only melanoma cells showed a significant depletion of XBP-1 at 5 μM concentrations (One-way Anova with Dunnett's post hoc corrections, for CHL-1 and WM266-4 = $P < 0.0001$). All cell lines showed increasing significance of XBP-1s formation with dose (For melanoma and glioblastoma = $P < 0.0001$ or for neuroblastoma = $P < 0.005$). For the depletion of XBP-1, fenretinide influenced expression in melanoma and neuroblastoma significantly (One-way Anova with Dunnett's post hoc corrections, for CHL-1 and WM266-4, 5 & 10 μM = $P < 0.0001$, 15 μM for WM266-4 = $P < 0.01$), but showed no significant reduction in XBP-1 in glioblastoma cell lines ($P > 0.05$).

With respect to bortezomib, there was a significant dose induction of splicing of XBP-1 in all cell lines tested (Figure 3.11 B, D & F). For melanoma and glioblastoma cells a significant increase in XBP-1s occurred in response to 100 nM bortezomib (One way Anova with Dunnett's post hoc corrections, for WM266-4 = $P < 0.01$, CHL-1 and U251 = $P < 0.001$ or MO59J = $P < 0.0001$) while in neuroblastoma cell lines a significant increase in XBP-1s was detected by 10 nM concentrations (One-way Anova with Dunnett's post hoc corrections, SH-SY5Y = $P < 0.005$, NGP = $P < 0.001$). All cell lines demonstrated higher significance with dose (all cell lines reaching = $P < 0.0001$). The effect of bortezomib on expression of XBP-1 expression demonstrated a significant reduction (One-way Anova with Dunnett's post hoc corrections, for melanoma 200 nM bortezomib = $P < 0.01$, U251 cells treat with 100 nM = $P < 0.05$, glioblastoma treated

with 200 nM or above = $P < 0.001$ or SH-SY5Y treat with 20 nM bortezomib = $P < 0.01$, neuroblastoma with = 30 nM bortezomib $P < 0.001$).

These data demostrate a significant induction of splicing by fenretinide or bortezomib. Comparing individual cell lines, for glioblastoma cells there was a significant difference between XBP-1s formation ($F_{4, 72} = 22.3$, $P < 0.0001$), however for melanoma and neuroblastoma for both XBP-1s formation and XBP-1 depletion or glioblastoma for XBP-1 depletion, there was no significant difference in cellular response to either agent ($P > 0.05$). These data parallel the conclusions for the activation of the ATF6 arm of the UPR where a similar response was achieved. Thus, with regards to XBP-1 splicing, these data demonstrate a significant difference between cancer types and their response to either fenretinide and bortezomib (analysis by 2 Way ANOVA $F_{2, 24} = 38.2$ or 64.5, $P < 0.001$ for both), highlighting a difference in the degree of UPR activity across melanoma, glioblastoma and neuroblastoma cancer models.

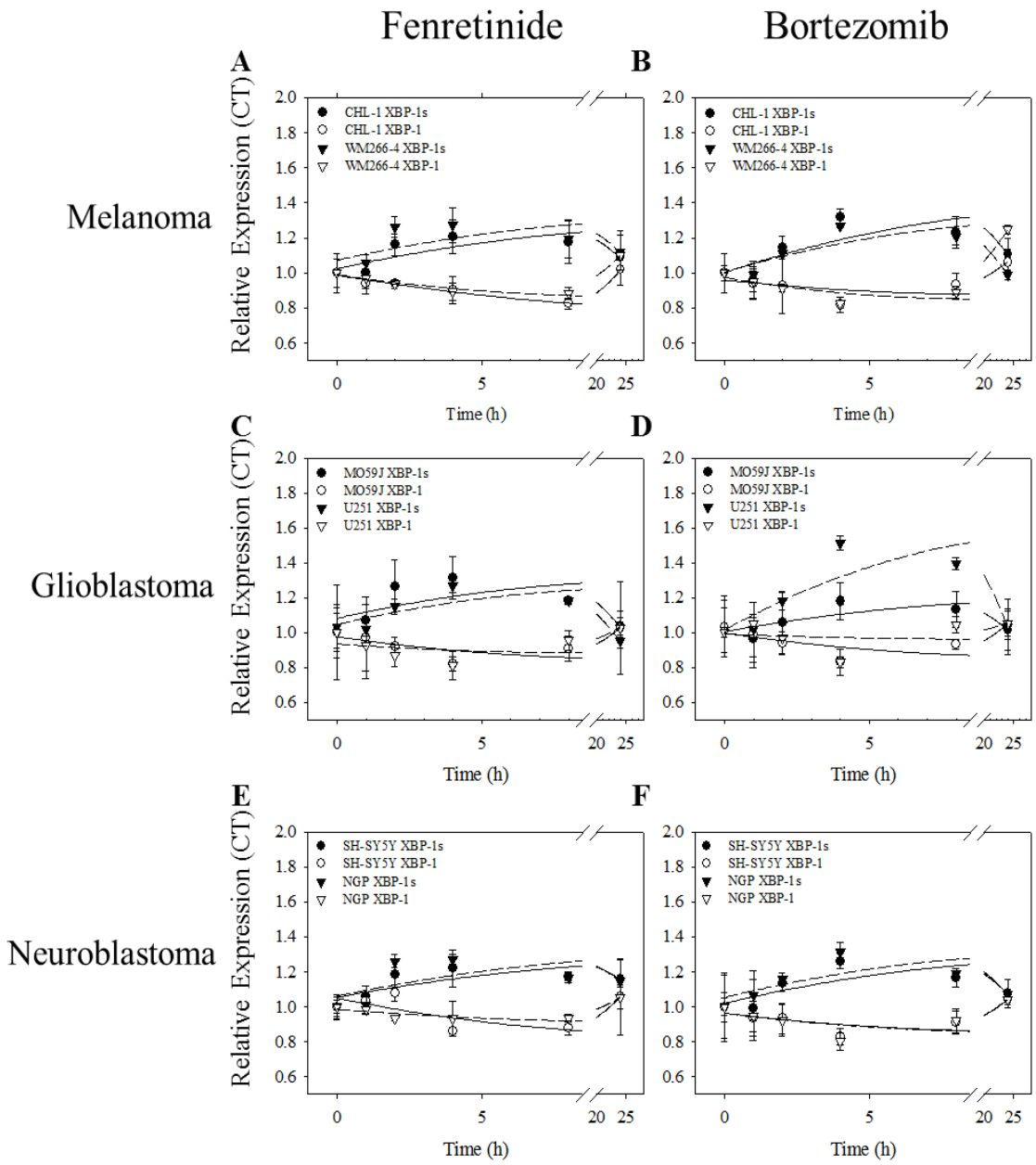

Figure 3.12: *Assessing the effect of fenretinide and bortezomib induced XBP-1 splicing over time. CHL-1, WM266-4 (melanoma), MO59J, U251 (glioblastoma), NGP and SH-SY5Y (neuroblastoma) cell lines were treated with fenretinide (FenR, 10 µM for melanoma or glioblastoma or 5 µM for Neuroblastoma) or bortezomib (Bort, 200 nM for melanoma or glioblastoma or 20 nM for Neuroblastoma) for 0, 1, 2, 4, 8 and 24 h prior to harvesting. Cells were then counted and assessed by real time PCR for XBP-1 and XBP-1s expression over time, using actin as control. Data were expressed as the mean of 3 independent experiments ± 95% CI.*

Investigating the activity of the IRE1 branch of the UPR over time to stress, cells were treated with either fenretinide or bortezomib (10 μM fenretinide and 200 nM bortezomib for metastatic melanoma and glioblastoma cell lines or 5 μM fenretinide and 20 nM bortezomib for neuroblastoma cell lines for 0, 1, 2, 4, 8 and 24 h prior to analysis for the formation of XBP-1s in comparison to the expression of XBP-1, in relation to β-Actin (Figure 3.12).

For the effect of fenretinide on the formation of XBP-1s, all cells showed a significant increase in XBP-1s by 2 h (Figure 3.12 A, C & E, One-way Anova with Dunnett's post hoc corrections, for CHL-1 = $P < 0.05$, WM266-4 and both glioblastoma and neuroblastoma cell lines = $P < 0.0001$), however, only metastatic melanoma and NGP neuroblastoma cells demonstrated a significant depletion in endogenous XBP-1 at 2 h (One-way Anova with Dunnett's post hoc corrections, for CHL-1 and WM266-4 melanoma cells = $P < 0.001$ or NGP = $P < 0.005$), and showed a significant increase in XBP-1s up to the 4 h time point (One-way Anova with Dunnett's post hoc corrections, for all cell lines = $P < 0.0001$) or a depletion up to the 8 h time point (One-way Anova with Dunnett's post hoc corrections, for both melanoma and neuroblastoma cell lines = $P < 0.0001$) or up to the 4 h for glioblastoma (both cell lines = $P < 0.005$). Data demonstrated a normalisation in either XBP-1 or XBP-1s expression levels, as the system returned to equilibrium, at 24 h, except for neuroblastoma cells that still demonstrated a significant expression of XBP-1s (Both cell lines = $P < 0.0001$).

The effect of bortezomib on XBP-1 splicing over time (Figure 3.12 B, D & F) showed a response similar to that of fenretinide (Figure 3.11 A, C & E). Data showed a significant induction of XBP-1s formation by 2 h in all cells (One-way Anova with Dunnett's post hoc corrections, for NGP and SH-SY5Y = $P < 0.05$, CHL-1 = $P < 0.005$, WM266-4 and U251 = $P < 0.001$), except for MO59J that showed a significant induction by 4 h ($P < 0.05$).

Bortezomib, for all cell lines, demonstrated maximal induction of XBP-1s formation (One-way Anova with Dunnett's post hoc corrections, for MO59J cells = $P < 0.05$ and for all other cell lines = $P < 0.0001$) and XBP-1 depletion (For metastatic melanoma and neuroblastoma cell lines = $P < 0.0001$ or both glioblastoma cell lines) by 4 h, followed by a gradual normalisation of expression to basal by 24 h. XBP-1 expression, like that of ATF6 is induced by the UPR to recover the system and allow for a prolonged activation of the UPR and therefore recovery is required to reset the system.

These data thus indicate the basic characteristics of both the IRE1 and ATF6 arm of the UPR respond to stress over a similar period of time, with no discrimination between the types of stress. Further investigation demonstrated no significant difference between the responses to fenretinide across cancer types ($P > 0.05$), with regard to XBP-1s formation. However, data demonstrated a significant difference between cancer cell types in their response to bortezomib induced ER stress ($F_{6, 108} = 62.9$, $P < 0.01$).

Therefore this work demonstrated a cancer types capacity to activate UPR can vary within each arm of the UPR. Melanoma demonstrated significantly higher induction of ATF4 than glioblastoma or neuroblastoma, yet activated XBP-1 splicing and ATF6 cleavage to a similar magnitude. This study also demonstrated that XBP1 splicing occurred for significantly longer in neuroblastoma.

3.2.4: Results Summary.

- Cellular concentrations of GRP78 differed across neural-crest-derived cancer types with human metastatic melanoma cells demonstrating significantly higher expression.
- Cell lines within a certain cancer types expressed GRP78 to the same extent, demonstrating a cell type-specific requirement.
- In neural-crest-derived cancer models, expression of the UPR activators did not correlate with GRP78 expression, with IRE1 showing a significantly higher expression than either PERK or ATF6.
- Co-localisation analysis of GRP78 to calnexin demonstrated differences in GRP78 distribution between cancer types. However, GRP78 was predominantly cytoplasmic within all cancer types.
- Induction of stress by either fenretinide or bortezomib increased co-localisation, suggesting a stress triggered migration of GRP78.
- Exposure to fenretinide or bortezomib induced UPR, demonstrated by induction of ATF4, splicing of XBP-1 or cleavage of ATF6.
- Cancer types demonstrated differences in the magnitude of response to ER stress stimulated ATF4 induction, with melanoma cells showing greater response to that of glioblastoma or neuroblastoma.
- Neural-crest-derived cancer cells showed similar levels of induction of XBP-1s, however neuroblastoma demonstrated activation for significantly longer than either glioblastoma and neuroblastoma cells.
- ER stress-induced ATF6 cleavage by fenretinide and bortezomib, as for XBP-1 splicing, was observed to a similar extent across cancer types.

3.3: Discussion.

Investigating the UPR across differing neural-crest-derived cancer cells demonstrated differences in cellular concentrations of GRP78. Furthermore, the cellular concentrations of UPR activators did not correlate with GRP78 expression, demonstrating a cell line-dependent concentration of PERK, IRE1 or ATF6. The expression of the UPR activators also showed a significant difference in cellular concentrations within all cancer types, with IRE1 demonstrating the highest expression. Furthermore, comparing GRP78 to the cellular concentration of total UPR activators, melanoma and glioblastoma cancer types demonstrated higher expressions of GRP78, compared to neuroblastoma cells, however, neuroblastoma cells displayed higher concentrations of UPR activators compared to levels of GRP78.

Differences in GRP78 cellular concentrations between cancer types suggested the existence of a cell type specific requirement. Although these cells have all originated from the neural-crest, significant differentiation occurs to generate cells designed for specialized jobs. The significantly higher expression of GRP78 in melanoma in comparison to melanocytes suggests a disease-related increase. These findings confirm that of Zhuang *et al.*, which demonstrated an increase in GRP78 expression with melanoma disease state [115]. In addition, melanoma and glioblastoma may display significantly higher expression of GRP78 as a consequence of an increase in protein synthesis, which in turn has influenced ER capacity and chaperone expression [228].

Depending on cancer type, chaperones may be expressed at different cellular concentrations and although GRP78 expression was lower in neuroblastoma cells, other members of the heat shock protein family may be more highly expressed. Studies have shown that total chaperone expression counters any changes in overall expression by up or down regulating family members to maintain equilibrium [229]. Although GRP78 expression levels in the present study were significantly higher in melanoma, compared to neuroblastoma, GRP94 has been shown to be over-expressed in neuroblastoma and hence GRP78 was observed to be expressed to a lesser extent [230]. Nevertheless, these findings do not necessarily confirm a cancer type specific difference in total chaperone expression. However, results derived from the present study may suggest a difference between cancer types in their dependence on GRP78 and the UPR as a mechanism to buffer cellular insults or for protein turn-over in general.

Quantification of UPR activator expression highlighted the importance of IRE1. The evolutionary conserved component of the UPR [231] showed a significantly higher cellular concentration than either of the other two UPR activators, suggesting that IRE1 may still function as the primary UPR activator in the cellular response to stress and although the mammalian UPR has developed a complex and diverse set of cascades [226], IRE1 signalling is still essential.

Stoichiometric analysis also showed that melanoma and glioblastoma cell lines exhibited significantly higher cellular concentrations of GRP78 compared to the combined concentrations of PERK, IRE1 and ATF6; however, in neuroblastoma the opposite was observed (For melanoma 1 : 0.65 , Glioblastoma 1 : 0.7 and neuroblastoma 1 : 1.5, averaged between cell lines of the same cancer type). These data suggest differences between GRP78 and the UPR activators with regard to the dynamic equilibrium of the UPR. It is well established that GRP78 acts as a central inhibitory hub of the UPR, binding to PERK, IRE1 and ATF6 under periods of normal physiology [209]. These data suggest that for melanoma and glioblastoma a large reservoir of free GRP78 exists which may interact with unfolded of mis-folded protein substrates, reducing the probability that a GRP78 molecule, that is inhibiting a PERK, IRE1 or ATF6, will come into contact with a substrate. However for neuroblastoma this relationship was reversed, indicating a population of cells with free UPR activators under periods of normal physiology, suggesting that these cells have the capability to present an active UPR at any time.

The observed differences in cell line co-localisation of GRP78 and ER resident calnexin suggests differences in ER capacity. As GRP78 has been shown to exist in the nucleus, peri-nucleus, cytoplasm and cell membranes of a number of different cell type, differences in co-localisation suggests cell types exert differing ER capacity, and demonstrating lower co-localisation to calnexin. When melanoma and glioblastoma cells were stressed by either fenretinide or bortezomib, a significant increase in co-localisation was observed, suggesting ER stress related recruitment of GRP78 to the ER. This would result in an increase in the concentration of GRP78 within the ER and allow a cell to buffer higher levels of stress, prior to the activation of the UPR, increasing the probability of cell survival, by increasing the ER chaperone activity.

Mapping the activation of the UPR over time using fenretinide and bortezomib as inducers of ER stress demonstrated cancer types respond differently, depending on the

type of stress present. Research by Lin *et al.,* showed that time of activation of each arm of the UPR is critical in determining a cells fate to stress and requires prolonged activation of PERK after other UPR activators had been attenuated [225]. The present study demonstrated that all three cancer types respond differently to ER stress, with bortezomib showing a greater ability to activate the UPR than fenretinide. These observations suggest differences in the mechanism of action and ultimately the manner to which either agent perturbs the ER, can affect the response outcome. Bortezomib induces inhibition of the 26S proteasome exerting a more ER specific stress, rather than the accumulation of ROS by fenretinide [82, 201, 203, 232-240]. Interestingly, although fenretinide has been shown to induce cell death via ER stress, the activation of the PERK arm never exceeded that of the IRE1 arm, suggesting that time difference between UPR branches is not the determining factor for life or death, with regards to ROS induced ER stress [225]. Data demonstrated a significantly greater induction of ATF4 in melanoma than glioblastoma and neuroblastoma, yet there was no significant difference between PERK expression. This suggests that differences may exist in ATF4 mRNA transcription and/or translation.

The effect of ER stress on UPR within neuroblastoma highlighted a prolonged activation of IRE1, showing a significantly different response to that of melanoma and glioblastoma. This difference was present when neuroblastoma cells were treated with either fenretinide or bortezomib and may suggest that there is an imbalance of GRP78 to UPR activator expression within this cancer type. Studies have indicated the importance of the PERK arm of the UPR for the induction of the pro-apoptotic transcription factor Gadd153 [112, 220, 241], however it has also been shown that IRE1 is capable of promoting cell death, either by the induction of Gadd153 transcription or via JNK activation [213]. These data suggest that although the PERK cascade demonstrates activity under ER stress-induced by either fenretinide or bortezomib, IRE1 maybe essential within the response of the UPR.

However, the differences in the activation of IRE1 over time observed in neuroblastoma cells would also imply the presence of another regulatory body for IRE1 activation, as the formation of XBP-1s was only present after stimulation by ER stress-inducing agents. Research into the activation of IRE1 in yeast has demonstrated the requirement of IRE1 to interact with an unfolded protein after dissociation from GRP78 to become active. This work did not correlate with human IRE1, but does suggest that IRE1 may

undergo a more complex activation, requiring release from GRP78 and a secondary trigger prior to becoming capable of signalling to the nucleus [242].

The activity of the ATF6 element of the UPR demonstrated a significant response from 2 h until the UPR induction of ATF6 and IRE1 replenished the system after 8 h [243]. The present study however, could only demonstrate significant activation of the ATF6 arm of the UPR (and therefore loss of full length protein) from 2 h and was unable to demonstrate the presence of the activated cleaved ATF6 fragment, which would allow for a conclusive assessment of the total activity of this arm of the UPR.

For the effect of ER stress on the activation of the UPR, neuroblastoma cells were treated with significantly lower doses of either fenretinide or bortezomib, compared to melanoma and glioblastoma due to their increased sensitivity to death by either agent. Although neuroblastoma cells were more sensitive to fenretinide/bortezomib-induced cell death compared to the utilised melanoma cells, induction of ATF4 was markedly decreased. Induction of XBP-1 splicing and ATF6 cleavage however was similar across all cancer cell types. These data thus suggest ATF4 mediated Gadd153-induced cell death is not crucial for neuroblastoma cells in response to either fenretinide or bortezomib.

Due to the differences observed within the UPRs response to ER stress, further research into the effect of the dynamic equilibrium between GRP78 and UPR activators across cancer types and their response to cellular stress is required. Developing a more comprehensive understanding of the UPR and the role that it plays in cancer cell resistance, aggression and overall survival to either natural or pharmaceutical stimuli is warranted and may allow for a more specific targeting strategy and overall improvement in prognosis for cancer patients. Previous studies have correlated GRP78 expression with tumour stage and progression, as well as chemo-resistance. In a vast number of solid tumours including the neural-crest-derived melanoma and glioblastoma cancer types [113, 115], increased GRP78 expression correlated with a poor prognosis, however in studies of acute myeloid leukaemia and neuroblastoma, increased GRP78 correlated with a favourable outcome [116]. Further studies were therefore required to establish the role of GRP78 and the relationship with UPR activation and to test the hypothesis that GRP78 expression influences cellular UPR signalling and downstream activation of death stimuli, ultimately affecting cellular survival.

3.4: Conclusion.

This study highlights a cancer type specific expression of GRP78, which does not correlate to the individual expressions of the UPR activators. Comparing GRP78 and the UPR activators showed that unlike melanoma or glioblastoma, neuroblastoma contained a higher concentration of UPR activators than GRP78 to inhibit them. ER stress-induced ATF4 expression highlighted that cancer types respond differently to stressors, as well as possess different capacity to induce ATF4 expression, with melanoma capable of inducing greater levels. Although differences were observed between ATF4 induction, the magnitude of response for both XBP-1 splicing and ATF6 cleavage were similar across cancer types, with neuroblastoma showing detectable levels of XBP-1s longer than melanoma and glioblastoma.

Chapter 4:

Reduction in GRP78 expression affects the response of cancer cells to ER stress-induced cell death.

4.1: Introduction.

In eukaryotic cells, proteins (both membrane and secretory) are folded and assembled within the ER before transport to the cell surface or destination organelle [206]. Newly-synthesised proteins enter the lumen of the ER where they often undergo glycosylation [206]. For a protein to reach its functional tertiary or quaternary structural state, it must undergo physical processing, where bonds are actively added to maintain the complex structures required for a functional state. This is often achieved by the addition of disulphide bonds [206]. Cellular insults can hinder these processes by altering environmental conditions within the lumen of the ER, achieving a state that no longer promotes correct secondary structure formation or affects the ability of bond formation, as a direct consequence of changes to the ER redox state [206]. As a consequence, cells activate intracellular signalling pathways which regulate protein folding capacity of the cell [91, 111]. The UPR consists of 3 individual signalling cascades initiated by IRE1, PERK and ATF6 [91, 111]. Upon activation of these three UPR signalling proteins, the outcome is initially a pro-survival response to any cellular insult that has perturbed the functioning of the ER followed by the activation of cell death pathways if the stress is too severe or persistent. To regulate this homeostatic response, each UPR activator binds to and is inhibited by the central stress regulator GRP78 [168, 209, 244-246].

Studies by Kohmo, Shen and Bertolotti *et al.,* have demonstrated a direct interaction between PERK, IRE1 and ATF6 [168, 209, 210, 247]. Using pull down experiments, Kohmo and Bertolotti *et al.,* demonstrated a dynamic interaction between GRP78 and either IRE1 or PERK. This interaction results in the prevention of self-association of PERK and IRE1, as the interaction with GRP78 masks the required luminal domain sequences, preventing homo-dimerization to the active complex (Figure 4.1) [209, 247-249]. Kohno *et al.,* demonstrated that upon ER stress, IRE1 dissociates from the substrate binding domain of GRP78 [248], allowing IRE1 to homodimerise and activate a signalling cascade to the nucleus with a consequent up-regulation of chaperone mRNA, including GRP78 [249].

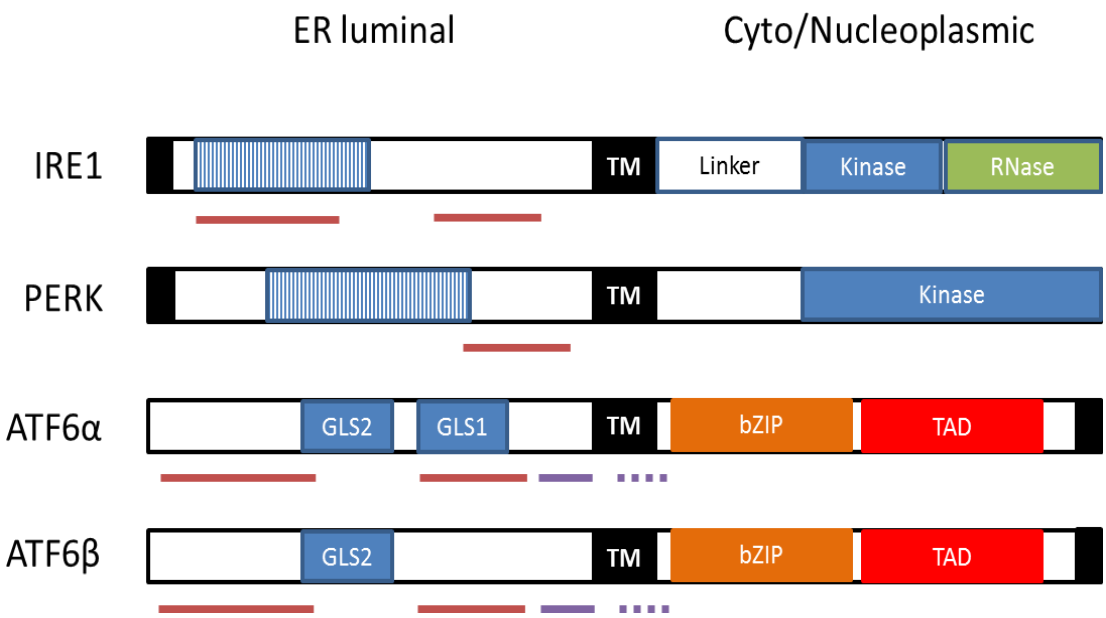

Figure 4.1: *The primary structure of the ER stress sensors: inositol requiring kinase 1(IRE1), protein kinase-like endoplasmic reticulum kinase (PERK), and activating transcription factor 6 (ATF6). Red lines represent regions interacting with BiP. The black boxes represent the signal peptides, and the blue lined boxes depict the region of limited homology between IRE1 and PERK as well as regions sufficient for signal transduction or oligomerization. Purple lines full and dotted represent the sites for site 1 protease and site 2 protease respectively. The other abbreviations are bZIP, basic leucine zipper; GLS1 and GLS2, Golgi localization sequences 1 and 2; TAD, transcriptional activation domain; and TM, trans-membrane domain. Picture modified from Schröder et al [91].*

Using a similar approach, Prywes et al, demonstrated a dynamic relationship between ATF6 and GRP78 in which dissociation occurred under periods of stress induced by DTT treatment [244-246]. These studies [244-246] demonstrated the presence of Golgi localization sequences within the luminal domain of ATF6 [168, 210] and also showed the requirement of Golgi localisation sequences for ATF6 activation. Furthermore, Shen *et al.*, also demonstrated over expression of GRP78 can prevent ATF6 activation under periods of stress by masking the Golgi localisation sequences, thus retaining ATF6 within the ER [246].

Collectively these studies clearly show an inhibitory role of GRP78, acting as a stress sensor for the activation of the UPR within mammalian cells. However, there have been

numerous studies demonstrating a correlation between GRP78 expression and UPR activation [250, 251]. These findings suggest the presence of a dynamic equilibrium between GRP78 and the UPR activators that if altered can influence the outcome of the UPR.

The fact that increased expression of GRP78 prevents the activation of ATF6 [210] suggests that the up-regulation of GRP78 as a downstream consequence of the UPR may not only function to aid ER recovery, but may also act to negatively regulate the UPR [168, 210]. Studies in melanoma, breast, colon, liver, lung and many other solid tumour types, have demonstrated increased expression of GRP78 relative to non-tumour tissue [115, 252-255], particularly in metastatic tumour cells [256]. Experiments to understand the consequence of GRP78 expression have demonstrated that, in certain cancer types such as melanoma, increased levels of GRP78 results in a more malignant and chemo-resistant phenotype. The association of UPR activators with GRP78 therefore prevents activation of death induction in the absence of stress. However, in cancerous cells, adaptations in cellular mechanisms to evade cell death and altered cellular proliferation result in a harsh environmental condition: these cells demonstrate changes in GRP78 and UPR activity. Conditioning of a cancer cell to such stress results in a favourable up-regulation of GRP78 expression, as well as the negative regulation of the UPR, that maybe suppressing the activation of UPR and the ability to induce cell death.

Suzuki et al, Sun *et al.,* and Lee *et al.,* demonstrated that knockdown of GRP78 expression increased cell sensitivity to apoptosis [251, 257, 258]. Using a Hela cell model, Suzuki *et al.,* demonstrated the activation of UPR signalling in cells with reduced GRP78, confirming the presence of a dynamic equilibrium (Figure 4.2) [251]. These data, using a p5 x ATF6-GL3 or pGL3-GRP78 luciferase assay, showed significant induction of UPR-related promoters in cells with reduced GRP78, in comparison to control. Moreover, these studies indicated the activation of XBP-1 splicing in knockdown cells and importantly demonstrated a significant induction of GADD153 [251]. Sun *et al.,* and Lee *et al.,* showed that a decrease in GRP78 significantly decreased cell proliferation and highlighted GRP78 as crucial mediator of angiogenesis, by regulating cell proliferation, survival and migration [257, 258]. Sun *et al.,* also demonstrated, in an RKO cell model, an increase in spontaneous apoptosis in cells with reduced GRP78 expression [257].

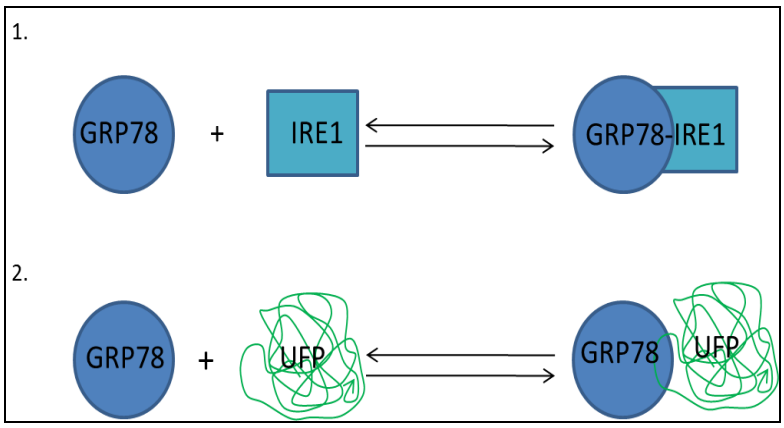

Figure 4.2: *The dynamic equilibrium of GRP78 and the activation of the UPR. The relationship that exists between GRP78 and the UPR activators PERK, IRE1 and ATF6 is crucial for life. GRP78 binds to and inactivates PERK, IRE1 and ATF6 (diagram uses IRE1 as an example). However, GRP78 has a higher affinity for unfolded or mis-folded substrates and therefore on exposure to a substrate dissociates from the UPR activator to function as a chaperone, aiding protein synthesis and ER recovery. GRP78 interaction with a substrate is dependent on the presence of either ATP/ADP. When bound to ADP, GRP78 demonstrates a stronger affinity for unfolded substrates. On replacement of ADP with ATP a much weaker attraction is present and GRP78 dissociates. The now free GRP78 is capable of binding to another protein substrate or to a UPR activator depending on proximity and substrate concentration. Therefore the expression levels of GRP78, UPR activators and unfolded protein substrates all affect the dynamic relationship present within the UPR [259].*

Studies into the effect of GRP78 expression on patient prognosis reveal a significant difference in outcome, depending on cancer type. Research specifically investigating the role of GRP78 within neural-crest-derived tumours demonstrated in melanoma and glioblastoma, an increase in GRP78 expression directly correlated with disease progression and resistance [113, 114, 224], however in the case of neuroblastoma a more favourable prognosis was associated with increased GRP78 [116]. Therefore, the aim of this study was to investigate the effect of GRP78 expression on neural-crest-derived cancer cell sensitivity to ER stress. Studies into the effect of fenretinide or bortezomib have been carried out previously, demonstrating both agents act as potent inducers of ER stress and cell death in neural-crest-derived cancer types, however to date no direct comparison has been made between differing cancer types and sensitivity to ER stress or the underlying differences in the mechanism of UPR in relation to patient prognosis [82, 203, 235, 240, 260-262].

4.2: Results.

4.2.1: Fenretinide and Bortezomib induced ER stress.

To test the hypothesis that the cellular expression of GRP78 can affect the outcome of ER stress, with regards to triggering cell death, experiments were designed to test the effect of reducing GRP78 expression on neural-crest-derived cancer cell sensitivity to ER stress-induced cell death in response to fenretinide or bortezomib. Previous studies within the group have demonstrated that fenretinide and bortezomib both potently induce cell death in melanoma and neuroblastoma cancer cell lines *in vitro* [82, 112, 203]. However, to confirm the activity of ER stress-inducing agents within this study and to determine the effect of fenretinide and bortezomib as well as the ability of either agent to induce cell death of glioblastoma cells, CHL-1 and WM266-4 (metastatic melanoma), NGP and SH-SY5Y (neuroblastoma) as well as MO59J and U251 glioblastoma cells were therefore treated with a dose range of both drugs

Using previous reports as a guide, melanoma and glioblastoma cells were treated with 2-fold or 10-fold higher concentrations of fenretinide or bortezomib respectively [82, 112], compared to concentrations of either agent used to treat neuroblastoma cells. To determine a standardised dose of both fenretinide and bortezomib for further studies, and to allow for a comparison of the UPR across cancer types as well as investigate the effect of manipulating the UPR on stress induced cell death, cells were compared for the induction of death or inhibition of cell viability for a drug dose that:

1. Gave a measurable effect for both death and viability
2. Was biologically significant in response, in comparison to control
3. Was less than the maximally inducible level for each drug (upper asymptote of dose response curves)
4. Was within the clinically-achievable dose range (below 15 μM for fenretinide or 300 nM for bortezomib)
5. Gave a significant biological and statistical affect for both cell lines of the same cancer type.

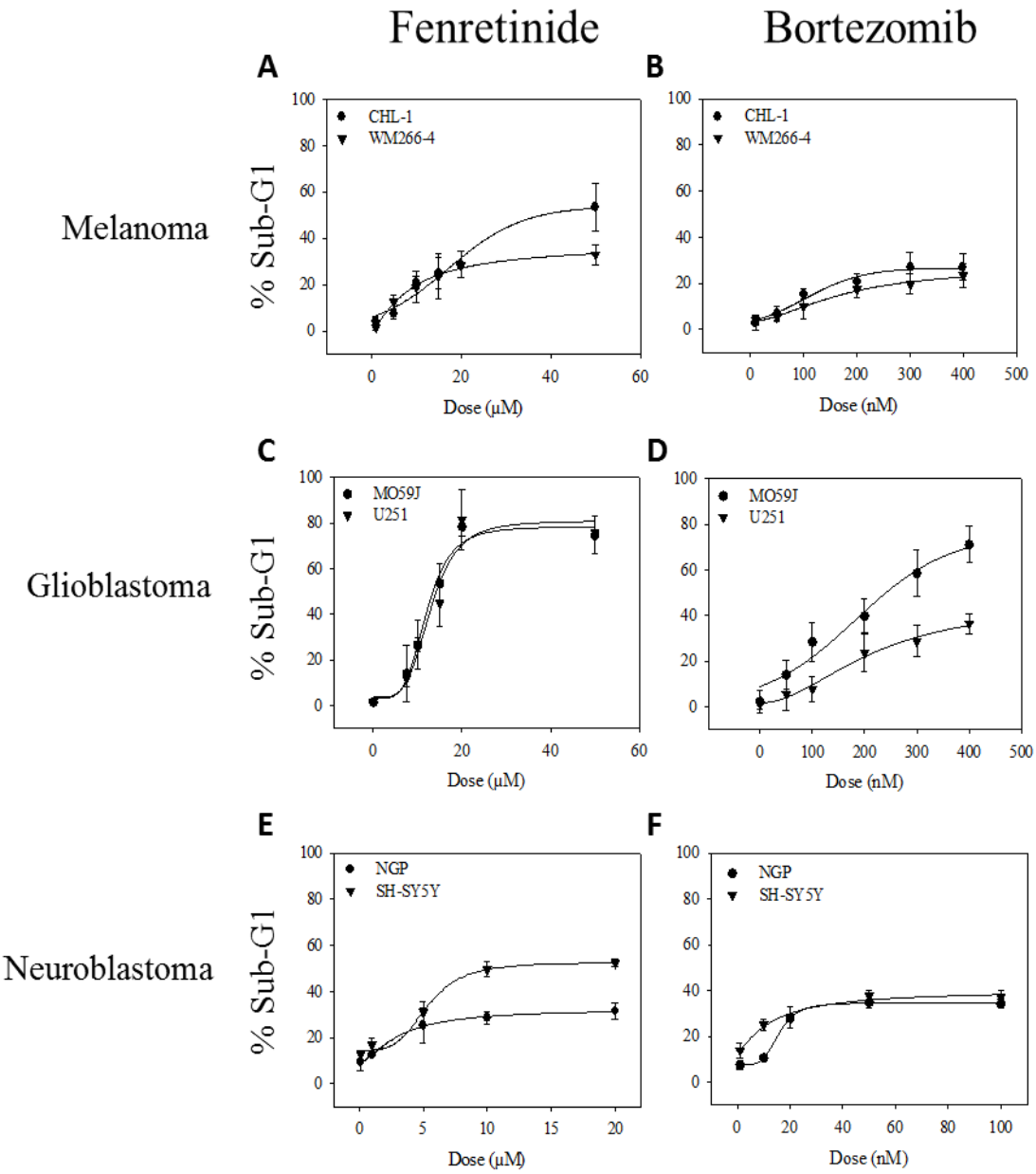

Figure 4.3: *Fenretinide- or Bortezomib-induced cell death in a panel of neural-crest-derived cancer cells. Melanoma (A & B), glioblastoma (C & D) and neuroblastoma (E & F) cells were treated with increasing doses of either fenretinide (0 – 50 µM for melanoma and glioblastoma or 0 – 20 µM for neuroblastoma cell lines) or bortezomib (0 – 400 nM for melanoma and glioblastoma or 0 – 100 nM for neuroblastoma cell lines) for 24 h prior to harvesting, and samples analysed for cell death by propidium iodide staining and flow cytometry to quantify the proportion of cells with SubG1 DNA content. Data are the mean of 3 repeat experiments ± 95% CI.*

Dose response experiments of fenretinide- or bortezomib- induced cell death of metastatic melanoma, glioblastoma and neuroblastoma cancer cells were carried out in order to determine optimal doses for subsequent experiments for the effect of GRP78 expression on cell line sensitivity. Cells were treated with increasing doses of fenretinide (0 – 50 μM for both melanoma and glioblastoma or 0 – 20 μM for neuroblastoma) or bortezomib (0 – 400 nM for melanoma and glioblastoma or 0 – 100 nM for neuroblastoma) and apoptosis assessed by flow cytometry (Figure 4.3). Data demonstrated a dose-dependent increase in cell death in response to either fenretinide or bortezomib but with no significant difference in EC_{50} values between individual cell lines ($P > 0.05$) across a single tumour type. However, significant differences in the maximum achievable level of cell death (in the achieved upper asymptote) were evident between differing tumour types.

Metastatic melanoma and neuroblastoma cells showed a significant difference in response to either fenretinide or bortezomib (Figure 4.3 A & E, One-way ANOVA comparing melanoma cells; $F_{4, 34} = 27$ or 12.8, $P < 0.0001$ for either agent, respectively, or for neuroblastoma; $F_{4, 28} = 104.9$, $P < 0.0001$ with fenretinide and $F_{4, 28} = 49.3$, $P < 0.01$ with bortezomib), with CHL-1 and SH-SY5Y suffering higher levels of cell death. The data also demonstrated differences between cell lines in the level of cell death induced by each ER stress-inducing agent. For glioblastoma cells, there was a significant difference between cell lines treated with bortezomib (Figure 4.3 D, One-way ANOVA comparing glioblastoma cell lines; $F_{4, 34} = 113.4$, $P < 0.0001$), with MO59J being the most sensitive. When treated with fenretinide, both glioblastoma cell lines responded in a similar way (Figure 4.3 C). These data showed that the susceptibility of glioblastoma to death differed depending on the ER stress-inducing agent used. Thus, cells differed in their sensitivity to death in a drug-dependant manner.

Based on the data derived in figure 4.3, optimal doses of fenretinide or bortezomib were determined; for melanoma or glioblastoma cell lines, 10 μM fenretinide or 200 nM bortezomib or for neuroblastoma, 5 μM fenretinide or 20 nM bortezomib, were subsequently used as single agent concentrations and importantly at doses which induce biologically-reproducible effects below the maximum-tolerated dose.

The effects of fenretinide or bortezomib-induced cell death as determined by FACS analysis of SubG1 were confirmed by the analysis of cell viability (Figure 4.4). Data indicated a dose-dependent increase in fenretinide or bortezomib- induced inhibition of

cell viability for all cell lines (One-way ANOVA with Dunnett's post hoc corrections, $P \leq 0.001$ for all cell lines, with either agent). Melanoma cells demonstrated differences in responses to both fenretinide and bortezomib (Figure 4.4 A & B) with regards to the maximally achievable levels of inhibition of cell viability (Figure 4.4 A, Two-way ANOVA comparing drug, $F_{4, 95} = 42.4$ or 12.3, $P < 0.01$). For glioblastoma and neuroblastoma, differences in cell line response to bortezomib were also observed, showing U251 and SH-SY5Y cells as the most sensitive (Figure 4.4 D & F, Two-way ANOVA, $F_{4, 95} = 12.6$ or 9.4, respectively, $P \leq 0.01$). However, in response to fenretinide, both cancer types responded in the same way (Figure 4.4 C & E, $P > 0.05$). Comparing cancer cell types, there was a significant difference in the Ec_{50} for fenretinide and the maximum achievable effect (Nested ANOVA, For Ec_{50} $F_{2, 12} = 16.4$, $P < 0.001$ and asymptote $F_{2, 12} = 121.4$, $P < 0.01$), with no significant differences in bortezomib response ($P > 0.05$).

Comparing the data for death and inhibition of cell viability showed that although a given cell line maybe more sensitive to death, this does not necessarily correlate with inhibition of cell viability. These data thus confirmed the single-drug dose concentrations of ER stress-inducing agents selected for use in subsequent knockdown experiments.

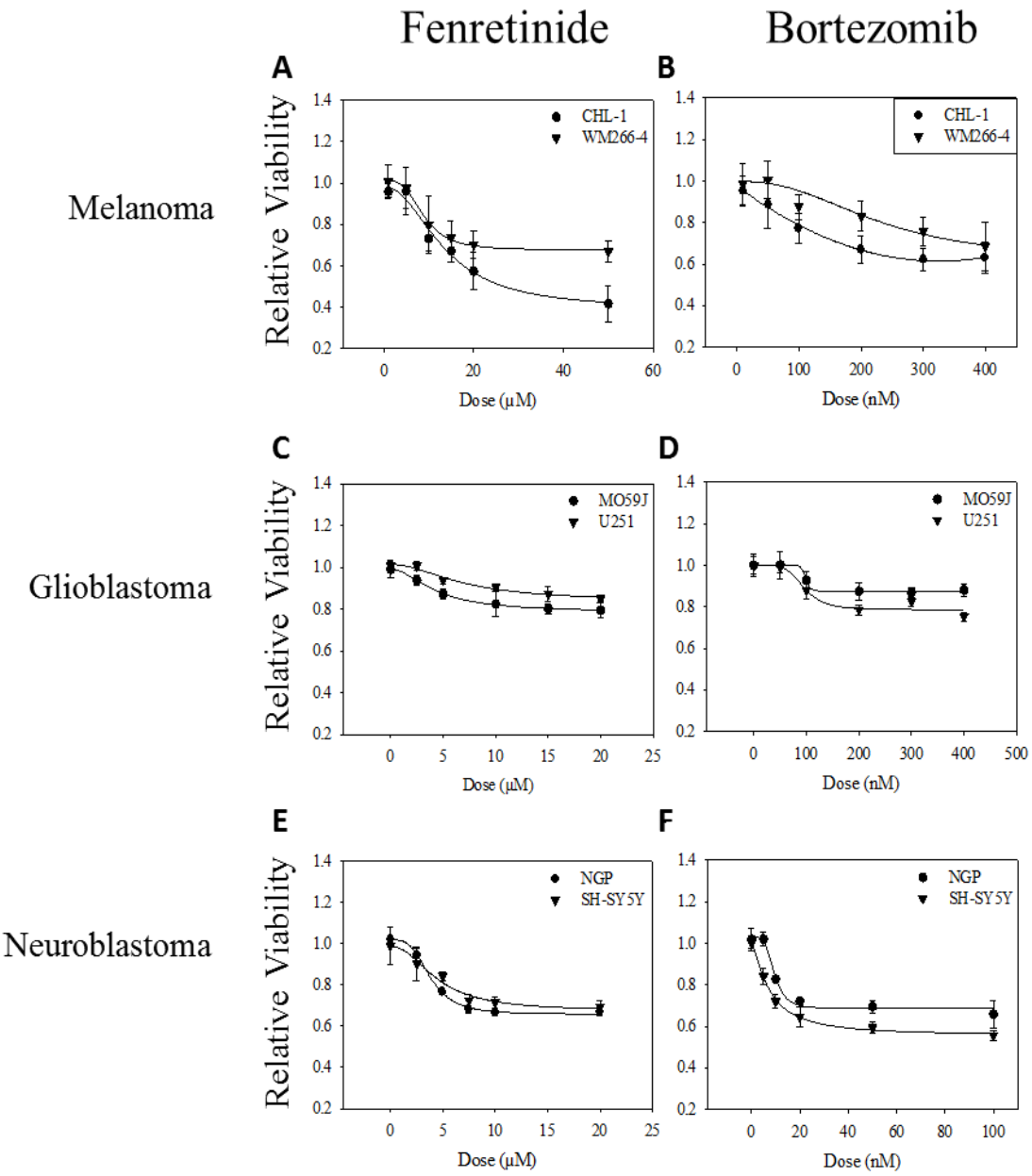

Figure 4.4: *Fenretinide and Bortezomib induced inhibition of cell viability in a panel of neural-crest-derived cancer cells. Melanoma (A & B), glioblastoma (C & D) and neuroblastoma (E & F) cells were treated with a dose response curve of either fenretinide (0 – 50 µM for melanoma and glioblastoma or 0 – 20 µM for neuroblastoma cell lines) or bortezomib (0 – 400 nM for melanoma and glioblastoma or 0 – 100 nM for neuroblastoma cell lines) for 24 h prior to harvesting and samples analysed for their effect on cell viability using the commercially available colorimetric based (MTS) metabolic assay. Experiments are the mean of 3 replicate experiments, each containing 3 replicates, ± 95% CI.*

To determine if fenretinide induces ROS accumulation and to compare the level of ER stress achieved between neural-crest-derived cancer types, cells were treated with fenretinide (10 μM for melanoma or glioblastoma and 5 μM for neuroblastoma) for 0 – 6 h prior to the assessment of ROS induction by flow cytometry of DCDHF stained cells (Figure 4.5). Cells were also treated with bortezomib (200 nM for melanoma or glioblastoma and 20 nM for neuroblastoma) for 0 – 24 h to determine if bortezomib-induced inhibition of the 26S proteasome results in protein accumulation, as measured by western blot analysis for ubiquitin and ubiquitin smears, in comparison to β-Actin as loading control (Figure 4.6).

Data (Figure 4.5) demonstrated a time dependant induction in ROS in all cell lines (One-way ANOVA with Dunnett's post hoc corrections, for all cell lines $P < 0.0001$) from a minimum of 30 minutes exposure to fenretinide (For WM266-4 melanoma cells, either neuroblastoma or glioblastoma cell line $P < 0.05$. For CHL-1 melanoma cells $P < 0.001$). Comparing cell lines of the same cancer type revealed no significant difference in response of glioblastoma or neuroblastoma ($P > 0.05$), however CHL-1 melanoma cells showed significantly higher induction of fenretinide-induced ROS, in comparison to WM266-4 cells (Two-way ANOVA, $F_{24, 47} = 59.2$, $P < 0.001$). Data for melanoma or glioblastoma demonstrated a significantly greater expression of ROS at 0 h, compared to neuroblastoma (Two-way ANOVA, $F_{6, 17} = 88.3$, $P < 0.0001$). However, over time there were no significant differences between cancer types for the induction of ROS ($P > 0.05$).

Investigating the effect of bortezomib on the accumulation of ubiquitin-tagged proteins (Figure 4.6, ubiquitin smears) demonstrated a significant increase in ubiquitin smears over time in all cell lines (One-way ANOVA with Dunnett's post hoc corrections, $P \leq 0.01$ for all cell lines). Ubiquitin was significantly induced in melanoma and glioblastoma cells by 4 h ($P \leq 0.05$), whereas induction was not significantly increased in neuroblastoma cells until 6 h ($P \leq 0.01$).

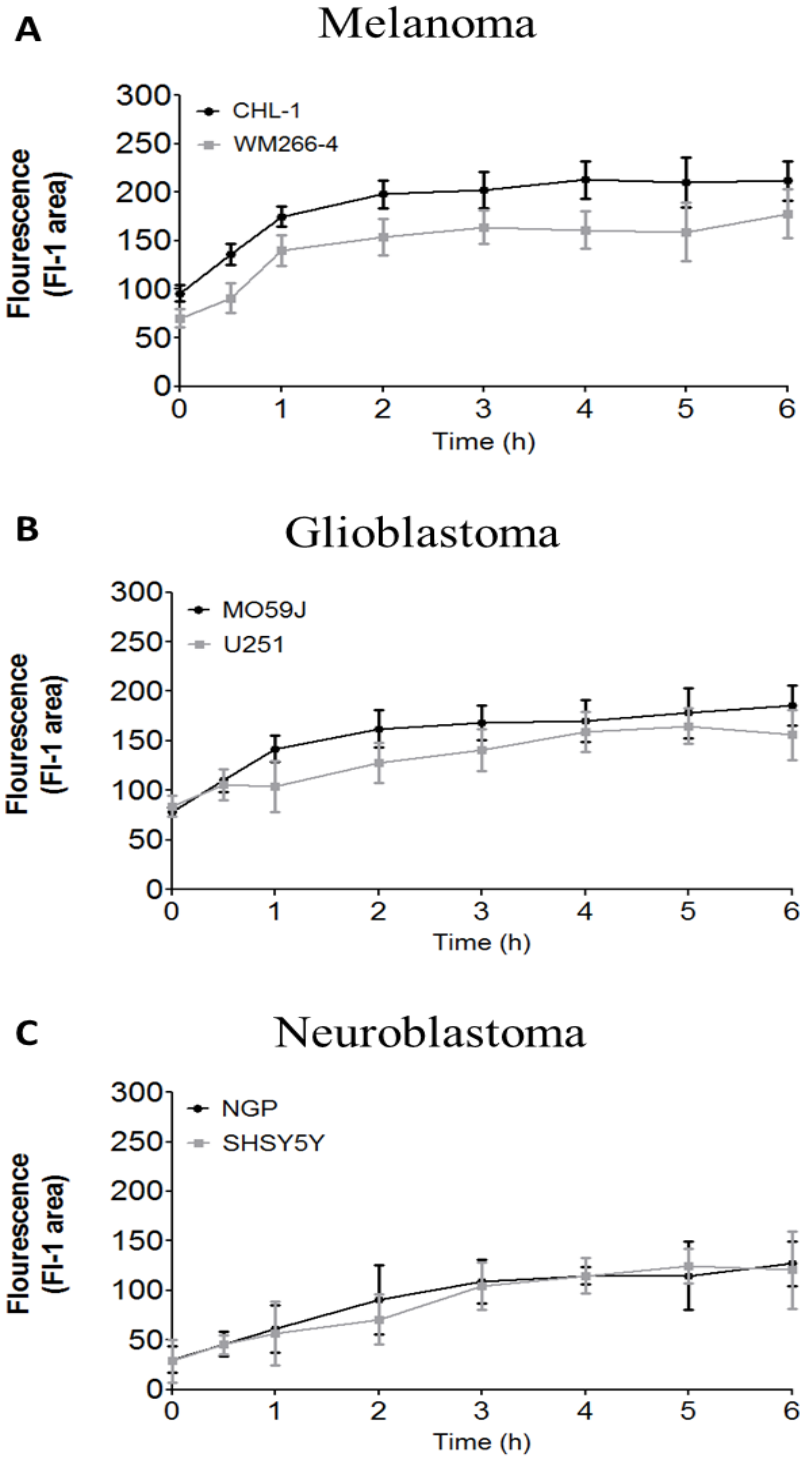

Figure 4.5: *The induction of ROS over time by fenretinide treatment. Melanoma (A), glioblastoma (B) or neuroblastoma (C) cells were treated with either 5 µM (neuroblastoma) or 10 µM (melanoma and glioblastoma) fenretinide and the induction of ROS assessed over a 6 hour time course by DCDHF staining and subsequent flow cytometry for FL-1 positivity. Data are the mean of 3 individual experiments for the FL-1 peak area ± 95% CI.*

A

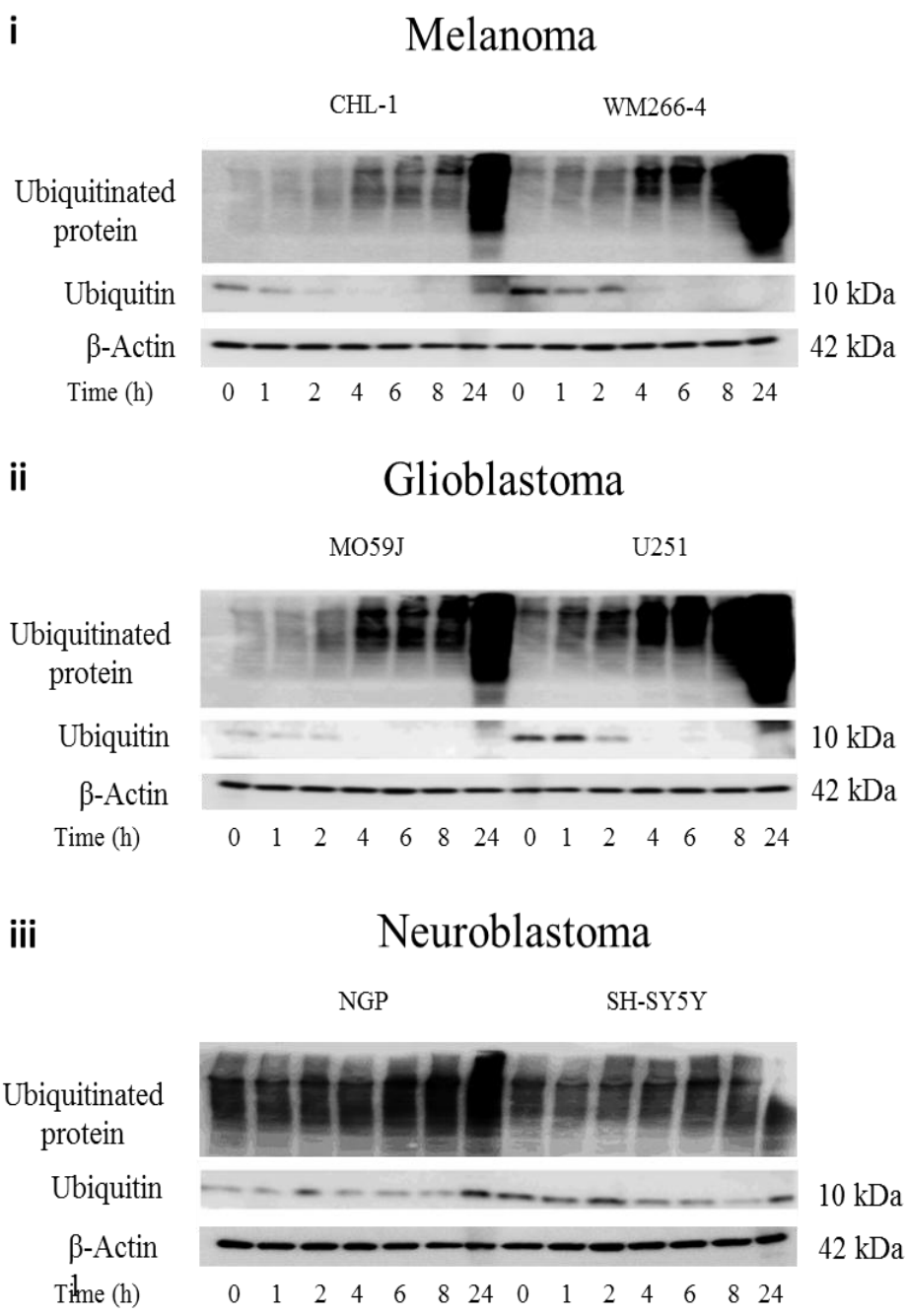
i
Melanoma
CHL-1
WM266-4
Ubiquitinated protein
Ubiquitin
β-Actin
10 kDa
42 kDa
Time (h)
0 1 2 4 6 8 24 0 1 2 4 6 8 24
ii
Glioblastoma
MO59J
U251
Ubiquitinated protein
Ubiquitin
β-Actin
10 kDa
42 kDa
Time (h)
0 1 2 4 6 8 24 0 1 2 4 6 8 24
iii
Neuroblastoma
NGP
SH-SY5Y
Ubiquitinated protein
Ubiquitin
β-Actin
10 kDa
42 kDa
Time (h)
0 1 2 4 6 8 24 0 1 2 4 6 8 24

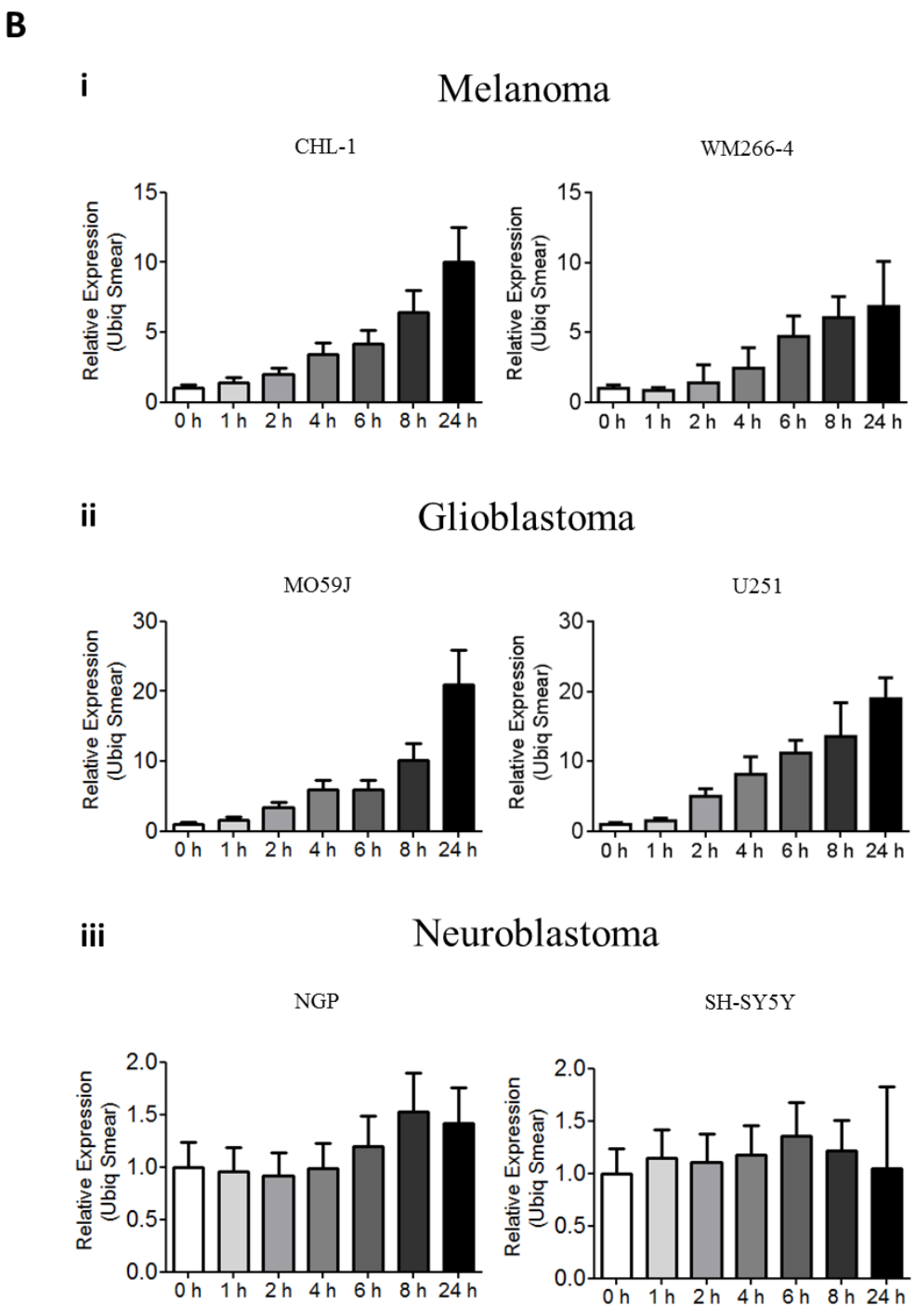

Figure 4.6: *The effect of Bortezomib treatment on 26S proteasome inhibition in neural-crest-derived-cancer cells.* ***(A)*** *Melanoma (i), glioblastoma (ii) or neuroblastoma (iii) cells were treated with either 20 nM (neuroblastoma) or 200 nM (melanoma and glioblastoma) bortezomib and samples harvested over a 24 hour time course and processed for ubiquitin smears in comparison to free ubiquitin, using β-actin as a loading control.* ***(B)*** *Densitometry analysis for the induction of ubiquitin smears by bortezomib treatment. Data are the mean of 3 individual experiments ± 95% CI.*

Data also demonstrated that ubiquitin smears were significantly increased in CHL-1 and MO59J cell lines compared to their partner cell lines, WM266-4 and U251 respectively (Two-way ANOVA, $F_{21, 41} = 94.6$ for melanoma and 129.3 for glioblastoma, $P < 0.0001$) On the other hand, data for neuroblastoma demonstrated no significant differences in effect between cell lines ($P < 0.05$).

Analysing the magnitude of response over cancer types demonstrated a significant difference in the accumulation of ubiquitin tagged proteins between melanoma or glioblastoma, compared to neuroblastoma (Two-way ANOVA, $F_{42, 125} = 45.3$ for melanoma or 94.9 for glioblastoma, $P < 0.0001$), with no significant difference observed between melanoma and glioblastoma ($P > 0.05$). Collectively these data therefore demonstrate that fenretinide and bortezomib increase ER stress, fenretinide via induction of ROS and bortezomib via the inhibition of the 26S proteasome.

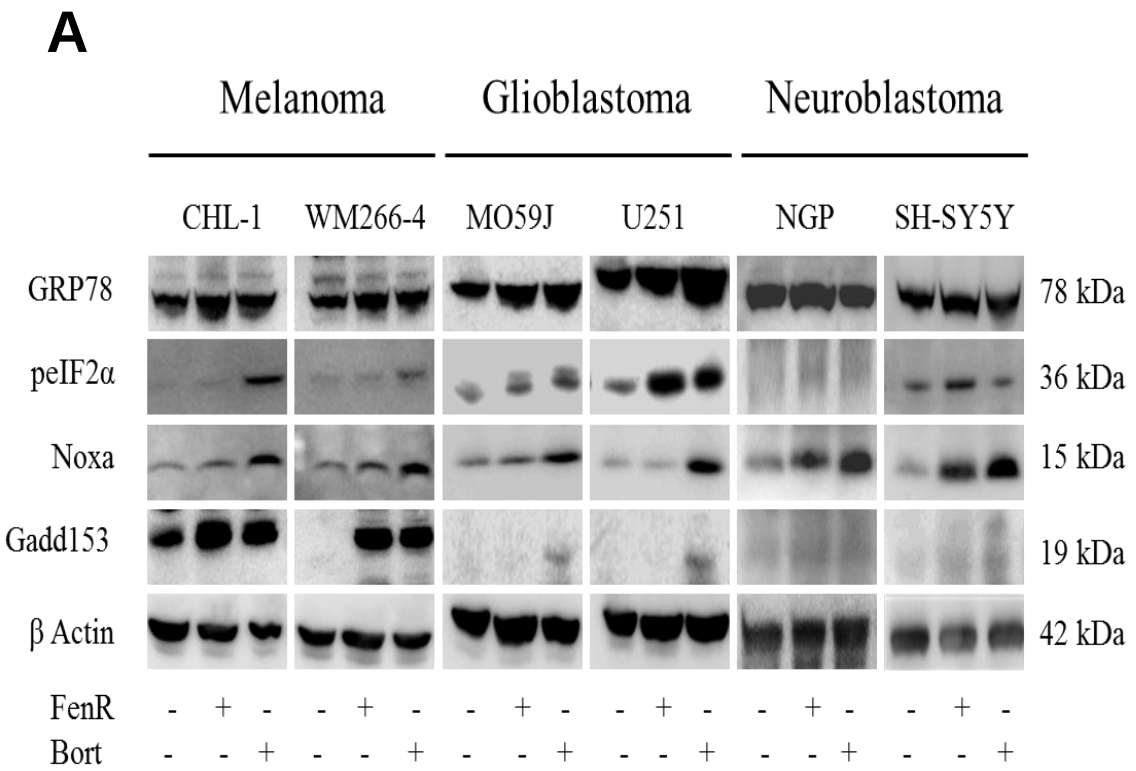

Figure 4.7: *The effect of fenretinide and bortezomib on ER stress-induced cancer cell death.* ***(A)*** *Cell lines were treated with single dose of either fenretinide (10 µM for melanoma and glioblastoma cell lines or 5 µM for neuroblastoma cell lines) or Bortezomib (200 nM for melanoma and glioblastoma cell lines or 20 nM for neuroblastoma cell lines) and incubated for 8 h prior to harvesting. Samples were than assessed by western blot for GRP78, peIF2α, Noxa, Gadd153 and β-Actin as loading control. Experimental design allows for the interpretation of UPR activation (peIF2α), induction of pro-survival chaperones (GRP78), pro-death stimuli (Gadd153) and ER to mitochondria cross talk (Noxa).* ***(B)*** *Densitometry data (data on next page) for the activation of the UPR in melanoma (i + ii), glioblastoma (iii + iv) or neuroblastoma (v + vi) by either fenretinide (grey bars) or bortezomib (black bars) were carried out on blots of 3 independent experiments in comparison to control (white bars). Data were expressed relative to β-Actin and relative to control samples (no treatment) ± 95% CI.*

B

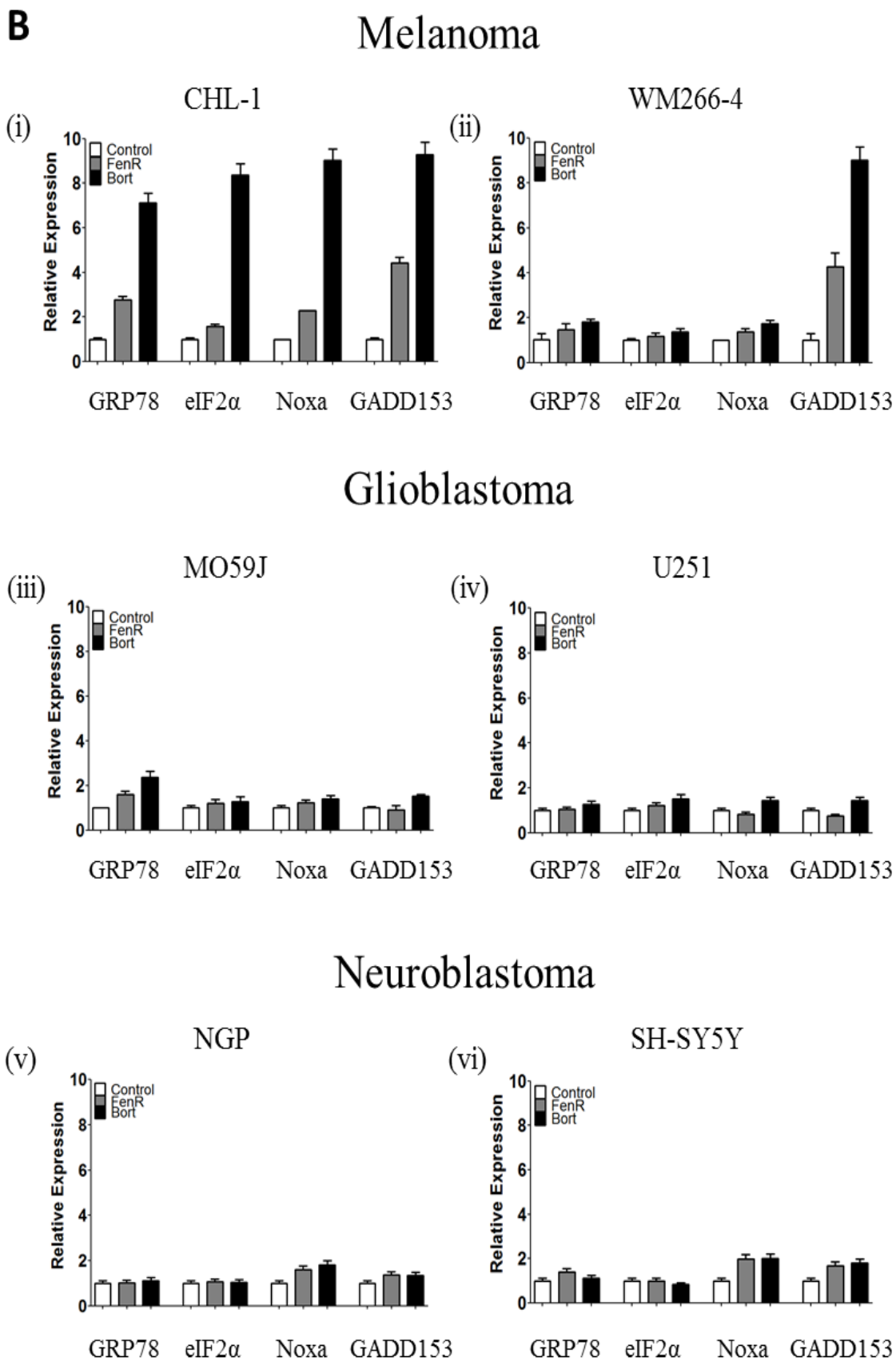
Melanoma
CHL-1
(i)
WM266-4
(ii)
Glioblastoma
MO59J
(iii)
U251
(iv)
Neuroblastoma
NGP
(v)
SH-SY5Y
(vi)
Control
FenR
Bort
Relative Expression
0
2
4
6
8
10
GRP78
eIF2α
Noxa
GADD153

To test the hypothesis that the induction of cell death in all neural-crest-derived cell lines was stimulated through ER stress activation of the UPR (Figure 4.7), cells were treated with fenretinide (10 μM for both melanoma and glioblastoma or 5 μM for neuroblastoma) or bortezomib (200 nM for both melanoma and glioblastoma or 20 nM for neuroblastoma) for 8 h prior to assessment of GRP78 and ATF4 expression by western blotting as a measure of UPR activation, GADD153 as a pro-death stimulus of the UPR and Noxa as a marker of ER-mitochondrial cross talk [184, 263].

Data demonstrated that both fenretinide and bortezomib induced a significant increase in GRP78 expression in melanoma (Figure 4.7 B; One-way ANOVA with Dunnett's post hoc correction for the effect of fenretinide in CHL-1 $P < 0.0001$ and WM266-4 $P < 0.01$ or bortezomib; CHL-1 $P < 0.0001$ and WM266-4 $P < 0.01$) and glioblastoma cells (One-way ANOVA with Dunnett's post hoc correction for the effect of fenretinide in MO59J $P < 0.01$ or bortezomib; MO59J $P < 0.0001$ and U251 $P < 0.05$). Fenretinide, however had no significant effect on GRP78 induction in U251 cells, and only fenretinide induced a significant effect in SH-SY5Y neuroblastoma cells (Figure 4.7 B; One-way ANOVA with Dunnett's post hoc correction, $P < 0.01$). There was also a significant difference between the ability of fenretinide or bortezomib to induce GRP78 expression in melanoma and glioblastoma (One-way ANOVA for treatment with either fenretinide or bortezomib for melanoma $F_{11, 25} = 438$ or 1058 and glioblastoma $F_{11, 25} = 68.2$ or 131.3 with $P < 0.0001$ respectively), with no significant difference observed in neuroblastoma. When comparing either fenretinide or bortezomib -induced GRP78 expression between cancer types, significant differences in effect between each agent were observed (Figure 4.7 B; One-way ANOVA for either fenretinide or bortezomib; $F_{5, 8} = 277.7$ or $F_{5, 8} = 1938$, $P < 0.0001$, respectively).

GRP78 induction is a consequence of UPR activation and indicative of a UPR response; however, phosphorylation of eIF2α was also assessed as an indicator of UPR activation (Figure 4.7 B); the phosphorylation of eIF2α at serine 51 is the critical step in global protein synthesis [264]. Phosphorylation results in promotion of a more specialized protein synthesis via an alternative internal ribosomal entry site (IRES), allowing for the up-regulation of key chaperones and folding machinery capable of aiding ER folding capacity during stress [264].

As for GRP78, there was a significant induction of eIF2α phosphorylation after fenretinide or bortezomib treatment in melanoma (One-way ANOVA with Dunnett's

post hoc correction, for fenretinide and bortezomib in CHL-1 $P < 0.0001$ or WM266-4 $P < 0.05$ for either agent) and glioblastoma (One-way ANOVA with Dunnett's post hoc correction for fenretinide and bortezomib in MO59J $P < 0.05$ or U251 $P < 0.05$ and $P < 0.01$, respectively), with no significant induction seen in neuroblastoma cells. Comparing fenretinide and bortezomib-induced eIF2α phosphorylation across cell lines of the same cancer type, results demonstrated a significant difference between melanoma cell lines in response to either ER stress-inducing agent, but not between glioblastoma and neuroblastoma cell types (Comparing CHL-1 $F_{2, 8} = 340.8$, and WM266-4 $F_{2, 8} = 39$, $P < 0.0001$). Induction of GRP78 also differed across cancer types (One-way ANOVA with Bonferroni post hoc correction to compare melanoma with either glioblastoma or neuroblastoma $P < 0.0001$ for both, respectively, and glioblastoma with neuroblastoma $P < 0.01$).

The induction of GADD153 (Figure 4.7 B) was compared between differing cell lines to correlate UPR activation with cell death stimulation. Results showed both fenretinide and bortezomib induced a significant induction of GADD153 in melanoma (One-way ANOVA with Dunnett's post hoc correction, for CHL-1 and WM266-4 cells with either agent $P < 0.0001$), glioblastoma (MO59J cells treated with fenretinide $P < 0.005$ or MO59J and U251 treated with bortezomib, $P < 0.01$) and neuroblastoma (Fenretinide in which fenretinide $P < 0.001$ or bortezomib $P < 0.001$ for either cell lines), except for U251 cells in which there was no significant effect. With respect to the effect of either fenretinide or bortezomib on GADD153 induction between differing cell lines, there was no difference in effect amongst cell lines of the same cancer type, but significant differences were observed between melanoma and the other cancer types (One-way ANOVA with Bonferroni post hoc correction, $P < 0.0001$).

Noxa, a member of the BCL-2 family, is a key mediator of ER stress [265] and is important for the downstream events of ER stress-induced cell death in response to fenretinide and bortezomib [184]. Results demonstrated Noxa was significantly induced by either fenretinide or bortezomib in melanoma, glioblastoma and neuroblastoma cell lines (One-way ANOVA with Dunnett's post hoc correction, for CHL-1 and WM266-4, with either fenretinide or bortezomib $P < 0.0001$, NGP and SH-SY5Y with either fenretinide or bortezomib $P < 0.001$ or MO59J and U251 with bortezomib $P < 0.01$), except for each glioblastoma cell line treated with fenretinide in which there was no significant effect. As for all other proteins tested, bortezomib was a more potent inducer of Noxa compared to fenretinide. There was a significant difference in fenretinide and

bortezomib- induced Noxa expression levels between CHL-1 and WM266-4 melanoma cells (One-way ANOVA with Bonferroni post hoc correction, for fenretinide $P < 0.005$ or bortezomib $P < 0.0001$). Except for a higher induction of Noxa in CHL-1 cells, all other cell lines demonstrated similar changes in expression, although no response was observed in glioblastoma cells treated with fenretinide (Figure 4.7 B).

Collectively these results show that fenretinide and bortezomib induced ER stress in all three cancer types, but with some variability. Melanoma cells demonstrated the greatest sensitivity to either ER stress-inducing agent with respect to inhibition of cell viability but were less sensitive to ER stress-induced cell death (Figure 4.3) compared to glioblastoma cell lines, despite this, melanoma demonstrated the most UPR activity. These data suggest the possibility of more than one pathway conferring cellular resistance to ER stress. To further evaluate the ability of fenretinide or bortezomib to induce cell death and confirm that both agents induce apoptosis, the activation of pro-caspase-3 was measured as an additional marker.

All cells lines were treated for 24 h with increasing doses of fenretinide (1 – 20 µM for melanoma and glioblastoma or 1 – 10 µM for neuroblastoma) or bortezomib (10 – 300 nM for melanoma and glioblastoma or 1 – 30 nM for neuroblastoma) within clinically-achievable dose ranges prior to analysis of caspase 3 cleavage by western blotting (Figure 4.8). Results revealed a significant difference between fenretinide and bortezomib-induced caspase-3 cleavage (One-way ANOVA, $F_{1, 23} = 15.4$, $P < 0.001$) across all cell lines. Treatment with fenretinide resulted in a dose dependent and a significant increase of caspase-3 cleavage in melanoma (Figure 4.8 A, One-way ANOVA with Dunnett's post hoc correction, for CHL-1 cells 10 µM & 20 µM $P < 0.01$ and WM266-4 10 µM & 20 µM $P < 0.05$ or $P < 0.01$ respectively), glioblastoma (Figure 4.8 C, for MO59J cells 10 µM & 20 µM $P < 0.05$ and $P < 0.01$ respectively and U251 cells 20 µM $P < 0.001$) and neuroblastoma cells (Figure 4.8 E, for NGP and SH-SY5Y cells 5 µM & 10 µM $P < 0.005$ and NGP cells treated with 2.5 µM $P < 0.05$) and these data showed no significant difference in effect between cell lines of the same cancer type and hence demonstrated a similar drug-dependent sensitivity (in terms of signal intensity) to caspase-dependent cell death.

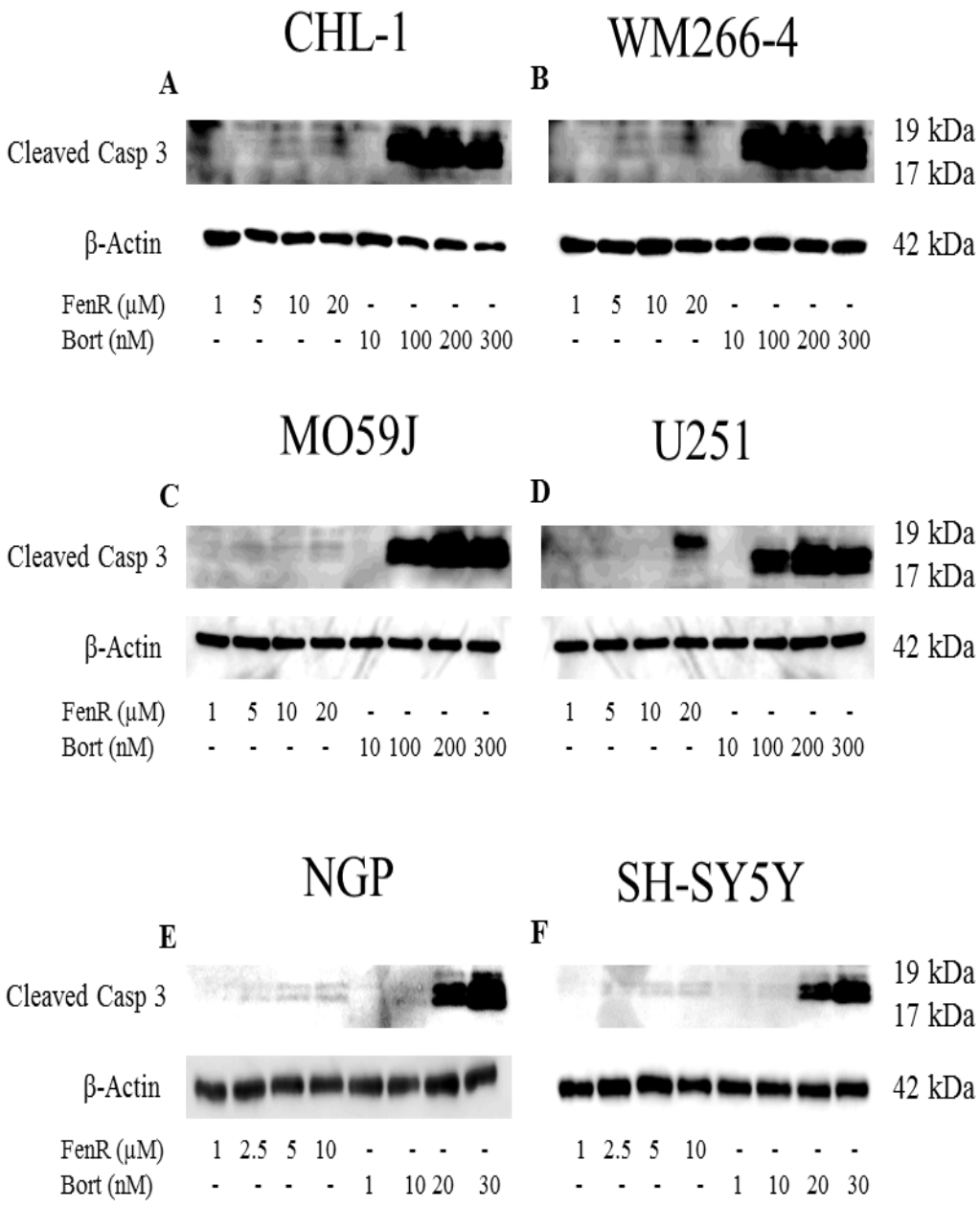

Figure 4.8 continued on next page.

Figure 4.8 continued.

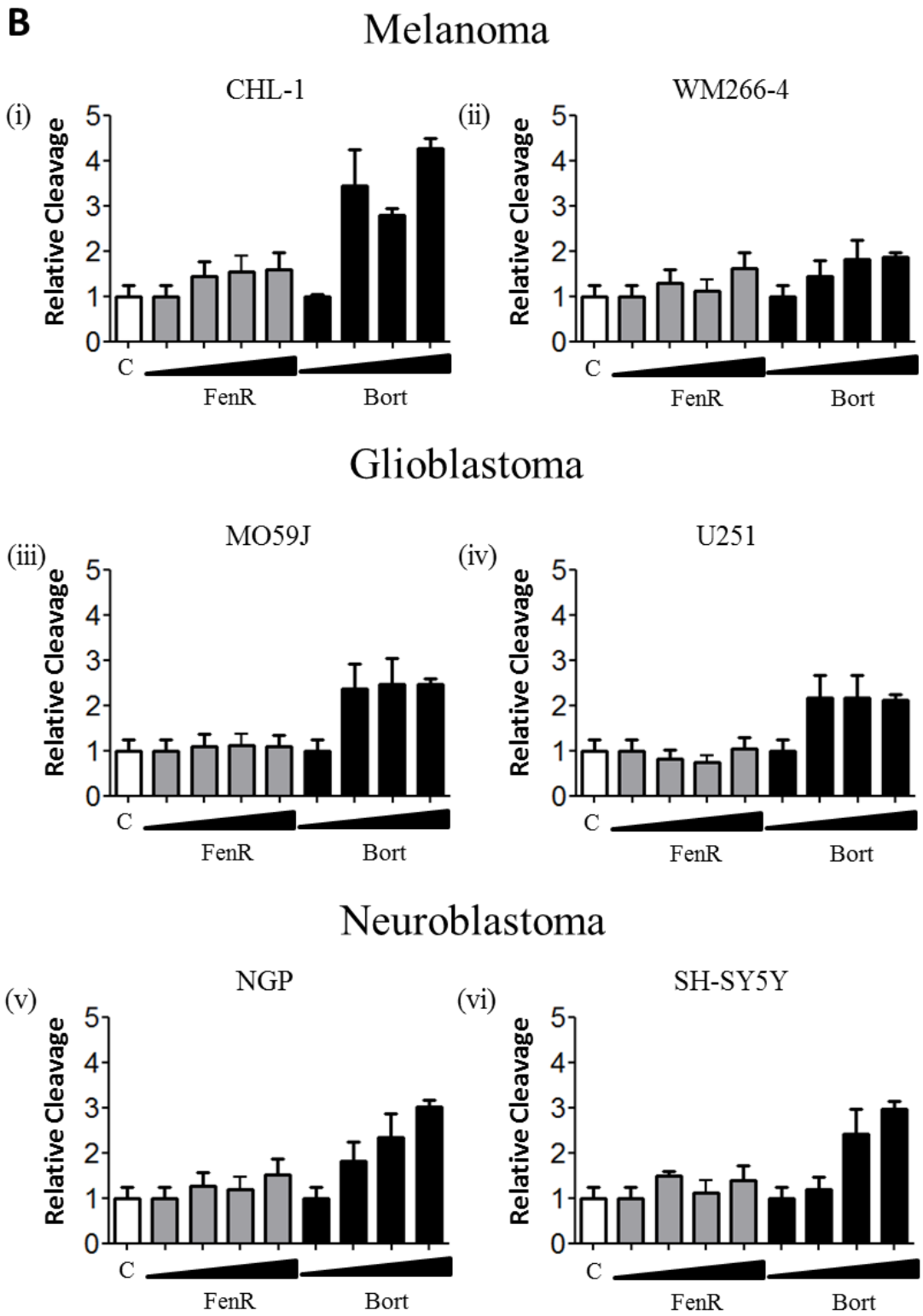

Figure 4.8 legend on next page.

Figure 4.8: *The effect of fenretinide and bortezomib on inducing Caspase 3 cleavage as a marker of apoptosis.* ***(A)*** *Neural-crest-derived cancer cells were treated with increasing doses for both fenretinide (0 – 50 µM for melanoma and glioblastoma or 0 – 20 µM for neuroblastoma cell lines) or bortezomib (0 – 400 nM for melanoma and glioblastoma or 0 – 100 nM for neuroblastoma cell lines) and incubated for 24 h prior to harvesting. Cell lysates were analysed by western blotting for the formation of the two cleaved products of pro-caspase 3, indicative of active caspase 3 (17 kDa and 19 kDa active Caspase-3 fragments). Figure 4.8 is a representative blot of 3 individually replicated experiments.* ***(B)*** *Densitometry data (data on next page) for the caspase 3 cleavage in melanoma (i + ii), glioblastoma (iii + iv) or neuroblastoma (v + vi) cells by increasing doses of either fenretinide (grey bars) or bortezomib (black bars) were carried out in comparison to control (white bars). Data were expressed relative to β-Actin and relative to control samples (no treatment) ± 95% CI.*

Data for the effect of bortezomib indicated a significant increase in the expression of cleaved Caspase 3 in melanoma (Figure 4.8 B, One-way ANOVA with Dunnett's post hoc correction, for CHL-1 cells 100 nM – 300 nM $P < 0.0001$ and WM266-4 100 nM – 300 nM $P < 0.05$, $P < 0.001$ or $P < 0.001$ respectively), glioblastoma (Figure 4.8 D, for MO59J and U251 cells treated with 100 nM – 300 nM $P < 0.0001$) and neuroblastoma (Figure 4.8 F, for NGP and SH-SY5Y cells treated with 20 nM & 30 nM $P < 0.0001$ and NGP cells with 10 nM $P < 0.001$). Furthermore, bortezomib-induced Caspase 3 cleavage was significantly higher in CHL-1 compared to WM266-4 cells (Two-way ANOVA, $F_{1, 23} = 12.1$, $P < 0.001$), although there was no significant difference in response amongst glioblastoma or neuroblastoma cell lines ($P > 0.05$). However, differences in response were observed with respect to bortezomib dose; WM266-4 cells showed bortezomib induced a dose-dependent increase in cleaved caspase 3, but for CHL-1, MO59J and U251 cells concentrations of 100 nM or above induced caspase 3 cleavage to the same extent. These data suggest therefore, that CHL-1 and glioblastoma cells were more sensitive to bortezomib-induced apoptosis compared to WM266-4 cells. Comparing the responses to 100 nM demonstrated significant differences in expression between cell lines (One-way ANOVA with Dunnett's post hoc corrections, WM266-4, $P < 0.0001$). With respect to the sensitivity of neuroblastoma cells to fenretinide or bortezomib, these cell lines were significantly more sensitive to either agent compared to melanoma and glioblastoma cells.

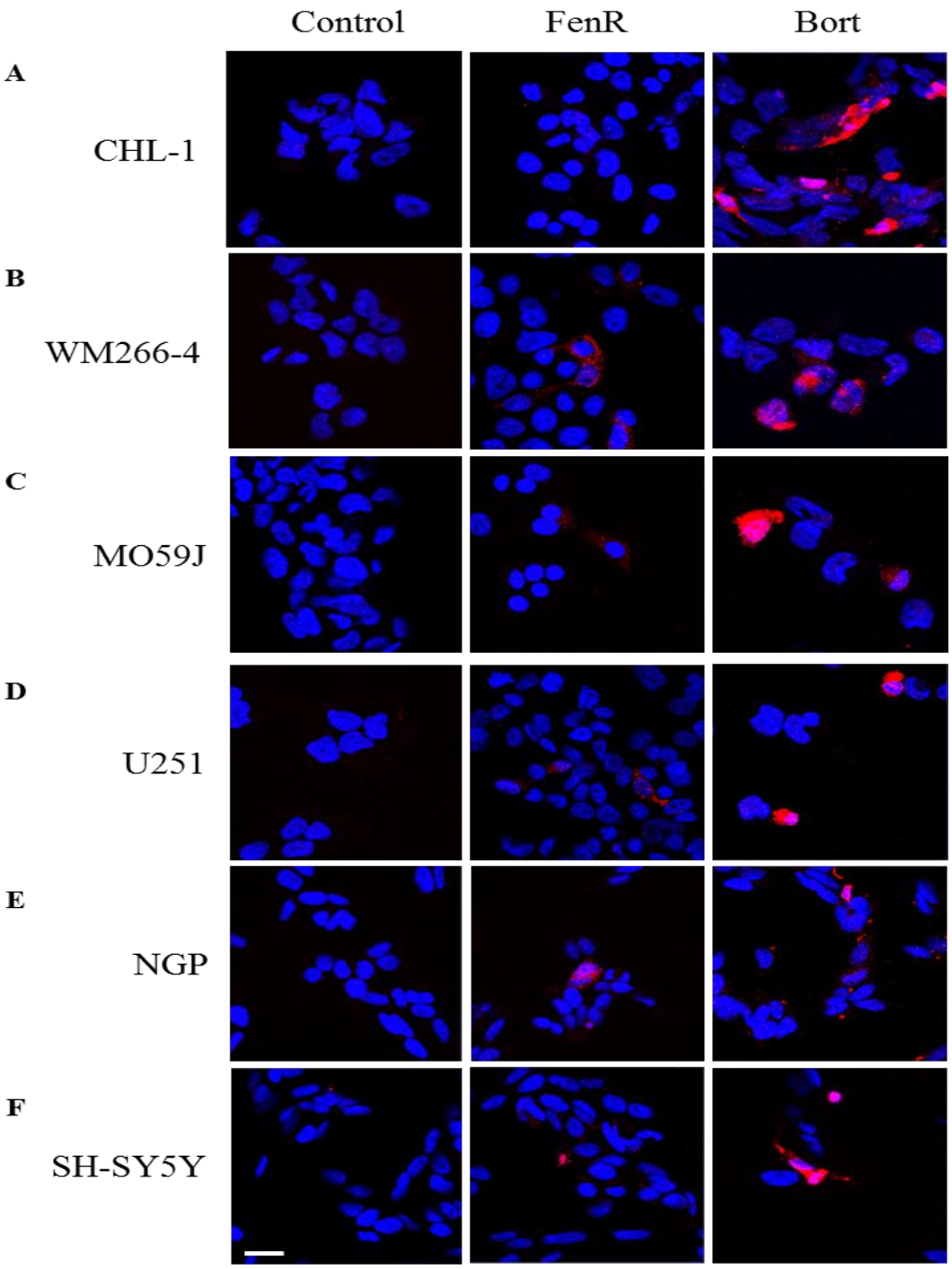

Figure 4.9: *Immunofluorescent analysis of fenretinide and bortezomib induced caspase 3 cleavage, as a marker of cancer cell apoptosis. Neural-crest-derived cancer cells were treated with increasing doses for both fenretinide (10 µM for melanoma and glioblastoma cell lines or 5 µM for neuroblastoma cell lines) or Bortezomib (200 nM for melanoma and glioblastoma cell lines or 20 nM for neuroblastoma cell lines) and incubated for 24 h prior to fixation in 4% PFA. Samples were then stained for active caspase-3, using DAPI as a marker of the cell nucleus. Immunofluorescence images are representative of 3 individual experiments. Scale bar on SH-SY5Y control = 20 µm.*

Caspase 3 cleavage in response to fenretinide or bortezomib was also assessed by immunofluorescence (figure 4.9). While Western blot data demonstrated a significant induction of cleaved caspase-3 by either fenretinide or bortezomib (One-way ANOVA with Dunnett's post hoc correction, for fenretinide $P < 0.05$ for all cell lines, and for bortezomib, CHL-1 and WM266-4 $P < 0.001$, MO59J and U251 cells $P < 0.0001$ or for NGP and SH-SY5Y neuroblastoma cells $P < 0.001$ or $P < 0.0001$ respectively), as well as a significant difference between fenretinide and bortezomib treatment (Figure 4.9; CHL-1 and WM266-4 cells $F_{2, 17} = 1.3$, $F_{2, 17} = 2.7$, $P < 0.01$, NGP cells $F_{2, 17} = 5.8$, $P < 0.001$ or for MO59J, U251 and SH-SY5Y cells $F_{2, 17} = 15.6$, $F_{2, 17} = 11.9$, $F_{2, 17} = 15.9$, $P < 0.0001$ respectively), immunofluorescence studies demonstrated a non-homogenous response to either fenretinide or bortezomib within a population of each individual cell line. Instead of an increase in the basal expression a significant increase in cleaved caspase 3 expression was only evident in a subset of cells within each population. For melanoma cells, CHL-1 18% and 21%, WM266-4 16% and 19% or glioblastoma cells MO59J 22% and 26%, U251 18% and 21 % or neuroblastoma cell lines NGP 26% and 32%, SH-SH5Y 20% and 29% were positive (demonstrating higher staining intensity than control cells) for cleaved caspase 3 after treatment with either fenretinide (10 µM for melanoma and glioblastoma or 5 µM for neuroblastoma) or bortezomib (200 nM for melanoma and glioblastoma or 20 nM for neuroblastoma), respectively.

These data demonstrate that fenretinide and bortezomib induce ER stress-induced cell death in all cell lines representing three neuronal or neuro-ectodermally-derived cancers. To gain a better understanding for the role that GRP78 plays in cellular sensitivity to ER stress and gain a better understanding of how changes in GRP78 expression can affect the outcome of ER stress, subsequent experiments were designed to reduce GRP78 expression and therefore alter the dynamic equilibrium of the UPR. Cellular sensitivity to ER stress-induced by fenretinide and bortezomib was then evaluated by propidium iodide stained flow cytometry for the induction of cell death or the inhibition of viability by MTS assay.

4.2.2: The role of GRP78 in UPR

To test the hypothesis that the UPR in relation to ER stress is regulated by a dynamic equilibrium between GRP78 and the UPR activators PERK, IRE1 and ATF6, the expression of GRP78 was reduced by RNA interference. SiRNA mediated knock-down of GRP78 was optimised in comparison to a scrambled control (Figure 4.10) and required double transfection in order to achieve a significant reduction in GRP78 expression. For all cell lines, GRP78 expression was significantly reduced by more than 50% (One-way ANOVA with Dunnett's post hoc correction $P < 0.0001$ for all cell lines). The mean reduction of GRP78 levels, compared to control SiRNA, was 56.3% for CHL-1, or 58.9% in WM266-4 melanoma, and 62.8% in MO59J and 82.3% in U251 glioblastoma cells, and 63.8% in NGP and 60.3% in SH-SY5Y neuroblastoma cells. Following RNAi mediated knock-down of GRP78, cells were also treated with fenretinide or bortezomib to determine if GRP78 knock-down resulted in ER stress-induced GRP78 which demonstrated GRP78 expression was in fact increased by both agents in all three neural-crest-derived cancer types (Figure 4.10 A – C).

The effect of GRP78 specific knock-down resulted in a significant reduction in the ability of either fenretinide or bortezomib to induce the expression of GRP78 in either melanoma (Figure 4.10 A, analysis by One-way ANOVA with Dunnett's post hoc correction for CHL-1 cells treated with fenretinide $P < 0.05$ or both CHL-1 and WM266-4 cells with bortezomib $P < 0.01$), glioblastoma (Figure 4.10 B, for MO59J cells treated with fenretinide $P < 0.001$ or bortezomib $P < 0.0001$ and U251 treated with either fenretinide or bortezomib $P < 0.01$ respectively) or neuroblastoma cells (Figure 4.10 C, for NGP with either fenretinide or bortezomib $P < 0.01$ or SH-SY5Y with fenretinide $P < 0.01$ or bortezomib $P < 0.05$) in comparison to cells transfected with the scrambled control, except for WM266-4 melanoma cells that were treated with fenretinide.

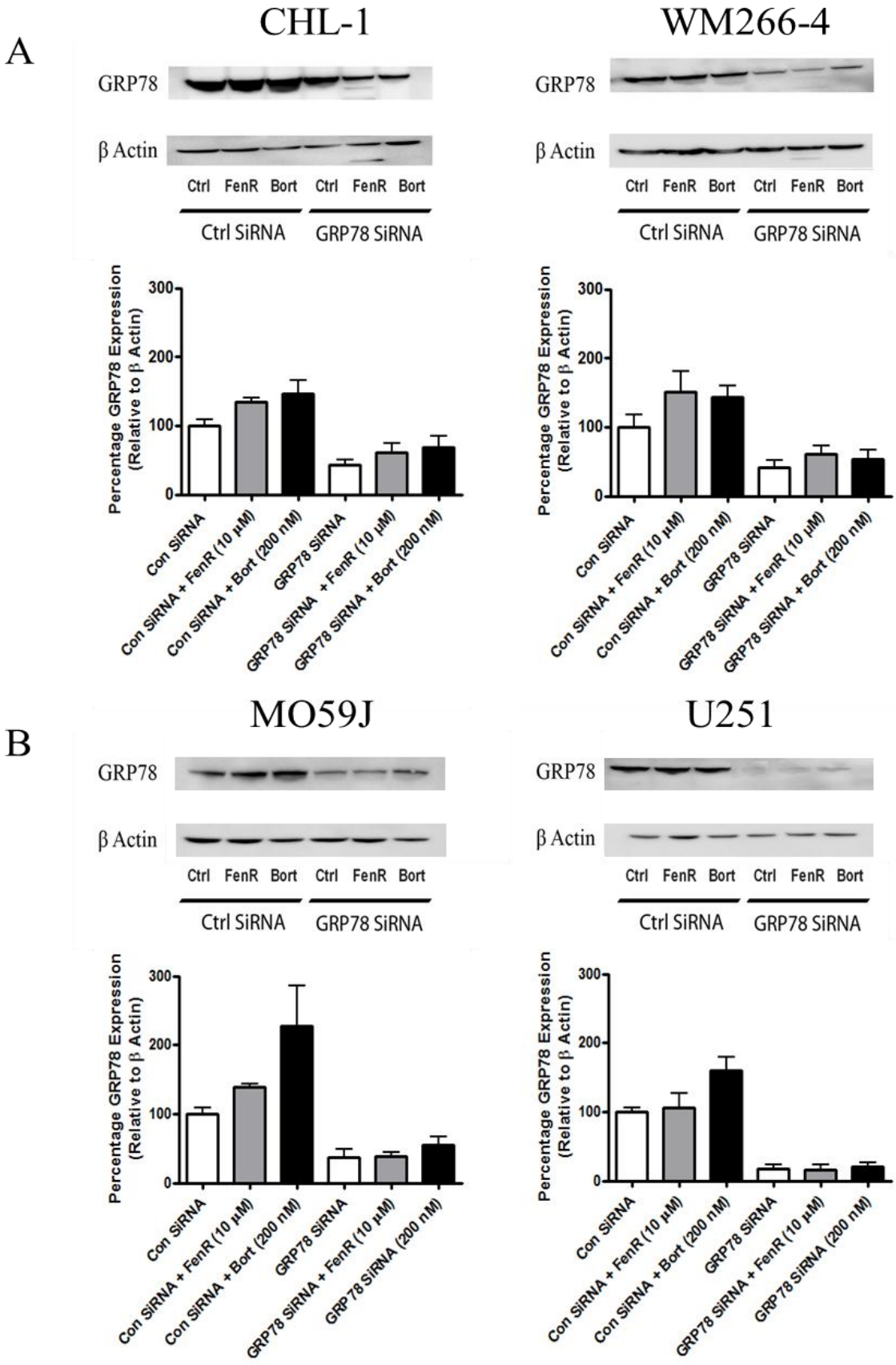
A
CHL-1
WM266-4
GRP78
β Actin
Ctrl FenR Bort Ctrl FenR Bort
Ctrl SiRNA
GRP78 SiRNA
Percentage GRP78 Expression (Relative to β Actin)
300
200
100
0
Con SiRNA
Con SiRNA + FenR (10 μM)
Con SiRNA + Bort (200 nM)
GRP78 SiRNA
GRP78 SiRNA + FenR (10 μM)
GRP78 SiRNA + Bort (200 nM)
B
MO59J
U251
GRP78 SiRNA (200 nM)

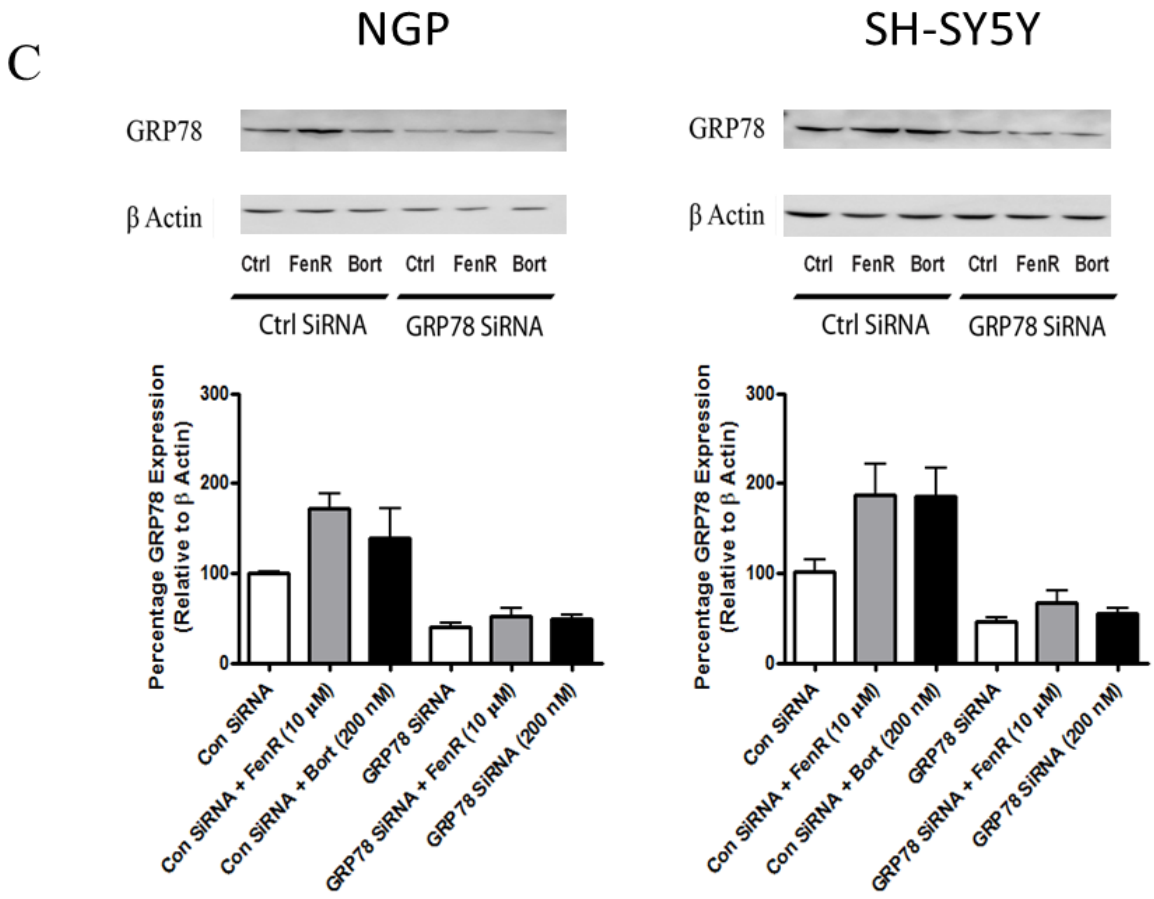

Figure 4.10: *The effect of GRP78 siRNA on neural-crest-derived cancer cell line expression of GRP78. The effect of GRP78 specific SiRNA, in comparison to control scrambled, on GRP78 expression in a panel of neural-crest-derived cancer cell lines. CHL-1 and WM266-4 metastatic melanoma (A), MO59J and U251 glioblastoma (B) or NGP and SH-SY5Y neuroblastoma cell lines (C) were transfected with 40 nM GRP78-specific siRNA in comparison to a scrambled control and incubated for 2 x 24 h prior to treatment with either fenretinide (grey bars, 10 μM for melanoma and glioblastoma cell lines or 5 μM for neuroblastoma cell lines) or Bortezomib (black bars, 200 nM for melanoma and glioblastoma cell lines or 20 nM for neuroblastoma cell lines) for a further 24 h. Samples were then harvested and analysed for GRP78 protein expression in comparison to β-Actin as a loading control. Densitometry is expressed as a percentage of control, relative to β-Actin as a mean of 3 replicate experiments ± 95 % CI. Data for the effect of siRNA on GRP78 expression in melanoma cells were previously published [266].*

The effect of GRP78 specific siRNA between cell lines, of the same cancer type, indicated a significant difference between the responses of either glioblastoma cell line ($F_{1, 17} = 65.2$, $P < 0.01$). Knock-down of GRP78 also resulted in a significant difference in sensitivity to ER stress-induced UPR induction of GRP78 observed between differing cancer types (Comparing melanoma to glioblastoma $F_{2, 53} = 11.1$, $P < 0.05$ or neuroblastoma $F_{2, 53} = 22.8$, $P < 0.01$ and glioblastoma to neuroblastoma $F_{2, 53} = 36.3$, $P < 0.01$).

These data demonstrate a significant reduction in GRP78 expression as well as a reduction in UPR-mediated up-regulation of GRP78. This potentially creates an UPR system where the dynamic equilibrium has been shifted towards an active or free UPR activator state.

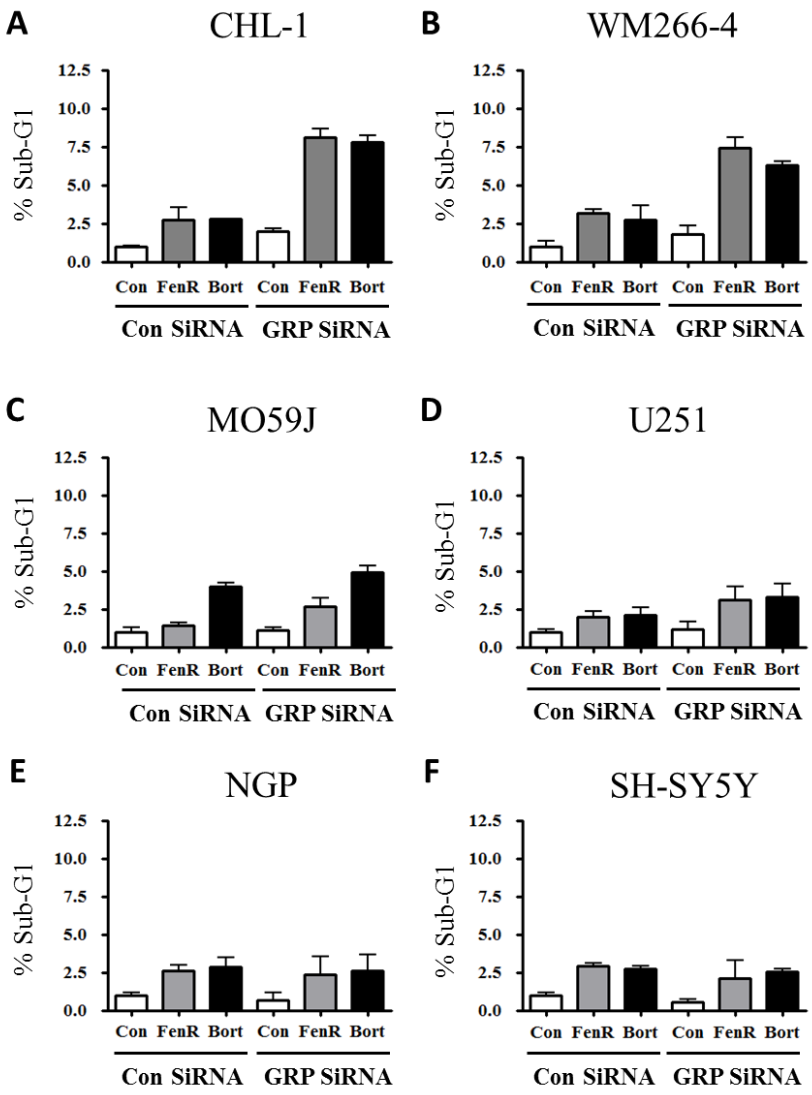

Figure 4.11: *The effect of GRP78 expression of neural-crest-derived cancer cell sensitivity to fenretinide and bortezomib induced cell death. CHL-1 and WM266-4 metastatic melanoma (A & B), MO59J and U251 glioblastoma (C & D) or NGP and SH-SY5Y neuroblastoma cell lines (E & F) were transfected with 40 nM GRP78 specific siRNA in comparison to a scrambled control and incubated for 2 x 24 h prior to treatment of the samples with either fenretinide (grey bars, 10 µM for melanoma and glioblastoma cell lines or 5 µM for neuroblastoma cell lines) or bortezomib (black bars, 200 nM for melanoma and glioblastoma cell lines or 20 nM for neuroblastoma cell lines) for a further 24 h. Samples were then assessed for changes in sensitivity to cell death by propidium iodide stained flow cytometry for the increase in the SubG1 population. Data are expressed as relative to control (no treatment) scrambles siRNA-treated cells and bars are the mean of 3 replicate experiments ± 95 % CI.* Data for the effect of reduced GRP78 expression on ER stress-induced melanoma cell death were previously published [266].

To determine if the shift in the dynamic equilibrium sensitizes neural-crest-derived cancer cells to ER stress-induced cell death, cells were transfected with scrambled or GRP78 siRNA, and subsequently treated with control vehicle, fenretinide or bortezomib for 24 h prior to the assessment of cell death and cell viability. Data demonstrated GRP78 knock-down resulted in a cancer type specific sensitivity to either fenretinide or bortezomib (Figure 4.11, comparing the effect of GRP78 SiRNA on fenretinide and bortezomib induced cell death over cancer types, $F_{3, 36} = 57.1$, $P < 0.001$). In melanoma cell lines (Figure 4.11 A & B) reduction in GRP78 expression resulted in significantly enhanced cell death in response to either fenretinide or bortezomib (One-way ANOVA with Dunnett's post hoc correction, to compare the effect of fenretinide or bortezomib across siRNA treatments $P < 0.0001$ respectively). Knock-down of GRP78 also significantly increased cell death in CHL-1 in absence of drug treatment, although this effect was not observed in WM266-4 cells.

The effect of GRP78 knock-down on fenretinide and bortezomib-induced cell death in glioblastoma (Figure 4.11 C & D) resulted in a significant increase in cell death, induced by either ER stress-inducing agent (Comparing fenretinide or bortezomib across siRNA treatments by One Way ANOVA with Dunnett's post hoc correction within MO59J $P < 0.0001$ or U251 $P < 0.001$ respectively). Furthermore, transfection of GRP78 siRNA in both melanoma and glioblastoma cells resulted in an increase in fenretinide and bortezomib- induced cell death. Significant differences between the responses of melanoma and glioblastoma were also observed, with melanoma cells being more susceptible to both ER stress-inducing agents compared to glioblastoma cells (One-way ANOVA with Dunnett's post hoc correction, $P < 0.001$ for either fenretinide or bortezomib). In neuroblastoma cells however, (Figure 4.11 E & F) in general there was no significant increase in ER stress-induced cell death in either cell line following GRP78 knock-down in comparison to basal levels of GRP78 expression ($P > 0.05$), although in SH-SY5Y cells treated with fenretinide there was a small but significant decrease in cell death (One-way ANOVA with Dunnett's post hoc correction, $P < 0.05$)

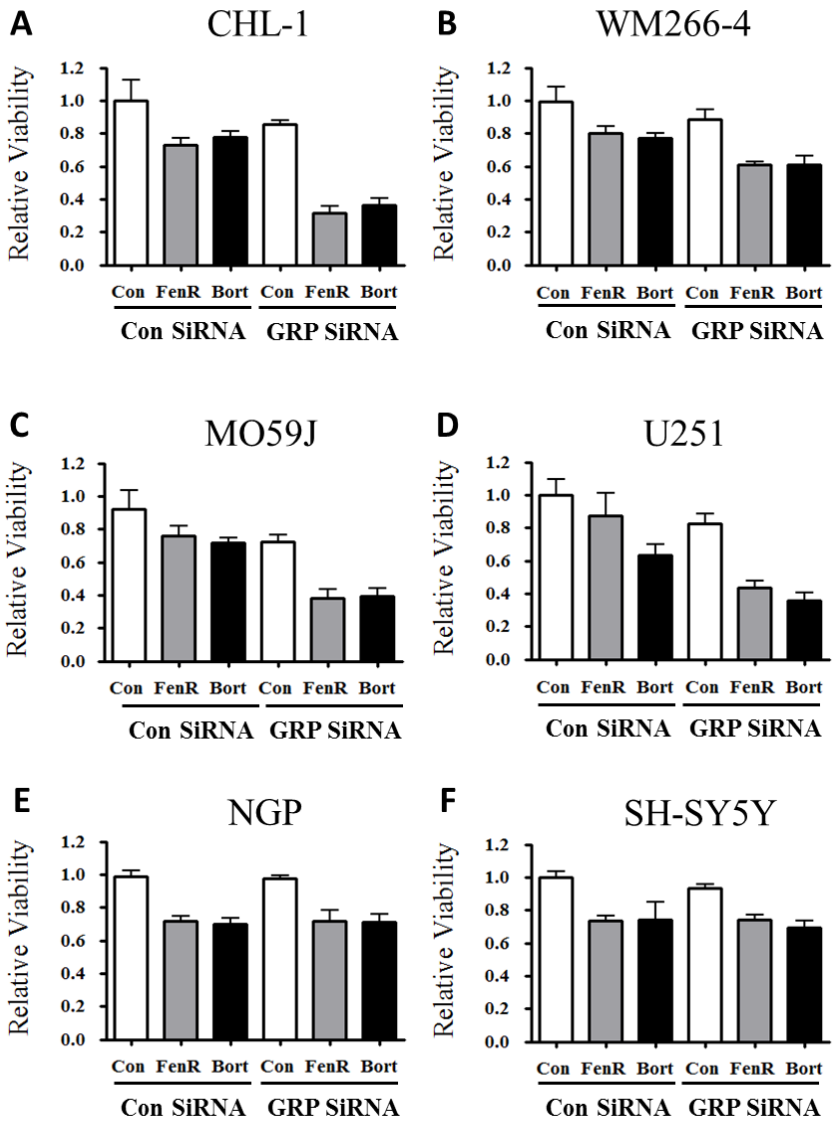

Figure 4.12: *The effect of GRP78 expression of neural-crest-derived cancer cell sensitivity to fenretinide and bortezomib induced inhibition of cell viability. CHL-1 and WM266-4 metastatic melanoma (A & B), MO59J and U251 glioblastoma (C & D) or NGP and SH-SY5Y neuroblastoma cell lines (E & F) were transfected with 40 nM GRP78 specific SiRNA in comparison to a scrambled control and incubated for 2 x 24 h prior to treating the samples with either fenretinide (grey bars, 10 µM for melanoma and glioblastoma cell lines or 5 µM for neuroblastoma cell lines) or bortezomib (black bars, 200 nM for melanoma and glioblastoma cell lines or 20 nM for neuroblastoma cell lines) for a further 24 h. Samples were then assessed for changes in cell viability using the MTS colorimetric based metabolic assay. Data are expressed as the mean of 3 replicate experiments ± 95 % CI. Data for the effect of reduced GRP78 expression on ER stress-induced inhibition of melanoma cell viability were previously published [266].*

Similar results were obtained for the effect of GRP78 knock-down on ER stress-induced inhibition of cell viability (Figure 4.12). In melanoma and glioblastoma cells (Figure 4.12 A & B for melanoma or C & D for glioblastoma), GRP78 knock-down resulted in a significant increase in either fenretinide or bortezomib-induced inhibition of cell viability (One-way ANOVA with Dunnett's post hoc correction for CHL-1 melanoma cells and either glioblastoma cell line treated with fenretinide $P < 0.001$ or WM266-4 with fenretinide and bortezomib or CHL-1, MO59J and U251 treated with bortezomib $P < 0.0001$, respectively). Although there was an apparent reduction in cell viability in untreated cells in response to a decrease in GRP78 expression, this was not significant ($P > 0.05$). CHL-1 and WM266-4 metastatic melanoma cells also demonstrated significant differences in response ($F_{1, 47} = 10.3$, $P < 0.01$), with WM266-4 cells being less affected by GRP78 knock-down. Data for the effect of GRP78 knock-down on ER stress-induced inhibition of neuroblastoma cell viability also demonstrated no significant differences between cells transfected with control or GRP78 specific siRNA ($P > 0.05$).

These results therefore demonstrate the importance of the UPR in cancer cell survival but the differing effects on reduction of cell viability and induction of cell death between cancer types (One-way ANOVA comparing melanoma and glioblastoma to neuroblastoma $F_{3, 96} = 68.1$ or $F_{3,96} = 138.5$ with $P < 0.001$ for both). Although GRP78 knock-down in melanoma cells resulted in a significantly higher level of cell death compared to the effects on glioblastoma-induced cell death ($P > 0.05$), cell viability data did not demonstrate any significant differences between cancer types. (Figure 4.12 A & B vs. C & D, $F_{3, 36} = 57.1$, $P < 0.001$).

This study shows that sensitivity to ER stress can be enhanced by a reduction in GRP78 expression and is cancer type dependent, with cancer expressing high levels of GRP78 being more susceptible to ER stress in the absence of GRP78. This demonstrates a cancer type-specific reliance on GRP78.

4.2.3: Results Summary.

- Fenretinide and bortezomib induced cell death and inhibit cell viability of neural-crest-derived cancer cells.

- There were differences in cell line sensitivity to ER stress-induced death or inhibition of cell viability between melanoma, glioblastoma and neuroblastoma.

- Fenretinide and Bortezomib significantly induced the UPR pro-death transcription factor Gadd153 in all cancer types, however a significant difference in the level of induction was observed (Melanoma > Glioblastoma > Neuroblastoma).

- Both fenretinide and bortezomib induced significant induction of Noxa in all cell types, a pro-apoptotic member of the BCL-2 family.

- Knockdown in GRP78 expression resulted in a more than 50% reduction in GRP78 expression within all neural-crest-derived cancer types.

- GRP78 siRNA decreased fenretinide and bortezomib-induced GRP78 in all cancer types, demonstrating the presence of on-going SiRNA mediated knockdown after transfection.

- Reduction in GRP78 expression increased the sensitivity of melanoma and glioblastoma cell lines to both fenretinide and bortezomib-induced death or inhibition of cell viability.

- GRP78 knock down had no significant effect on ER stress-induced cell death or inhibition of neuroblastoma cell viability.

4.3: Discussion.

The results from this study demonstrate that ER stress-inducing agents fenretinide or bortezomib induced cell death and inhibited cell viability of melanoma, glioblastoma and neuroblastoma cells. Fenretinide or bortezomib showed a significant induction of pro-death stimuli including Gadd153, as well as the BCL-2 family member Noxa in all cancer types, as a consequence of both ROS induction and ubiquitin-tagged protein accumulation, respectively [112, 184]. SiRNA mediated knock-down of GRP78 resulted in over 50% reduction in cellular expression in all cell lines with data demonstrating a cancer type specific effect on sensitivity to ER stress-induced cell death. Melanoma and glioblastoma cancer types demonstrated a significant increase in sensitivity to ER stress-induced cell death; however neuroblastoma showed no significant difference to control.

Dose response studies of fenretinide and bortezomib-induced cell death confirmed that both agents are potent inducers of cell death of neural-crest-derived cancer models [82, 83, 112, 201, 203, 240, 267]. Assessing fenretinide and bortezomib for their mechanism to induce ER stress, by monitoring ROS and ubiquitin tagged protein accumulation, respectively, showed that fenretinide induced a similar response in all cancer types. Interestingly, neuroblastoma showed the lowest basal level of ROS of all three cancer types tested, coupled with similar levels of ROS induction with half the concentration of fenretinide (5 μM). These findings highlight the sensitivity of neuroblastoma to ROS accumulation, in comparison to other neuro-ecto-dermal derived cancers. Bortezomib had a cell line dependant effect, with neuroblastoma cells demonstrating significantly lower levels of protein accumulation.

Interestingly, the sensitivity of neuroblastoma cells to bortezomib-induced cell death was comparable to the sensitivity of melanoma cells, even though they do not receive the same magnitude of protein build-up (ER stress). The differences in protein accumulation may therefore be a direct consequence of the lower dose of bortezomib used to treat neuroblastoma, cells, further emphasising the sensitivity of these cells to ER stress-induced death [268, 269].

In all cell lines fenretinide and bortezomib treatment induced Gadd153, the down-stream inducible transcription factor of the UPR, that triggers cell death via ER stress [204]. A significant induction of the pro-apoptotic BCL-2 family member Noxa was

also observed, highlighting the cross talk required between the ER and mitochondria to successfully induce cell death [184]. Variation between cancer models was observed for the induction of GRP78 and peIF2α (markers of UPR induction) in response to fenretinide and bortezomib with glioblastoma and neuroblastoma showing minimal activation.

Previous data, for the activation of the UPR over time (Chapter 3, Figure 3.8) highlighted ATF4 was detectable at 4 h but lost by 8 h. Therefore, the lack of detectable induction of peIF2α and GRP78 in glioblastoma and neuroblastoma cells may have been a time-dependent consequence. Mapping the induction of ATF4 over time (Chapter 3, figure 3.8) also indicated that for neuroblastoma, the response was significantly smaller than that of melanoma or glioblastoma, which is confirmed by the minimal induction of eIF2α phosphorylation detected in these experiments. Differences within the extent of GRP78 induction across cancer types, conforms to the data generated for the induction of ATF4 (Figure 3.6), were a greater response was observed in melanoma cells, than in glioblastoma or neuroblastoma, suggesting the presence of a more active or greater UPR capacity within these cancers.

Comparing the induction levels of pro-apoptotic stimuli Gadd153 and Noxa (Figure 4.7 A & B) to the levels of cell death achieved within differing cell lines (propidium iodide stained flow cytometry data), indicated that for CHL-1 cells ER stress-induced Noxa and Gadd153 were significantly higher compared to induction in WM266-4 cells, which also directly correlated with the levels of achievable cell death or inhibition of cell viability. Melanoma cells have been shown to have significant up-regulation of anti-apoptotic BCL-2 family members, such as BCL-XL, resulting in an increase resistance to cell death [270]. However, this explanation is down-stream of these experimental observations. Moreover, WM266-4 cells harbour a $BRAF^{V600E}$ mutation [271], which is well documented to increase cellular resistance to death and may therefore influence the outcome of ER stress due to the activation of other pro-survival pathways.

The effects of either fenretinide or bortezomib on neuroblastoma or glioblastoma-induced cell death or inhibition of cell viability also differed to the effects on induction of either Gadd153 or Noxa, suggesting the involvement of another mechanism that may also contribute to glioblastoma and neuroblastoma cell line sensitivity to bortezomib. For example, NGP and SH-SY5Y cells differ in MYCN status, with NGP cells demonstrating amplification of MYCN expression compared to SH-SY5Y [272].

MYCN amplification status has been demonstrated to alter cell line sensitivity to death and therefore could hinder the outcome of ER stress-inducing agents [272].

The significant difference between fenretinide and bortezomib induced caspase 3 cleavage, with bortezomib showing greater induction, highlights bortezomib as a stronger inducer of ER stress stimulated cell death and a better candidate agent for future trials. Immunofluorescence studies showed high induction of cleaved caspase 3, in a sub-population of cells, rather than within all cells. This observation may relate to the probability of inducing cell death within any given population. Factors such as cell cycle, BCL-2 family expression and even cell-cell contact can alter a cells susceptibility to death, by priming a cell to a given stress, and therefore making that cell less resistant to death induced by fenretinide or bortezomib. Due to cells existing at different phases of the cell cycle, coupled with protein half-life suggests that within a given population, cells at any one time point can be more susceptible or resistant to death stimuli.

After GRP78 knock-down, metastatic melanoma and glioblastoma cells became more susceptible to ER stress-induced cell death, suggesting that GRP78 plays an important inhibitory role in the UPR and shift in the dynamic equilibrium of the UPR towards a free and active cascade. This shift towards an active response pre-primes the UPR; and therefore less stress is required to push a cell over the threshold of activation, and towards death. These data support the findings of Suzuki *et al*, where reduction of GRP78 expression increased basal UPR signalling, as measured by ATF4 induction and XBP-1 splicing. This increase in signalling prior to the induction of stress, primes melanoma and glioblastoma cells, shifting them closer to the threshold of death, before treatment with either fenretinide or bortezomib. Initial theories focused on the reduction in chaperone activity as the primary factor that enhances cell line susceptibility to stress, however, subsequent research has demonstrated that GRP78 reduction results in the up regulation of other chaperones to counter act its loss [251].

In neuroblastoma there was no significant increase in sensitivity to ER stress, despite more than a 60% reduction in GRP78 expression. Following on from the data (in Figure 3.3) that demonstrated that the expression of total UPR activators is greater than that of GRP78 within neuroblastoma, this may describe the evolution of a cell type that requires high UPR activity. Therefore, a further shift towards free UPR activators, induced by knocking-down GRP78, may not induce the same consequence as demonstrated in melanoma and glioblastoma. These findings therefore suggest a more complex network within the UPR where downstream induction of pro- and anti-

apoptotic stimuli is different not only depending on the type of stress [273], but also the cell type the stress occurs in.

When comparing the increase in cell line sensitivity, to samples with control basal expression of GRP78, data demonstrated higher basal expression (Figure 3.2) of GRP78 correlates with the greater influence it has on the outcome of the UPR (i.e. melanoma cell lines showed the highest cellular concentration of GRP78 and became the most sensitive to fenretinide or bortezomib induced death when GRP78 is reduced). Melanoma cells demonstrated a greater response to GRP78 knock-down compared to either glioblastoma or neuroblastoma, while glioblastoma showed a significant difference in response compared to neuroblastoma. GRP78 knock-down also resulted in a decrease in GRP78 induction in response to either fenretinide or bortezomib, suggesting that there was an on-going effect of the siRNA, within all cancer types, up to 48 h post transfection.

Studies by Chen *et al.,* have correlated an increase in GRP78 expression with a favourable prognosis within neuroblastoma [116]. Findings from the present study indicate that reduction in GRP78 expression does not sensitize neuroblastoma cells to ER stress-induced cell death, as for melanoma or glioblastoma. Therefore, to confirm the outcome of these data, experiments were designed to test the hypothesis that increasing the expression of GRP78 decreases melanoma and glioblastoma cell line sensitivity to death, but increases the sensitivity of neuroblastoma cell lines by altering the activity of the UPR as a result of changes in the dynamic equilibrium. These experiments form the basis of chapter 5.

4.4: Conclusion

This study showed that there was a difference in cancer type sensitivity to ER stress, with neuroblastoma cells being significantly more sensitive to ER stress-induced cell death than melanoma or glioblastoma; even though they demonstrate lower levels of ER stress (ROS or ubiquitin build-up). There was a cancer type specific outcome for the effect of reduced GRP78 on ER stress-induced cell death, with melanoma cells showing enhanced sensitivity.

Chapter 5:

Over-expression of GRP78 affects the response of cancer cells to ER stress *in vitro*.

5.1: Introduction.

Solid tumours could be classified as organs, consisting of both cancerous and non-cancerous cells. The non-cancerous cells include: myofibroblasts, endothelial cells, pericytes, cancer-associated fibroblasts, mesenchyme stem cells and immune inflammatory cells [274-277]. These non-cancerous cells are important within the tumour and provide support for cancer cell growth, angiogenesis and metastasis [276, 278-280]. Tumour growth often occurs faster than the stimulation of blood vessel production, resulting in a hypoxic, glucose-deprived and acidic (lactic acid) environment. The interaction of cancer cells with and the severity of the tumour microenvironment plays a critical role in modulation of tumour growth, metabolism and metastasis [276, 280, 281].

These extracellular noxae of the tumour microenvironment are intrinsic stressors, affecting the biosynthesis of larger macro-molecules, glycoproteins and lipids by cancer cells. Errors in protein synthesis induce the UPR. Mounting evidence for solid tumours has documented the importance of UPR activation for cancer-cell growth and disease progression. Studies in breast, liver, colon and brain cancers have described UPR-induced GRP78 and ATF6 expression, as well as XBP-1 splicing in cancer cells. However, no induction of the UPR was observed in the non-cancerous peritumoral areas [282].

Lee *et al.,* demonstrated a critical role of GRP78 in tumour proliferation, survival and tumour angiogenesis. Mice heterozygous for GRP78 (+/-) were crossed with MMTVPyVT mice (expressing the polyoma middle T oncogene (PyT) and therefore genetically susceptible to mammary tumours) and offspring monitored for changes in tumour progression, with results demonstrating no significant differences in animal growth and development in comparison to wild type (wt) siblings [283]. Yet, with regard to tumour progression, mice heterozygous for GRP78 demonstrated an increased latency period before cancer was detectable. These mice also demonstrated a decreased proliferative capacity, coupled with an increased propensity to apoptosis. Further analysis identified a significant increase in Gadd153 and downstream caspase activity, suggesting a decrease in GRP78 expression may reduce the inhibitory role it plays upon the UPR and result in a shift within the dynamic equilibrium to an active state. Therefore, the priming of the UPR within these heterozygous tumour cells results in an

increase in the achievable levels of death induced by the tumour microenvironment [283]. Assessing tumour samples for differences in angiogenesis using the endothelial cell marker CD31 highlighted a reduction in heterozygous mice, compared to wt control [283].

Denko *et al.,* and Koong *et al.,* also demonstrated the importance of UPR signalling in tumour growth. Transformed mouse fibroblasts deficient in XBP-1 or fibroblasts with reduced XBP-1 expression, showed decreased ability to buffer hypoxic conditions as well as reduced growth and capacity to stimulate angiogenesis in comparison to control cells. These finding were consistent with data for human fibrosarcoma, where xenograft tumours with reduced XBP-1 expression also showed growth inhibition [284, 285]. Conversely, over-expression of XBP-1 in human fibrosarcoma cells expressing dominant-negative IRE1 resulted in the rescue of angiogenesis [284, 285]. PERK signalling has also been documented to support tumour cell growth. Inactivation of PERK or introduction of a dominant-negative form of PERK resulted in the formation of smaller tumours, with decreased growth capacity and angiogenic activity, when engrafted into immune-compromised mice models [286, 287].

Collectively, these studies highlight the importance of the UPR signalling cascade for tumour cell progression. However, increases in GRP78 expression have been documented in numerous cancer types. Enhanced GRP78 expression may be detectable as a downstream consequence of an increase in UPR signalling, rather than a change in the basal expression of GRP78 within the cancer cell. Lee *et al.,* demonstrated that although malignant glioma samples (TuBEC) demonstrated an increase in GRP78 expression, activation of other downstream UPR targets, including ATF4 and XBP-1s were not evident [288]. Kaufman *et al.,* also demonstrated in CHO cells stably over-expressing GRP78, a decrease in GRP78 and GRP94 mRNA translation when treated with tunicamycin [289]. These findings suggest that GRP78 may play a key role in stress-induced chaperone induction or that an increase in GRP78 expression buffers stress and therefore reduces UPR-induced chaperone induction [289].

The role of GRP78 in cancer is still not fully understood; however, there is growing evidence that GRP78 functions in a more diverse manner to that of normal cells. In normal cells, GRP78 is localised to the ER, due to the presence of ER localisation and KDEL sequences. Conversely, in cancer cells GRP78 is detectable in the cytosol, mitochondria, nucleus and at the cell surface [290, 291]. Global profiling of cell surface

proteome of tumour cells demonstrated a relative abundance of heat shock and glucose regulated proteins, including GRP78 [292]. Cell surface GRP78 has been implicated in tumour-specific targeting by circulating ligands and mediates the anti-angiogenic and pro-apoptotic activity of Kringle 5 in hypoxic and cytotoxic stressed tumours [293, 294].

Studies by Lee *et al.,* and Brodie *et al.,* demonstrated that in GRP78 over-expression models, stress-induced apoptosis is significantly decreased with a marked increase in cell growth was also observed. Lee *et al.,* also demonstrated higher expression of GRP78 in the vascular of human derived glioma, both *in situ* and *in vitro* cultures of TuBEC cells, than in surrounding non-malignant brain tissues (BEC) [288], correlating GRP78 expression directly to cellular resistance to apoptosis induced via ER stress.

Lee *et al.,* and Brodie *et al.,* also highlighted an interaction between GRP78 and caspase 7. Co-immunoprecipitation studies demonstrated GRP78 constitutively associates with caspase 7 and over-expression of GRP78 suppressed the activation of caspase 7 in response to etoposide and cisplatin treatment both *in vitro* and *in vivo* [113, 295]. The association of GRP78 with caspase 7 could be reversed by the addition of dATP, suggesting that the ATP binding domain of GRP78 was important for caspase 7 interaction. Further to this, using a mutant version of GRP78, which possessed a mutation within the ATP binding domain, studies demonstrated significant loss of caspase 7 binding capacity, as well as a reduction in resistance to etoposide treatment [113, 295].

In hepatocellular carcinoma, a positive correlation of GRP78 with both portal and intra-hepatic invasion has been demonstrated [296]. Over-expression of GRP78 in SMMC7721 cells promoted invasion both *in vitro* and *in vivo.* Mechanistic studies showed that GRP78 over-expression enhanced focal adhesion kinase (FAK). FAK plays an important role in tumour invasion and metastasis, by negatively regulating rock kinase activity, which although required at a basal expression, over activation of rock kinase prevents invasion [296].

Although the majority of cancer types demonstrate a correlation between GRP78 expression and poor patient prognosis, due to changes in cellular resistance and capacity to buffer ER stress, neuroblastoma demonstrates the converse [116]. Therefore, using neural-crest-derived cancer types, the aim of the present study was to test the hypothesis that over-expression of GRP78 increases resistance in melanoma and glioblastoma and decreases the resistance of neuroblastoma, to ER stress-induced cell death in response to either fenretinide or bortezomib.

5.2: Results.

5.2.1: Over-expression of GRP78

To test the effect of GRP78 over-expression on neural-crest-derived cancer types, one cell line of melanoma, glioblastoma and neuroblastoma was stably transfected with 4 µg pcDNA3.1 (+) GRP78 or vector control (pcDNA3.0) by selection with 1.5 mg/ml G418 for 10 passages as mixed populations of stably transfected cells. GRP78 expression was verified by western blotting, relative to β-Actin as loading control (Figure 5.1). Although it was preferable to do this work with all six cell lines, despite much effort, stable transfection of SH-SY5Y cells could not be achieved, therefore only one cell line of each cancer type was used to ensure a balanced approach.

Results confirmed a significant increase in GRP78 expression in WM266-4 melanoma, MO59J glioblastoma and NGP neuroblastoma cells (Figure 5.1 B, One-way ANOVA, $F_{2, 54} = 65.054$, $P < 0.0001$) after transfection with GRP78 plasmid compared to either wild-type cells or cells stably transfected with control plasmid. These data also demonstrate no significant effect of the antibiotic selection (1500 µg/ml G418) on GRP78 expression ($P > 0.05$). The increase in GRP78 expression was 1.7-fold for melanoma (One-way ANOVA with Bonferroni post hoc correction, $P < 0.0001$), 1.96-fold for glioblastoma of ($P < 0.0001$) and 1.5-fold for neuroblastoma of ($P < 0.01$). Comparing cells lines individually demonstrated a significant difference between glioblastoma and neuroblastoma (One-way ANOVA with Bonferroni post hoc correction, $P < 0.001$).

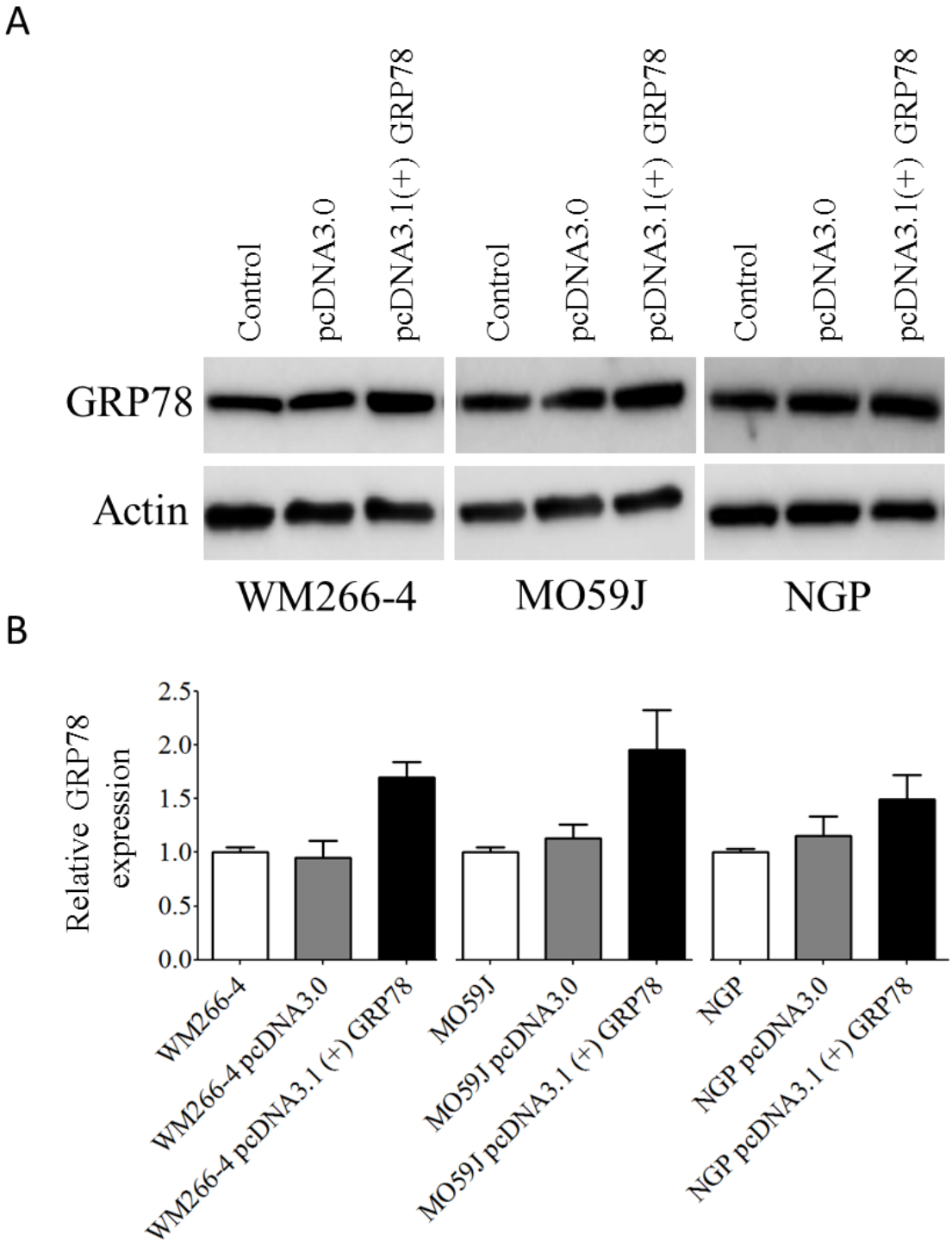

Figure 5.1: *Over-expression of GRP78 in neural-crest-derived cancer cells. WM266-4 metastatic melanoma, MO59J glioblastoma and NGP neuroblastoma cells were stably transfected with pcDNA3.0 or pcDNA3.1 (+) GRP78 and western blot analysis carried out to confirm GRP78 expression (A). Densitometry was performed on a minimum of 4 individual experiments for the expression of GRP78 in comparison to β-Actin loading control (B). Experimental data are expressed as mean values ± 95% CI.*

To confirm the western blot data for the over-expression of GRP78 protein, Real time PCR analysis also revealed a significant increase in GRP78 mRNA in all cell types, again using β-Actin mRNA as loading control (Figure 5.2). Data demonstrated significant difference between plasmid-transfected cell types with pcDNA3.1 (+) GRP78 significantly increasing GRP78 mRNA (One-way ANOVA, $F_{2, 54} = 187.6$, $P < 0.0001$) by 1.8-fold for melanoma cells (One-way ANOVA with Bonferroni post hoc corrections, $P < 0.0001$), 1.75-fold for glioblastoma ($P < 0.0001$) and 1.45-fold for neuroblastoma ($P < 0.0001$), compared to pcDNA3.0 control vector and wild-type cell lines.

With respect to GRP78 mRNA over-expression between cancer types, there was no difference between melanoma and glioblastoma ($P > 0.05$) but a significant difference between either melanoma or glioblastoma compared to neuroblastoma (Figure 5.2, One-way ANOVA with Bonferroni post hoc corrections, comparing neuroblastoma to melanoma $P < 0.001$ and glioblastoma $P < 0.01$).

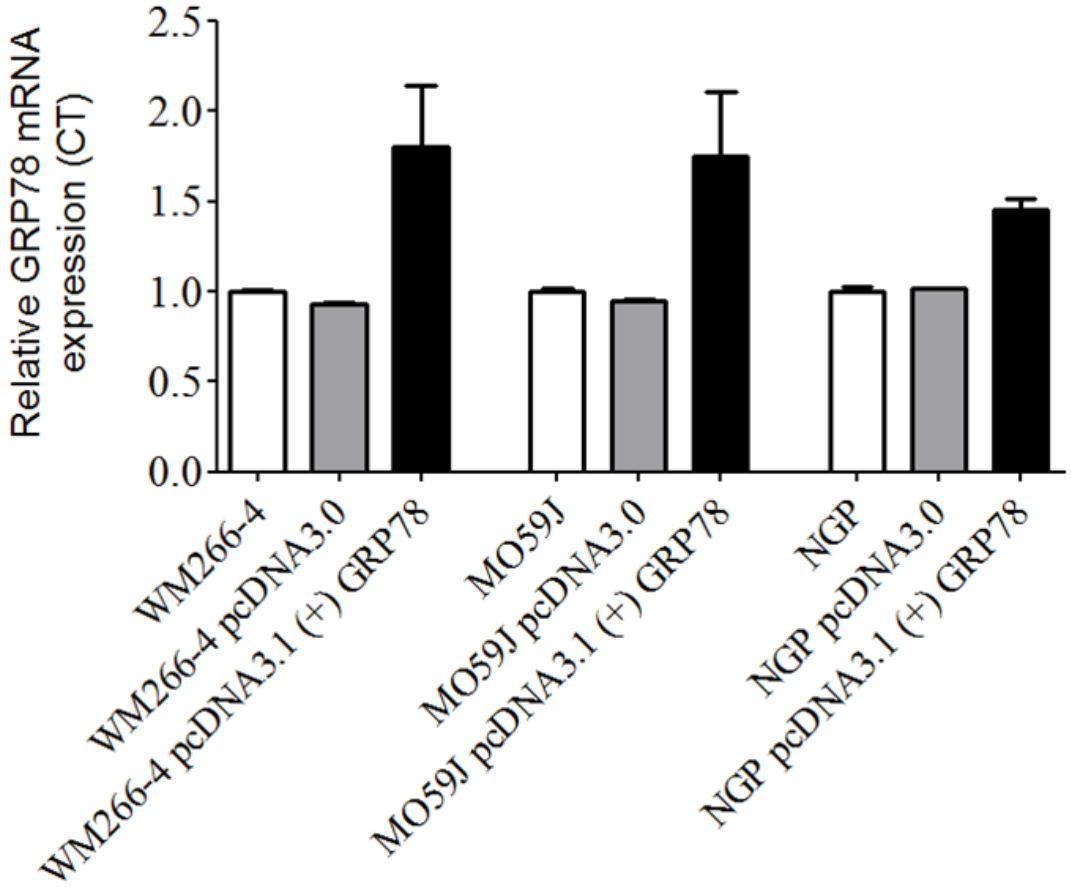

Figure 5.2: *The effect of pcDNA3.1 (+) GRP78 on GRP78 mRNA expression. WM266-4 melanoma, MO59J glioblastoma and NGP neuroblastoma neural-crest-derived cancer cells were stably transfected with control pcDNA3.0 or pcDNA3.1 (+) GRP78 (as described in methods) and the expression of GRP78 and β-Actin mRNA were analysed by real time PCR in comparison to wild type cell lines. Data are the mean of 3 individual experiments and expressed as relative to loading control ± 95% CI.*

Immunofluorescence staining was also used to determine the effect of transfection on GRP78 expression and cellular localisation. Confocal microscopy images (Figure 5.3 A) showed that although GRP78 intensity was significantly different between cell types (One-way ANOVA $F_{8, 89} = 45.4$, $P < 0.0001$), the effects of transfection resulted in similar GRP78 distribution. Data revealed that GRP78 cellular expression was cytoplasmic in localisation with an increased staining surrounding the peri-nuclear zone. A comparison of staining intensities for cells stably over-expressing GRP78 or control plasmid demonstrated a significant increase for melanoma (Figure 5.3 B, One-way ANOVA with Bonferoni post hoc correction, $P < 0.0001$), glioblastoma ($P < 0.0001$) and neuroblastoma ($P < 0.01$); and there was no significant difference between the wild-type cell lines and control vector-transfected cells ($P > 0.05$). Furthermore, comparing neural-crest-derived cancer types, over-expressing GRP78, data also demonstrated significant differences between the relative mRNA expression of melanoma or glioblastoma and neuroblastoma (Figure 5.2, One-way ANOVA with Bonferroni post hoc corrections, for the comparison of neuroblastoma to melanoma or glioblastoma $P < 0.0001$).

Light microscopy (Figure 5.4) analysis also demonstrated that over-expression of GRP78 resulted in a morphological change in NGP neuroblastoma cells (Figure 5.4). Photomicrographs also revealed a swelling of the cells with a decrease in dendrites, representing a significant increase in NGP cell size (Figure 5.4 B, One-way ANOVA, $F_{2, 29} = 62.4$, $P < 0.0001$). Melanoma and glioblastoma cells however, showed no apparent change in cell morphology.

These data indicate a significant increase in GRP78 mRNA and protein expression, that has not altered cellular distribution, however has induced a morphological change in neuroblastoma.

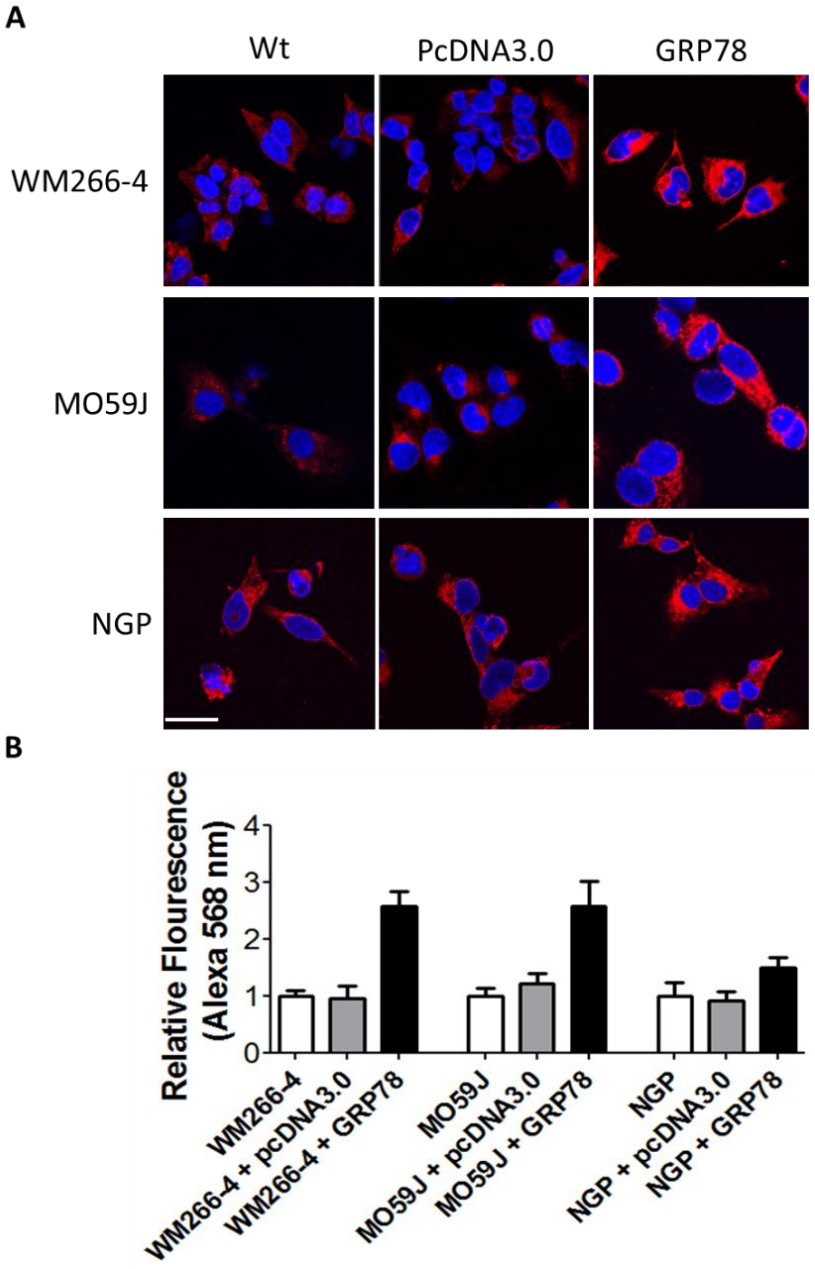

Figure 5.3: *The effect of pcDNA3.1 (+) GRP78 on GRP78 expression and localisation.* ***(A)*** *WM266-4 melanoma, MO59J glioblastoma and NGP neuroblastoma neural-crest-derived cancer cells were stably transfected with control pcDNA3.0 or pcDNA3.1 (+) GRP78 and the expression of GRP78 assessed by immunofluorescence. Cells were fixed in 100% ice cold methanol for 30 min, prior to staining for GRP78, using DAPI as control dye for the nucleus. Data are representative images of 3 individual experiments. Scale bar on NGP wt = 20 µm.* ***(B)*** *Cellular fluorescent intensities for the effect of GRP78 over-expression (black) in comparison to vector (grey) on GRP78 staining are the average of 30 cells per condition and data expressed as relative to control wild type (white) ± 95% CI.*

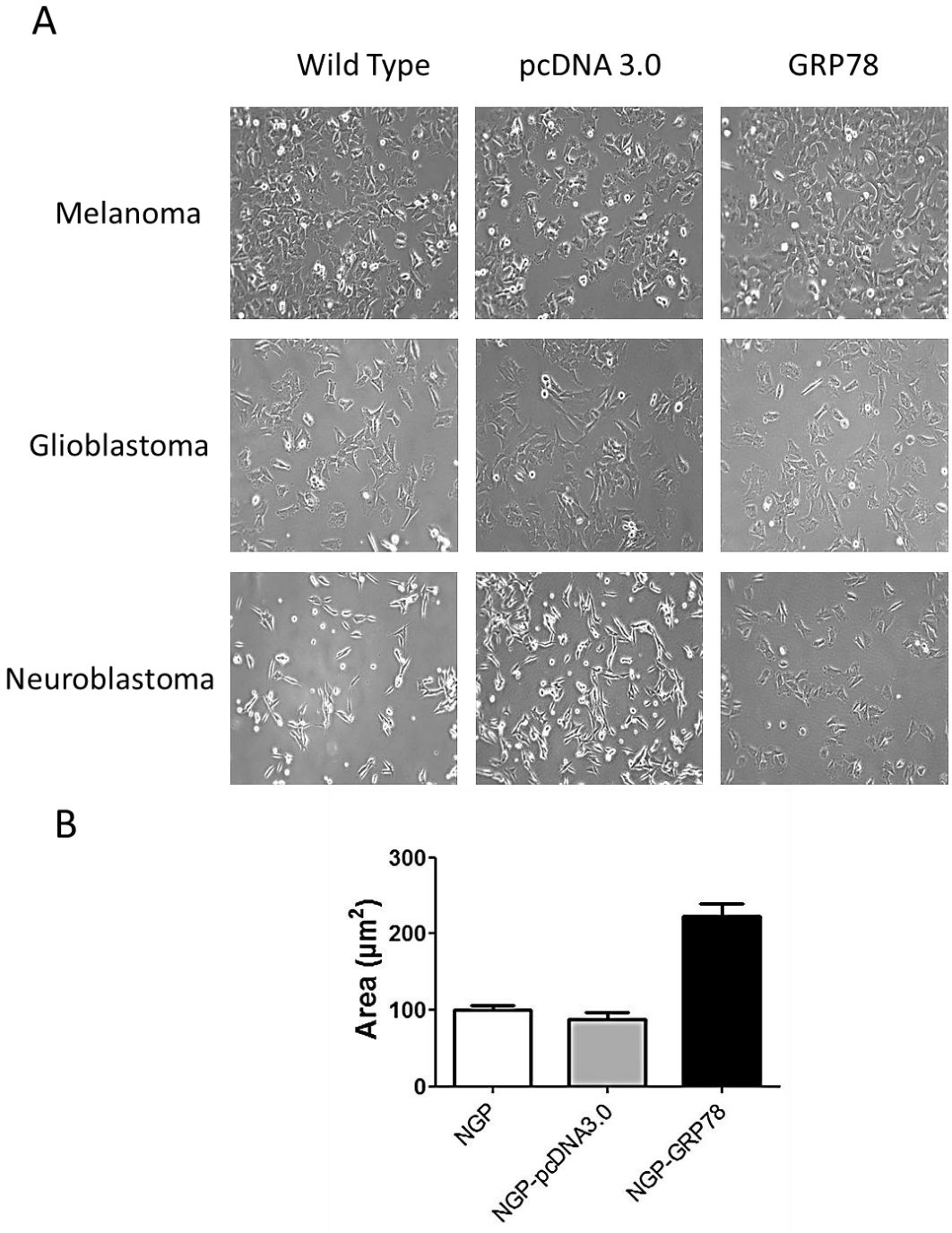

Figure 5.4: *The effect of GRP78 expression on cell line morphology. (A) Neural-crest-derived melanoma, glioblastoma and neuroblastoma cancer cells that were stably over-expressing GRP78 in comparison to control empty vector were assessed by light microscopy for the effect of transfection and GRP78 over-expression on morphology, in comparison to control wild-type cell lines. (B) Cell area for NGP neuroblastoma cell lines were calculated and data expressed as mean area of 30 cells over 3 individual experiments ± 95% CI.*

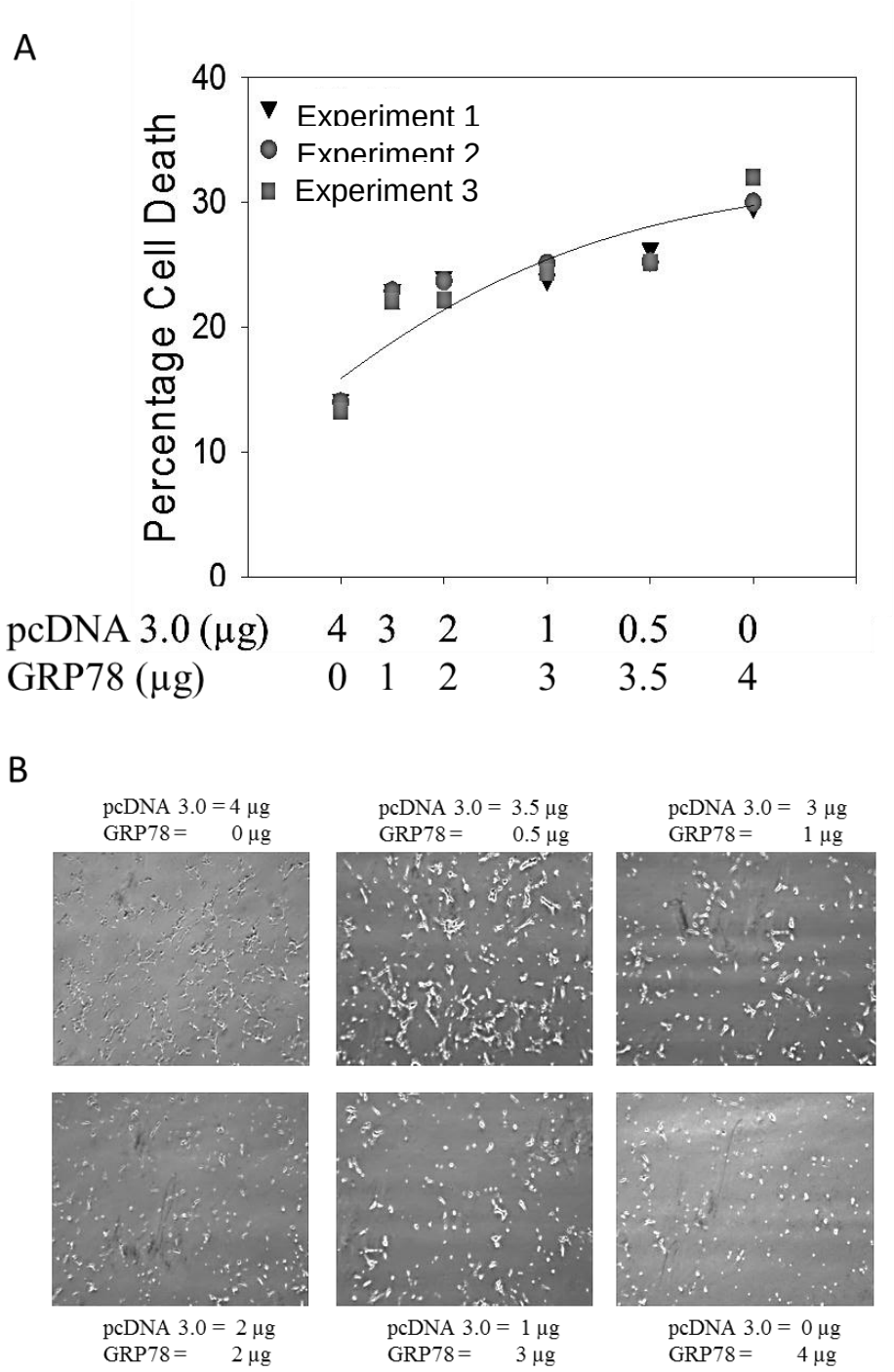

Figure 5.5: *The effect of GRP78 over-expression on neuroblastoma.* ***(A)*** *NGP neuroblastoma cells were transiently transfected with increasing concentrations of pcDNA3.1 (+) GRP78 to a maximum of 4 µg. Each individual transfection contained the same amount of total plasmid DNA by supplementing with pcDNA3.0 control vector and the effect of GRP78 on cell death assessed by propidium iodide stained flow cytometry. Flow cytometry data are the means of 3 individual experiments ± 95%.* ***(B)*** *Light microscopy images were acquired prior to flow cytometry to highlight the effect of GRP78 expression.*

Over-expression of GRP78 also resulted in a noticeable induction of cell detachment in neuroblastoma, but not in melanoma or glioblastoma cells. To check that the consequence of GRP78 over-expression were dose-dependent, NGP cells were transiently transfected with increasing amounts of pcDNA3.1 (+) GRP78. The final amount of plasmid DNA was kept at 4 µg/ml by the addition of pcDNA3.0. After transfection (24 h), cells were imaged prior to the analysis of cell death by flow cytometry of propidium iodide stained cells (Figure 5.5). Results demonstrated a significant increase in cell death of NGP cells with increasing amounts of transfected GRP78 (Figure 5.5 A, One-way ANOVA, $F_{5, 17} = 138.1$, $P < 0.0001$). Light microscopy images (Figure 5.5 B) also showed increasing concentrations of GRP78 transfection resulted in an increase in detached cells and a decrease in attached, flat cells. This suggests that an increase in GRP78 expression impacts on neuroblastoma cellular stress and survival.

5.2.2: The effect of GRP78 over-expression on cellular resistance to death.

The effect of stable GRP78 over-expression in neural-crest-derived cell models on ER stress-induced cell death was also evaluated by flow cytometry of propidium iodide stained cells after treatment with either fenretinide (10 μM for melanoma and glioblastoma or 5 μM for neuroblastoma) or bortezomib (200 nM for melanoma and glioblastoma or 20 nM for neuroblastoma) (Figure 5.6). Results clearly demonstrated over-expression of GRP78 affected the sensitivity of all neural-crest-derived cancer types. Comparing the effect of control transfection to transfection with GRP78, data revealed that there were no significant differences due the contrasting outcomes observed between melanoma or glioblastoma, to that of neuroblastoma ($P > 0.05$). However, results comparing the effect of GRP78 transfection across cancer type showed significant differences (Two-way ANOVA, $F_{2, 26} = 193.7$, $P < 0.0001$).

In melanoma or glioblastoma cells, over-expression of GRP78, resulted in a significant decrease in fenretinide- or bortezomib-induced cell death compared to either wild-type cells or cells stably transfected with vector control (Figure 5.6 A & B, One-way ANOVA with Bonferroni post hoc corrections, $P < 0.0001$ for either agent in both cancer types). Conversely, in neuroblastoma cells over-expressing GRP78 resulted in a significant increase in sensitivity to fenretinide- and bortezomib-stimulated ER stress-induced death (Figure 5.6 C, One-way ANOVA with Bonferroni post hoc corrections, $P < 0.01$ or $P < 0.0001$ for either fenretinide or bortezomib, respectively). Although stable transfection of GRP78 affected the response of cells to both fenretinide and bortezomib, a significantly greater inhibition of response was observed in melanoma cells treated with bortezomib (Figure 5.6 A, One-way ANOVA with Bonferroni post hoc corrections, $P < 0.0001$). In glioblastoma and neuroblastoma cells, however, there was no significant difference between responses to either fenretinide or bortezomib, with regards to the capacity of either agent to induce cell death in the presence of GRP78 over-expression ($P > 0.05$).

Investigating the effect of GRP78 over-expression on the ability of fenretinide or bortezomib to induce inhibition of cell viability, data demonstrated a significant effect on melanoma, glioblastoma and neuroblastoma cancer types (Figure 5.7). These data showed significant differences in response between both plasmid and cell type (Two-way ANOVA, $F_{2, 27} = 406.6$, $P < 0.001$ for cell and $F_{2, 27} = 12.3$, $P < 0.0001$ for plasmid).

These data highlight a significant influence of GRP78 on fenretinide and bortezomib induced cell death, as well as a significant difference in response type within neuroblastoma.

Data for melanoma and glioblastoma demonstrated a significant reduction of fenretinide and bortezomib induced inhibition of cell viability, in comparison to controls (Figure 5.7 A & B, One-way ANOVA with Bonferroni post hoc corrections, $P < 0.0001$ for either agent, in both cancer types). Neuroblastoma cells overexpressing GRP78 showed an increase in sensitivity to ER stress (Figure 5.7 C, One-way ANOVA with Bonferroni post hoc corrections $P < 0.001$ for fenretinide and $P < 0.0001$ for bortezomib).

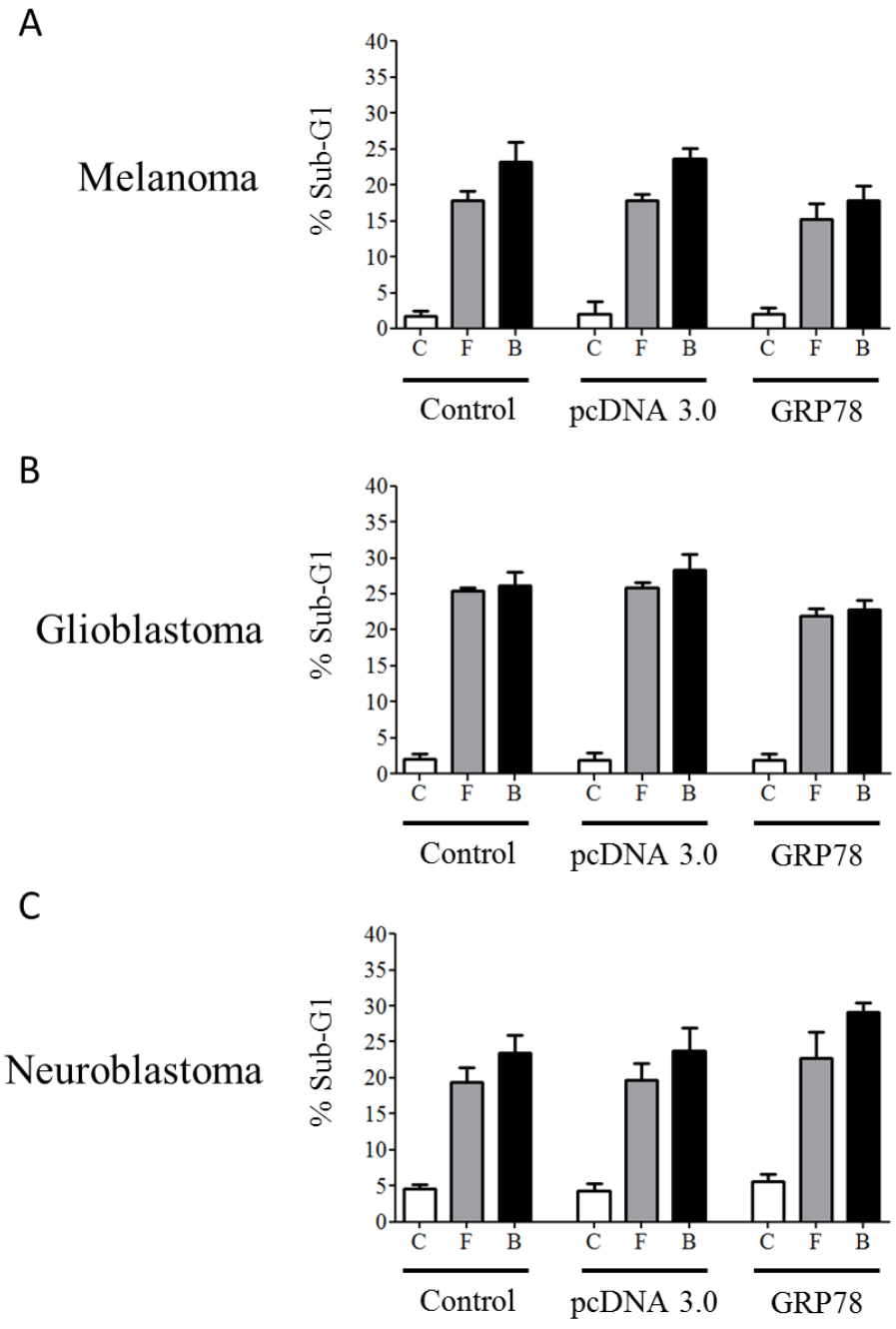

Figure 5.6: *The effect of GRP78 over-expression on neural-crest-derived cancer cell sensitivity to ER stress-induced cell death. Melanoma (A), glioblastoma (B) and neuroblastoma (C) cells stably over-expressing GRP78 were assessed for any changes in cellular resistance to death induced by either fenretinide (F, 10 µM for melanoma and glioblastoma or 5 µM for neuroblastoma) or bortezomib (B, 200 nM for melanoma and glioblastoma or 20 nM for neuroblastoma) compared to control (C, vehicle treated) for 24 h, in comparison to control transfected and wild type cells. Cell death was compared by propidium iodide stained flow cytometry on 70% ethanol fixed cells. Data were expressed as mean values of 3 independent experiments ± 95% CI.*

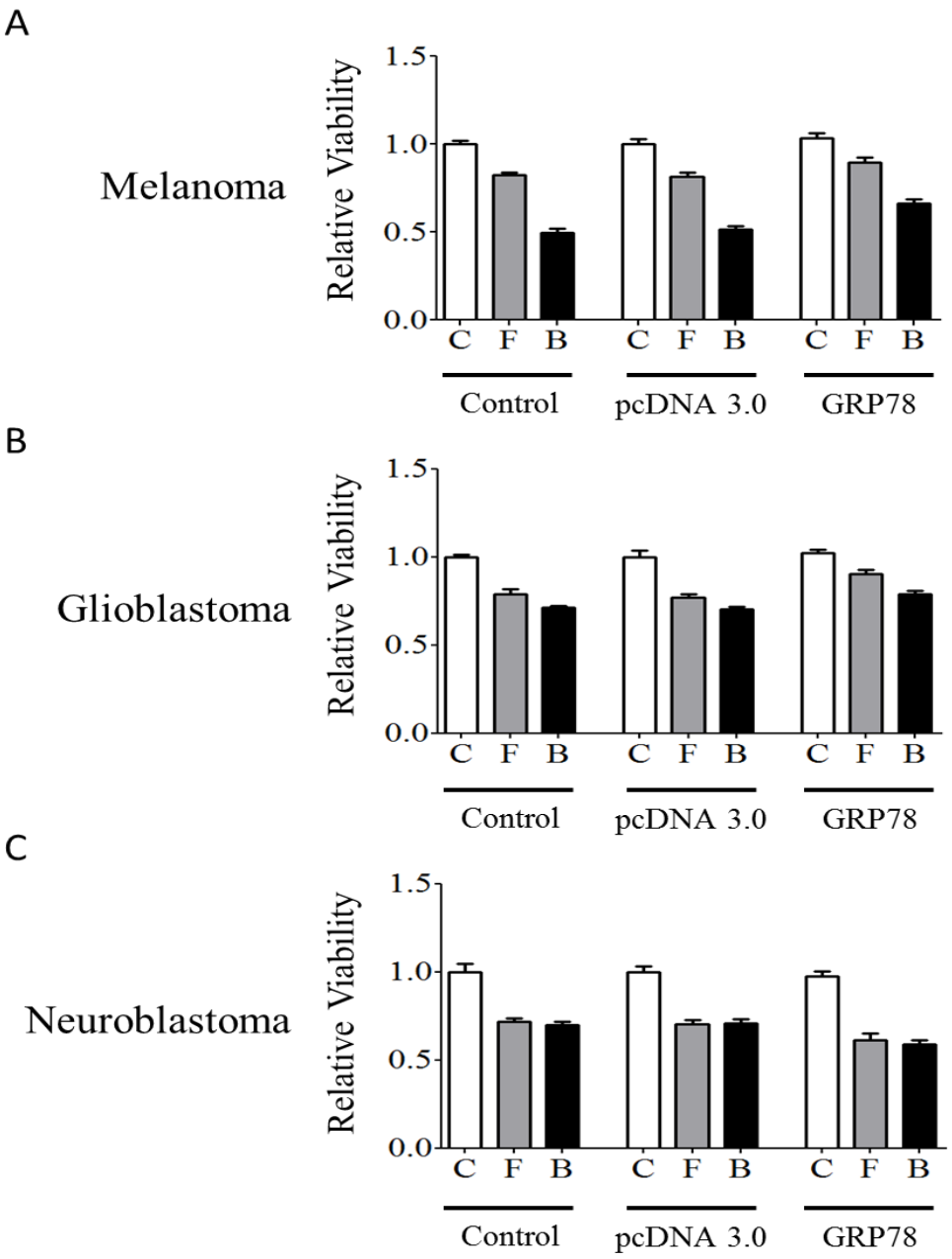

Figure 5.7: *The effect of GRP78 over-expression on cancer cell sensitivity to ER stress -induced inhibition of cell viability. Melanoma (A), glioblastoma (B) and neuroblastoma (C) cells that were stably over-expressing GRP78 were assessed for any changes in cellular resistance to inhibition of cell viability in comparison to control vector transfected or wild type cell lines, induced by either fenretinide (F, 10 µM for melanoma and glioblastoma or 5 µM for neuroblastoma) or bortezomib (B, 200 nM for melanoma and glioblastoma or 20 nM for neuroblastoma) in comparison to control (C, vehicle treated) for 24 h. Cell viability was assessed by the commercially available MTS assay. Data were expressed as the mean values of 3 independent experiments of 8 individual replicates ± 95% CI.*

To test the hypothesis that neural-crest-derived cancer cell sensitivity to ER stress is altered by GRP78 expression, due to changes in UPR activation as a consequence of manipulating the dynamic equilibrium between GRP78 and the UPR activators PERK, IRE1 and ATF6, the induction of ATF4 was investigated. Melanoma, glioblastoma and neuroblastoma stably expressing GRP78 were treated with fenretinide or bortezomib for 4 h in comparison to control pcDNA3.0 vector transfected cells, prior to analysis of ATF4 induction (Figure 5.8). Results demonstrated a significant effect on UPR induction in cells over-expressing GRP78 (Two-way ANOVA comparing the response across plasmid type or cancer type, $F_{1, 28} = 12.5$ $P < 0.001$ for plasmid and $F_{2, 28} = 406.9$, $P < 0.0001$ for cell line), with decreased ATF4 induction observed in response to fenretinide or bortezomib in melanoma and glioblastoma cells over-expressing GRP78 (Figure 5.8, One-way ANOVA with Bonferroni post hoc corrections, for melanoma treated with fenretinide $P < 0.0001$ or bortezomib $P < 0.001$ and for glioblastoma treated with fenretinide $P < 0.001$ or bortezomib $P < 0.0001$).

These data indicated an increased induction in response to ER stress in neuroblastoma cells over-expressing GRP78 and, therefore, highlighted a difference in mechanistic outcome in neuroblastoma, compared to either melanoma or glioblastoma. In this context, GRP78 over-expression in neuroblastoma cells resulted in significantly reduced induction of ATF4 in both control and fenretinide treated (Figure 5.8 A & B iii, One-way ANOVA with Bonferroni post hoc corrections, $P < 0.0001$ for either condition). Conversely, when treated with bortezomib, neuroblastoma cells demonstrated an increase in UPR activity, as shown by increased ATF4 induction ($P < 0.0001$).

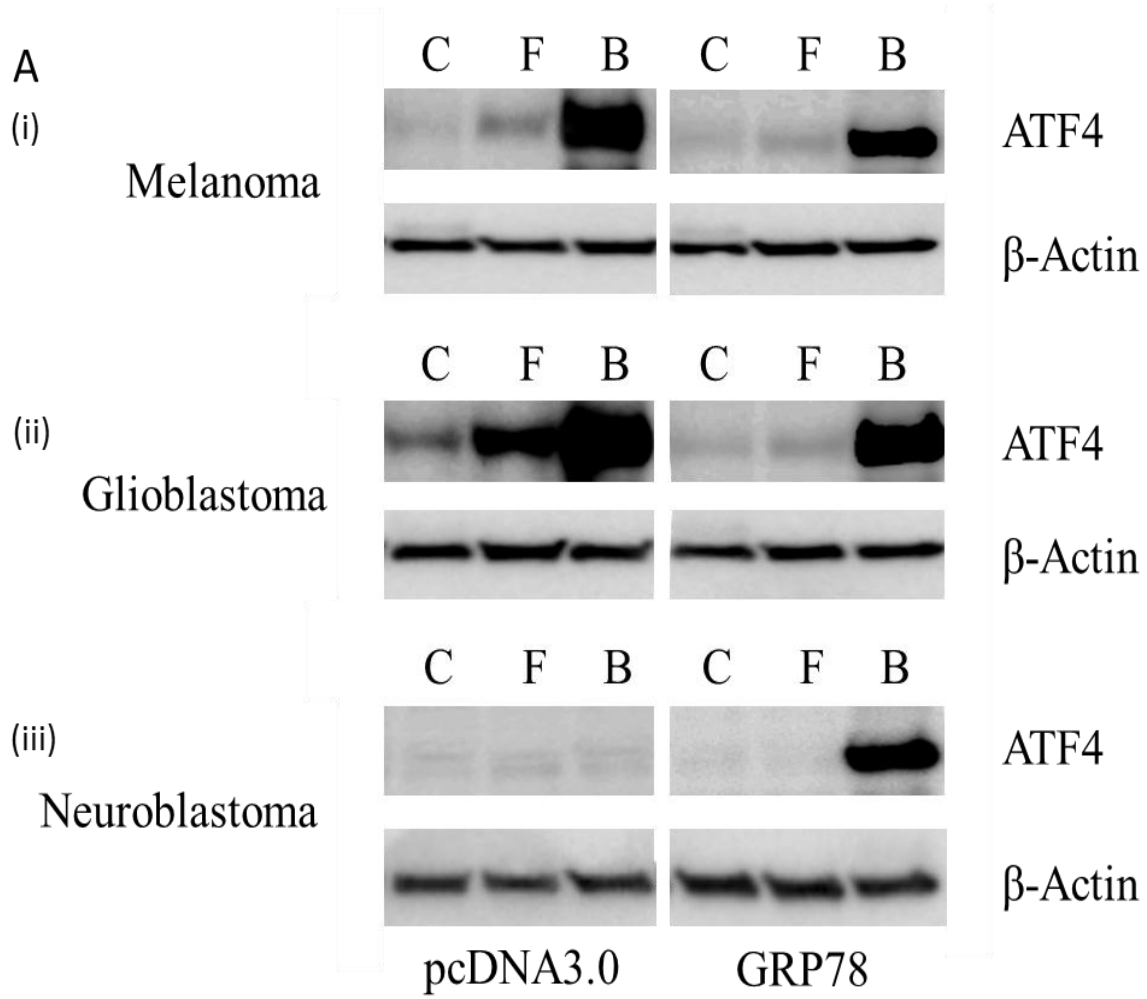

Figure 5.8 continued on next page

Figure 5.8 continued

B

(i)

Melanoma

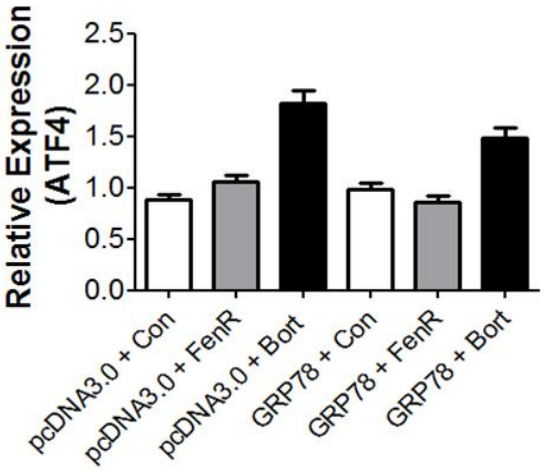

(ii)

Glioblastoma

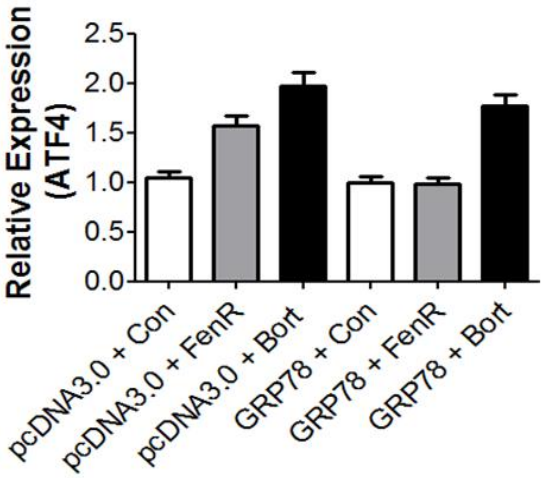

(iii)

Neuroblastoma

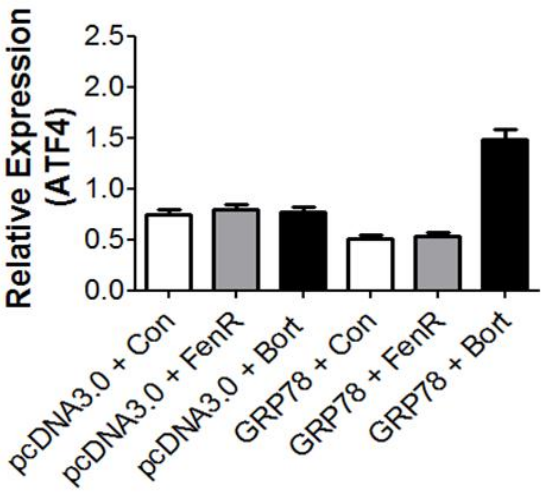

Figure 5.8 legend on next page

Figure 5.8: *The effect of GRP78 over-expression on UPR activity.* ***(A)*** *WM266-4 melanoma, MO59J glioblastoma and NGP neuroblastoma neural-crest-derived cancer cells stably over-expressing GRP78 in comparison to control vector were treated with fenretinide (10 µM for melanoma and glioblastoma or 5 µM for neuroblastoma) or bortezomib (200 nM for melanoma and glioblastoma or 20 nM for neuroblastoma) for 4 h. Western blot analysis for the induction of ATF4 were carried out in comparison to β-Actin as a loading control. Western blot data are representative blots of 3 repeat experiments. Figure 5.8 A; Cells treated with control = C, Fenretinide = F and Bortezomib = B.* ***(B)*** *Densitometry data for the effect of GRP78 expression on fenretinide (FenR, grey bars) or bortezomib (Bort, black bars) (graphs on next page) capacity to induce ATF4 in comparison to control (Con, white bars) are the average of triplicate experiments and bars are expressed as mean data relative to control (white bars, no treatment) ± 95% CI.*

To investigate if GRP78 modulation and the effects on ER stress-induced cell death resulted in downstream caspase activation, melanoma, glioblastoma and neuroblastoma cells over-expressing GRP78 were treated with fenretinide or bortezomib for 24 h and the effects on caspase 3 cleavage determined by western blotting (Figure 5.9). Data demonstrated GRP78 over-expression resulted in the inhibition of both fenretinide and bortezomib-induced caspase 3 cleavage in all neural-crest-derived cancer types (Figure 5.9, One-way ANOVA with Bonferroni post hoc corrections, for melanoma treated with fenretinide $P < 0.001$ or bortezomib $P < 0.0001$ and glioblastoma or neuroblastoma treated with either ER stress-inducing agent $P < 0.0001$). Investigating these effects between cancer types also demonstrated a significant difference between melanoma and either glioblastoma or neuroblastoma (Figure 5.9, One-way ANOVA with Dunnett's post hoc correction, $P < 0.001$ or $P < 0.0001$ respectively).

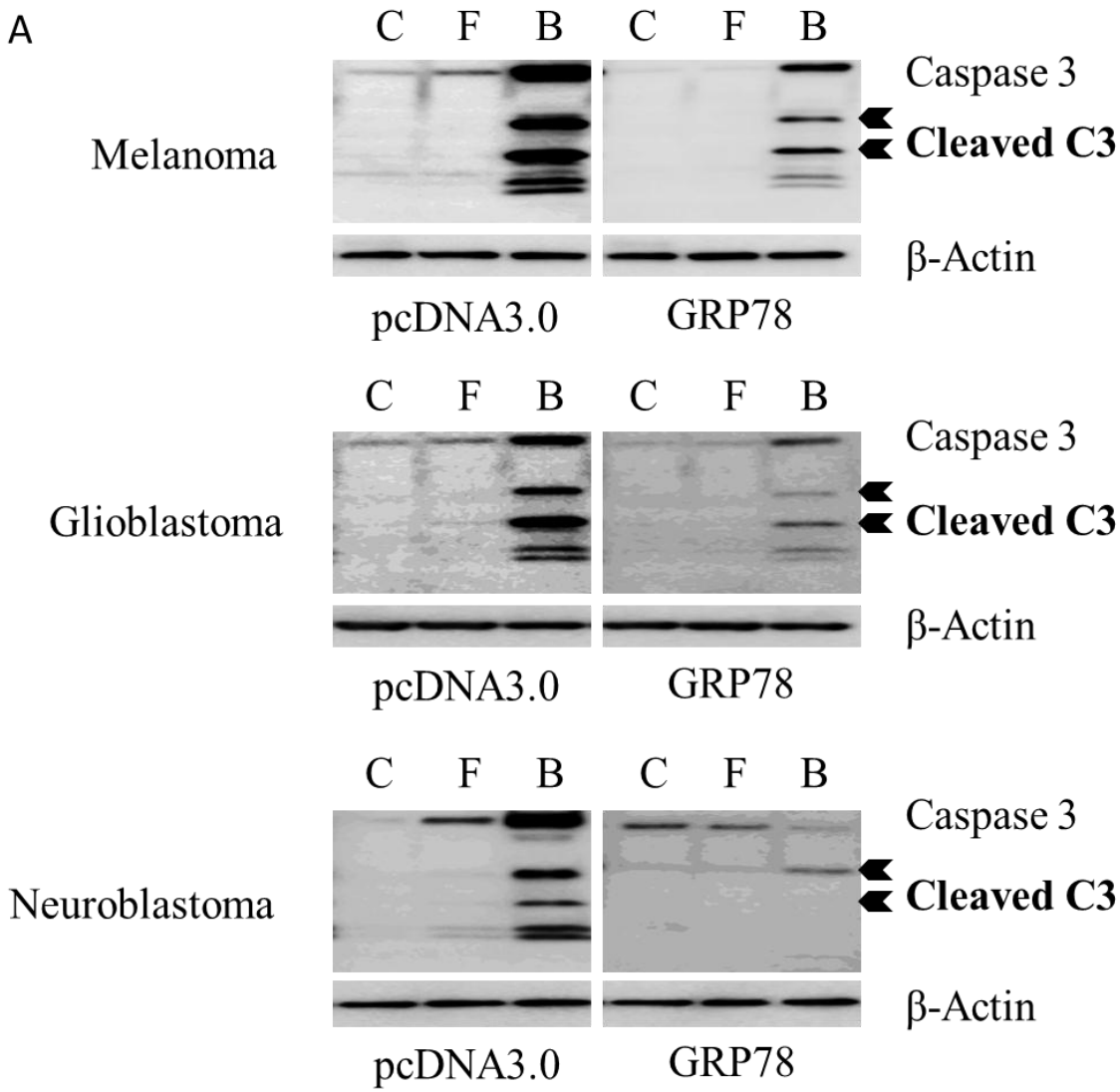

Figure 5.9 continued on the next page

Figure 5.9 continued

B

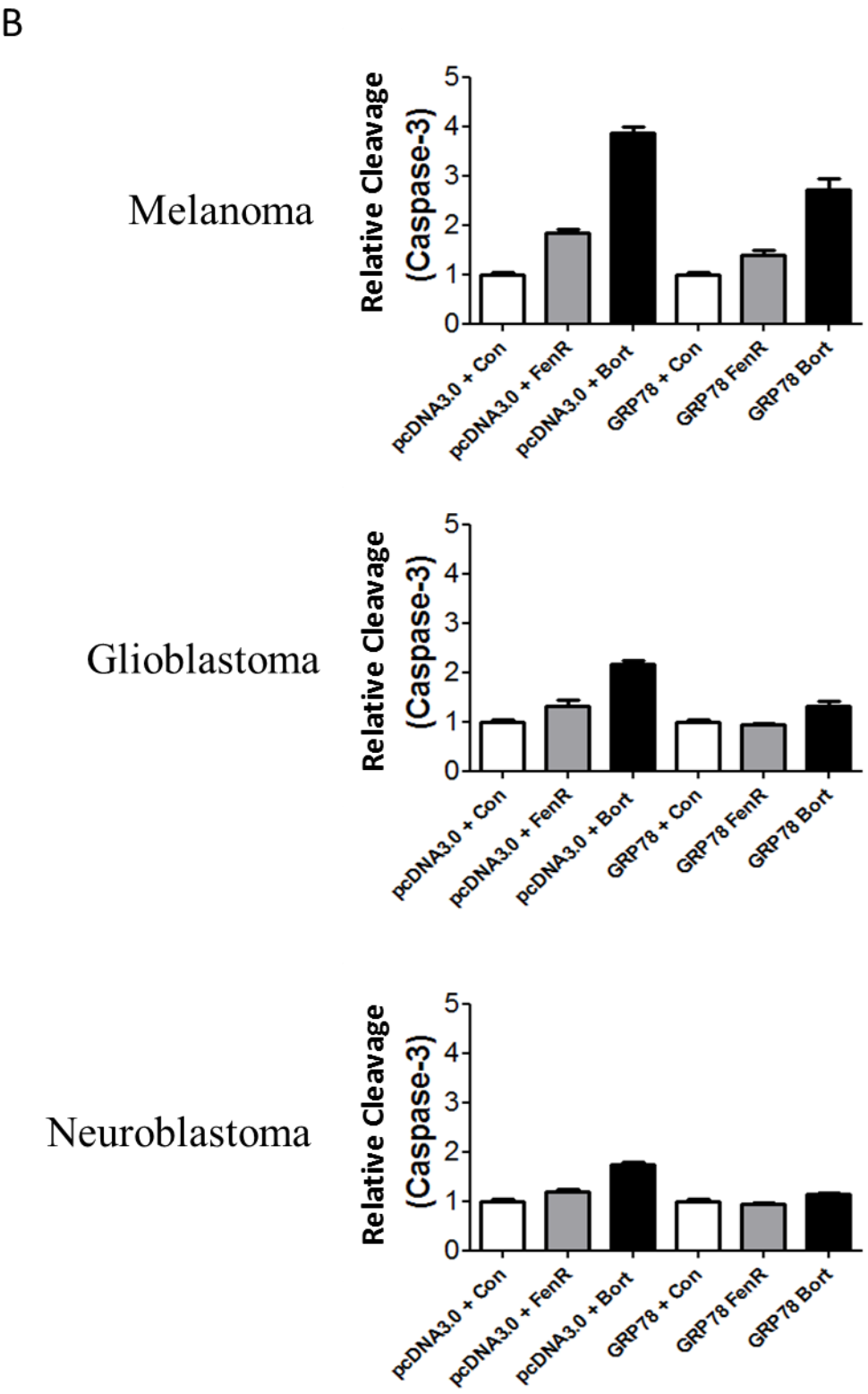

Figure 5.9 legend on next page

Figure 5.9: *The effect of GRP78 over-expression on the induction of caspase dependant cell death.* ***(A)*** *WM266-4 melanoma, MO59J glioblastoma and NGP neuroblastoma neural-crest-derived cancer cells stably over-expressing GRP78 in comparison to control vector were treated with fenretinide (10 µM for melanoma and glioblastoma or 5 µM for neuroblastoma) or bortezomib (200 nM for melanoma and glioblastoma or 20 nM for neuroblastoma) for 24 h. Western blot analysis for the induction of caspase 3 cleavage were carried out in comparison to β-Actin as a loading control. Western blot data are a representative blot of 3 repeat experiments. Figure 5.9 A; Cells treated with control = C, Fenretinide = F and Bortezomib = B.* ***(B)*** *Densitometry data for the effect of GRP78 expression on fenretinide (FenR, grey bars) or bortezomib (Bort, black bars) on caspase 3 cleavage, in comparison to control (Con, white bars, vehicle treated) are the average of triplicate experiments and bars are expressed as mean data relative to control (white bars, no treatment) ± 95% CI. For caspase 3 cleavage the accumulative intensity of the 17 and 19 kDa bands were used.*

To test the hypothesis that GRP78 over-expression alters its dynamic equilibrium with PERK, IRE1 and ATF6, the expression of each protein was evaluated in all neural-crest-derived cells over-expressing GRP78 compared to vector control or wild type cell lines (Figure 5.10). Results revealed a significant effect of GRP78 over-expression on the expression levels of each UPR activator, as well as significant differences between cancer types and the relative change in expression of each UPR activator (Figure 5.10, Two-way ANOVA, comparing plasmid and cell line expression, $F_{11,\ 107} = 77.1$, $P < 0.0001$ or $P < 0.005$ respectively).

Analyses highlighted that changes in UPR activator expression, with regard to the magnitude of protein expression, was altered by GRP78 over-expression and was also significantly different for all cancer types (Figure 5.10, One-way ANOVA, comparing UPR activators, $F_{11,\ 35} = 77.1$ for melanoma, 20.1 for glioblastoma and 67.8 for neuroblastoma, $P < 0.001$ for all cancer types).

With respect to PERK, IRE1 or ATF6 expression, there were no significant differences between wild type and control vector-transfected cell lines for each tumour type. Melanoma cells over-expressing GRP78 showed a significant increase in IRE1 and a significant decrease in ATF6 expression (Figure 5.10, One-Way ANOVA with Dunnett's post hoc correction, comparing stable transfected cells to wild type, $P < 0.0001$ for IRE1 and $P < 0.01$ for ATF6) while glioblastoma cells stably over-expressing GRP78 demonstrated a significant reduction in PERK expression ($P < 0.001$). Over-expression of GRP78 in neuroblastoma cells on the other hand resulted in a significant increase in all three UPR activators (Figure 5.10, comparing the expression of control wild type cells to GRP78 over-expressing for the expression of PERK $P < 0.05$, IRE1 or ATF6 $P < 0.0001$ for both).

Overall, changes in UPR activator concentration (fold increases in comparison to control) were significantly greater in neuroblastoma compared to either melanoma or glioblastoma (Figure 5.10, One-way ANOVA with Dunnett's post hoc correction, $P < 0.001$ for PERK and IRE1, or $P < 0.0001$ for ATF6).

Further analysis of relative changes in GRP78 and the UPR activator expression in neural-crest-derived cell lines stably over-expressing GRP78, in comparison to control vector were carried out to determine if over-expression of GRP78 altered the existing dynamic equilibrium with the UPR activators PERK, IRE1 and ATF6. Data

demonstrated a significant effect of GRP78 over-expression on the dynamic equilibrium that GRP78 exists in with the UPR activators (Figure 5.11).

There were also significant differences between cancer types (Figure 5.11, Two-way ANOVA, $F_{9, 35} = 72.4$, $P < 0.0001$). Melanoma and glioblastoma cells exhibited a significantly greater fold increase in GRP78 expression, compared with the changes to the UPR activators (One-way ANOVA with Bonferroni post hoc corrections, $P < 0.0001$ for both cancer types). Conversely, over-expression of GRP78 in neuroblastoma cells resulted in a greater fold induction of UPR activators compared to the fold increase in GRP78 itself (One-way ANOVA with Bonferroni post hoc corrections, $P < 0.0001$).

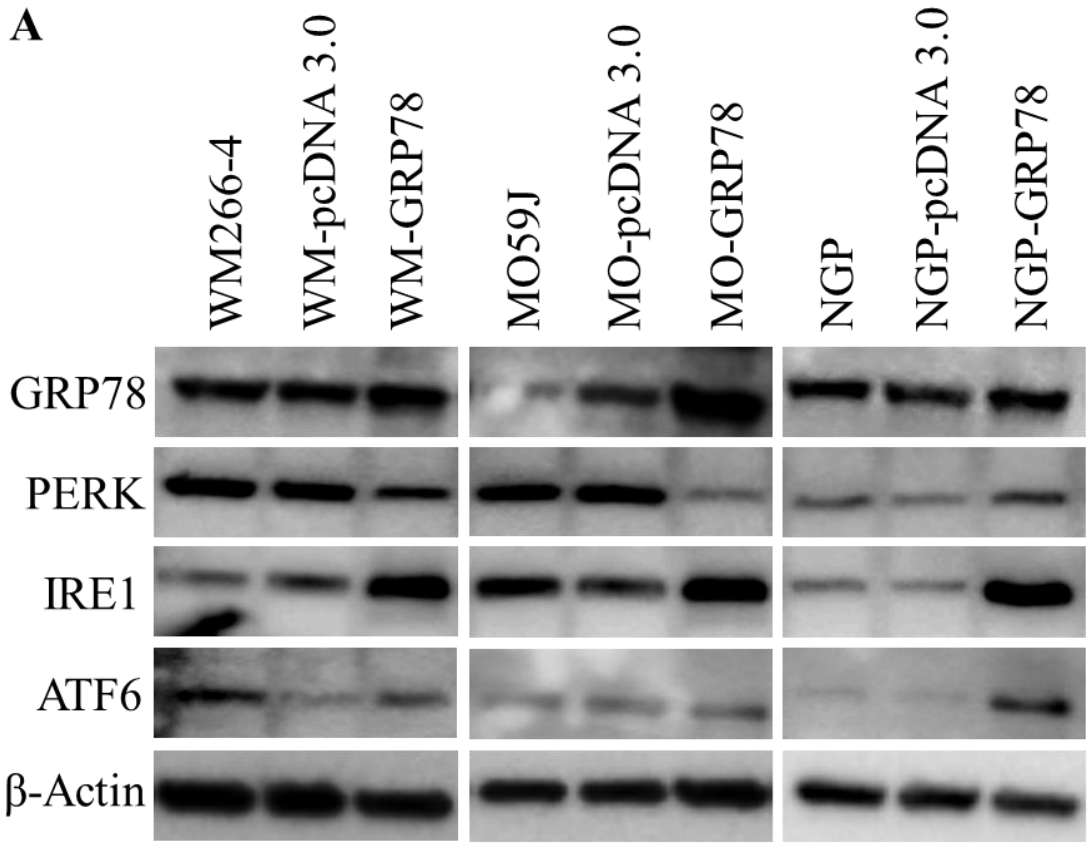

Figure 5.10: *The effect of GRP78 on UPR activator expression.* ***(A)*** *WM266-4 melanoma, MO59J glioblastoma and NGP neuroblastoma neural-crest-derived cancer cells stably over-expressing GRP78 in comparison to control vector or wild type cell line were assessed for changes in the expression of PERK, IRE1 and ATF6 in comparison to β-Actin as a loading control.* ***(B)*** *Densitometry analyses were performed for melanoma (i), glioblastoma (ii) and neuroblastoma (iii) western blotting data and were expressed as relative to control. Data on next page) and each bar is the mean of 3 replicate experiments ± 95% CI.*

Figure 5.10 continued on next page

Figure 5.10 continued

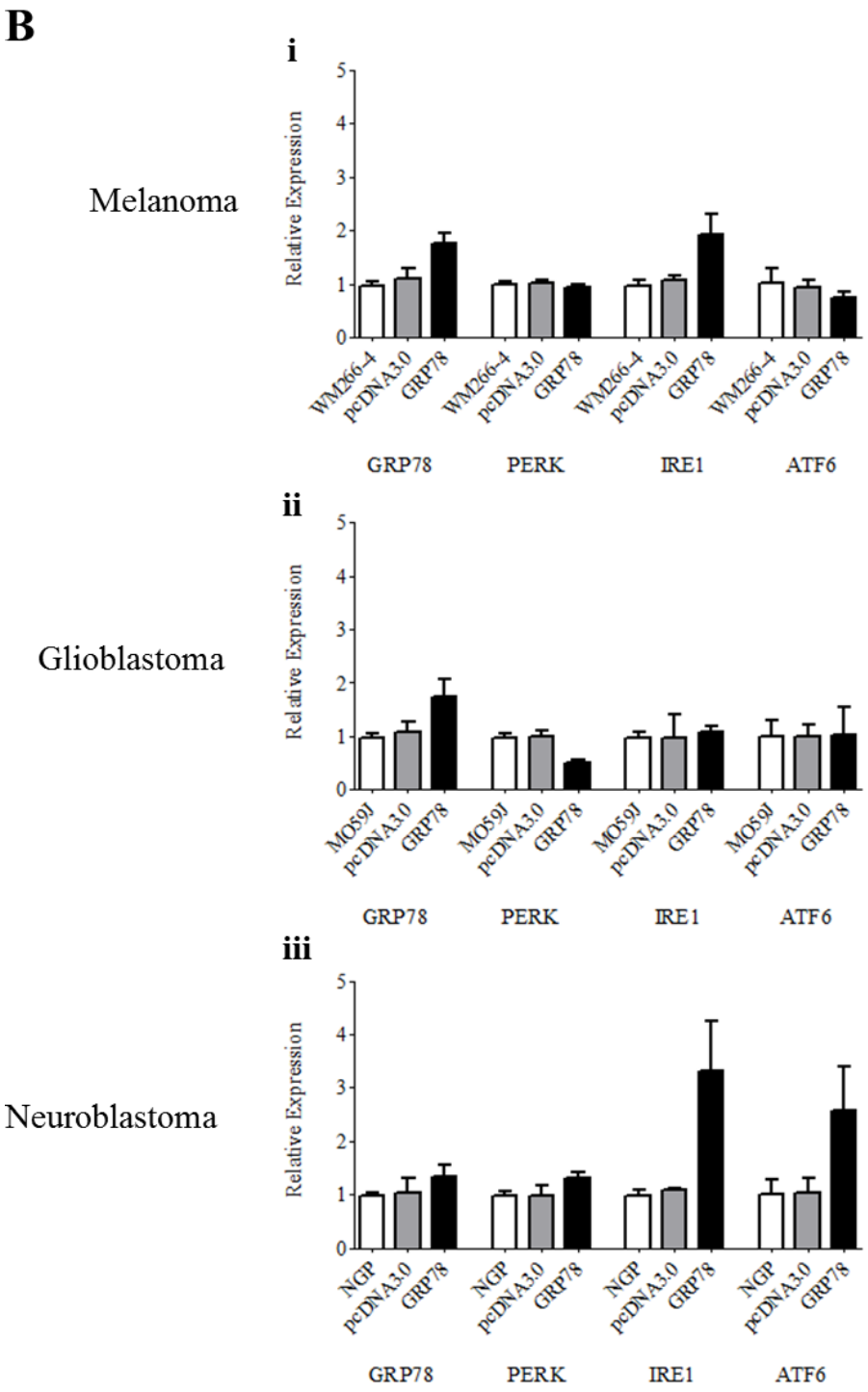

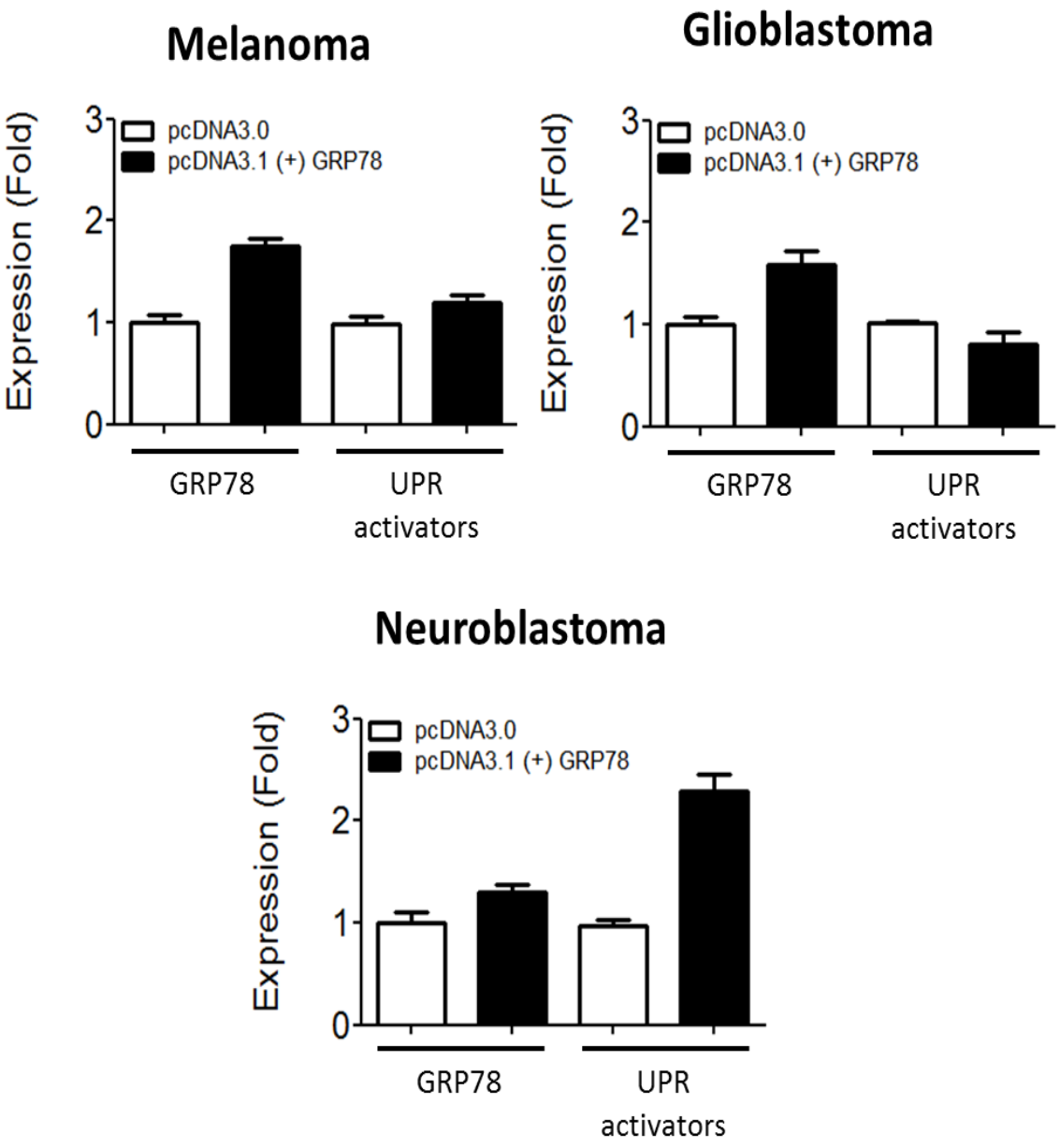

Figure 5.11: *The effect of GRP78 over-expression on relative expression of the UPR activators. Melanoma, glioblastoma and neuroblastoma cells stably over-expressing GRP78 (black bars) in comparison to control pcDNA3.0 (white bars) were analysed for the changes in GRP78 and UPR activator proteins expression and data expressed as relative fold changes of either GRP78 or combined UPR activator expression. Data expressed as relative to β-Actin prior to control vector compensation. Data were the mean of 3 independent experiments ± 95% CI.*

To check that the decrease in fenretinide or bortezomib-induced cell death resulting from GRP78 over-expression was a result of changes to signalling downstream of GRP78 and not the amount of stress resulting from drug treatment, the amount of ROS or ubiquitin tagged proteins was measured under control and over-expression conditions. Cells were treated with either fenretinide (Figure 5.12) for 6 h or bortezomib (Figure 5.13) for 8 h or 24 h. Subsequent analysis demonstrated GRP78 over-expression in melanoma and glioblastoma cells resulted in significant inhibition of fenretinide induced ROS (Figure 5.12, One-way ANOVA with Bonferroni post hoc corrections, $P < 0.0001$ for both cancer types). Conversely, GRP78 over-expression had no significant effect on ROS accumulation in neuroblastoma cells (One-way ANOVA with Bonferroni post hoc corrections, $P < 0.05$).

Treatment of cells with bortezomib resulted in a build-up of ubiquitin-tagged proteins and this was significantly reduced by GRP78 over-expression in melanoma and glioblastoma cells compared to control-transfected and wild-type cell lines, following treatment with bortezomib for either 8 or 24 h (Figure 5.13 B, One-way ANOVA with Bonferroni post hoc corrections, for melanoma $P < 0.005$ and $P < 0.01$ or glioblastoma $P < 0.05$ and $P < 0.01$ at 8 h and 24 h, respectively). Conversely, neuroblastoma cells over-expressing GRP78 showed an increase in ubiquitin-tagged proteins ($P < 0.001$ for both time points) in response to bortezomib. Comparisons across cancer types showed a significant difference between melanoma and glioblastoma, to neuroblastoma (Figure 5.13, One-way ANOVA with Bonferroni post hoc corrections comparing neuroblastoma to either melanoma or glioblastoma at either 8 h or 24 h, $P < 0.0001$). Comparing the 8 h and 24 h time points, results demonstrated that there was no significant difference for ubiquitin build-up across cancer type.

Data demonstrate a difference in response outcome to ER stress between cancer types with melanoma and glioblastoma showing increased resistance. This study also showed that an increase in GRP78 expression alters UPR activator expression in a cancer type-specific manner resulting in a significant increase in UPR activators in neuroblastoma, which may prime this cancer type to ER stress induced death.

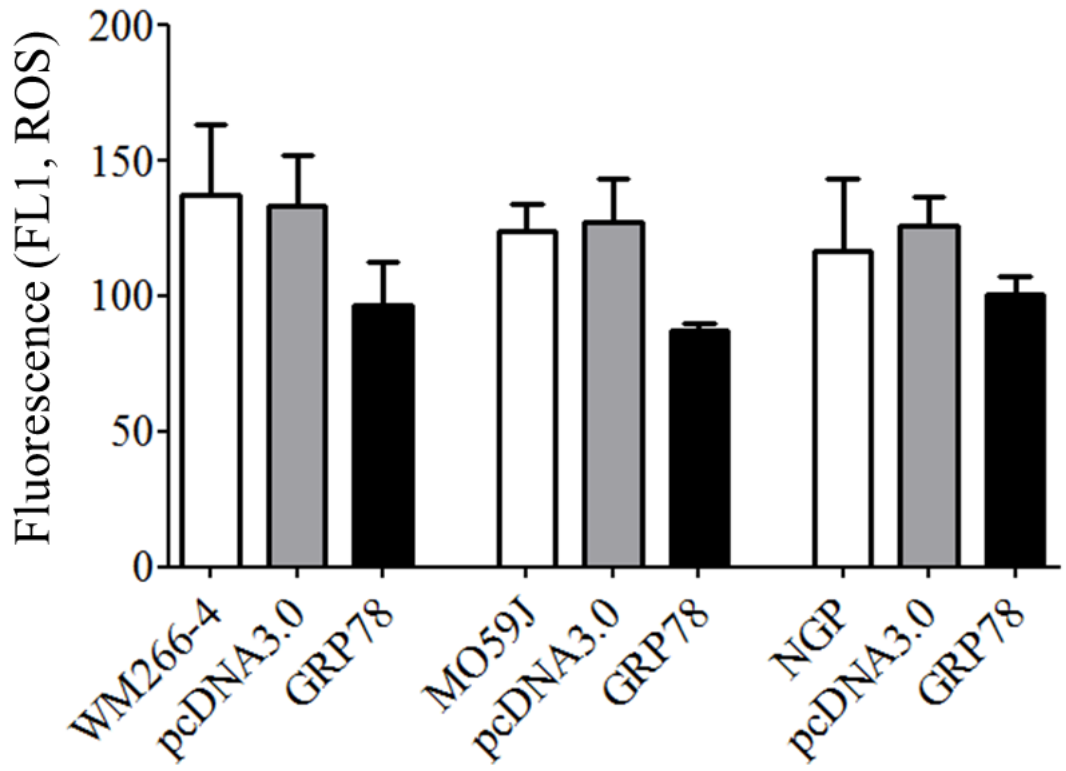

Figure 5.12: *The effect of GRP78 over-expression on ROS production. WM266-4 melanoma, MO59J glioblastoma and NGP neuroblastoma neural-crest-derived cancer cells stably over-expressing GRP78 (black bars) in comparison to control vector (grey bars) and wild type cell lines (white bars) were treated with fenretinide (10 µM fenretinide for melanoma and glioblastoma or 5µM for neuroblastoma) for 6 h, prior to staining with H2DCFDA for 20 min (as described in methods) and assessed for fluorescent induction by flow cytometry (FL-1). Data were expressed as mean values of 3 experiments ± 95% CI.*

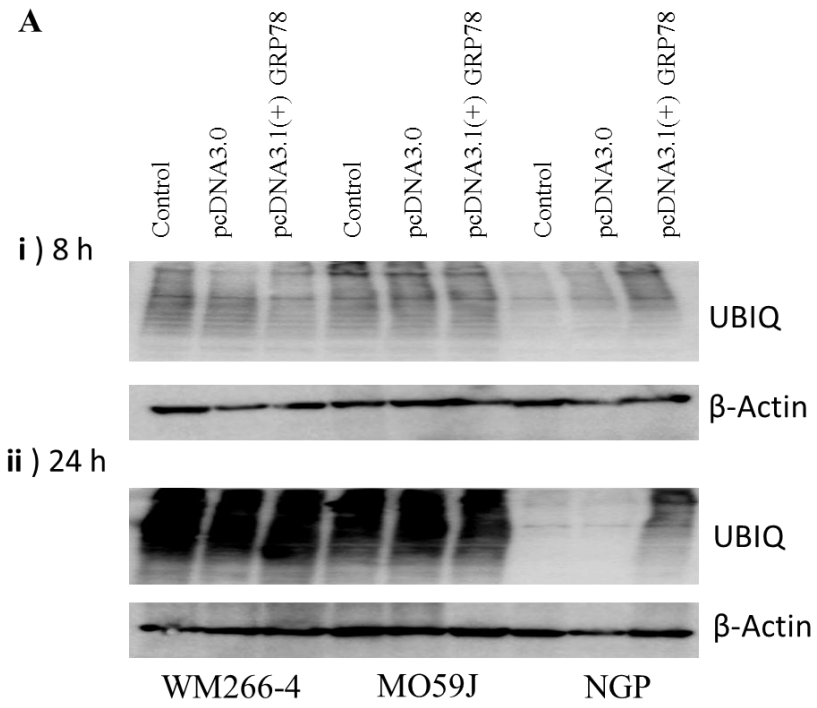

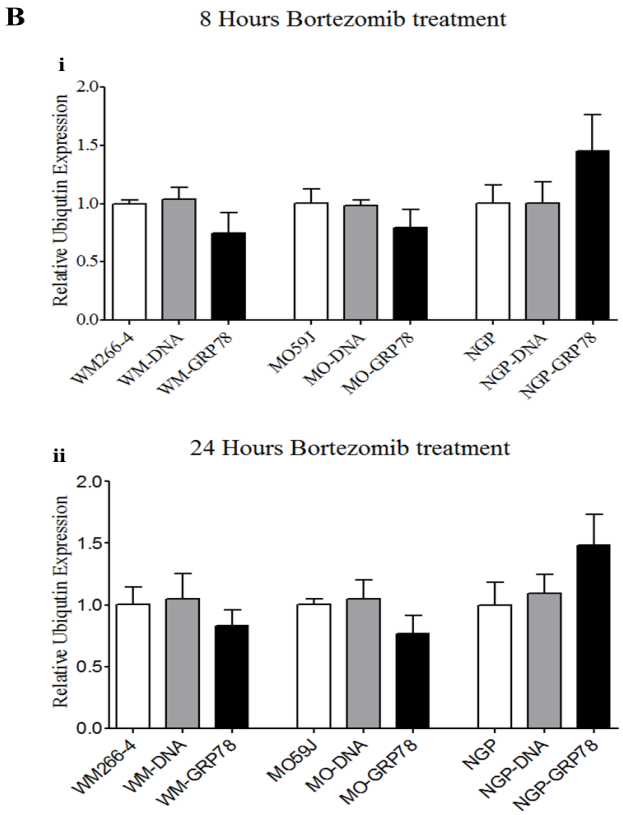

Figure 5.13 legend is on the next page

Figure 5.13: *The effect of GRP78 over-expression on ER stress-induced protein degradation.* ***(A)*** *Neural-crest-derived melanoma (WM266-4), glioblastoma (MO59J) and neuroblastoma (NGP) cancer cell lines that were stably over-expressing pcDNA3.0 (grey bars) or pcDNA3.1 (+) GRP78 (black bars), in comparison to wild type cells (white bars), were treated with bortezomib (200 nM for melanoma and glioblastoma or 20 nM for neuroblastoma) for 8 (i) and 24 (ii) h, prior to harvesting. Cell lysates were assessed by western blot analysis for ubiquitin smears (indicative of proteins tagged for degradation) in comparison to β-Actin as a loading control.* ***(B)*** *Densitometry was carried out for Ubiquitin smears and data expressed as relative to control. Each bar is the mean of 3 individual experiments ± 95& CI.*

5.2.3: Results Summary.

- Neural-crest-derived cancer types demonstrated significant differences in the ability to over-express GRP78. Glioblastoma cells showed the greatest increase in GRP78 expression.

- The ability to increase the expression of GRP78 did not correlate with basal expression, as neuroblastoma cell lines demonstrated the lowest cellular concentration and the smallest increase when transfected with pcDNA3.1(+) GRP78

- Over-expression of GRP78 significantly reduced melanoma and glioblastoma cell line sensitivity to ER stress-induced cell death. However, neuroblastoma cells showed an increase in cellular sensitivity to either fenretinide or bortezomib induced cell death.

- Melanoma and glioblastoma cells with increased GRP78 expression demonstrated a decrease in fenretinide and bortezomib induced inhibition of cell viability. Neuroblastoma cells, over-expressing GRP78, were significantly more sensitive to ER stress-induced inhibition of cell viability.

- The induction of caspase-3 cleavage by fenretinide or bortezomib was significantly reduced in neural-crest-derived cancer types that demonstrated a significant increase in GRP78 expression.

- Investigating the effect of GRP78 over-expression on UPR activation, demonstrated a significant reduction in induction of ATF4 in melanoma and glioblastoma cells in response to ER stress, but neuroblastoma cells showed a significant increase in ATF4 expression in response to fenretinide and bortezomib.

- Stable over-expression of GRP78 resulted in changes to the expression levels of the UPR activators PERK, IRE1 and ATF6. Neuroblastoma showed the greatest alteration in UPR activator expression, with an increase overall.

- Melanoma and glioblastoma cells with increased expression of GRP78 demonstrated a significant reduction in fenretinide or bortezomib ROS or Ubiquitin tagged protein accumulation, respectively. Neuroblastoma cells demonstrated no changes in ROS accumulation, however demonstrated a significant increase in ubiquitin tagged proteins in response to bortezomib treatment.

- Transient increase in GRP78 expression in neuroblastoma cells induced cell death.

5.3: Discussion.

Data from the present chapter demonstrate that increased GRP78 expression altered the sensitivity of neural-crest-derived cancer cells to ER stress-induced cell death and inhibition of cell viability. As a consequence of GRP78 over-expression, ER stress-induced UPR activation in melanoma and glioblastoma was reduced (as measured by ATF4 induction). However, neuroblastoma cells showed an increase in cellular sensitivity to ER stress-induced cell death, demonstrating the capacity to induce significantly higher levels of ATF4 during periods of ER stress. Unexpectedly, the data for neuroblastoma, in contrast to that of either melanoma or glioblastoma, demonstrated a marked decrease in caspase-3 activation. Over-expression of GRP78 also modulated the expression of the UPR activators PERK, IRE1 or ATF6 as well as the induction of spontaneous cell death in neuroblastoma cells. Furthermore, GRP78 over-expression altered the level of stress "seen" by the cells as measured by ROS and ubiquitin-tagged protein accumulation.

Stable clones of all cancer types over-expressing GRP78 were generated and demonstrated a significant increase in cellular expression of GRP78 in comparison to cells transfected with pcDNA3.0 vector control or wild type cells. GRP78 expression increased at both the mRNA and protein level, with expression of mRNA correlating with achievable protein induction. Optimisation of over-expression generated cells with a 1.5 (neuroblastoma) to 2.0 (melanoma and glioblastoma)-fold increase in expression. Previous studies have evaluated the role of GRP78, by generating a range of cell types over-expressing GRP78: in these studies GRP78 over-expression was to a similar degree as in the present study, ranging from 1.5 to 3 fold [295-301]. These studies were carried out in a range of differing cell types and demonstrate the cell line models developed in this study are within the achievable range for GRP78 over-expression. The over-expression of GRP78 showed that the ability of a particular cell line to increase its expression of GRP78 is not related to the basal concentration. Neuroblastoma cells demonstrated the lowest cellular concentrations of GRP78 and the smallest amount of inducible GRP78 compared to glioblastoma and melanoma cells. These findings suggest differences between cell types and their capacity to allow protein concentrations to fluctuate. These data also highlight the differential importance of GRP78 in different cancer types and thereby allow a greater promotion of GRP78 translation.

Evaluation of the effect of GRP78 over-expression on the sensitivity of neural-crest-derived cells to ER stress-induced cell death or inhibition of cell viability demonstrated increased resistance in melanoma and glioblastoma cells. This suggests that GRP78 aids melanoma and glioblastoma survival during periods of ER stress. These findings may be a direct consequence of changes to the dynamic equilibrium of the UPR. An increase in GRP78 may reduce UPR activation, as increased GRP78 would result in a decreased probability of a substrate binding to a GRP78 molecule, interacting with a UPR activator at such time. Confirming GRP78 over-expression reduces fenretinide or bortezomib-induced cell death, demonstrated a significant reduction in caspase-3 cleavage.

To test whether GRP78 over-expression resulted in a decrease in ER stress-induced UPR signalling, downstream ATF4 induction was analysed after treatment with either fenretinide or bortezomib. Results demonstrated a significant reduction in UPR activation with increased GRP78 expression. These findings suggest that GRP78 over-expression results in an increased inhibition of the UPR, with cells becoming more resistant to cell death due to a reduction in the translation of pro-apoptotic stimuli. Previous studies of GRP78 have indicated that GRP78 expression correlates with chemo-resistance [288, 296], suggesting changes in cellular stress regulation.

However, changes in UPR signalling are only part of the story an increase in GRP78 expression significantly reduced both ROS and ubiquitin-tagged protein accumulation. An increase in GRP78 would result in an enhanced cellular chaperone activity and therefore a reduction in proteins tagged for degradation would be a direct consequence of increased folding capacity of the cells [293]. A decrease in UPR activity, as a result of an increase in GRP78 inhibition of the UPR activators may have decreased ER stress-induced ERAD activation. This reduction in ERAD may be the reason why GRP78 over-expression reduced bortezomib-induced ubiquitin-tagged protein accumulation. However, the decrease in ROS accumulation with increased GRP78 was an unexpected observation, indicating a role of GRP78 in buffering ROS, or in prevention of fenretinide interference within the ceramide synthesis pathway.

Previously, it was reported that capsaicin, an ingredient of red pepper, induces apoptosis and also promotes cytoplasmic Gadd153 expression and nuclear translocation of GRP78 in human hepatoma HepG2 cells [302]. These studies showed that capsaicin-induced apoptosis was mediated through elevation of intracellular production of ROS, and

regulation of the mitochondrial Bcl-2 family and caspase 3. In another example, knockdown of GRP78 sensitized cells to ROS-induced cell death, primarily due to an impaired DNA repair capacity [303]. Taken together, these observations suggest a nuclear form of GRP78 might play a role against DNA-damage-induced cell death through a distinct regulatory mechanism in the nucleus.

To confirm that changes in the dynamic equilibrium of the UPR are important for melanoma and glioblastoma resistance to ER stress-induced cell death, the expression of the UPR activators; PERK, IRE1 and ATF6 were determined in cells over-expressing GRP78, in comparison to cells transfected with vector control or wild type cells. Data demonstrated that changes in expression of the UPR activators occurred as a direct consequence of GRP78 over-expression. IRE1 expression was increased in melanoma cells and PERK expression decreased in glioblastoma cells. These data suggest that interfering with the protein expression of GRP78, therefore results in changes to the UPR stoichiometry. However for glioblastoma, only a decrease in PERK expression was observed, which would further emphasise the shift within the dynamic equilibrium towards an inactive UPR.

Comparing the expression of GRP78 to the combined expression of UPR activators, relative to pcDNA3.0 transfected cells allowed for a direct comparison of the relationship between GRP78 expression and cancer type. Data demonstrated a significantly greater fold increase in GRP78 in comparison to the combined UPR activators in melanoma and glioblastoma cells. This represents a shift in the dynamic equilibrium in favour of the UPR being inhibited; suggesting that a greater amount of stress would be required to activate this signalling cascade. However, neuroblastoma cells demonstrated a significantly greater fold induction of UPR activators, compared to the achievable fold increase in GRP78 expression. This outcome would result in a shift of the dynamic equilibrium within neuroblastoma to favour a system that is switched on to a greater extent. These findings are supported by studies demonstrating that melanoma and glioblastoma cells become more resistant to death with increased GRP78 expression, in addition to studies in neuroblastoma showing the converse [113, 116, 224].

Data for the effect of GRP78 expression on neuroblastoma cell sensitivity to death and inhibition of cell viability, demonstrated an increase in fenretinide or bortezomib induced cell death or inhibition of cell viability. These data correlate with previous

studies, where GRP78 expression was shown to improve patient prognosis [116]. Analysis of the UPR in neuroblastoma cells showed a significant increase in PERK, IRE1 and ATF6 expression in cells over-expressing GRP78. These data suggest that one consequence of GRP78 over-expression, in neuroblastoma, is to induce the expression of the UPR activators. However, data demonstrated that wild-type neuroblastoma cells, unlike melanoma and glioblastoma cells, exhibit more UPR activator molecules than GRP78 molecules, present to inhibit them. Therefore, an increase in the UPR activators PERK, IRE1 and ATF6 would further shift the dynamic equilibrium of the UPR toward an active cascade in neuroblastoma. To investigate the downstream effects of this significant increase in UPR activators, cells were treated with either fenretinide or bortezomib prior to the analysis of ATF4 induction. Data derived from studies in neuroblastoma cells showed GRP78 over-expression resulted in significant ATF4 induction. However, when investigating downstream caspase activation, neuroblastoma cells showed a reduction in caspase 3 cleavage, suggesting that the increased UPR activity induced cell death in a caspase independent manner.

Previous research in multiple myeloma has highlighted that when the expression of a single UPR activator was deregulated by siRNA, this resulted in the promotion of cell death via autophagy, but represses apoptosis of multiple myeloma cells [304]. Multiple myeloma, as for neuroblastoma, demonstrates a favourable prognosis with increased GRP78 expression [304]. Assuming that the UPR can simultaneously activate survival and apoptosis mediators, the fate of a stressed cell is predictable at both extremes of the ER stress spectrum. However, there may be a range of stress signals of intermediate intensity, where the balance between protective and cytotoxic pathways does not allow a clear-cut decision between survival and death. The ER stress generated, coupled with the deregulation of the UPR sensor expression, and thus may fall into this category.

Neuroblastoma cells over-expressing GRP78 showed a significant increase in IRE1. Previous studies have proposed a link between IRE1 and JNK [305]. The JNK signalling pathway has been implicated in apoptosis-inducing factor (AIF)-dependent cell death and therefore an increase in IRE1 stimulated JNK activation may result in an increase in cell death in response to ER stress [306, 307].

Optimisation of stable GRP78 over-expressing neuroblastoma cells showed an increase in cell death in response to GRP78 specific plasmid transfection, in comparison to experimental control. To test the hypothesis that GRP78 over-expression induces

spontaneous cell death in neuroblastoma cells, NGP cells were transfected within increasing doses of pcDNA3.1 (+) GRP78 normalised to a final 4 µg/ml by the addition of control pcDNA3.0 (Figure 5.5). Data showed that enhancing GRP78 expression significantly induced neuroblastoma cell death. Therefore the lower fold increase in neuroblastoma over-expressing clones may be a balance between sufficient plasmid to be resistant to antibiotic selection, but low enough induction of GRP78 expression to prevent cell death from being induced too much, with cells demonstrating extremes of either too much or too little plasmid dying.

To date, the effect of GRP78 over-expression on neural-crest-derived cancer types UPR is poorly understood. These data demonstrate differences between cancer types with respect to the effect of GRP78 over-expression on UPR activator expression. Changes in neuroblastoma cells, whereby UPR activator expression significantly increased in comparison to GRP78, may tip the balance of the UPR. The resulting hyperactive UPR in this case may sensitize neuroblastoma cells to ER stress significantly more than the achieved 1.5 fold increase in GRP78 (enhanced chaperone activity and capacity to inhibit the UPR) can prevent it via its pro-survival mechanism. This concept is supported by data for neuroblastoma cells demonstrating that enhanced GRP78 expression had no significant effect on ROS accumulation together with the observed increase in ubiquitin tagged proteins (ER stress) in response to bortezomib. These findings highlight that in neuroblastoma cells, although a significant increase in GRP78 was achieved, no significant aid from GRP78 chaperone activity was observed. The increase in ubiquitin-tagged proteins may be a consequence of downstream ERAD activation as a consequence of the increase in UPR activators [308], which allows these neuroblastoma cells to induce UPR to a higher extent (determined by the increase in ATF4 induction).

Collectively, these data highlight the importance of understanding the stoichiometry of UPR activators, as well as GRP78 in the response of cancer cells to ER stress. To further investigate the importance of GRP78 as a therapeutic target, neural-crest-derived cancer cells were treated with a panel of GRP78 inhibitors, alone and in combination with ER stress-inducing agents.

5.4: Conclusion

This study, like that for the reduction of GRP78 expression, showed that increases in GRP78 altered sensitivity to ER stress in a cancer type-specific manner. Melanoma and glioblastoma observed increased resistance to ER stress-induced death, whereas neuroblastoma became more sensitive. Interpreting the effect of over-expression on UPR signalling showed that changes in resistance were linked with the activity of the UPR but not with caspase induction. Finally, this study demonstrated that over-expression of GRP78 results in downstream changes to the UPR activator expressions, and the effect of this is cancer type specific. Neuroblastoma resulted in a further increase in UPR activators, further activating the cascade. For melanoma and glioblastoma, on the other hand, there was more GRP78 induction than UPR activators, increasing the negative regulation of the UPR.

Chapter 6:

The effect of GRP78 inhibition on the survival of cancer cells

6.1: Introduction.

Demonstrating that the expression of GRP78 is enhanced in metastasis and late-stage cancer have highlighted GRP78 as a protein of interest in cancer signalling [114, 115, 258]. Research within this study has shown that reduction in GRP78 expression sensitizes only certain cancer types to ER stress-induced death; an outcome that was further confirmed when GRP78 over-expression models demonstrated opposing outcomes, with regards to the response to ER stress-inducing agents fenretinide or bortezomib across differing cancer types. However, to date studies using siRNA-mediated knock-down have demonstrated the importance of GRP78 expression in cancer-cell survival in response to both environmental and chemical stress [309]. Although siRNA targeted knock-down of GRP78 has shown beneficial outcomes *in vitro,* difficulties arise in clinical application of this technique and therefore another approach to target GRP78 is required [288]. To date, GRP78 activity can be disrupted using nucleoside analogues, specific antibodies [11], as well as by natural inhibitors, such as epigallocatechin gallate (EGCG) [288] or inhibited by AB_5 Subtilase cytotoxin ($SubAB_5$) [198-200]. Recently, Jack Arbiser and colleagues have demonstrated an interaction between honokiol and GRP78 (unpublished data, personal communications). Honokiol may represent a novel inhibitor of GRP78.

Like all large chaperones of the heat shock protein family, GRP78 is dependent on ATP for its chaperone activity; the processing of ATP to ADP alters the substrate binding domain and increases the affinity of GRP78 for unfolded or mis-folded proteins [310], and more recently Polizzi *et al.,* demonstrated that GRP78 interaction with ATP is required for GRP78 interaction with either PERK or IRE1 [311]. Palleros *et al.,* showed that on addition of Mg-ATP to HSP70-substrate complex, dissociation occurred [312]. However, when ATP-γS (a slowly metabolised ATP analogue) was used, there was no dissociation [312]. Therefore, these results suggest that the conversion of ATP to ADP is an important step for substrate release. This research also highlighted the importance of Mg-ATP binding, rather than hydrolysis as the essential step required for protein-substrate dissociation and that without K^+ present within the reaction, substrate dissociation was again significantly reduced [312]. This study highlighted the importance of the ATPase domain of the HSP70 family in their ability to interact with substrates [312] and demonstrates that targeting ATPase activity is a viable route to inhibit the functioning of chaperones.

Rao *et al.,* and Reddy *et al.,* also demonstrated the importance of ATPase activity in GRP78 function. Using Jurkat cells over-expressing GRP78 or a mutant variant, deficient in the ATP binding domain, the importance of the ATPase domain was demonstrated in protection against etoposide cytotoxicity [295], and the treatment of HEK293T cells with dATP, resulted in the dissociation of GRP78 complexes from caspase-7 and -12 [313]. These studies suggest that nucleoside analogues which could bind to the ATPase domain and result in dissociation, could activate pro-death stimuli, as well as disrupt the ability of GRP78 to bind/release substrates (cycling reaction) and, along with directly competing with ATP for the GRP78 binding site, would decrease the ability of GRP78 to react to ER stress efficiently by hindering chaperone activity.

Targeting the ATP binding domain was further evaluated between GRP78 and HSP70, demonstrating that designed quinolone (C9H7N) ligands potently bound to GRP78 and showed slow off-rates [314], However, dichlorophenyl ligands showed a greater inhibition of HCT116 cell proliferation [315]. Mapping the ATPase domain of GRP78 in comparison to HSP70, by X-Ray crystallography, highlighted that although most residues were the same between proteins, GRP78 contains a non-polar Ile61 instead of a Thr37 seen in HSP70. This change results in GRP78 having a more hydrophobic binding site [316], capable of interacting with a more diverse group of substrates.

EGCG, the most abundant catechin found in green tea, is reported to block the ATPase domain of GRP78, suppressing its anti-apoptotic property [317]. For example, TuBEC cells treated with EGCG in combination with temozolamide or etoposide demonstrated the induction of cell death, whereas single agents showed no significant cell death [301]. However, EGCG also has the ability to inhibit the 26S proteasome and NFκB signalling cascades and, therefore, is an ideal candidate as a drug to overcome chemoresistance in solid tumours [318]. Alastair Hawkins and Heather Lamb recently demonstrated that EGCG can bind to the unfolded form of the GRP78 ATPase domain (unpublished data).

The $SubAB_5$ cleaves GRP78 specifically at the di-leucine bridge between the ATPase and substrate binding domains; this specificity is due to the Sub A domain having an unusually deep active-site cleft [198]. AB_5 toxins are key virulence factors of a range of bacteria, including shiga toxigenic *Escherichia coli* (*E.coli*), which is part of a diverse group of *E.coli* strains that are capable of producing shiga toxins [198]. This subtilase cytotoxin, named because the 'A' subunit shares sequence homology with a subtilase-like serine protease of Bacillus anthracis, comprises a single A subunit and a pentamer

of substrate-targeting B subunits [319]. $SubAB_5$ comprises of a single 35 kDa A subunit and a pentamer of 13 kDa B subunits [200]. Cell death is induced as a direct consequence of GRP78 cleavage [200], and treatment with $SubAB_5$ at high doses results in the activation of the UPR, characterised by the induction of eIF2α phosphorylation and XBP-1 splicing [320], leading to the induction of Gadd153, characteristic changes in protein synthesis and EDEM. Thus, treatment with $SubAB_5$ can induce ER stress signalling [320].

Jack Arbiser and colleagues using biotinylated honokiol bound to strepdavadin beads demonstrated that GRP78 from SVR angiosarcoma cell lysates interacted with honokiol. Alastair Hawkins and Heather Lamb, as for EGCG, have demonstrated an interaction between GRP78 and honokiol. Again this work demonstrated interaction with the ATPase domain (Unpublished data). Honokiol is a lignan, a chemical component of plant cell walls, in this case present in the cones, bark, and leaves of *Magnolia grandiflora* and has been used in the traditional Japanese medicine *Saiboku-to* as an anxiolytic, antithrombotic, anti-depressant, anti-emetic, and anti-bacterial. While early research on the effective compounds in traditional remedies have simply used whole magnolia bark extracts, known as houpu magnolia, recent work has identified honokiol and its structural isomer magnolol as the active compounds in magnolia bark [323]. In the late 1990s, honokiol saw a revival in western countries as a potent and highly tolerable anti-tumorigenic and neurotrophic compound. More recently, honokiol has been shown to be anti-oxidant, anti-inflammatory and a bio-available, non-toxic inhibitor of angiogenesis [323].

Honokiol induces apoptosis as a result of ER stress in chondrosarcoma cells with the concomitant up-regulation of GRP78, Bax and Bak and down-regulation of Bcl-xl [324]. It is noteworthy that, in this model, a reduction in GRP78 expression resulted in a decrease in honokiol mediated cell death. *In vivo* treatment with honokiol saw a 53% reduction in tumour volume [324].

The aim of this study was to test the effect of the known inhibitors of GRP78 $SubAB_5$ and EGCG on ER stress-induced cell death of neural-crest-derived cancer cells in response to either fenretinide or bortezomib. As honokiol demonstrated an interaction with GRP78, an additional aspect of this work was to determine if honokiol, like EGCG could inhibit GRP78. Inhibitors were tested alone or in combination with either ER stress-inducing agent. To assess the effect of drug combinations on death and viability,

fixed-dose-ratio experiments for inhibitors alone and in combination were carried out by propidium iodide-stained flow cytometry and MTS or SRB (for EGCG) -based cell viability assays, as well as western blot analysis for caspase-3 cleavage. A final aim of this study was to test the prediction from GRP78 over-expression and knockdown studies that neuroblastoma cells would show different responses to GRP78 inhibitors compared to melanoma and glioblastoma cells.

6.2: Results

6.2.1: $SubAB_5$ synergistically enhances ER stress-induced death of melanoma and glioblastoma, but not neuroblastoma.

The effect of the GRP78 inhibitor $SubAb_5$ (toxin) on death and viability of melanoma, glioblastoma and neuroblastoma cancer cell lines was tested in comparison to the inactive mutant $SubA_{A272}B_5$ (mutant toxin). The effect of $SubAB_5$ on GRP78 protein levels was also investigated in parallel to confirm toxin activity by measuring the formation of the 28 kDa product resulting from toxin-specific cleavage of GRP78 between the functional domains. Toxin-mediated cleavage of GRP78 was detected using a C-terminal-specific GRP78 antibody which detects the 28 kDa cleavage product.

There was a significant dose-dependent increase in cell death (Figure 6.1) and inhibition of cell viability (Figure 6.2) in all cancer types tested (One-Way ANOVA with Dunnett's post hoc corrections, for cell death: all cell lines from 100 ng/ml $P < 0.0001$, CHl-1 cells with 50 ng/ml $P < 0.05$, WM266-4, MO59J, NGP and SH-SY5Y cell lines with 20 and 50 ng/ml toxin $P < 0.05$ and 0.0001 respectively or U251 cells 20 and 50 ng/ml toxin $P < 0.0001$; for inhibition of cell viability: melanoma and neuroblastoma cell lines from 5 ng/ml toxin upwards $P < 0.001$, or glioblastoma cells from 50 ng/ml toxin $P < 0.0001$). The mutant toxin had no significant effect on the induction of cell death ($P > 0.05$). Comparing the effect of the toxin to the mutant toxin to confirm that the toxin is different to the mutant control in all cell lines showed a significant difference in response within all cell lines (Two-way ANOVA, for cell death: CHL-1 $F_{1, 41} = 36$, WM266-4 $F_{1, 41} = 8.6$, MO59J $F_{1, 41} = 52$, U251 $F_{1, 41} = 14.7$ NGP $F_{1, 41} = 17.7$ and SH-SY5Y $F_{1, 41} = 18.6$, $P < 0.0001$. For inhibition of cell viability: CHL-1 $F_{1, 111} = 111.9$, MO59J $F_{1, 111} = 42.5$, U251 $F_{1,111} = 17.3$ NGP $F_{1, 111} = 16.3$ and SH-SY5Y $F_{1, 111} = 19.4$, $P < 0.0001$ or WM266-4 $F_{1, 111} = 9.6$, $P < 0.01$). Interestingly, high doses of mutant toxin had a small but significant effect on melanoma cell viability ($P < 0.001$ for both melanoma cell lines).

Comparing the effect of toxin between cell lines demonstrated a significant difference in all cancer types for cell death and a difference between melanoma and glioblastoma cell lines for inhibition of cell viability (Two-way ANOVA: Cell death data for: Melanoma $F_{3, 83} = 36.8$, glioblastoma $F_{3, 83} = 54.8$ or neuroblastoma $F_{3, 83} = 33.8$, $P < 0.001$. Cell

viability data for: Melanoma; $F_{3, 223}$ = 83.5, glioblastoma; $F_{3, 223}$ = 59.7, P < 0.001 or 0.01 respectively).

Western blot analyses for the effect of toxin on GRP78 protein (Figure 6.3) demonstrated a significant decrease in GRP78 levels with increasing toxin (One-way ANOVA with Dunnett's post hoc correction, CHL-1, WM266-4 and from 50 ng/ml or MO59J and U251 from 20 ng/ml P 0.001. NGP cells from 10 ng/ml or SHSY-5Y cells from a dose of 2.5 ng/ml; P < 0.001). There was also a significant increase in GRP78 cleaved product with dose (One-way ANOVA with Dunnett's post hoc correction, CHL-1, WM266-4, U251 and SH-SY5Y cell lines treated with toxin from; 0.5 ng/ml P < 0.001. MO59J cells from 1 ng/ml P < 0.001 and NGP cells treated with toxin from; 20 ng/ml P < 0.05). Comparing cell lines within the same cancer type demonstrated no significant difference (P > 0.05), however significant differences were observed between cancer types, with melanoma cells (Figure 6.3 A & B, i, ii) showing significantly greater induction of cleaved product than either glioblastoma (Figure 6.3 A & B, iii, iv) or neuroblastoma (Figure 6.3 A & B, v, vi, Two Way ANOVA, $F_{37, 371}$ = 427.3, P < 0.0001). There were no significant differences between glioblastoma and neuroblastoma (P > 0.05)

Comparing the effect of toxin to siRNA mediate knock-down in GRP78 expression demonstrated that for all cell lines where a more than 50%, reduction in GRP78 expression by toxin cleavage resulted in higher levels of cell death than when GRP78 was reduced by siRNA (One-way ANOVA, for CHL-1, WM266-4 and SH-SY5Y cells F1, 5 = 15.6, 11.1 or 21.6 respectively, P ≤ 0.01)

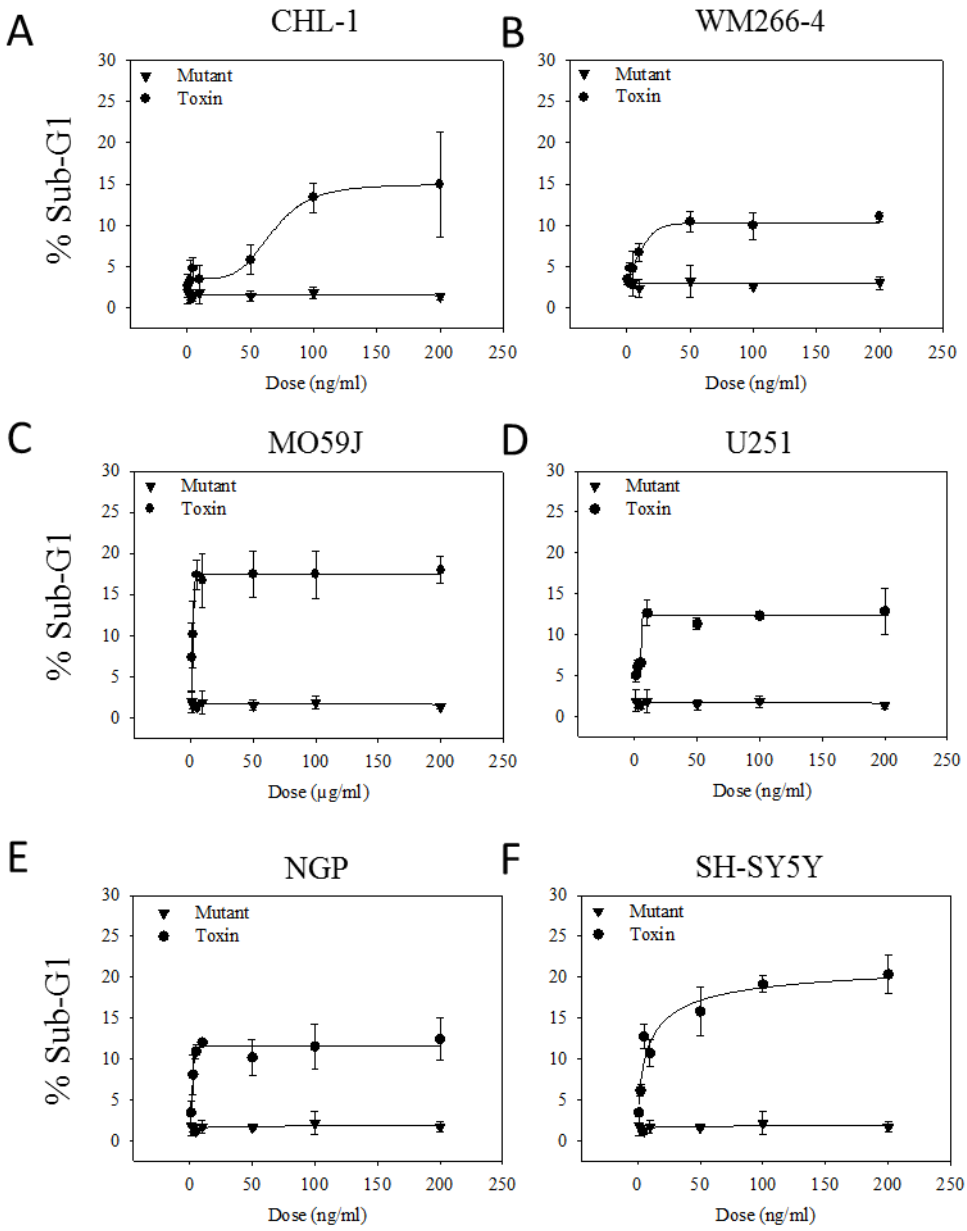

Figure 6.1: *The effect of GRP78 specific SubAB$_5$ on neural-crest-derived cancer cell death. CHL-1 and WM266-4 melanoma (A & B), MO59J glioblastoma (C & D) and neuroblastoma (E & F) cells were treated with increasing doses of subtilase cytotoxin (SubAB$_5$, doses 0 – 200 ng/ml) in comparison to an inactive mutant (SubA$_{272}$B$_5$) for 24 h prior to cell death analysis by flow cytometry for the percentage SubG1 peak of propidium iodide stained cells. Each point is the mean SubG1 peak percentage of 3 individual experiments ± 95% CI.*

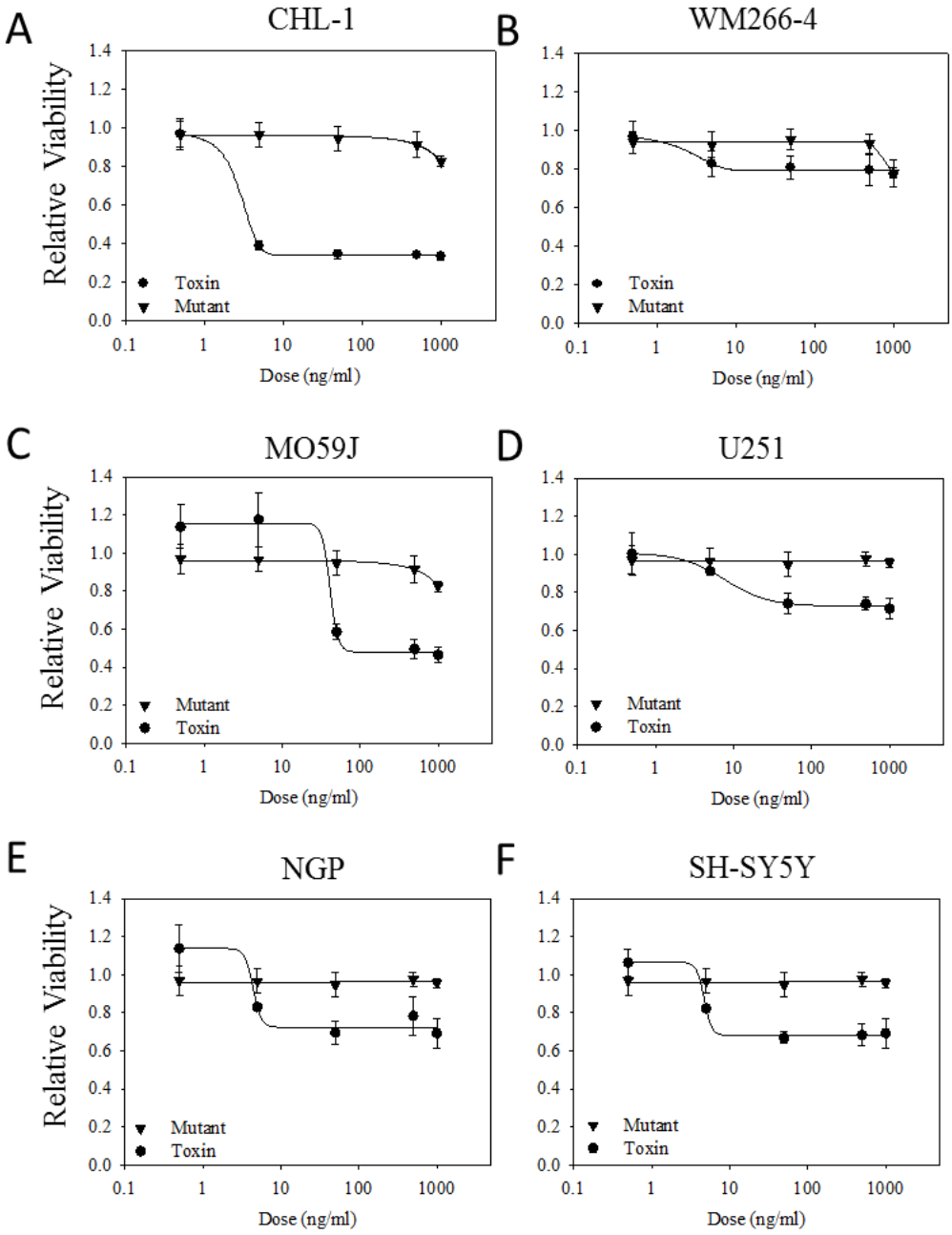

Figure 6.2: *The effect of GRP78 specific SubAB$_5$ on the inhibition of neural-crest-derived cancer cell viability. CHL-1 and WM266-4 melanoma (A & B), MO59J glioblastoma (C & D) and neuroblastoma (E & F) cells were treated with increasing doses of subtilase cytotoxin (SubAB$_5$, doses 0 – 200 ng/ml) in comparison to an inactive mutant (SubA$_{272}$B$_5$) for 24 h prior to analysis for the effect of GRP78 inhibition on neural-crest-derived cancer cell viability by MTS assays. Each point is the mean of 8 replicates over 3 individual experiments ± 95% CI.*

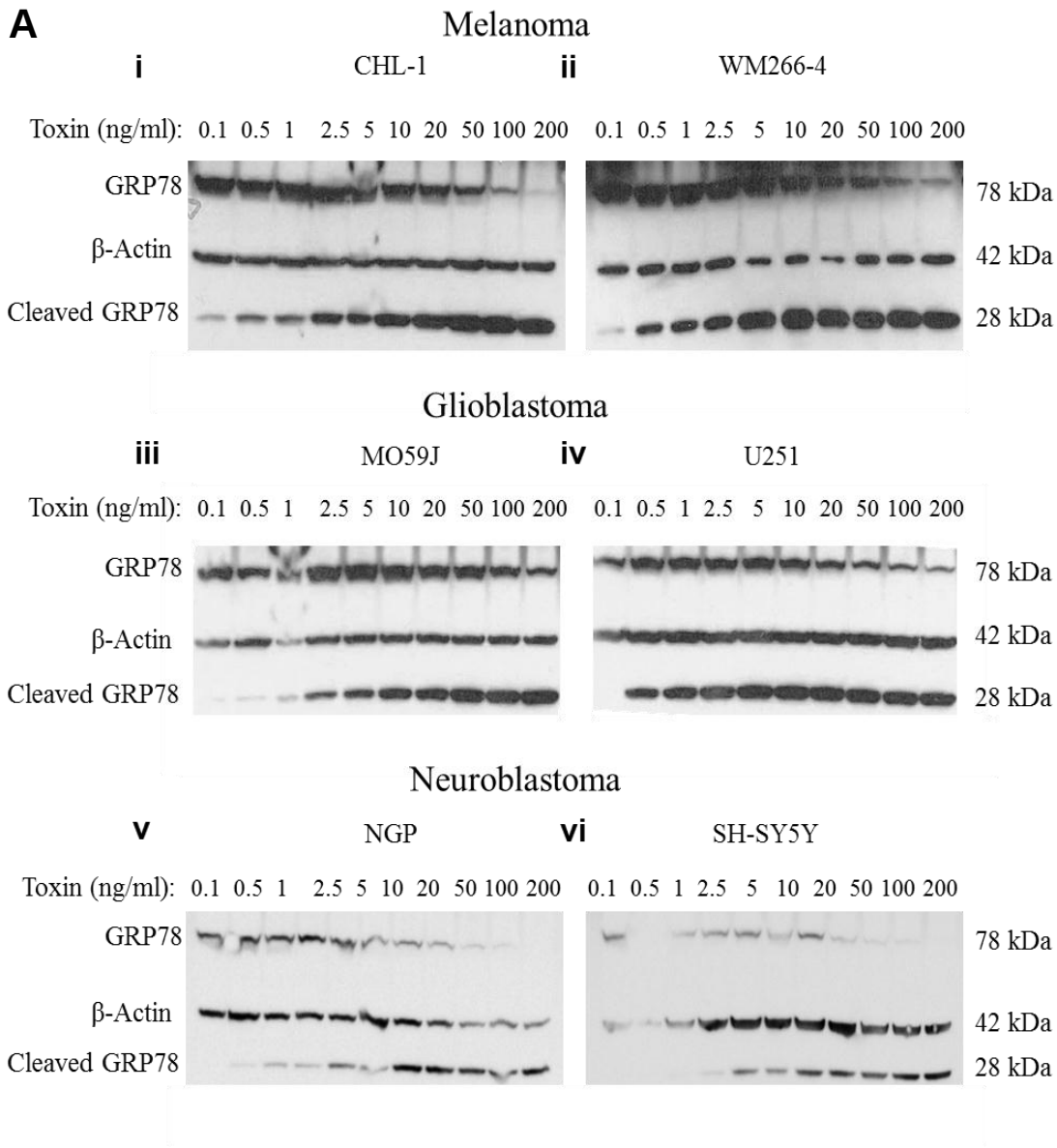

Figure 6.3: *The effect of $SubAB_5$ on GRP78 expression and cleavage.* ***(A)*** *Melanoma (i & ii), glioblastoma (iii & iv) and neuroblastoma (v & vi) cell lines were treated with increasing doses of $SubAB_5$ (Toxin, dose range = 0.1 – 200 ng/ml) for 24 h prior to western blot analysis for GRP78 and cleaved product, in comparison to β-Actin as loading control, which is the intermediate band.* ***(B)*** *Densitometry data for the effect of $SubAB_5$ on the expression of GRP78 (grey bars) or cleaved product (black bars, data are on the next page) is the mean of 3 individual experiments ± 95% CI. Data are corrected for loading control β-Actin and relative to lowest dose (because lowest dose had no effect on GRP78 expression relative to control.*

B

Melanoma

i **CHL-1**

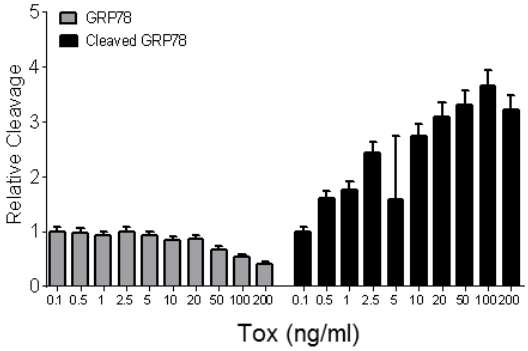

ii **WM266-4**

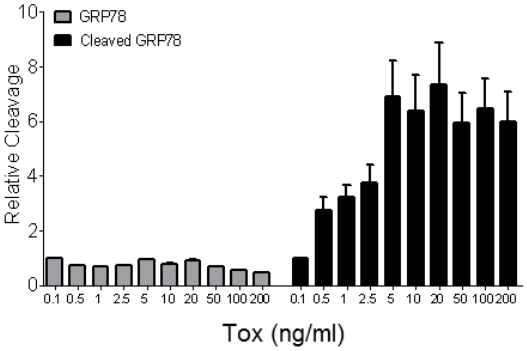

Glioblastoma

iii **MO59J**

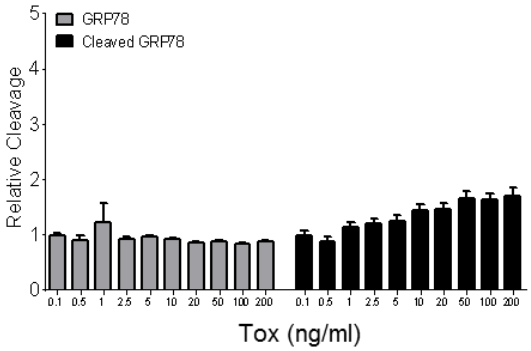

iv **U251**

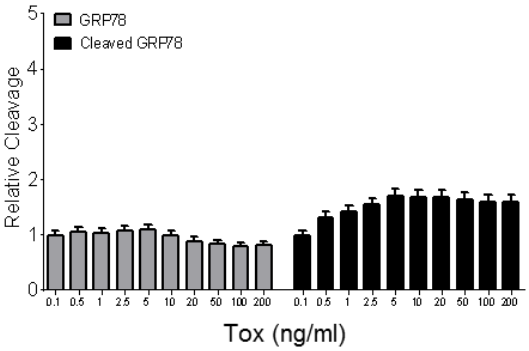

Neuroblastoma

v **NGP**

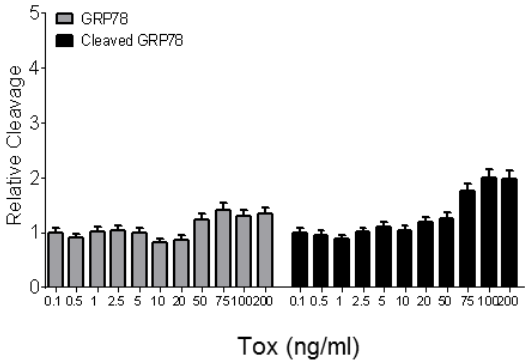

vi **SH-SY5Y**

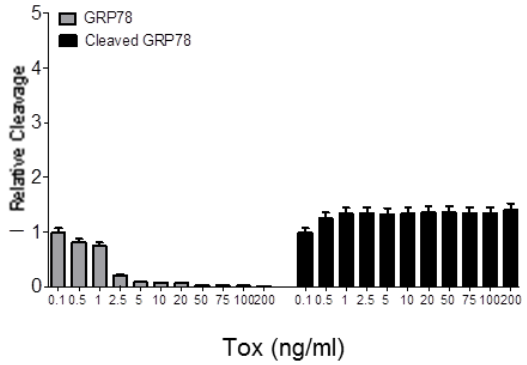

To investigate the response to toxin with regards to activity over time and the exposure required to induce a biologically-significant response, time course studies were carried out in melanoma cells, either under constant exposure to toxin (Figure 6.4 A – F) or where samples were treated for 1 h with toxin in comparison to inactive mutant and then washed (Figure 6.4 G – J) and samples tested for the effect on induction of cell death in comparison to achieved cleavage of GRP78.

In the continuous presence of 5 ng/ml of toxin, cell death increased with time in both melanoma cell lines, producing similar levels of apoptosis up to 24 h (Figure 6.4). There was a time-dependent increase in GRP78 cleavage in both cell lines detectable within 1 h of exposure to toxin, and with a concomitant decrease in full length GRP78 (Figure 6.4). The increase in GRP78 cleavage correlated with increased levels of cell death; the inactive $SubA_{A272}B$ mutant toxin had no effect on apoptosis and did not cleave GRP78.

The length of exposure to toxin required to induce apoptosis was assessed by treating cells with wild-type or mutant toxin for 1, 2, 4, 8 and 24 h, then continuing incubation in the absence of toxin for the time remaining to 24 h after initial exposure. There was a significant difference in response to toxin between the two cell lines (2-Way ANOVA; effect of cell type $F_{1, 20}=13.8$, $P < 0.001$). Using the 1 h exposure time as a reference for CHL-1 cells, cell death was only significantly increased after 24 h exposure (One-way ANOVA, Dunnett's test, up to 8 h, $P \geq 0.2$; 24 h, $P < 0.001$). Conversely, for the WM266-4 cells, cell death was significantly elevated after 4 h exposure (One-way ANOVA, Dunnett's test, 4, 8 and 24 h, $P \leq 0.05$). This difference between the cell lines was mirrored by higher levels of cleaved GRP78 in WM266-4 cells after even a short 1 h exposure to toxin (Figure 6.4).

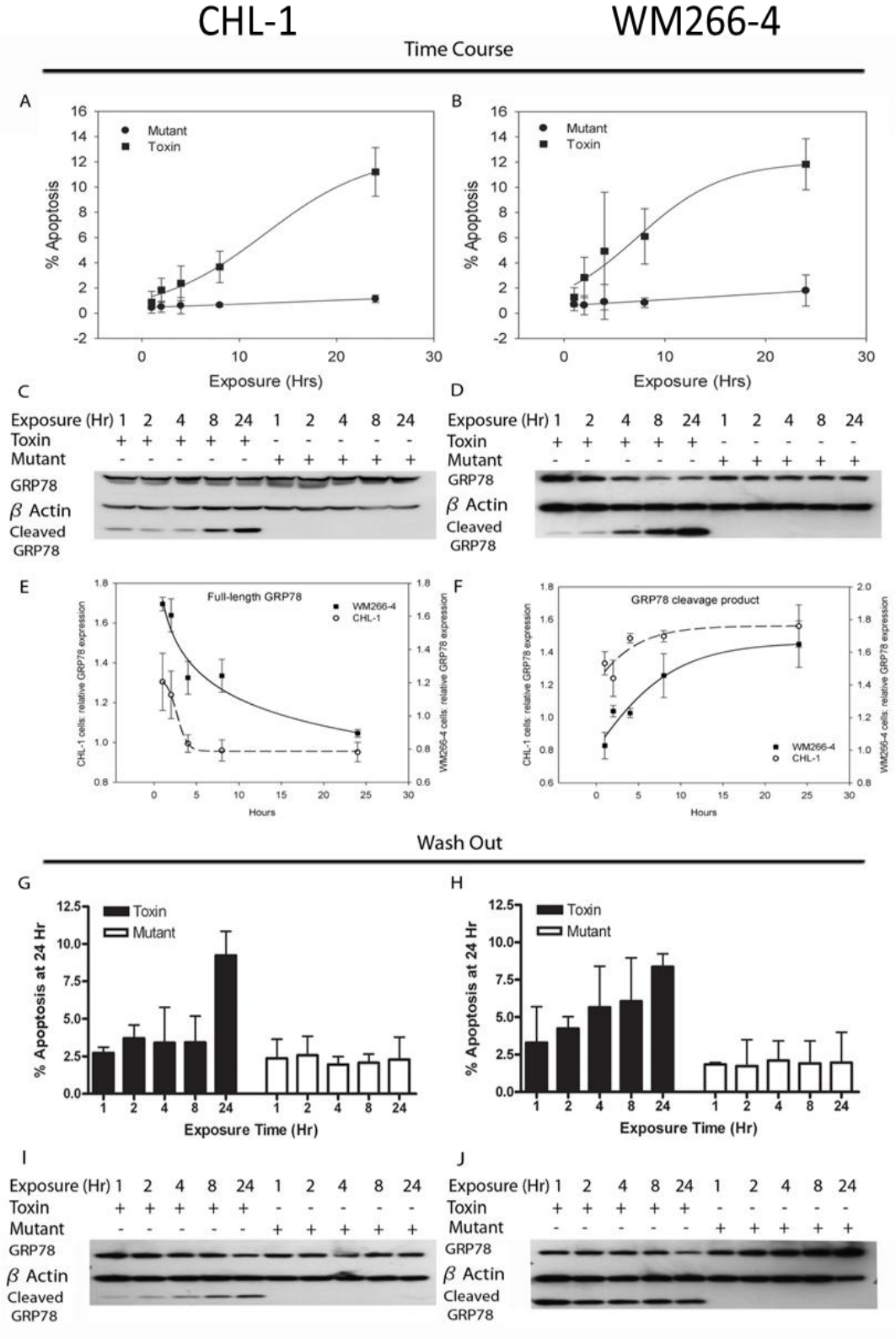
CHL-1
WM266-4
Time Course
A
B
Mutant
Toxin
% Apoptosis
Exposure (Hrs)
C
D
Exposure (Hr) 1 2 4 8 24 1 2 4 8 24
Toxin
Mutant
GRP78
β Actin
Cleaved GRP78
E
F
Full-length GRP78
GRP78 cleavage product
WM266-4
CHL-1
CHL-1 cells: relative GRP78 expression
WM266-4 cells: relative GRP78 expression
Hours
Wash Out
G
H
% Apoptosis at 24 Hr
Exposure Time (Hr)
I
J

Figure 6.4: *Time-course of apoptosis in response to continuous (Time Course) or pulsed exposure (Wash Out) to $SubAB_5$ treatment. CHL-1 and WM266-4 cells were treated with 5 ng/ml $SubAB_5$ for 1, 2, 4, 8 and 24 h and harvested for flow cytometry (A & B) and to assess GRP78 cleavage by Western blotting (C & D); blots were probed simultaneously for GRP78 and β-actin and the β-actin band is intermediate in size between full length GRP78 and the cleavage product. Densitometry data for full length GRP78 (E) and the cleavage product (F), relative to the β-actin loading control from three independent experiments were combined and are shown in panels E & F. Error bars in E & F are ± ± 95% CI. To investigate the length of exposure to toxin required to induce apoptosis after 24 h, cells were treated with 5 ng/ml $SubAB_5$ continuously for 24 h, or for 1, 2, 4, or 8 h then washed and cultured in the absence of $SubAB_5$ in the medium to the time remaining until 24 h after initial exposure; at 24 h the cells were harvested for measurement of apoptosis (G & H) or GRP78 cleavage as above (I & J). Flow cytometry data are means ± 95% confidence intervals. Data for the effect of $SubAB_5$ compared to mutant over time on GRP78 cleavage and apoptosis of melanoma cells were previously published [266].*

In summary these data show that $SubAB_5$ cleaved GRP78 in all cell lines, resulting in a decrease in GRP78 expression and increase in cleaved product. This cleavage resulted in the induction of apoptosis in all cell lines and when comparing the effect of $SubAB_5$ reduction in GRP78 on cell death (as single agent) to the level of cell death in cells with reduced GRP78 expression (by siRNA treatment), $SubAB_5$ induced significantly higher levels of death.

Fixed-dose-ratio experiments were performed for $SubAB_5$ combined with either fenretinide (Melanoma and glioblastoma for fenretinide with $SubAB_5$ 2000:1 and neuroblastoma 1000:1) or bortezomib (Melanoma and glioblastoma for fenretinide with $SubAB_5$ 1:40 and neuroblastoma 1:4) to test the hypothesis that GRP78 cleavage enhanced ER stress -induced cell death, as well as to test the hypothesis that differences in response outcome would exist between melanoma and glioblastoma, to that of neuroblastoma cancer cells (Figure 6.5). When melanoma and glioblastoma cells were treated with $SubAB_5$ and fenretinide or bortezomib there was increasing synergy with dose (Figure 6.5 A – P, combination indices listed in Table 6.1). For melanoma cells there were moderate levels of synergy (ci > 0.6), in comparison to mild synergy seen for glioblastoma (ci > 0.9 but < 0.6).

Comparing the combination indices for melanoma cells with respect to death and viability (Figure 6.5: A – D vs. E – H) showed that CHL-1 cells treated with bortezomib responded more with regards to death than viability. Investigating the combination of $SubAB_5$ with either fenretinide or bortezomib on cell death in neuroblastoma (Figure 6.5 Q – T) demonstrated no correlation with dose. Combination index values showed that the combination of $SubAB_5$ with either ER stress-inducing agent was inhibitory (ci > 1). For the effect of the combination on neuroblastoma cell viability (Figure 6.5 U – X) there was a decrease in favourable outcome with increased dose, represented by an increase in combination indices with dose (Table 6.1).

Assessing the combination indices values generated for the effect of $SubAB_5$ combined with either fenretinide or bortezomib (data summarised in graphs alongside table 6.5) demonstrated differences in response between cancer types. Comparing combination indices values to cell line demonstrated a significant difference in response to combination. When combining $SubAB_5$ with fenretinide, a dose dependent effect was only observed in all cell lines (One-Way ANOVA with Tukeys post hoc analysis, $P \leq 0.05$), and for $SubAB_5$ combined with Bortezomib, a dose dependent effect was

observed for U251 and NGP cell lines ($P \leq 0.05$). Comparing the combination of either fenretinide or bortezomib with $SubAB_5$ elicited a significant response between cancer types when treated with bortezomib ($P \leq 0.001$ for both), however no significant difference was observed across cancer types for the fenretinide combinations ($P > 0.05$).

Melanoma

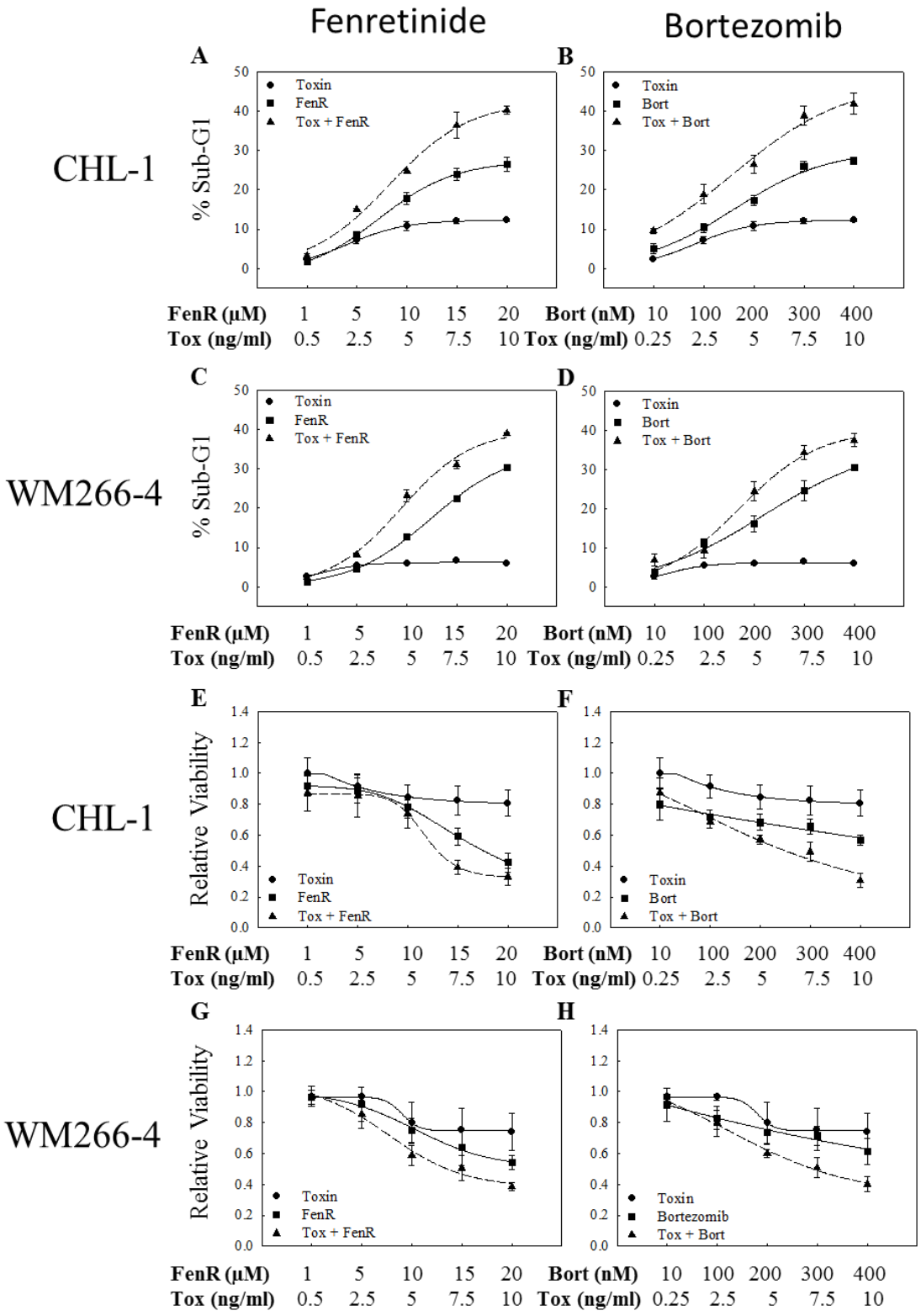
Fenretinide
Bortezomib
A
B
C
D
E
F
G
H
CHL-1
WM266-4
CHL-1
WM266-4
% Sub-G1
% Sub-G1
Relative Viability
Relative Viability
Toxin
FenR
Tox + FenR
Bort
Tox + Bort
Bortezomib
FenR (µM) 1 5 10 15 20
Tox (ng/ml) 0.5 2.5 5 7.5 10
Bort (nM) 10 100 200 300 400
Tox (ng/ml) 0.25 2.5 5 7.5 10

Glioblastoma

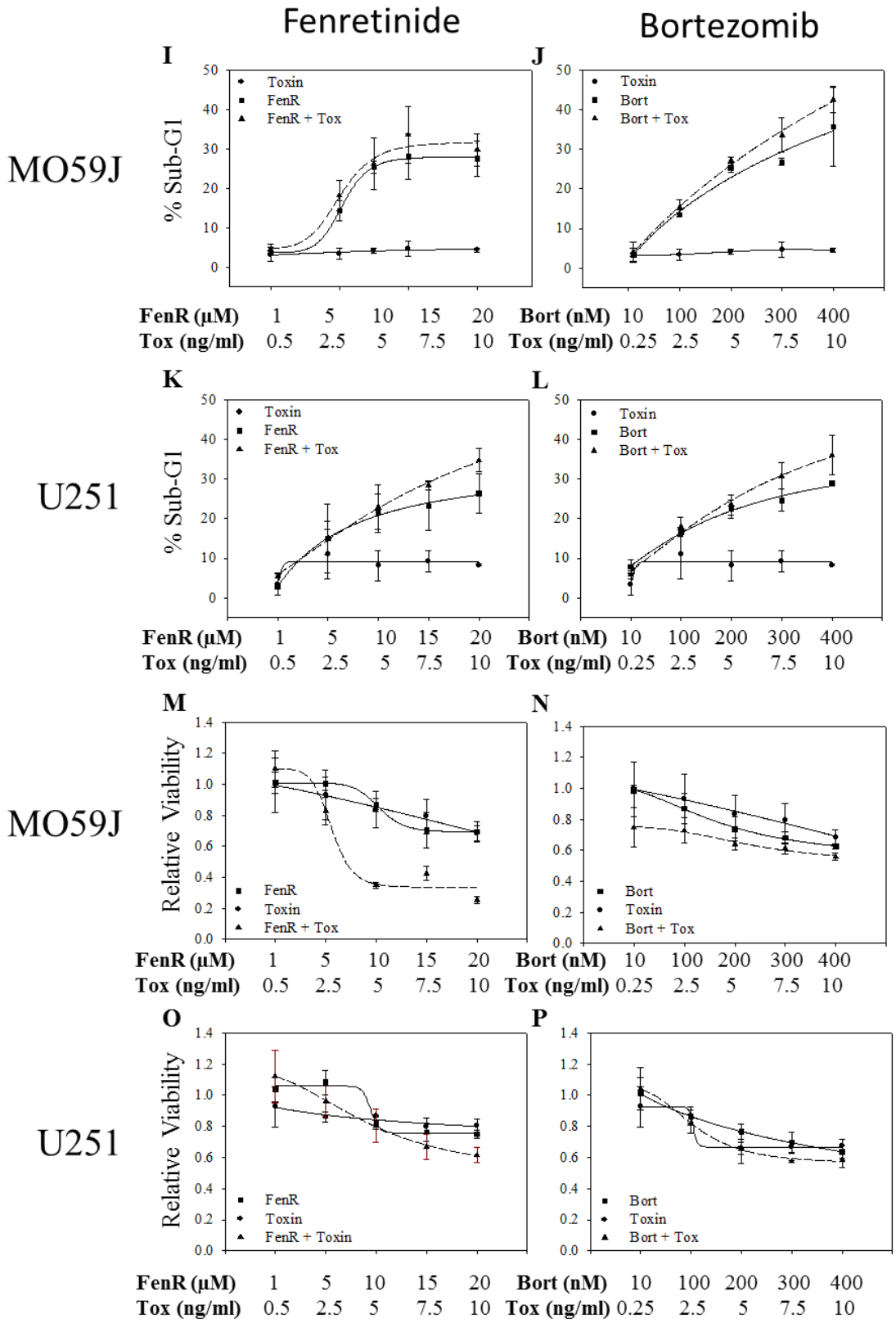

Neuroblastoma

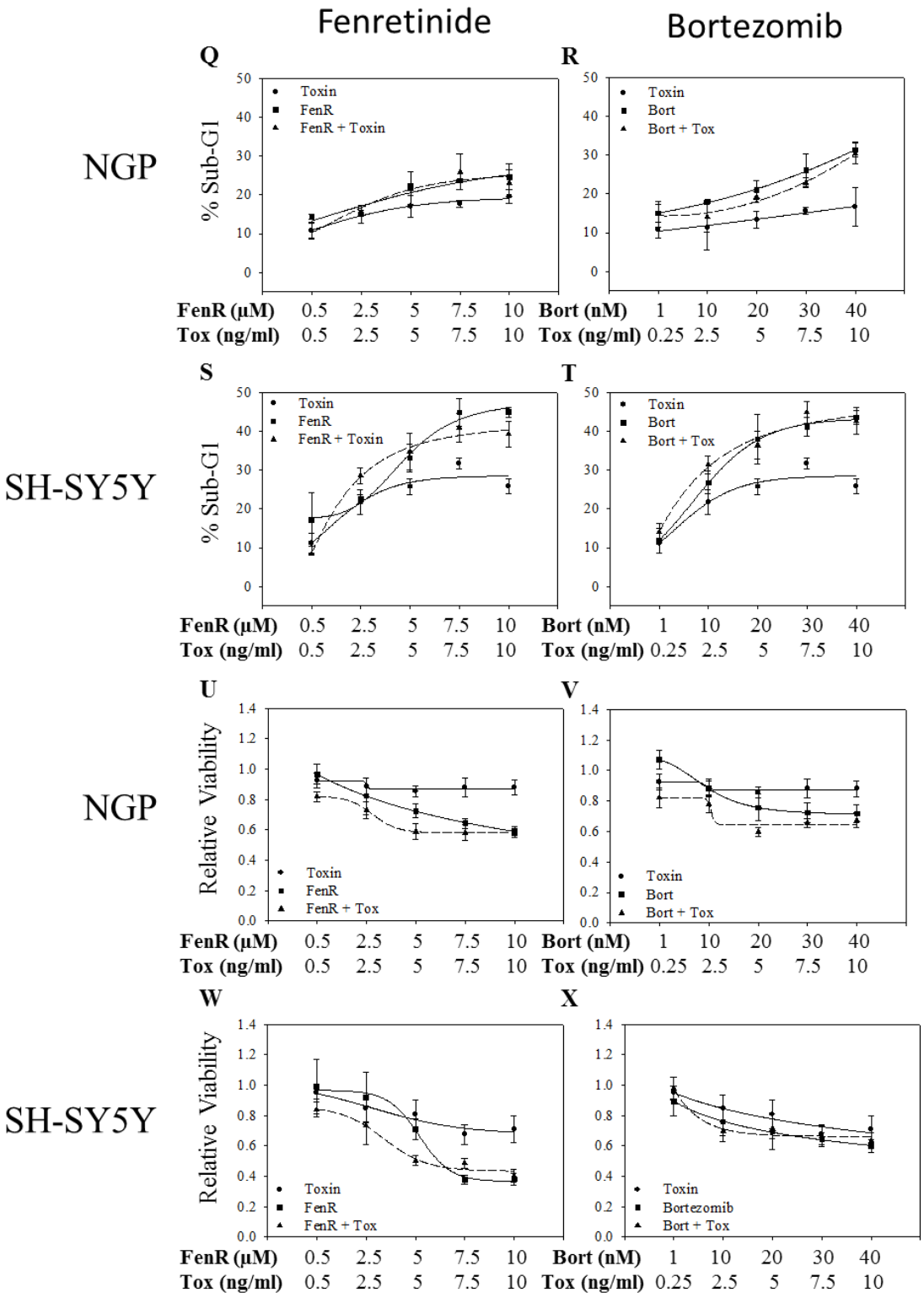

Figure 6.5: *Effect of GRP78 specific SubAB$_5$ on fenretinide and bortezomib induced apoptosis or inhibition of cell viability. CHL-1 (A & B, E & F) or WM266-4 (C & D, G & H) melanoma, MO59J (I & J, M & N) or U251 (K & L, O & P) glioblastoma and NGP (Q & R, U & V) or SH-SY5Y (S & T, W & X) neuroblastoma cells were treated with fenretinide (dose range = 1 – 20 µM for melanoma and glioblastoma or 1 – 10 µM for neuroblastoma), bortezomib (dose range = 10 – 400 nM for melanoma and glioblastoma or 1 – 40 nM for neuroblastoma) and* SubAB$_5$ *(Toxin, dose range = 0.5 – 10 ng/ml) alone and in combination for 24 h at fixed dose ratios of 2000:1 or 1000:1 (nM fenretinide: ng/ml* SubAB$_5$*) and 40:1 or 4:1 (nM bortezomib: ng/ml* SubAB$_5$*) for melanoma and glioblastoma or neuroblastoma , respectively. Samples were analyzed for cell death (A – D, I – L, Q –T for melanoma, glioblastoma and neuroblastoma cell lines treated with either fenretinide or bortezomib, respectively) or inhibition of cell viability (E – H, M – P, U - X. T for melanoma, glioblastoma and neuroblastoma cell lines treated with either fenretinide or bortezomib, respectively). Note that fenretinide units are expressed in µM on the figure. Apoptosis data are the mean of 3 experiments for cell death or 8 individual replicates for inhibition on cell viability ± 95% confidence intervals. CalcuSyn was used to determine the outcome of drug combinations (Combination indices for the outcome of drug interactions are given in Table 6.1). Data for the effect of SubAB$_5$ on fenretinide and bortezomib-induced cell death and inhibition of cell viability of melanoma cells was previously published [266].*

Cell Line	ER stress inducing agent	GRP78 Inhibitor	Cell Death (ci)	Viability (ci)
CHL-1	1. FenR (1 µM)	1. Tox (0.5 ng/ml)	1.281	0.476
	2. FenR (5 µM)	2. Tox (2.5 ng/ml)	0.781	1.826
	3. FenR (10 µM)	3. Tox (5 ng/ml)	0.755	1.835
	4. FenR (15 µM)	4. Tox (7.5 ng/ml)	0.637	0.705
	5. FenR (20 µM)	5. Tox (10 ng/ml)	0.7	0.755
	1. Bort (10 nM)	1. Tox (0.25 ng/ml)	0.026	15.552
	2. Bort (100 nM)	2. Tox (2.5 ng/ml)	0.073	17.402
	3. Bort (200 nM)	3. Tox (5 ng/ml)	0.073	2.391
	4. Bort (300 nM)	4. Tox (7.5 ng/ml)	0.051	0.838
	5. Bort (400 nM)	5. Tox (10 ng/ml)	0.057	0.18
WM266-4	1. FenR (1 µM)	1. Tox (0.5 ng/ml)	1.956	1.493
	2. FenR (5 µM)	2. Tox (2.5 ng/ml)	0.995	1.375
	3. FenR (10 µM)	3. Tox (5 ng/ml)	0.599	0.791
	4. FenR (15 µM)	4. Tox (7.5 ng/ml)	0.648	0.787
	5. FenR (20 µM)	5. Tox (10 ng/ml)	0.654	0.636
	1. Bort (10 nM)	1. Tox (0.25 ng/ml)	0.221	27.733
	2. Bort (100 nM)	2. Tox (2.5 ng/ml)	1.463	4.497
	3. Bort (200 nM)	3. Tox (5 ng/ml)	0.6	2.256
	4. Bort (300 nM)	4. Tox (7.5 ng/ml)	0.513	0.918
	5. Bort (400 nM)	5. Tox (10 ng/ml)	0.572	0.652
MO59J	1. FenR (1 µM)	1. Tox (0.5 ng/ml)	0.975	41.6
	2. FenR (5 µM)	2. Tox (2.5 ng/ml)	0.883	0.981
	3. FenR (10 µM)	3. Tox (5 ng/ml)	0.873	0.036
	4. FenR (15 µM)	4. Tox (7.5 ng/ml)	0.882	0.13
	5. FenR (20 µM)	5. Tox (10 ng/ml)	0.815	0.052
	1. Bort (10 nM)	1. Tox (0.25 ng/ml)	1.993	0.041
	2. Bort (100 nM)	2. Tox (2.5 ng/ml)	0.862	0.263
	3. Bort (200 nM)	3. Tox (5 ng/ml)	0.893	0.862
	4. Bort (300 nM)	4. Tox (7.5 ng/ml)	0.799	0.912
	5. Bort (400 nM)	5. Tox (10 ng/ml)	0.763	0.986
U251	1. FenR (1 µM)	1. Tox (0.5 ng/ml)	27.62	33.621
	2. FenR (5 µM)	2. Tox (2.5 ng/ml)	4.839	7.632
	3. FenR (10 µM)	3. Tox (5 ng/ml)	3.62	1.463
	4. FenR (15 µM)	4. Tox (7.5 ng/ml)	0.844	0.886
	5. FenR (20 µM)	5. Tox (10 ng/ml)	0.711	0.763
	1. Bort (10 nM)	1. Tox (0.25 ng/ml)	43.4	29.83
	2. Bort (100 nM)	2. Tox (2.5 ng/ml)	4.663	417.62
	3. Bort (200 nM)	3. Tox (5 ng/ml)	1.431	22.63
	4. Bort (300 nM)	4. Tox (7.5 ng/ml)	0.812	0.86
	5. Bort (400 nM)	5. Tox (10 ng/ml)	0.786	0.73
NGP	1. FenR (0.5 µM)	1. Tox (0.5 ng/ml)	16.83	0.843
	2. FenR (2.5 µM)	2. Tox (2.5 ng/ml)	22.63	0.91
	3. FenR (5 µM)	3. Tox (5 ng/ml)	8.621	0.93
	4. FenR (7.5 µM)	4. Tox (7.5 ng/ml)	1.473	0.981
	5. FenR (10 µM)	5. Tox (10 ng/ml)	9.62	1.124
	1. Bort (1 nM)	1. Tox (0.25 ng/ml)	6.36	0.901
	2. Bort (10 nM)	2. Tox (2.5 ng/ml)	11.6	0.973
	3. Bort (20 nM)	3. Tox (5 ng/ml)	9.4	0.843
	4. Bort (30 nM)	4. Tox (7.5 ng/ml)	11.1	0.916
	5. Bort (40 nM)	5. Tox (10 ng/ml)	3.4	0.984
SH-SY5Y	1. FenR (0.5 µM)	1. Tox (0.5 ng/ml)	17.6	0.791
	2. FenR (2.5 µM)	2. Tox (2.5 ng/ml)	0.841	0.761
	3. FenR (5 µM)	3. Tox (5 ng/ml)	1.013	0.684
	4. FenR (7.5 µM)	4. Tox (7.5 ng/ml)	3.6	2.31
	5. FenR (10 µM)	5. Tox (10 ng/ml)	5.8	1.610
	1. Bort (1 nM)	1. Tox (0.25 ng/ml)	0.932	1.23
	2. Bort (10 nM)	2. Tox (2.5 ng/ml)	0.916	0.94
	3. Bort (20 nM)	3. Tox (5 ng/ml)	2.1	0.996
	4. Bort (30 nM)	4. Tox (7.5 ng/ml)	0.994	1.433
	5. Bort (40 nM)	5. Tox (10 ng/ml)	1.31	2.136

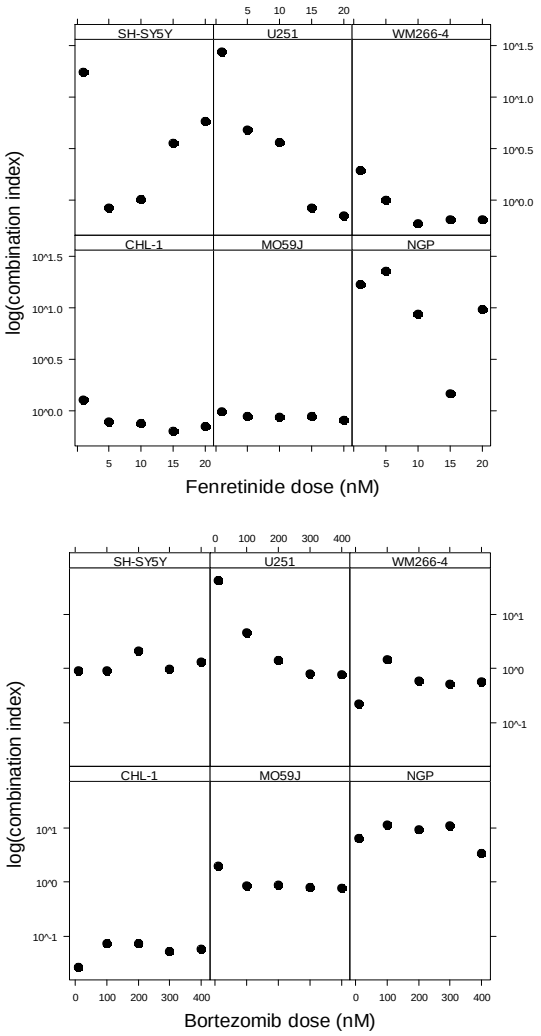

Table 6.1: *Effect of GRP78 inhibition by SubAB$_5$ treatment on ER stress-induced cell death or inhibition of melanoma cell viability. Drug interaction reviewed by fixed-dose-ratio analysis for the effect of GRP78 specific SubAB$_5$ (Tox) on fenretinide (FenR) or bortezomib (Bort) induced cell death or inhibition of cell viability of melanoma, glioblastoma and neuroblastoma cells. Combination indices (ci) values; < 1 = Synergy (green), ≤ 1 = Additive (black) and > 1 = inhibitory (red). Data are given in Figure 6.5. Alongside the combination indices data are graphs summarising the combination indices over dose range were obtained for the effect of combining SubAB$_5$ with either fenretinide or bortezomib for all cell lines individually.*

To determine if the increase in cell death and inhibition of cell viability observed when GRP78 cleavage was combined with an ER stress-inducing agent was a consequence of changes in the UPR response, western blots for GRP78 expression, ATF4 induction and caspase 3 cleavage (Figure 6.6) were performed for the effect of fenretinide (For melanoma and glioblastoma: F1 = 5 μM and F2 = 10 μM or neuroblastoma F1 = 2.5 μM and F2 = 5 μM), bortezomib (B1 = 100 nM and B2 = 200 nM or neuroblastoma B1 = 10 nM and B2 = 20 nM) or toxin (T1 = 5 ng/ml and T2 = 10 ng/ml) alone or in combination (FT1, FT2, BT1 and BT2) in melanoma, glioblastoma and neuroblastoma cell lines. In cells exposed to $SubAB_5$, there was induction of cleaved product for all cancer types (Figure 6.6, One-way ANOVA with Bonferroni post hoc corrections, for all cell lines treated with T1 = $P < 0.01$, or T2 = $P < 0.001$). $SubAB_5$ treatment in combination with ER stress-inducing agents resulted in a decrease in expression of GRP78 after exposure to BT1, BT2 or FT1, FT2 (One-way ANOVA with Bonferroni post hoc corrections, $P < 0.01$).

Treatment of $SubAB_5$ alone or in combination significantly induced the expression of cleaved GRP78 in all samples (One-way ANOVA with Bonferroni post hoc corrections, $P < 0.01$), except for SH-SY5Y cells treated with FT1 ($P > 0.05$). Combining an ER stress-inducing agent with the $SubAB_5$ resulted in significant changes in the production of the cleaved product (Figure 6.6 A iii – F iii). Data showed that treatment with FT2 in comparison to $SubAB_5$ alone significantly reduced GRP78 cleavage in all cell lines (One-way ANOVA with Bonferroni post hoc corrections, All cell line $P \leq 0.05$), except in U251 cells, where treatment with FT1 demonstrated the capacity to hinder toxin induced GRP78 cleavage ($P < 0.001$). Treatment of CHL-1, WM266-4, MO59J and NGP cells with BT2 demonstrated a significant increase in cleaved product (One-way ANOVA with Bonferroni post hoc corrections, All cell line $P \leq 0.05$). WM266-4, MO59J and NGP cells, as well as SH-SY5Y cells showed a significant increase in GRP78 cleavage when treated with BT1 ($P \leq 0.05$).

With respect to the induction of ATF4 or cleavage of caspase 3, the combination of fenretinide and $SubAB_5$ showed a significant increase in ATF4 induction with either dose in both melanoma cell lines and MO59J cells (One-way ANOVA with Bonferroni post hoc corrections, for all cell lines with either concentration $P \leq 0.001$), as well as showing a significant effect with high dose (FT2) in U251 glioblastoma and both neuroblastoma cell lines ($P \leq 0.001$). For the combination of $SubAB_5$ with bortezomib, a decrease in ATF4 induction was observed in melanoma cell lines and NGP

neuroblastoma cells with either dose (One-way ANOVA with Bonferroni post hoc corrections, for all cell lines with either concentration $P \leq 0.001$), as well as MO59J cells with BT2 treatment ($P \leq 0.005$).

Combining $SubAB_5$ with fenretinide demonstrated a reduction in caspase 3 cleavage for either FT1 or FT2 treatments in both melanoma cells lines, U251 glioblastoma and NGP neuroblastoma cell lines (One-way ANOVA with Bonferroni post hoc corrections, for all cell lines with either concentration $P \leq 0.001$), and resulted in a decrease in FT2 treatment in MO59J cells ($P \leq 0.01$). For bortezomib, with $SubAB_5$, data showed that the BT2 treatment for WM266-4 cells of either BT1 or BT2 for neuroblastoma cells showed a decrease in caspase 3 cleavage (One-way ANOVA with Bonferroni post hoc corrections, for all cell lines with either concentration $P \leq 0.001$). Conversely, both glioblastoma cell lines demonstrated an increase in cleaved caspase 3 when treated with the BT2 combination ($P \leq 0.01$).

In summary, these data show that in melanoma and glioblastoma treatment of $SubAB_5$ with either ER stress-inducing agent fenretinide or bortezomib resulted in a synergistic enhancement of cell death and inhibition of cell viability. However, for neuroblastoma there was an inhibitory effect. Investigation into the effect of these combinations by western blotting for GRP78, ATF4 and cleaved caspase 3 demonstrated no clear effect on ER stress or apoptosis.

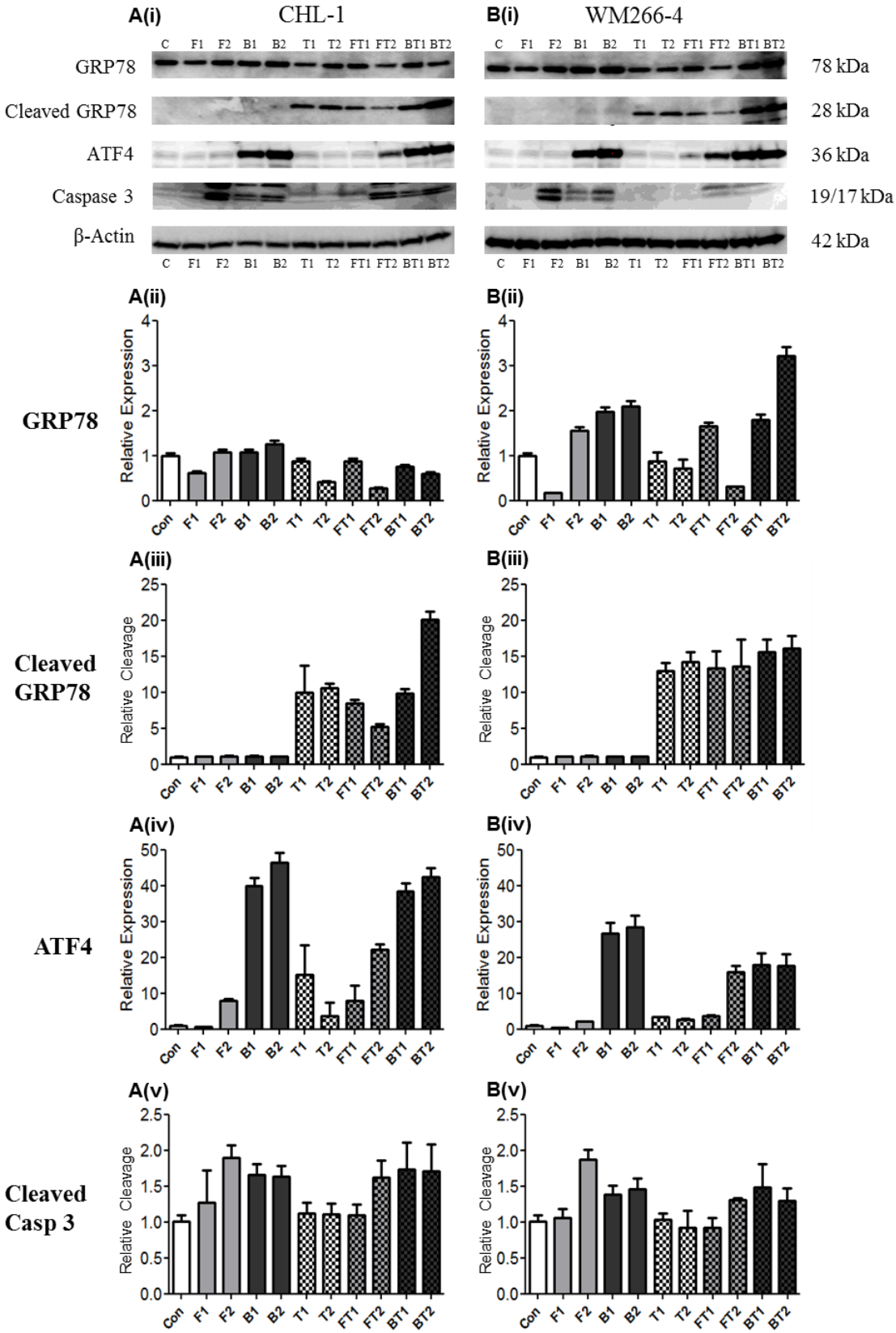
A(i)
CHL-1
B(i)
WM266-4
C F1 F2 B1 B2 T1 T2 FT1 FT2 BT1 BT2
GRP78
Cleaved GRP78
ATF4
Caspase 3
β-Actin
78 kDa
28 kDa
36 kDa
19/17 kDa
42 kDa
A(ii)
B(ii)
GRP78
Relative Expression
A(iii)
B(iii)
Cleaved GRP78
Relative Cleavage
A(iv)
B(iv)
ATF4
Relative Expression
A(v)
B(v)
Cleaved Casp 3
Relative Cleavage
Con F1 F2 B1 B2 T1 T2 FT1 FT2 BT1 BT2

Glioblastoma

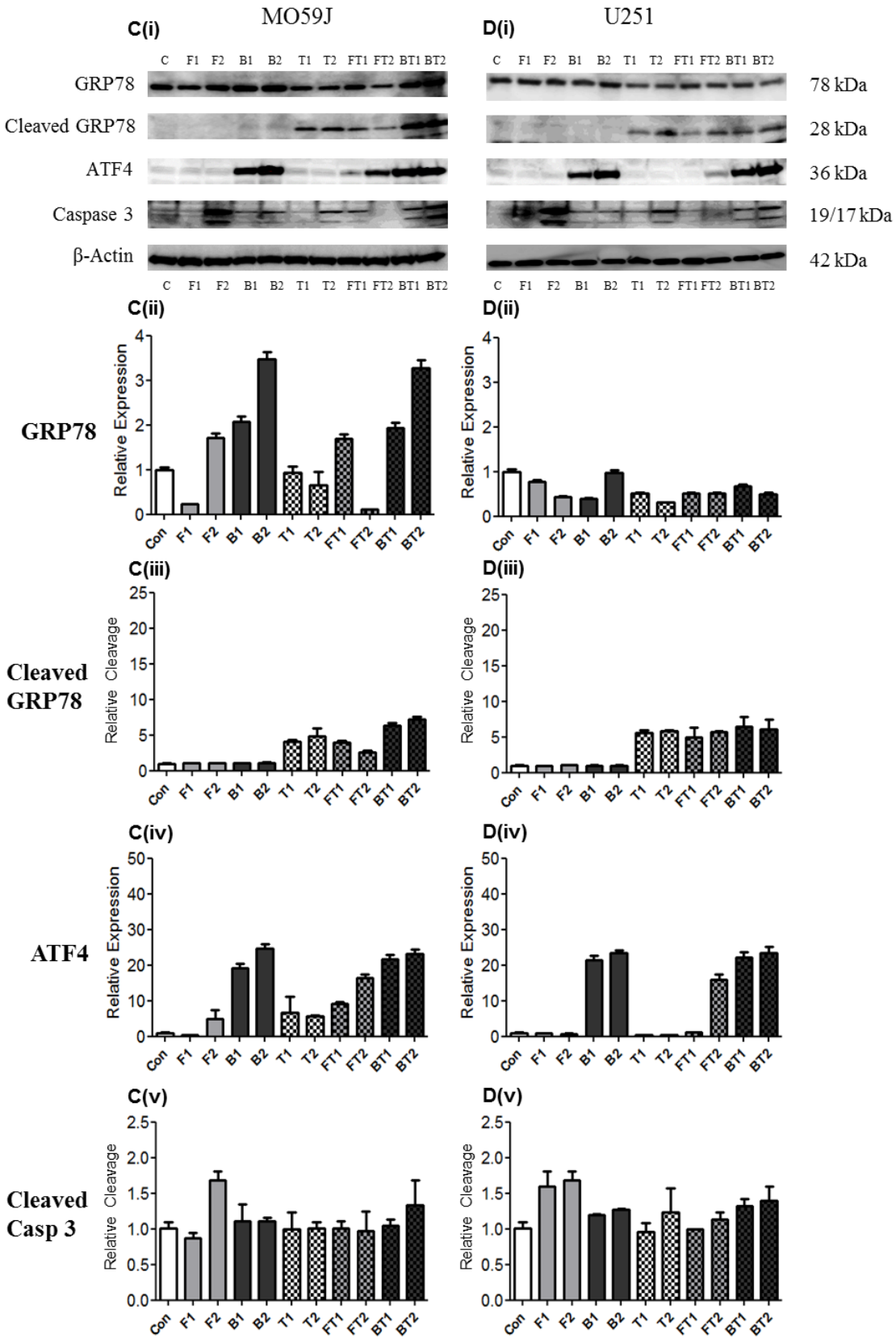

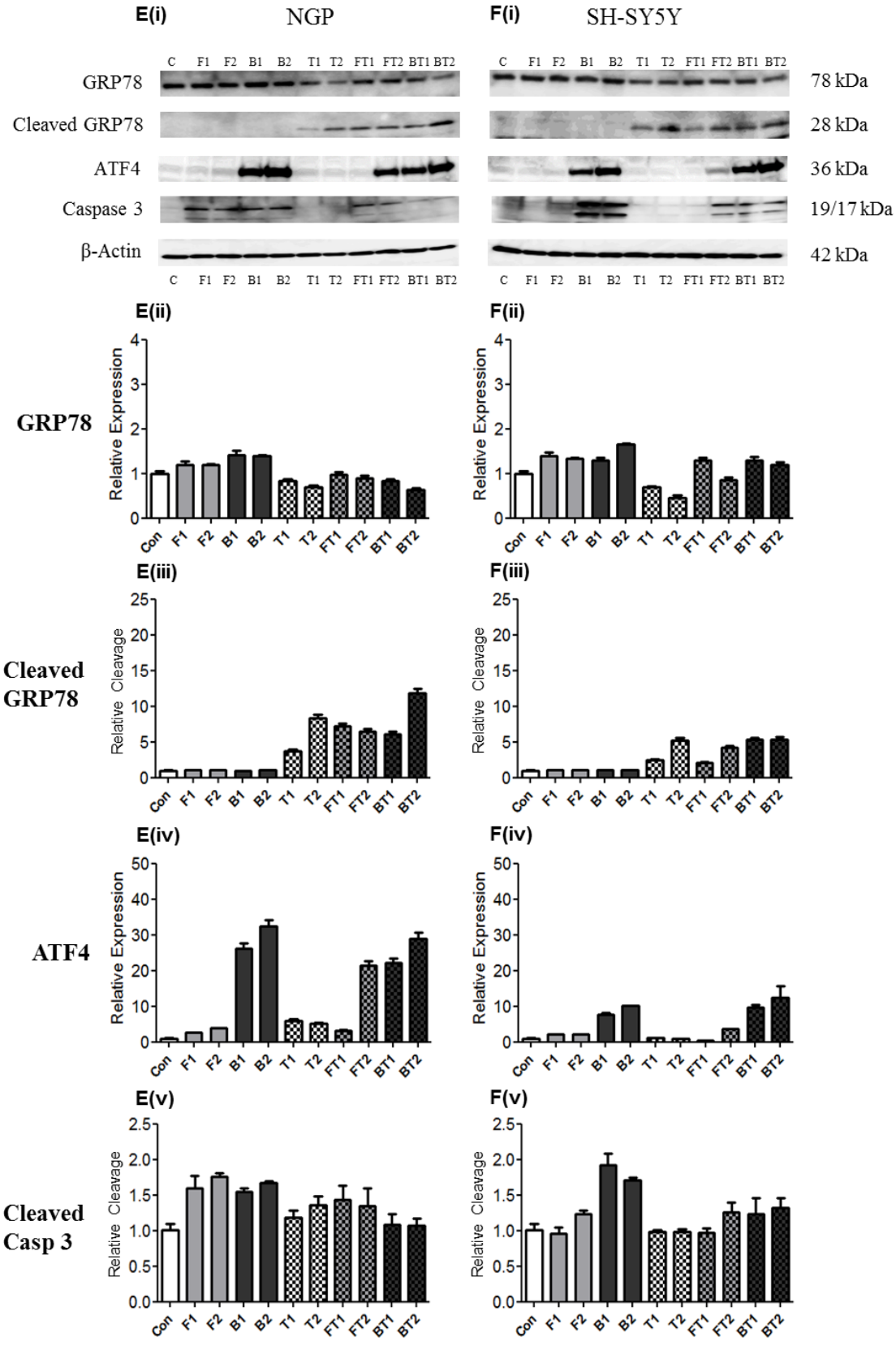
E(i)
NGP
F(i)
SH-SY5Y
C F1 F2 B1 B2 T1 T2 FT1 FT2 BT1 BT2
GRP78
Cleaved GRP78
ATF4
Caspase 3
β-Actin
78 kDa
28 kDa
36 kDa
19/17 kDa
42 kDa
E(ii)
F(ii)
GRP78
Relative Expression
E(iii)
F(iii)
Cleaved GRP78
Relative Cleavage
E(iv)
F(iv)
ATF4
Relative Expression
E(v)
F(v)
Cleaved Casp 3
Relative Cleavage
Con F1 F2 B1 B2 T1 T2 FT1 FT2 BT1 BT2

Figure 6.6: *The effect of $SubAB_5$ treatment on fenretinide or bortezomib induced ER stress and induction of apoptosis. Melanoma (A & B), glioblastoma (C & D) and neuroblastoma (E & F) cells were treated with fenretinide (light grey bars, For melanoma and glioblastoma, F1 = 5 µM and F2 = 10 µM or neuroblastoma F1 = 2.5 µM and F2 = 5 µM), bortezomib (Dark grey bars, For melanoma and glioblastoma, B1 = 100 nM and B2 = 200 nM or neuroblastoma B1 = 10 nM and B2 = 20 nM) and $SubAB_5$ (Toxin, Dotted bars, T1 = 5 ng/ml and T2 = 10 ng/ml) alone or in combination (FT1, FT2, BT1and BT2) for 24 h. Western blot analysis (i) were performed for GRP78 expression, induction of UPR inducible ATF4 and cleavage of caspase 3, using β-Actin as a loading control. Densitometry analysis were performed on GRP78 (ii), ATF4 (iii) and cleaved caspase 3 (iv) and data expressed as mean values, relative to β-Actin as a loading control, of 3 independent experiments ± 95%. Graphs are scaled across cancer types, differing depending on the protein of interest to allow for a visual comparison for the effect of drug combinations.*

		Combination				
Cell Line	**Protein**	**FT1**	**FT2**		**BT1**	**BT2**
CHL-1	**GRP78**					
WM266-4						
MO59J						
U251						
NGP						
SH-SY5Y						
CHL-1	**Cleaved GRP78**					
WM266-4						
MO59J						
U251						
NGP						
SH-SY5Y						
CHL-1	**ATF4**					
WM266-4						
MO59J						
U251						
NGP						
SH-SY5Y						
CHL-1	**Cleaved Caspase 3**					
WM266-4						
MO59J						
U251						
NGP						
SH-SY5Y						

Table 6.2: *The effect of SubAB$_5$ treatment on ER stress and induction of cancer cell apoptosis. A Summary table for the effect of drug combination in comparison to ER stress-inducing agents (fenretinide + F, Bortezomib + B) or* SubAB$_5$ *treatment (Toxin = T). Data are the average of the response of 3 individual experiments and demonstrate an increase (green), decrease (red) or no significant difference (grey) in protein expression.*

6.2.2: The effect of natural GRP78 inhibitor epigallocatechin gallate on ER stress-induced neural-crest-derived cancer cell survival.

EGCG over a range of doses (0.1 – 200 μM) was used to investigate effects on cell death and viability of neural-crest-derived cancer cell lines (Figure 6.7). Cell viability was assessed by SRB assay, rather than MTS for all experiments including EGCG, due to auto-fluorescence affecting MTS readouts at high EGCG concentrations. There was a significant induction of cell death or inhibition of cell viability with increasing doses of EGCG in all cell lines tested (One-way ANOVA with Dunnett's post hoc corrections, for cell death: MO59J, U251 and SH-SY5Y cells treated with 5 μM, WM266-4 or NGP with 7.5 μM or CHL-1 with 10 μM up wards $P < 0.05$. For viability: NGP with 0.5 μM, SH-SY5Y with 1 μM, WM266-4 and MO59J with 5 μM, U251 with 7.5 μM and CHL-1 treated with 10 μM up wards $P \leq 0.05$).

There was a significant difference between melanoma cell lines, with regard to inhibition of cell viability (Two-way ANOVA, $F_{19,59} = 86.3$, $P < 0.001$), with no significant difference observed for glioblastoma and neuroblastoma ($P > 0.05$). Comparing cancer types for the induction of cell death showed melanoma cells responded significantly greater than either glioblastoma or neuroblastoma (Two-way ANOVA, for cell death melanoma vs. glioblastoma or neuroblastoma $F_{19, 59} = 23.2$ or 27.9, $P < 0.001$, respectively). For cell viability there was no significant difference between cancer types ($P > 0.05$).

The effect of EGCG on eliciting an ER stress response and activating apoptosis was carried out, looking at ATF4 and caspase 3 cleavage, this work demonstrated no significant induction in either proteins expression. This is represented in figure 6.9, as part of the fixed-dose-ratio work, where treatment with high and low dose of EGCG had no effect.

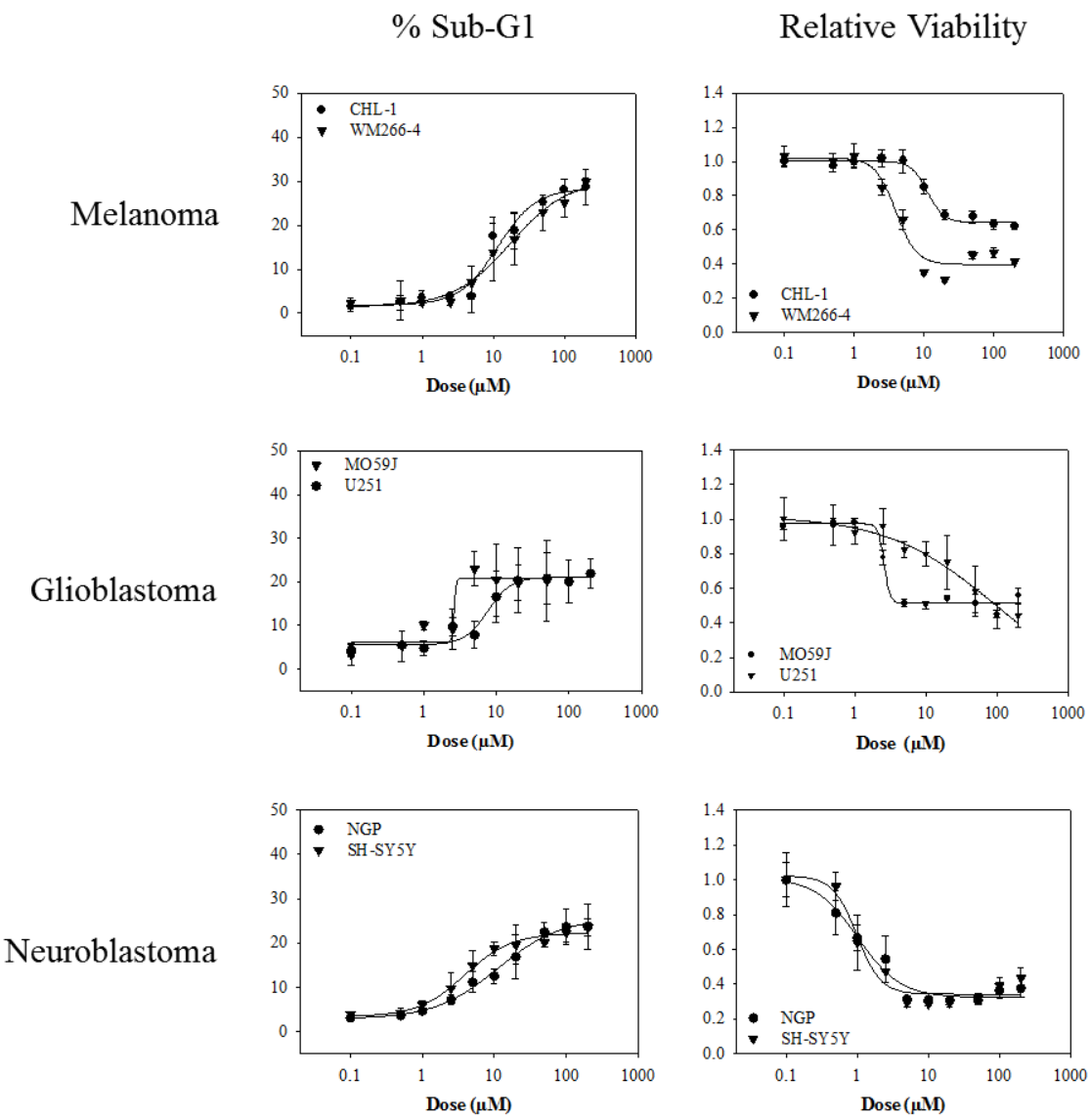

Figure 6.7: *The effect of GRP78 inhibitor EGCG on neural-crest-derived cancer cells. Melanoma (A & B), glioblastoma (C & D) and neuroblastoma (E & F) cells were treated with increasing doses of epigallocatechin gallate (EGCG, dose range = 0.1 – 200 µM) for 24 h. Cells were assessed for induction of cell death and inhibition of cell viability. Note; cell viability of cells treated with EGCG were performed by SRB assay due to the effect of auto-fluorescence. For cell death each point is the mean percentage SubG1 peak of 3 individual experiments or inhibition of cell viability 8 replicate experiments ± 95% CI.*

Fixed-dose-ratio experiments were performed for EGCG combined with either fenretinide or bortezomib (melanoma and glioblastoma were used at ratios of 1:1 for fenretinide and 1:50 with bortezomib, Neuroblastoma were used at 1:2 with fenretinide and 1:500 with Bortezomib) to test the hypothesis that inhibition of GRP78 enhanced ER stress-induced cell death, and to test the hypothesis that differences in response outcome would exist between melanoma and glioblastoma to neuroblastoma cancer cells (Figure 6.8). There was an increase in synergy with dose for the combination of EGCG with fenretinide on melanoma cell death (Figure 6.8 A & C, reaching a ci < 0.4, combination indices values listed in Table 6.3). However, when EGCG was combined with bortezomib the interaction was inhibitory (ci > 1, Table 6.3). Cell viability data showed an increase in inhibition of cell viability when either ER stress-inducing agent was combined with EGCG (Figure 6.8 E – H). Combination indices for inhibition of cell viability demonstrated a lower level of synergy for cell death (ci < 0.7, Table 6.3). For glioblastoma cells combination indices for the combination of EGCG with either fenretinide or bortezomib were not dose dependent (Table 6.3), with an overall inhibitory effect (ci > 1), except for U251 cells treated with fenretinide and EGCG where at high doses a weak synergistic interaction was achieved (ci < 0.7, Table 6.3). NGP and SH-SY5Y neuroblastoma cells demonstrated a weak synergy for the induction of cell death cell death in EGCG/fenretinide combinations and for NGP cells treated with EGCG/bortezomib (ci < 0.5, Table 6.3). For the effect of EGCG on either fenretinide- or bortezomib-induced inhibition of cell viability (Figure 6.8 U – X), there was an inhibitory effect on fenretinide response and an additive effect on bortezomib responses (ci > 1, Table 6.3).

Investigating the combination indices values generated for the effect of EGCG combined with either fenretinide or bortezomib (data summarised in graphs alongside table 6.3) demonstrated differences in response across cancer types. EGCG in combination with fenretinide- the cell type to cell line interaction was not significant ($P > 0.05$), so cell types were compared using Tukeys HSD where glioblastoma and melanoma differed significantly ($P < 0.05$) but there was no significant difference between neuroblastoma and glioblastoma ($P > 0.05$) or melanoma ($P > 0.05$). EGCG in combination with bortezomib- cell type to cell line interaction was significant ($P < 0.0005$) so the data were analysed by cell line. The combination overall was inhibitory but particularly for SH-SY5Y neuroblastoma cells which was significantly different compared to the other cell lines ($P < 0.05$).

Melanoma

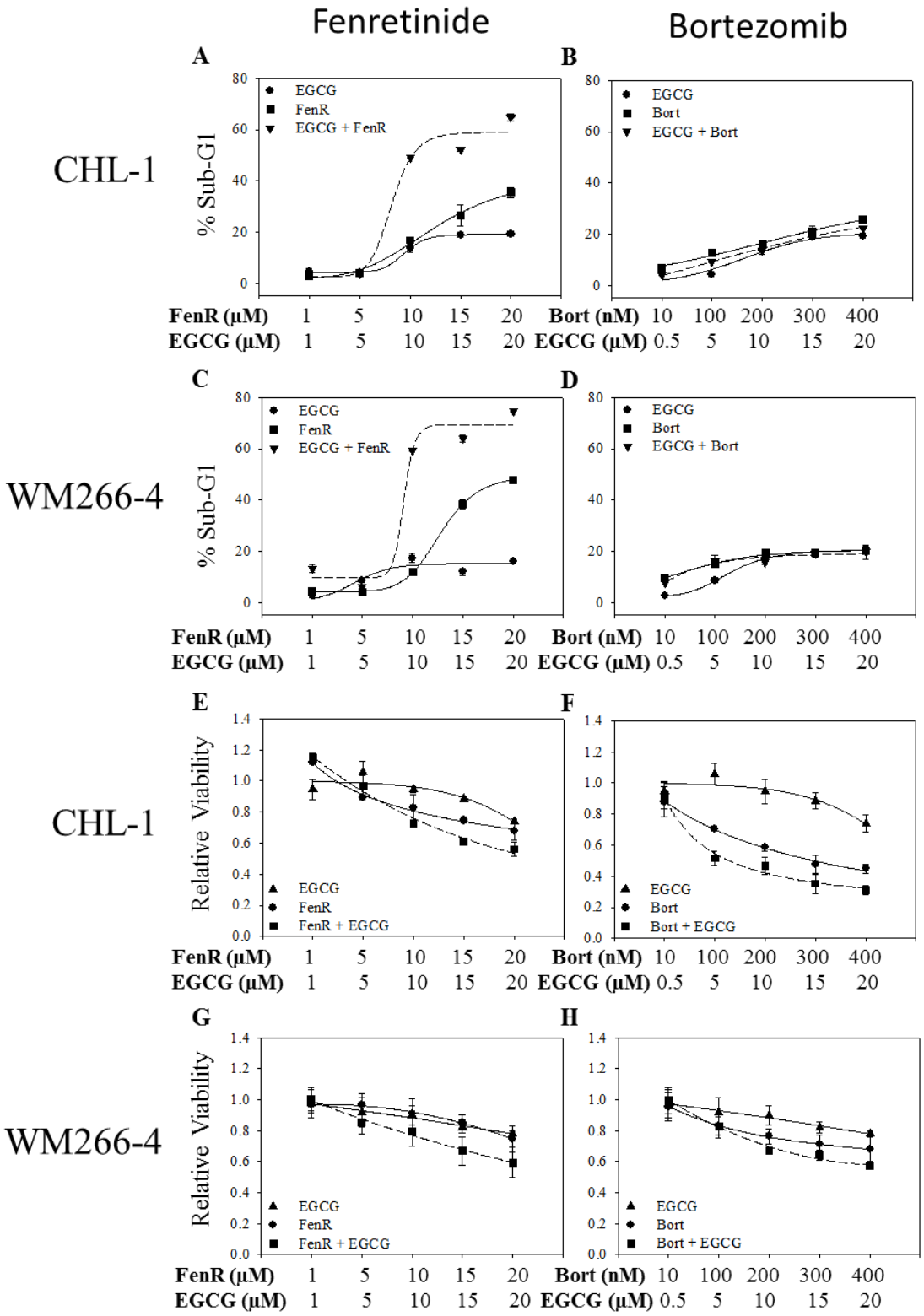
Fenretinide
Bortezomib
A
B
C
D
E
F
G
H
CHL-1
WM266-4
CHL-1
WM266-4
% Sub-G1
Relative Viability
EGCG
FenR
EGCG + FenR
Bort
EGCG + Bort
FenR + EGCG
Bort + EGCG
FenR (μM) 1 5 10 15 20
EGCG (μM) 1 5 10 15 20
Bort (nM) 10 100 200 300 400
EGCG (μM) 0.5 5 10 15 20

Glioblastoma

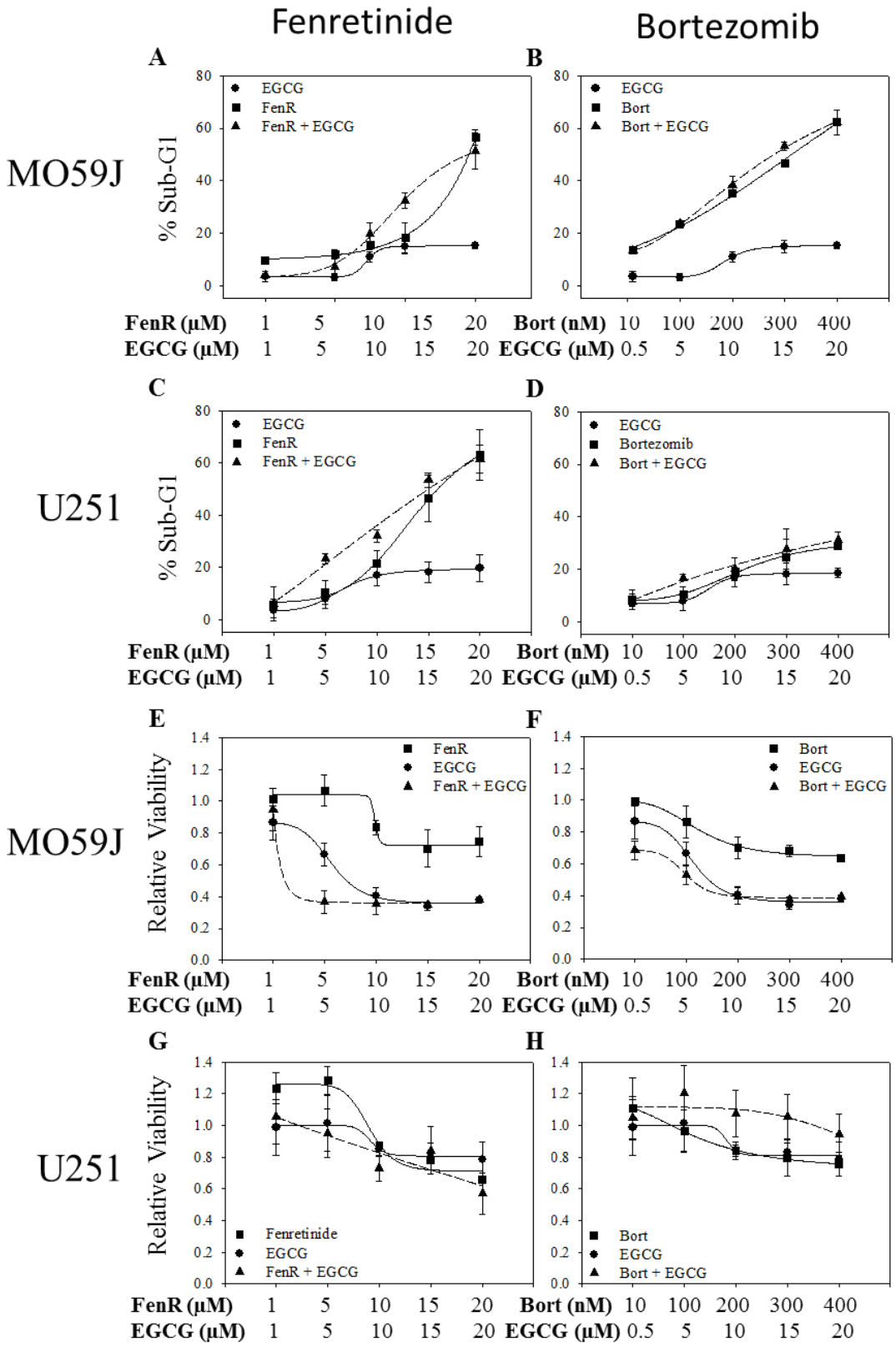

Neuroblastoma

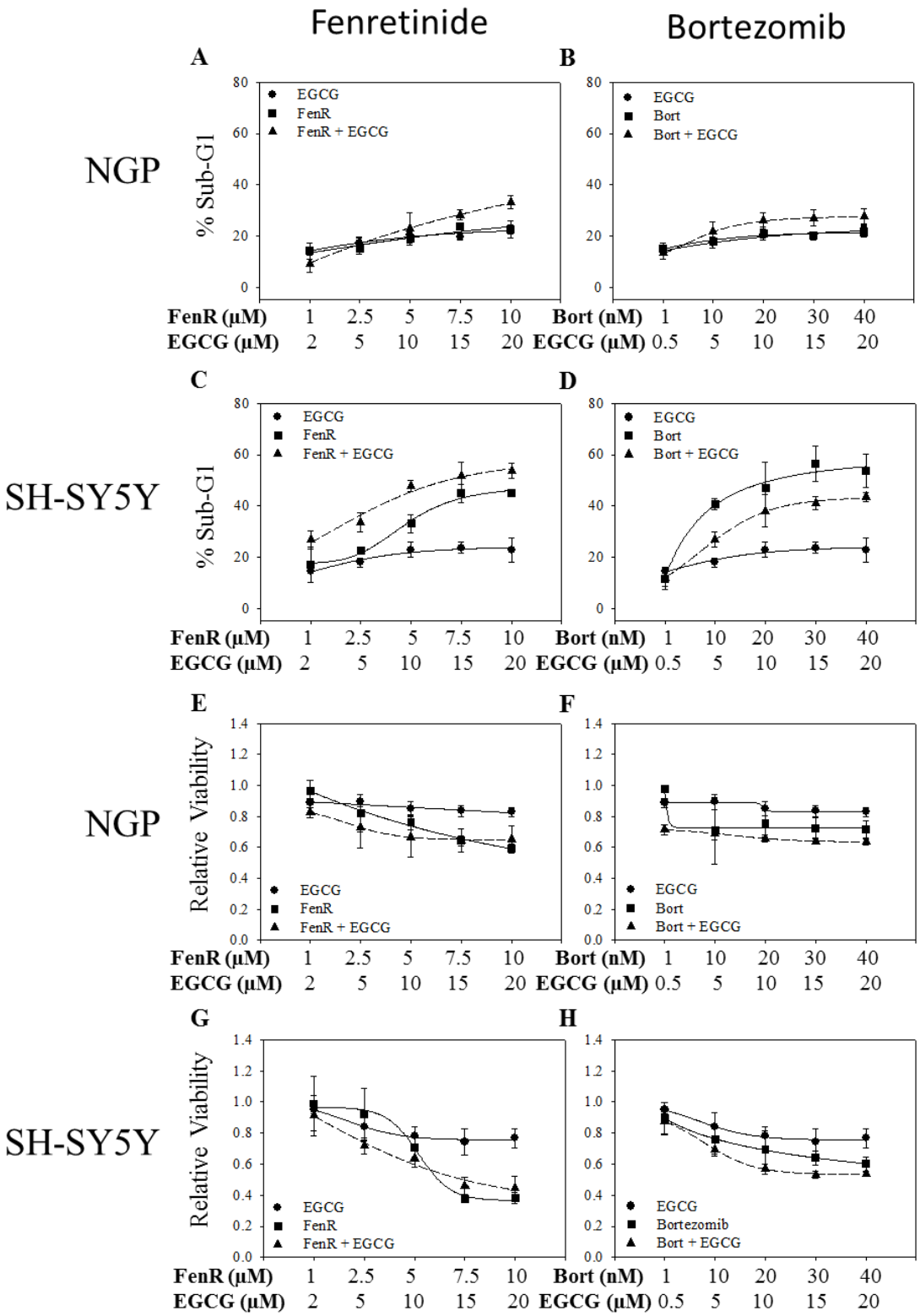

Figure 6.8: *Effect of GRP78 inhibitor EGCG on fenretinide and bortezomib induced apoptosis or inhibition of cell viability. CHL-1 (A & B, E & F) or WM266-4 (C & D, G & H) melanoma, MO59J (I & J, M & N) or U251 (K & L, O & P) glioblastoma and NGP (Q & R, U & V) or SH-SY5Y (S & T, W & X) neuroblastoma cells were treated with fenretinide (dose range = 1 – 20 µM for melanoma and glioblastoma or 1 – 10 µM for neuroblastoma), bortezomib (dose range = 10 – 400 nM for melanoma and glioblastoma or 1 – 40 nM for neuroblastoma) and epigallocatechin gallate (EGCG, dose range = 1 – 20 µM) alone and in combination for 24 h at fixed-dose-ratios of 1:1 or 2:1 (µM fenretinide: µM EGCG) and 1:50 or 1:500 (nM bortezomib: µM EGCG) for melanoma and glioblastoma or neuroblastoma , respectively. Samples were analyzed for cell death (A – D, I – L, Q –T for melanoma, glioblastoma and neuroblastoma cell lines treated with either fenretinide or bortezomib respectively) or inhibition of cell viability (E – H, M – P, U - X. T for melanoma, glioblastoma and neuroblastoma cell lines treated with either fenretinide or bortezomib, respectively). Apoptosis data are the mean of 3 experiments for cell death or 8 individual replicates for inhibition on cell viability ± 95% confidence intervals. CalcuSyn was used to determine the outcome of drug combinations (Combination indices for the outcome of drug interactions are given in Table 6.3).*

Cell Line	ER stress inducing agent	GRP78 Inhibitor	Cell Death (ci)	Viability (ci)
CHL-1	1. FenR (1 μM)	1. EGCG (1 μM)	1.062	1.986
	2. FenR (5 μM)	2. EGCG (5 μM)	1.019	2.34
	3. FenR (10 μM)	3. EGCG (10 μM)	0.376	0.68
	4. FenR (15 μM)	4. EGCG (15 μM)	0.412	0.761
	5. FenR (20 μM)	5. EGCG (20 μM)	0.316	0.68
	1. Bort (10 nM)	1. EGCG (0.5 μM)	2.63	1.94
	2. Bort (100 nM)	2. EGCG (5 μM)	3.14	0.74
	3. Bort (200 nM)	3. EGCG (10 μM)	2.62	0.83
	4. Bort (300 nM)	4. EGCG (15 μM)	1.93	0.79
	5. Bort (400 nM)	5. EGCG (20 μM)	2.014	0.69
WM266-4	1. FenR (1 μM)	1. EGCG (1 μM)	0.331	1.662
	2. FenR (5 μM)	2. EGCG (5 μM)	1.62	0.991
	3. FenR (10 μM)	3. EGCG (10 μM)	0.231	0.892
	4. FenR (15 μM)	4. EGCG (15 μM)	0.376	0.73
	5. FenR (20 μM)	5. EGCG (20 μM)	0.344	0.78
	1. Bort (10 nM)	1. EGCG (0.5 μM)	1.016	1.919
	2. Bort (100 nM)	2. EGCG (5 μM)	1.14	2.42
	3. Bort (200 nM)	3. EGCG (10 μM)	1.63	0.96
	4. Bort (300 nM)	4. EGCG (15 μM)	2.64	0.98
	5. Bort (400 nM)	5. EGCG (20 μM)	2.81	0.91
MO59J	1. FenR (1 μM)	1. EGCG (1 μM)	6.41	2.62
	2. FenR (5 μM)	2. EGCG (5 μM)	4.86	0.53
	3. FenR (10 μM)	3. EGCG (10 μM)	0.94	2.97
	4. FenR (15 μM)	4. EGCG (15 μM)	0.79	6.37
	5. FenR (20 μM)	5. EGCG (20 μM)	1.93	6.4
	1. Bort (10 nM)	1. EGCG (0.5 μM)	2.62	0.36
	2. Bort (100 nM)	2. EGCG (5 μM)	1.83	0.76
	3. Bort (200 nM)	3. EGCG (10 μM)	1.99	2.62
	4. Bort (300 nM)	4. EGCG (15 μM)	0.96	6.94
	5. Bort (400 nM)	5. EGCG (20 μM)	1.18	6.39
U251	1. FenR (1 μM)	1. EGCG (1 μM)	2.93	1.43
	2. FenR (5 μM)	2. EGCG (5 μM)	0.63	0.97
	3. FenR (10 μM)	3. EGCG (10 μM)	0.78	0.76
	4. FenR (15 μM)	4. EGCG (15 μM)	0.97	1.09
	5. FenR (20 μM)	5. EGCG (20 μM)	1.43	0.84
	1. Bort (10 nM)	1. EGCG (0.5 μM)	2.4	3.4
	2. Bort (100 nM)	2. EGCG (5 μM)	0.95	18.6
	3. Bort (200 nM)	3. EGCG (10 μM)	1.4	19.9
	4. Bort (300 nM)	4. EGCG (15 μM)	1.016	22.8
	5. Bort (400 nM)	5. EGCG (20 μM)	1.005	17.6
NGP	1. FenR (1 μM)	1. EGCG (2 μM)	4.99	1.01
	2. FenR (2.5 μM)	2. EGCG (5 μM)	2.063	0.87
	3. FenR (5 μM)	3. EGCG (10 μM)	2.011	0.93
	4. FenR (7.5 μM)	4. EGCG (15 μM)	0.83	1.83
	5. FenR (10 μM)	5. EGCG (20 μM)	0.48	3.7
	1. Bort (1 nM)	1. EGCG (0.5 μM)	8.6	0.62
	2. Bort (10 nM)	2. EGCG (5 μM)	0.93	1.1
	3. Bort (20 nM)	3. EGCG (10 μM)	0.89	0.96
	4. Bort (30 nM)	4. EGCG (15 μM)	0.84	0.99
	5. Bort (40 nM)	5. EGCG (20 μM)	0.87	0.98
SH-SY5Y	1. FenR (1 μM)	1. EGCG (2 μM)	0.036	0.96
	2. FenR (2.5 μM)	2. EGCG (5 μM)	0.29	0.89
	3. FenR (5 μM)	3. EGCG (10 μM)	0.48	0.94
	4. FenR (7.5 μM)	4. EGCG (15 μM)	0.79	4.3
	5. FenR (10 μM)	5. EGCG (20 μM)	0.83	3.3
	1. Bort (1 nM)	1. EGCG (0.5 μM)	6.23	1.42
	2. Bort (10 nM)	2. EGCG (5 μM)	24.6	0.91
	3. Bort (20 nM)	3. EGCG (10 μM)	29.3	0.81
	4. Bort (30 nM)	4. EGCG (15 μM)	27.6	0.83
	5. Bort (40 nM)	5. EGCG (20 μM)	28.1	0.91

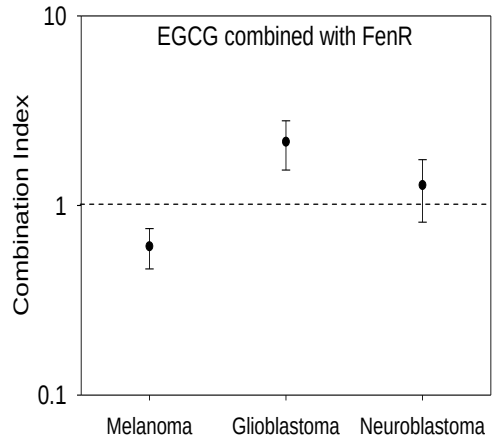

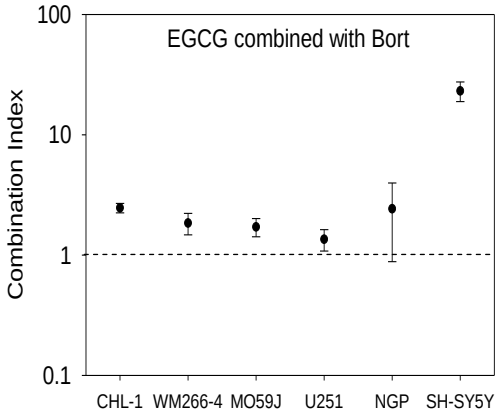

Table 6.3: The e*ffect of GRP78 inhibition by EGCG treatment on ER stress-induced cell death or inhibition of cancer cell viability. Drug interaction review by fixed dose ratio analysis for the effect of GRP78 epigallocatechin gallate (EGCG) on fenretinide (FenR) or bortezomib (Bort) induced cell death or inhibition of cell viability of melanoma, glioblastoma and neuroblastoma cells. Combination indices (ci) values; < 1 = Synergy (Green), ≤ 1 = Additive (Black) and > 1 = inhibitory (red). Data are given in Figure 6.8. Alongside the combination indices data are graphs summarising the combination indices obtained for the effect of combining EGCG with either fenretinide or bortezomib.*

To investigate the effect of combining EGCG with an ER stress-inducing agent on biochemical markers of ER stress and apoptosis cell lines were treated with fenretinide (For melanoma and glioblastoma: F1 = 5 μM and F2 = 10 μM or neuroblastoma F1 = 2.5 μM and F2 = 5 μM), bortezomib (B1 = 100 nM and B2 = 200 nM or neuroblastoma B1 = 10 nM and B2 = 20 nM) or EGCG (E1 = 5 μM and E2 = 10 μM) alone or in combination (FE1, FE2, BE1 and BE2, Figure 6.9).

Melanoma and glioblastoma cell lines demonstrated a reduction in GRP78 expression when treated with combinations of fenretinide or bortezomib with EGCG (Figure 6.9 A-D ii, One-way ANOVA with Bonferroni post hoc corrections, For all samples $P \leq 0.01$), except for CHL-1 and MO59J, where there was an increase in GRP78 expression in cells treated with the FE1 combination ($P < 0.0001$ for both).

For ATF4 there was a significant reduction in expression in CHL-1 and WM266-4 cells treated with FE2, BE1 and BE2 combinations (Figure 6.9 A-D iii, One-way ANOVA with Bonferroni post hoc corrections, for all samples $P \leq 0.01$). Significant increases in expression were demonstrated in the remaining combinations ($P < 0.0001$ for melanoma). MO59J and U251 glioblastoma cell lines for ATF4 expression, demonstrated no consistent change in response outcome for the combinations, respectively ($P < 0.0001$ for all). Where an increase in ATF4 expression was observed for MO59J with either bortezomib combination ($P \leq 0.01$) and a decrease in expression in U251 cells treated with FE1, FE2 and BE2 ($P \leq 0.01$)

For caspase 3 cleavage there was a significant reduction in melanoma and glioblastoma cell lines with either fenretinide or bortezomib combinations with EGCG (Figure 6.9 A-D iv, One-way ANOVA with Bonferroni post hoc corrections, For all samples $P \leq 0.01$), except for CHL-1 treated with the FE1 combination, were an increase in caspase 3 cleavage was observed ($P \leq 0.01$).

For the effect of EGCG combination with either fenretinide or bortezomib in neuroblastoma cell lines, data demonstrated a significant decrease in GRP78 expression, in NGP FE1, BE1 and BE2 combinations (Figure 6.9 E & F ii, One-way ANOVA with Bonferroni post hoc corrections, For all samples $P \leq 0.01$), and an increase in NGP cells treated with the FE2 combination or all SH-SY5Y combinations ($P < 0.05$). The effect of EGCG combination with fenretinide or bortezomib on ATF4 induction in neuroblastoma cell lines demonstrated significant increase in expression in NGP cells

with the FE1 combination (Figure 6.9 E & F ii, One-way ANOVA with Bonferroni post hoc corrections, for all samples $P \leq 0.01$). All other combinations demonstrated a significant reduction in ATF4 expression (For all samples $P \leq 0.01$), except NGP cells treated with FE2 ($P > 0.05$). Caspase 3 data showed an increase in cleavage for NGP cells treated with FE2 and BE1 combinations (Figure 6.9 E & Fiv, One-way ANOVA with Bonferroni post hoc corrections, for all samples $P \leq 0.01$) and a decrease for NGP cells treated with BE2 or all SH-SY5Y combinations ($P \leq 0.01$).

In summary, EGCG induced cell death and inhibition of cell viability in a dose dependent manner in all cell lines tested. When combining EGCG with an ER stress-inducing agent, a synergistic response was observed in melanoma cells treated with fenretinide. However no enhancement of was observed in glioblastoma and for neuroblastoma the combination with fenretinide showed an increase in inhibition of response with dose. Finally the assessment of ATF4 induction and caspase 3 cleavage for the combination of EGCG with either fenretinide or bortezomib showed no consistent effect.

Melanoma

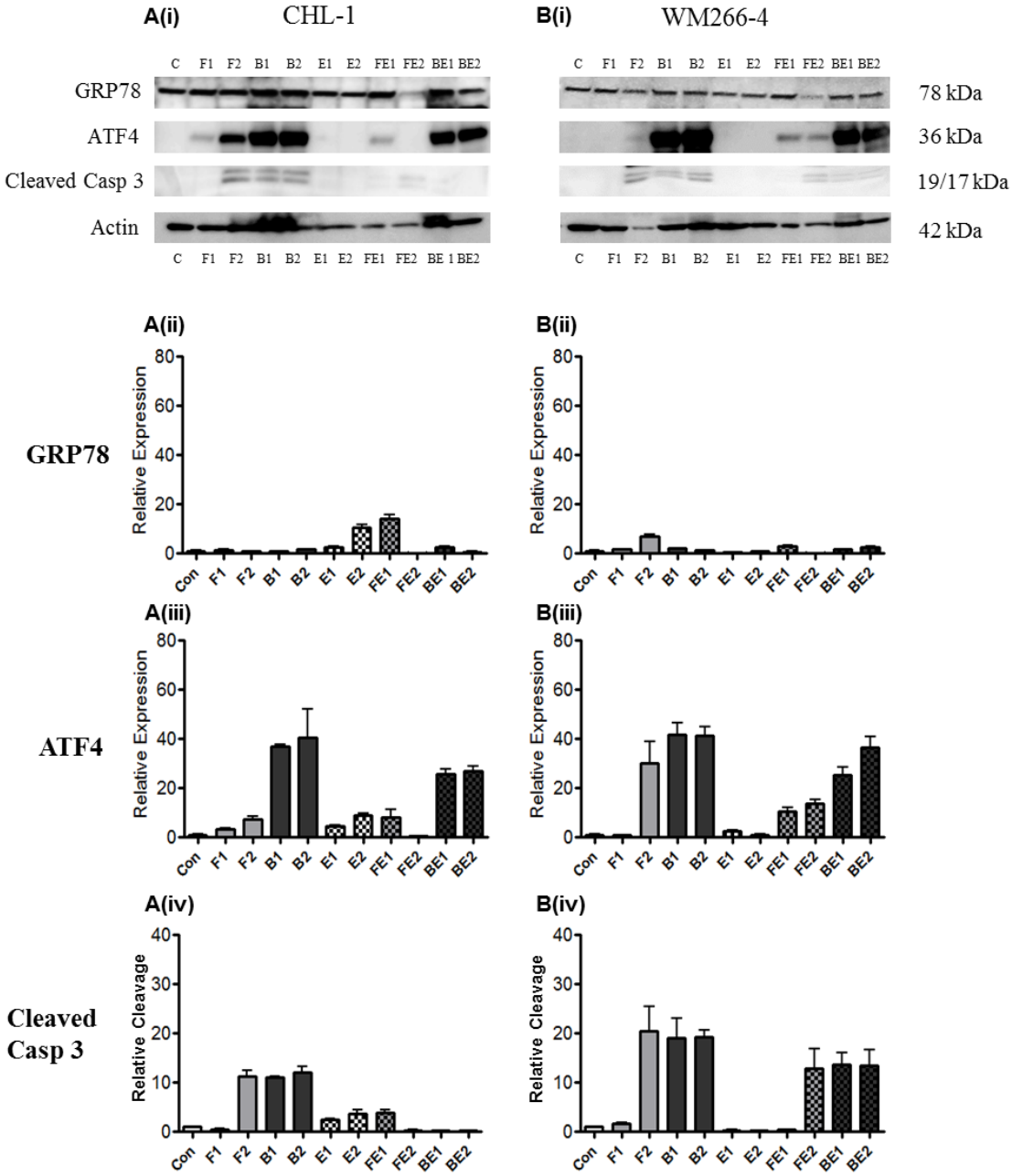
A(i)
CHL-1
B(i)
WM266-4
C F1 F2 B1 B2 E1 E2 FE1 FE2 BE1 BE2
GRP78
ATF4
Cleaved Casp 3
Actin
78 kDa
36 kDa
19/17 kDa
42 kDa
A(ii)
B(ii)
GRP78
A(iii)
B(iii)
ATF4
A(iv)
B(iv)
Cleaved Casp 3
Relative Expression
Relative Cleavage
Con F1 F2 B1 B2 E1 E2 FE1 FE2 BE1 BE2

Glioblastoma

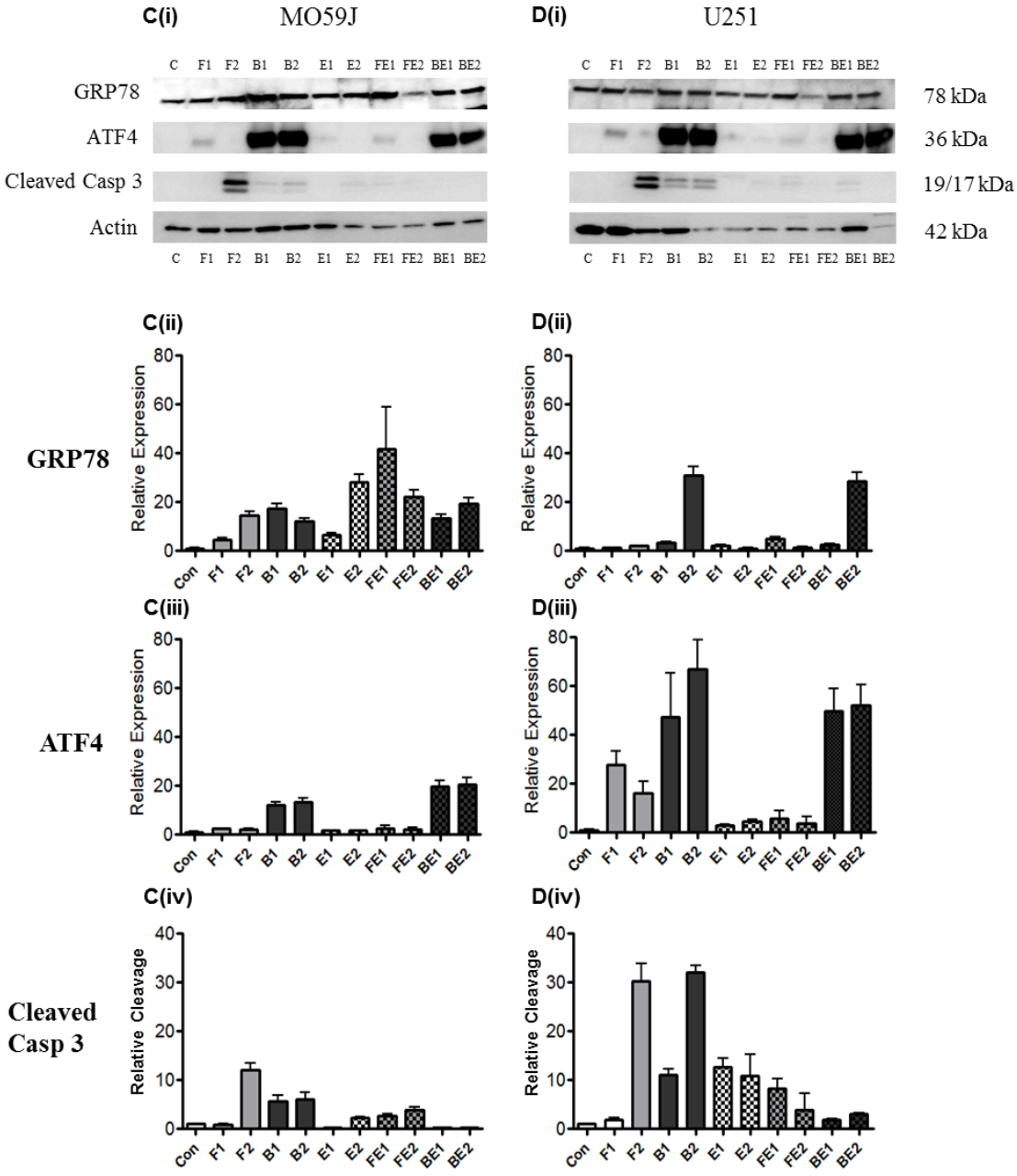

Neuroblastoma

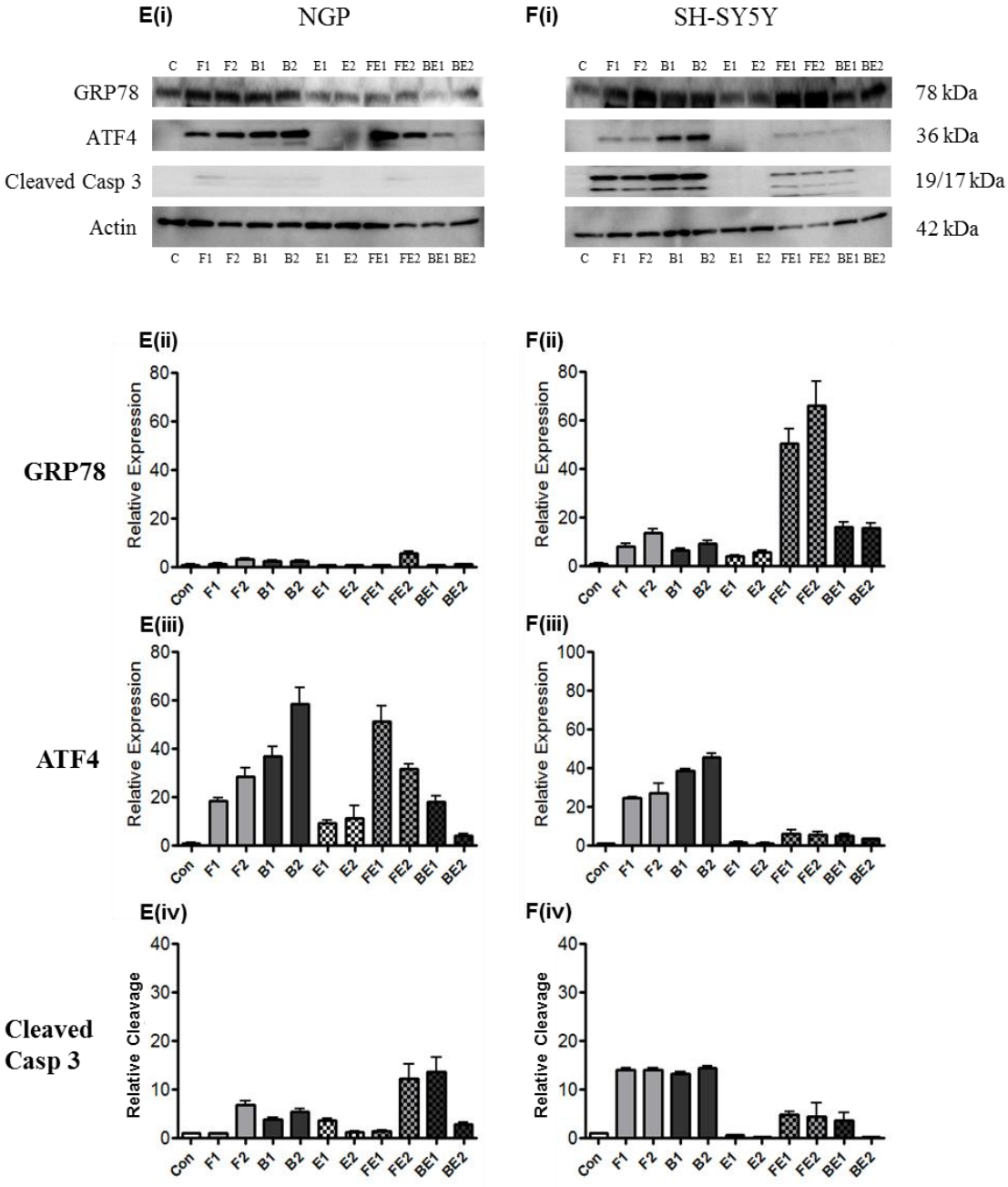

Figure 6.9: *The effect of EGCG treatment on fenretinide or bortezomib induced ER stress and induction of apoptosis. Melanoma (A & B), glioblastoma (C & D) and neuroblastoma (E & F) cells were treated with either fenretinide (light grey bars, For melanoma and glioblastoma, F1 = 5 µM and F2 = 10 µM or neuroblastoma F1 = 2.5 µM and F2 = 5 µM), bortezomib (Dark grey bars, For melanoma and glioblastoma, B1 = 100 nM and B2 = 200 nM or neuroblastoma B1 = 10 nM and B2 = 20 nM) or epigallocatechin gallate (EGCG, Dotted bars, E1 = 5 µM and E2 = 10 µM) alone or in combination for 24 h. Western blot analyses (i) were performed for GRP78 expression, induction of UPR inducible ATF4 and cleavage of caspase 3, using β-Actin as a loading control. Densitometry analysis were performed on GRP78 (ii), ATF4 (iii) and cleaved caspase 3 (iv) and data expressed as mean values, relative to β-Actin as a loading control, of 3 independent experiments ± 95%. Graphs are scaled across cancer types, differing depending on the protein of interest to allow for a visual comparison for the effect of drug combinations.*

		Combination				
Cell Line	**Protein**	**FE1**	**FE2**		**BE1**	**BE2**
CHL-1	**GRP78**					
WM266-4						
MO59J						
U251						
NGP						
SH-SY5Y						
CHL-1	**ATF4**					
WM266-4						
MO59J						
U251						
NGP						
SH-SY5Y						
CHL-1	**Cleaved Caspase 3**					
WM266-4						
MO59J						
U251						
NGP						
SH-SY5Y						

Table 6.4: *The effect of GRP78 inhibition, by EGCG treatment, on the induction of ER stress in neural-crest-derived cancer cells. A Summary table for the effect of drug combination in comparison to ER stress-inducing agents (Fenretinide = F, Bortezomib = B) or EGCG treatment control (EGCG = E). Data are the sum of the response of 3 individual experiments and demonstrate an increase (green), decrease (red) or no significant difference (grey) in protein expression.*

6.2.3: The effect of natural putative GRP78 inhibitor honokiol on ER stress and cell death of melanoma, glioblastoma and neuroblastoma cancer cells.

To Investigate the effect of honokiol on neural-crest-derived cancer cells, melanoma, glioblastoma and neuroblastoma cells were treated with increasing doses of honokiol and assessed for the induction of cell death or inhibition of cell viability (Figure 6.10, dose range = 0.1 – 100 μM).

There was a significant induction of cell death in all cancer lines (One-way ANOVA with Dunnett's post hoc correction, for CHL-1 and WM266-4 from 40 μM or MO59J, U251, NGP and SH-SY5Y cells from 10 μM $P \leq 0.05$) and inhibition of cell viability (For CHL-1 and WM266-4 from 20 μM or MO59J, U251, NGP and SH-SY5Y cells from 40 μM $P \leq 0.05$).

The response between cancer lines within each cancer type was similar ($P > 0.05$), but between cancer types there was a lower response in glioblastoma compared to either melanoma or neuroblastoma (Two-way ANOVA, for cell death glioblastoma vs. either melanoma or neuroblastoma $F_{19, 59} = 23.3$ or 17.6, $P < 0.001$, respectively). As well as differences in the magnitude of death induced across cancer types, there were differences in the kinetics of honokiol-induced cell death. Glioblastoma and neuroblastoma demonstrated an exponential rise to the maximum achievable level of cell death. On the other hand, melanoma showed a more classic sigmoidal effect of honokiol, requiring more drug to elicit a response than either glioblastoma or neuroblastoma (Melanoma requiring a minimum of 20 μM honokiol in comparison to glioblastoma 5 μM and Neuroblastoma 2.5 μM). The kinetic responses were also the same for each cell line of a certain cancer type, suggesting a cancer-type-specific mode of action.

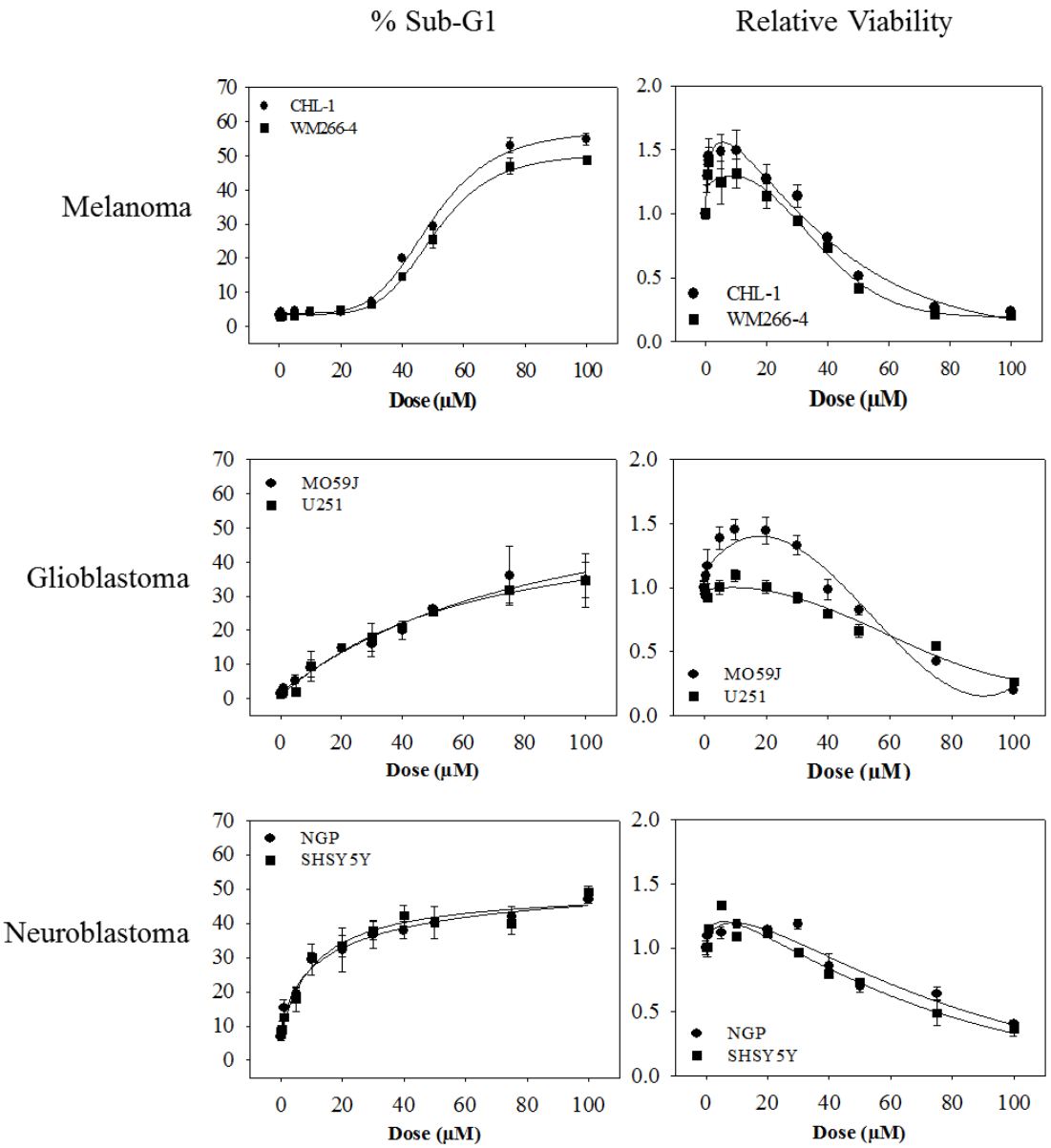

Figure 6.10: *The effect of honokiol on neural-crest-derived cancer cell death and inhibition of cell viability. Melanoma (A & B), glioblastoma (C & D) and neuroblastoma (E & F) cells were treated with increasing doses of Honokiol (dose range = 0.1 – 100 µM) for 24 h. Cells were assessed for the induction of cell death by propidium iodide stained flow cytometry and inhibition of cell viability by MTS assay. For cell death each point is the mean percentage SubG1 peak of 3 individual experiments or inhibition of cell viability of 8 replicates over 3 individual experiments ± 95% CI.*

To test the hypothesis that honokiol induces death and inhibition of cell viability by activating ER stress and downstream apoptosis signalling cascades, cancer cells were treated with increasing doses of honokiol (0 – 100 μM) and analysed by western blot for GRP78 expression, ATF4 induction and caspase 3 cleavage (Figure 6.11). The treatment of melanoma (Figure 6.11 A & B), glioblastoma (Figure 6.11 C & D) and neuroblastoma (Figure 6.11 E & F) cell lines with honokiol significantly induced the expression of GRP78 (One-way ANOVA with Dunnett's post hoc corrections, CHL-1; 20 – 75 μM, WM266-4; 1 – 50 μM, MO59J and U251; 0.5 μM up wards, NGP; 0.5 – 50 μM or SH-SY5Y; 0.5 – 75 μM $P \leq 0.05$). However, cancer types treated with high dose honokiol showed a reduction in GRP78 expression (One-way ANOVA with Dunnett's post hoc corrections, for CHL-1, WM266-4, U251, SH-SY5Y at 100 μM or NGP at 75 & 100 μM, $P \leq 0.001$). Comparing cancer types demonstrated no significant difference in GRP78 induction in response to honokiol ($P > 0.05$), but cell lines of the same cancer type show significant differences in sensitivity (Two-way ANOVA, for melanoma, glioblastoma and neuroblastoma $F_{33, 197} = 33.2$, 54.6 and 66.9, respectively, $P < 0.0001$).

The cell lines all demonstrated a significant dose-dependent increase in ATF4 expression (One-way ANOVA with Dunnett's post hoc corrections, melanoma cells from 20 μM, glioblastoma from 5 μM or NGP and SH-SY5Y neuroblastoma cells from 30 & 10 μM respectively, $P \leq 0.01$) and caspase 3 cleavage (One-way ANOVA with Dunnett's post hoc corrections, melanoma from 5 μM, glioblastoma from 50 μM and neuroblastoma from 1 μM, $P \leq 0.01$). WM266-4 melanoma cells treated with high doses of honokiol (75 & 100 μM) showed a loss of ATF4 induction, compared to lower doses (20 - 50 μM). Melanoma cells demonstrated significantly greater induction of ATF4 in comparison to glioblastoma or neuroblastoma (Two-way ANOVA, for melanoma vs. glioblastoma or neuroblastoma $F_{33, 197} = 127.5$, 144.6 respectively, $P < 0.0001$). Melanoma and neuroblastoma cells showed significantly higher stimulation of caspase 3 cleavage by honokiol treatment than glioblastoma (Two-way ANOVA, $F_{33, 197} = 41.2$, $P < 0.001$). Comparing cell lines of the same cancer type highlighted differences between CHL-1 and WM266-4 cell lines for the achievable level of caspase 3 cleavage (Two-way ANOVA, $F_{33, 65} = 21.8$, $P < 0.001$).

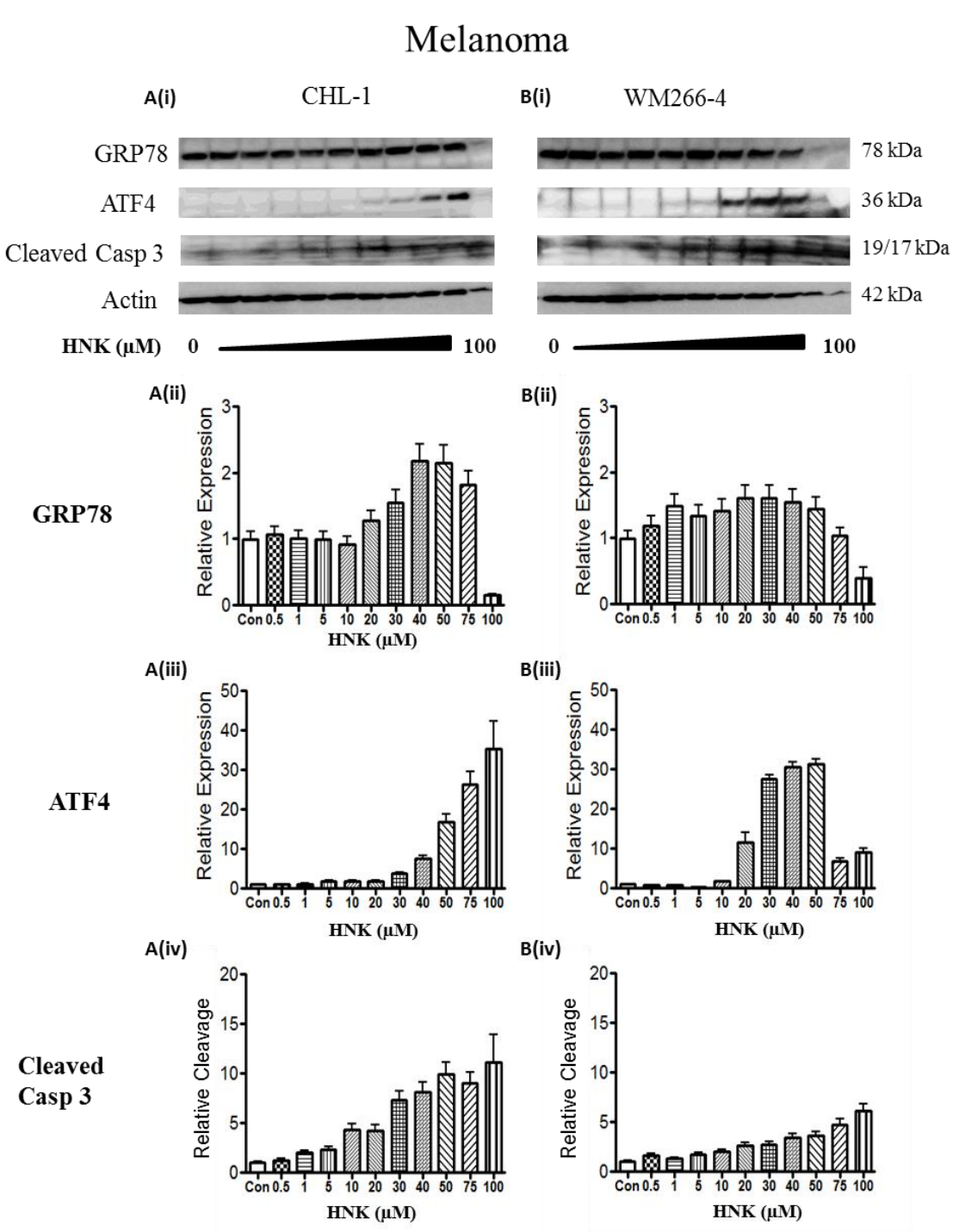
Melanoma
A(i)
CHL-1
B(i)
WM266-4
GRP78
ATF4
Cleaved Casp 3
Actin
78 kDa
36 kDa
19/17 kDa
42 kDa
HNK (µM)
0
100
0
100
GRP78
ATF4
Cleaved Casp 3
A(ii)
B(ii)
A(iii)
B(iii)
A(iv)
B(iv)
Relative Expression
Relative Cleavage
Con 0.5 1 5 10 20 30 40 50 75 100
HNK (µM)

Glioblastoma

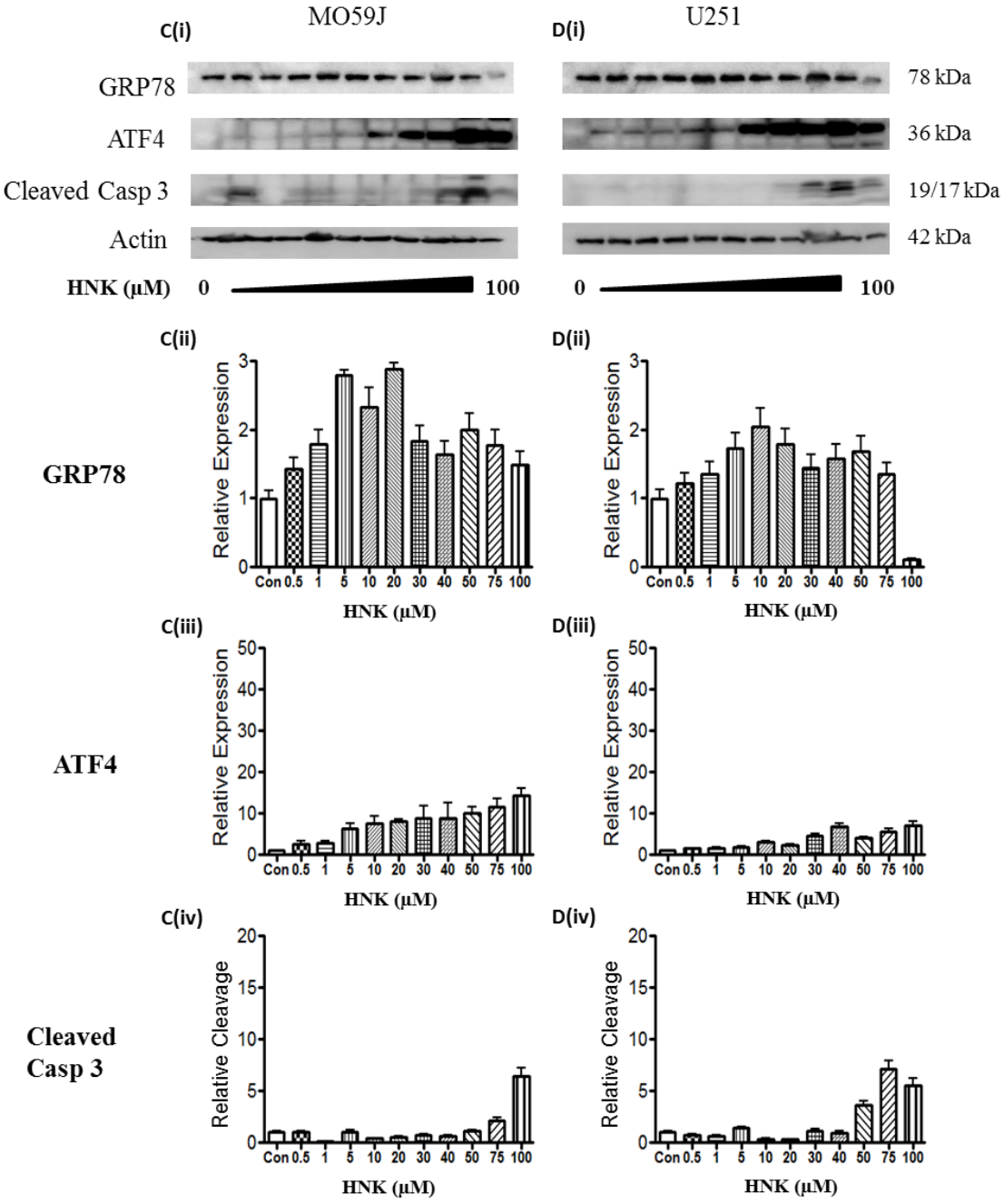

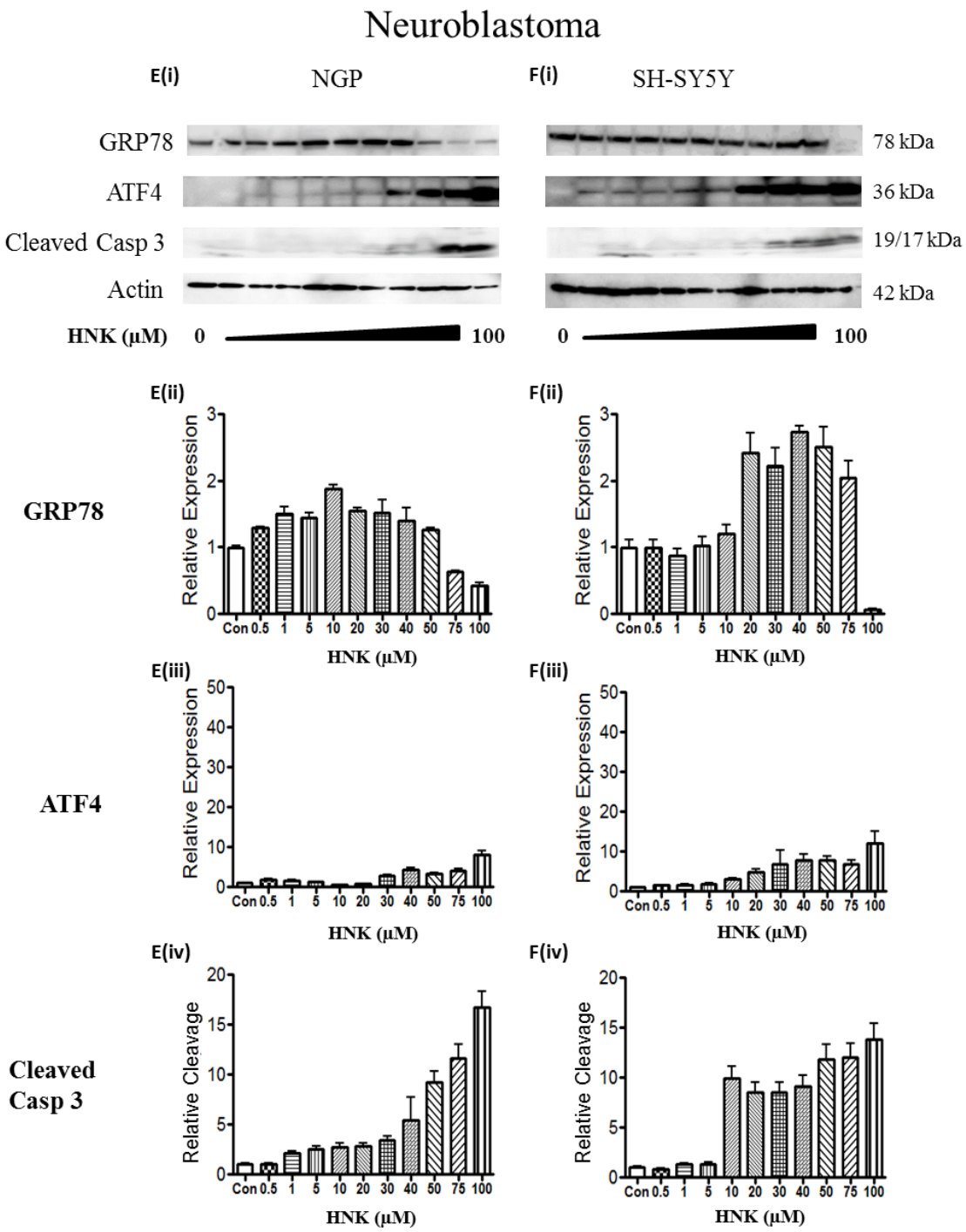
Neuroblastoma
E(i)
NGP
F(i)
SH-SY5Y
GRP78
ATF4
Cleaved Casp 3
Actin
78 kDa
36 kDa
19/17 kDa
42 kDa
HNK (µM) 0 100
0 100
E(ii)
F(ii)
GRP78
Relative Expression
Con 0.5 1 5 10 20 30 40 50 75 100
HNK (µM)
E(iii)
F(iii)
ATF4
Relative Expression
HNK (µM)
E(iv)
F(iv)
Cleaved Casp 3
Relative Cleavage
HNK (µM)

G. Summary

1 **CHL-1**

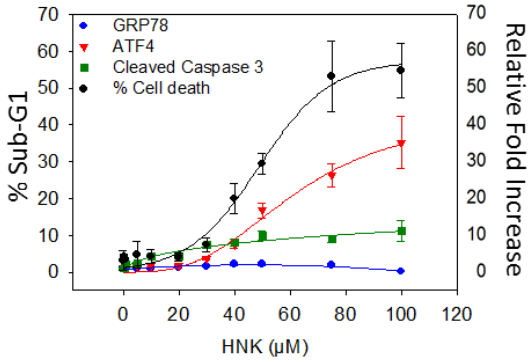

2 **WM266-4**

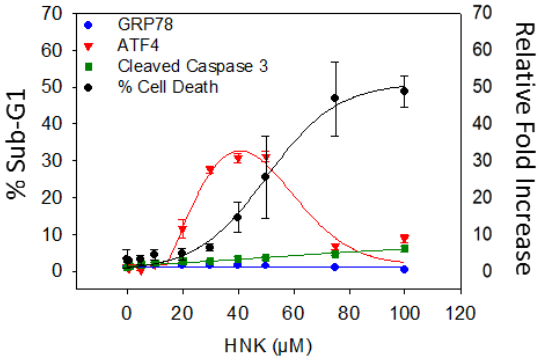

3 **MO59J**

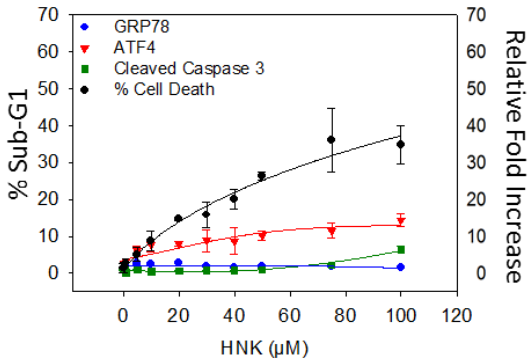

4 **U251**

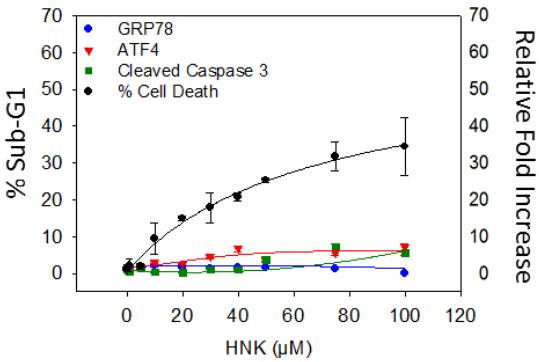

5 **NGP**

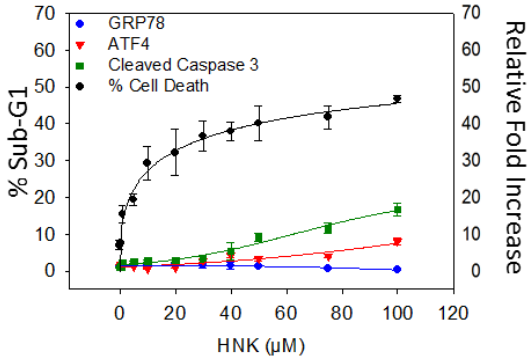

6 **SH-SY5Y**

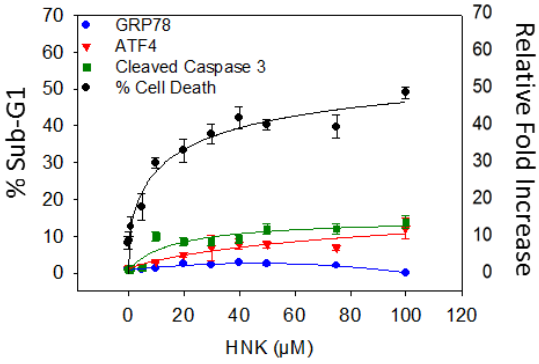

Figure 6.11: *The effect of honokiol dose on the induction of ER stress and apoptosis. Melanoma (A & B), glioblastoma (C & D) and neuroblastoma (E & F) cells were treated with increasing concentrations of honokiol (HNK, dose range = 0 – 100 µM) for 24 h prior to western blot analysis (i) for ER stress markers; GRP78 and ATF4, or the apoptotic marker; cleaved caspase 3. Densitometry analysis were performed on GRP78 (ii), ATF4 (iii) and cleaved caspase 3 (iv). G – Summary for the effect of honokiol dose response on cell death (black) in comparison to protein expression for ER stress (GRP78 + ATF4, blue and red respectively) and apoptosis (Cleaved caspase 3, green) induction. Data are expressed relative to β-Actin as a loading control (for western blot analysis) or as percentage of control (cell death). All are expressed as the mean values, of 3 independent experiments ± 95%. Graphs are scaled across cancer types, differing depending on the protein of interest to allow for a visual comparison for the effect of drug combinations.*

To test the hypothesis that GRP78 inhibition, using the natural inhibitor honokiol, would enhance cell death of neural-crest-derived cancer cells in response to ER stress, fixed-dose-ratio experiments were carried for the combination of honokiol with either fenretinide or bortezomib (melanoma and glioblastoma were used at ratios of 1:5 for fenretinide and 1:250 with bortezomib, Neuroblastoma were used at 1:10 with fenretinide and 1:2500 with Bortezomib) and the effect assessed by cell death and inhibition of cell viability (Figure 6.12). Melanoma (Figure 6.12 A – H) and glioblastoma (I – P) cells demonstrated a synergistic interaction with respect to both cell death and inhibition of cell viability, for the combination of honokiol with either fenretinide or bortezomib (for cell death ci < 0.3 or viability ci < 0.02). Data for the inhibition of viability demonstrated greater synergy than that of the cell death data (ci < 0.02, Table 6.5). Comparing combinations demonstrated no significant difference between interactions of either fenretinide or bortezomib ($P < 0.05$), with regards to the synergy achieved. Glioblastoma cells treated with high dose combinations demonstrate an inhibitory effect on the inhibition of cell viability (ci > 1, Table 6.5). Testing the effect of honokiol on fenretinide or bortezomib induced cell death or inhibition of cell viability in neuroblastoma (Figure 6.12 U – X) demonstrated an inhibitory interaction between honokiol and either ER stress-inducing agent (ci > 1, Table 6.5).

Assessing the combination indices values generated for the effect of honokiol combined with either fenretinide or bortezomib (data summarised in graphs alongside table 6.5) demonstrated differences in response between cancer types. Honokiol in combination with fenretinide, the cell type to cell line interaction was significant ($P < 0.005$); except for neuroblastoma cell lines, were no significant difference was observed ($P > 0.5$). Neuroblastoma were significantly different to other cell lines ($P < 0.05$); WM266-4 melanoma cells were similar to glioblastoma cells ($P > 0.05$) but significantly different to CHL-1 melanoma cells ($P < 0.01$). For honokiol in combination with bortezomib, no significant cell type to cell line interaction was observed ($P > 0.05$); neuroblastoma cells differed significantly from glioblastoma and melanoma cells ($P < 0.0001$).

Melanoma

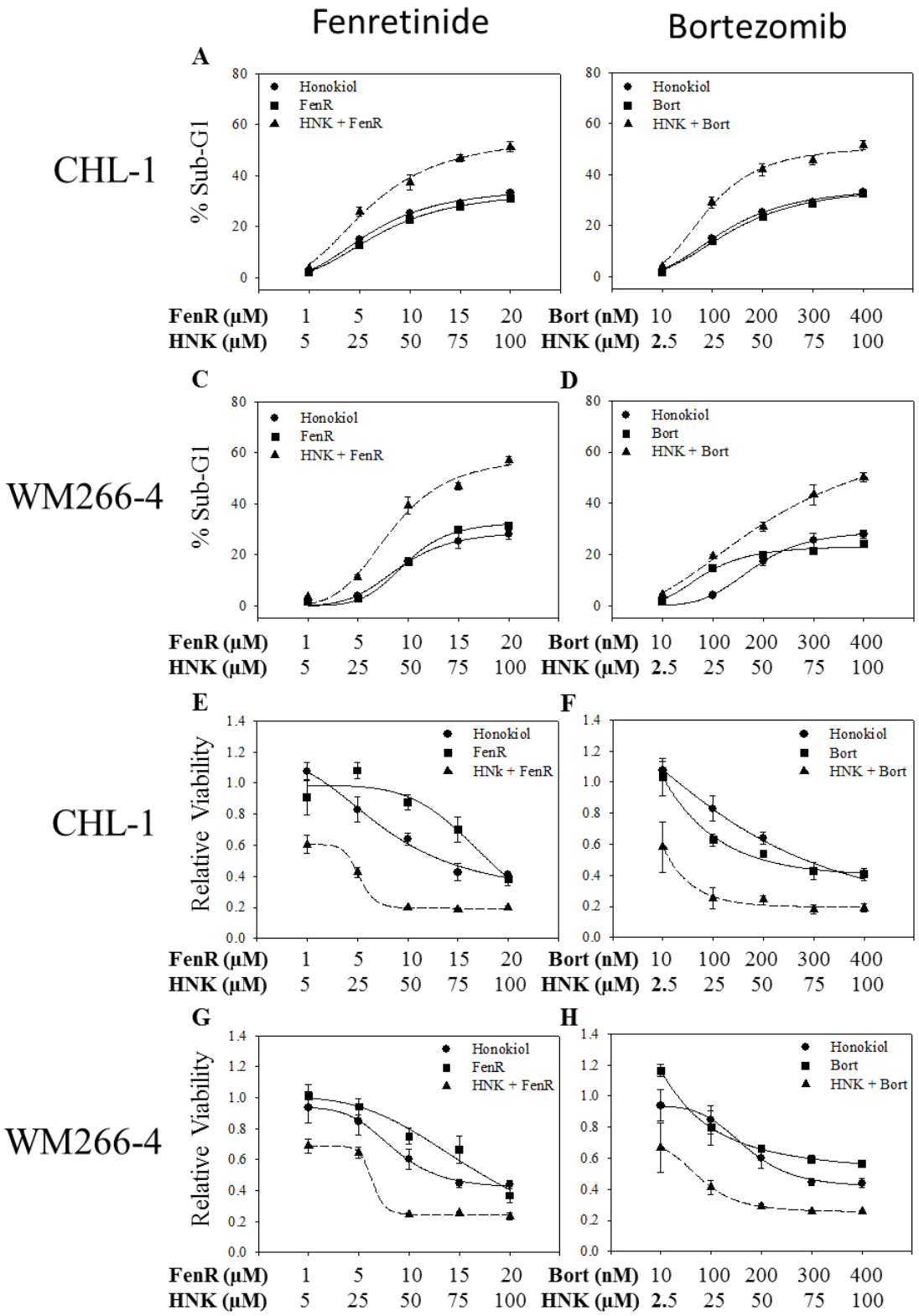
Fenretinide
Bortezomib
A
CHL-1
% Sub-G1
Honokiol
FenR
HNK + FenR
Bort
HNK + Bort
FenR (µM) 1 5 10 15 20
HNK (µM) 5 25 50 75 100
Bort (nM) 10 100 200 300 400
HNK (µM) 2.5 25 50 75 100
C
D
WM266-4
E
F
CHL-1
Relative Viability
HNk + FenR
G
H
WM266-4

Glioblastoma

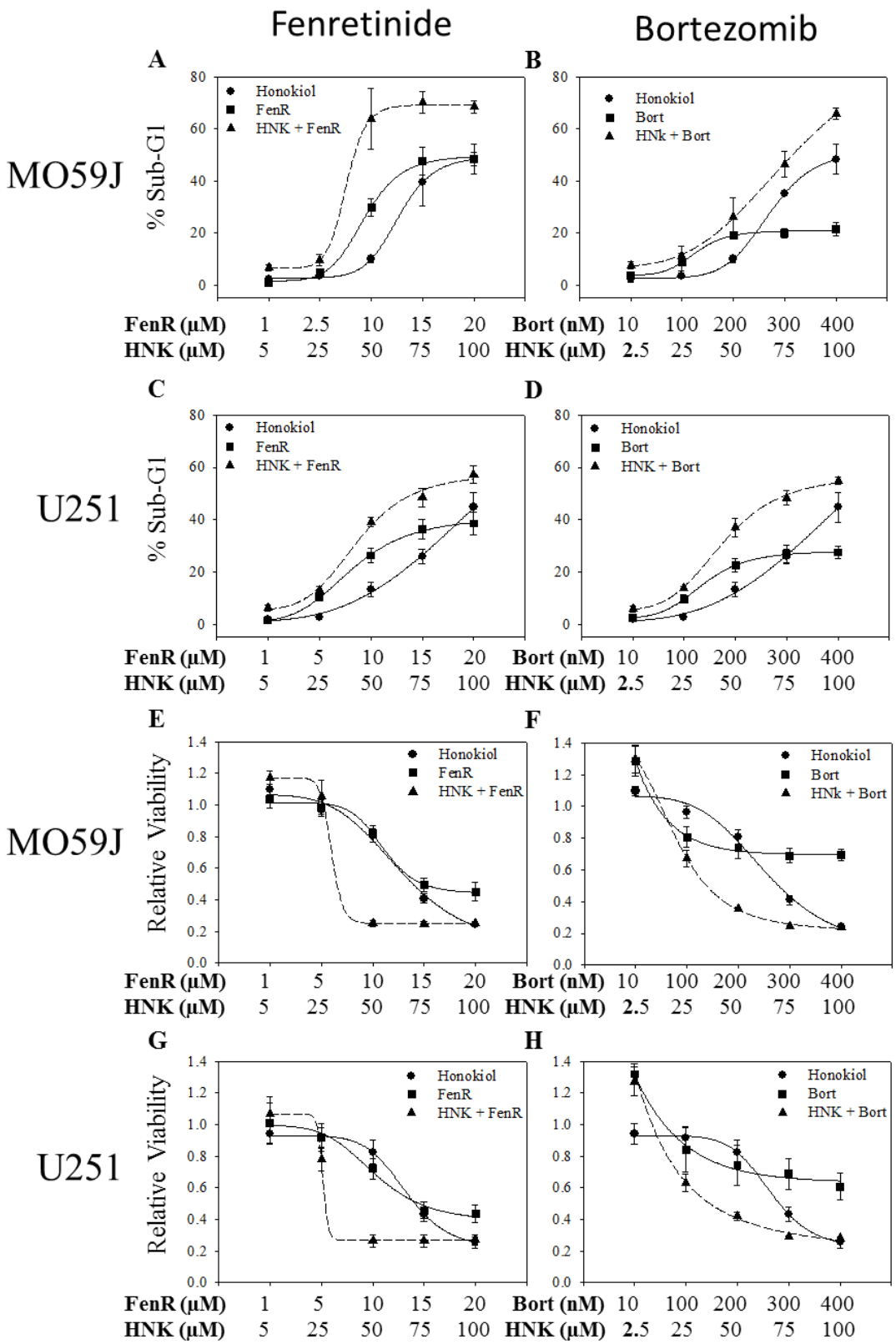

Neuroblastoma

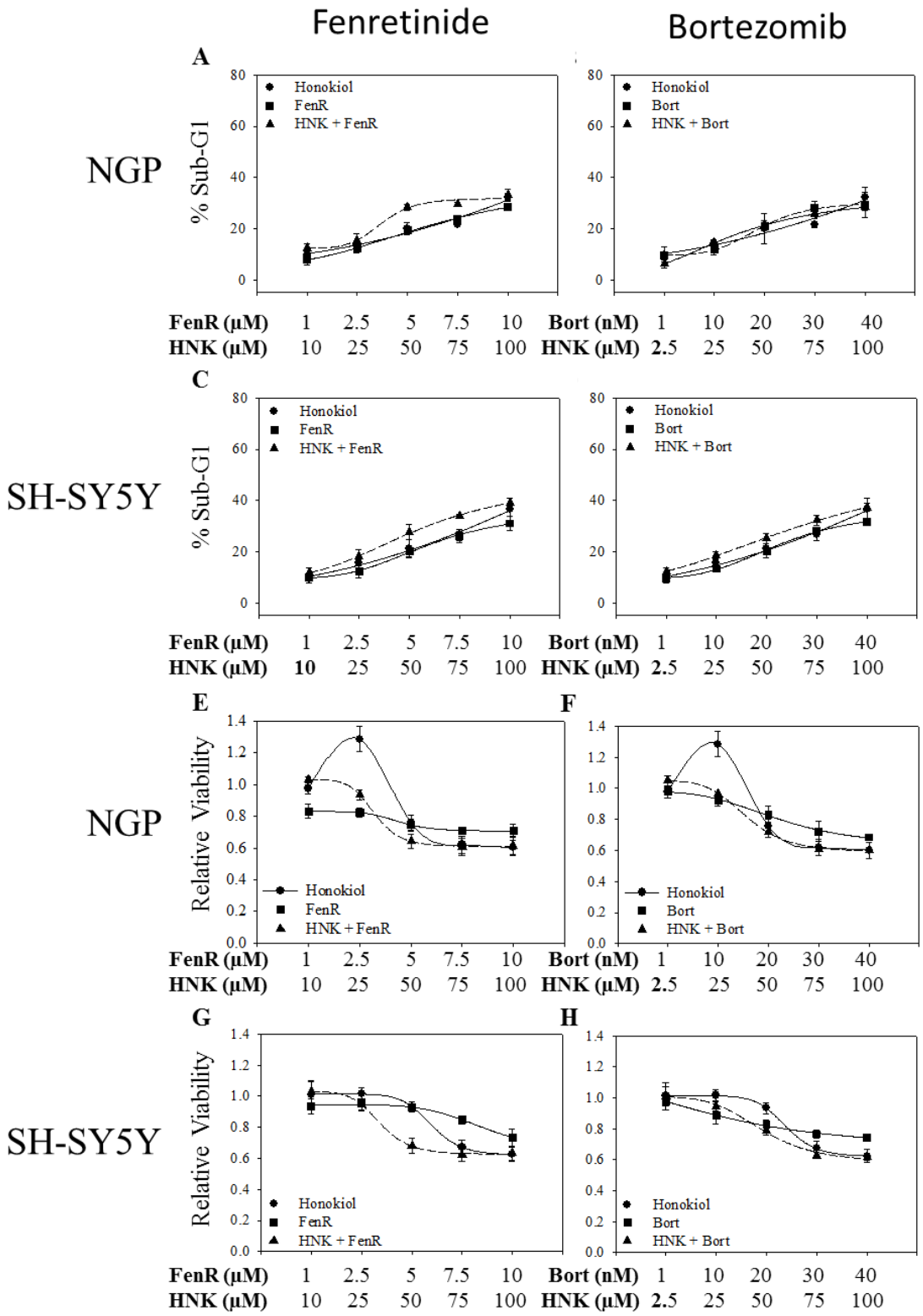

Figure 6.12: *Effect of honokiol on fenretinide and bortezomib induced cell death and inhibition of cancer cell viability. CHL-1 (A & B, E & F) or WM266-4 (C & D, G & H) melanoma, MO59J (I & J, M & N) or U251 (K & L, O & P) glioblastoma and NGP (Q & R, U & V) or SH-SY5Y (S & T, W & X) neuroblastoma cells were treated with fenretinide (dose range = 1 – 20 µM for melanoma and glioblastoma or 1 – 10 µM for neuroblastoma), bortezomib (dose range = 10 – 400 nM for melanoma and glioblastoma or 1 – 40 nM for neuroblastoma) and honokiol (HNK, dose range = 1 – 20 µM) alone and in combination for 24 h at fixed-dose-ratios of 1:5 or 1:10 (µM fenretinide: µM HNK) and 1:50 or 1:500 (nM bortezomib: µM HNK) for melanoma and glioblastoma or neuroblastoma , respectively. Samples were analyzed for cell death (A – D, I – L, Q –T for melanoma, glioblastoma and neuroblastoma cell lines treated with either fenretinide or bortezomib respectively) or inhibition of cell viability (E – H, M – P, U - X. T for melanoma, glioblastoma and neuroblastoma cell lines treated with either fenretinide or bortezomib, respectively). Apoptosis data are the mean of 3 experiments for cell death or 8 individual replicates for inhibition on cell viability ± 95% confidence intervals. CalcuSyn was used to determine the outcome of drug combinations (Combination indices for the outcome of drug interactions are given in Table 6.5).*

Cell Line	ER stress inducing agent	GRP78 Inhibitor	Cell Death (ci)	Viability (ci)
CHL-1	1. FenR (1 µM)	1. HNK (5 µM)	0.685	0.068
	2. FenR (5 µM)	2. HNK (25 µM)	0.772	0.218
	3. FenR (10 µM)	3. HNK (50 µM)	0.731	0.015
	4. FenR (15 µM)	4. HNK (75 µM)	0.603	0.023
	5. FenR (20 µM)	5. HNK (100 µM)	0.637	0.031
	1. Bort (10 nM)	1. HNK (2.5 µM)	0.354	0.064
	2. Bort (100 nM)	2. HNK (25 µM)	0.334	0.054
	3. Bort (200 nM)	3. HNK (50 µM)	0.294	0.015
	4. Bort (300 nM)	4. HNK (75 µM)	0.349	0.023
	5. Bort (400 nM)	5. HNK (100 µM)	0.329	0.031
WM266-4	1. FenR (1 µM)	1. HNK (5 µM)	0.205	0.054
	2. FenR (5 µM)	2. HNK (25 µM)	0.339	0.459
	3. FenR (10 µM)	3. HNK (50 µM)	0.242	0.001
	4. FenR (15 µM)	4. HNK (75 µM)	0.16	0.013
	5. FenR (20 µM)	5. HNK (100 µM)	0.136	0.001
	1. Bort (10 nM)	1. HNK (2.5 µM)	0.644	0.025
	2. Bort (100 nM)	2. HNK (25 µM)	1.398	0.018
	3. Bort (200 nM)	3. HNK (50 µM)	0.302	0.006
	4. Bort (300 nM)	4. HNK (75 µM)	0.274	0.009
	5. Bort (400 nM)	5. HNK (100 µM)	0.197	0.012
MO59J	1. FenR (1 µM)	1. HNK (5 µM)	0.016	23.6
	2. FenR (5 µM)	2. HNK (25 µM)	0.741	18.4
	3. FenR (10 µM)	3. HNK (50 µM)	0.286	0.021
	4. FenR (15 µM)	4. HNK (75 µM)	0.374	0.034
	5. FenR (20 µM)	5. HNK (100 µM)	0.398	1.013
	1. Bort (10 nM)	1. HNK (2.5 µM)	0.244	4.3
	2. Bort (100 nM)	2. HNK (25 µM)	0.962	0.96
	3. Bort (200 nM)	3. HNK (50 µM)	0.883	0.11
	4. Bort (300 nM)	4. HNK (75 µM)	0.816	0.39
	5. Bort (400 nM)	5. HNK (100 µM)	0.704	1.6
U251	1. FenR (1 µM)	1. HNK (5 µM)	0.172	5.4
	2. FenR (5 µM)	2. HNK (25 µM)	0.863	0.71
	3. FenR (10 µM)	3. HNK (50 µM)	0.412	0.021
	4. FenR (15 µM)	4. HNK (75 µM)	0.478	0.059
	5. FenR (20 µM)	5. HNK (100 µM)	0.526	1.6
	1. Bort (10 nM)	1. HNK (2.5 µM)	0.096	12.6
	2. Bort (100 nM)	2. HNK (25 µM)	0.79	0.71
	3. Bort (200 nM)	3. HNK (50 µM)	0.601	0.11
	4. Bort (300 nM)	4. HNK (75 µM)	0.319	0.36
	5. Bort (400 nM)	5. HNK (100 µM)	0.803	1.42
NGP	1. FenR (1 µM)	1. HNK (10 µM)	0.86	26.2
	2. FenR (2.5 µM)	2. HNK (25 µM)	1.12	16.3
	3. FenR (5 µM)	3. HNK (50 µM)	0.62	0.94
	4. FenR (7.5 µM)	4. HNK (75 µM)	0.83	1.16
	5. FenR (10 µM)	5. HNK (100 µM)	1.9	1.83
	1. Bort (1 nM)	1. HNK (2.5 µM)	4.9	7.3
	2. Bort (10 nM)	2. HNK (25 µM)	0.99	2.13
	3. Bort (20 nM)	3. HNK (50 µM)	1.43	0.94
	4. Bort (30 nM)	4. HNK (75 µM)	2.1	1.2
	5. Bort (40 nM)	5. HNK (100 µM)	2.6	1.41
SH-SY5Y	1. FenR (1 µM)	1. HNK (10 µM)	1.12	3.9
	2. FenR (2.5 µM)	2. HNK (25 µM)	1.01	2.6
	3. FenR (5 µM)	3. HNK (50 µM)	0.96	0.049
	4. FenR (7.5 µM)	4. HNK (75 µM)	0.88	0.99
	5. FenR (10 µM)	5. HNK (100 µM)	0.99	1.14
	1. Bort (1 nM)	1. HNK (2.5 µM)	0.84	2.9
	2. Bort (10 nM)	2. HNK (25 µM)	0.93	2.4
	3. Bort (20 nM)	3. HNK (50 µM)	0.97	1.1
	4. Bort (30 nM)	4. HNK (75 µM)	0.93	0.96
	5. Bort (40 nM)	5. HNK (100 µM)	1.16	1.68

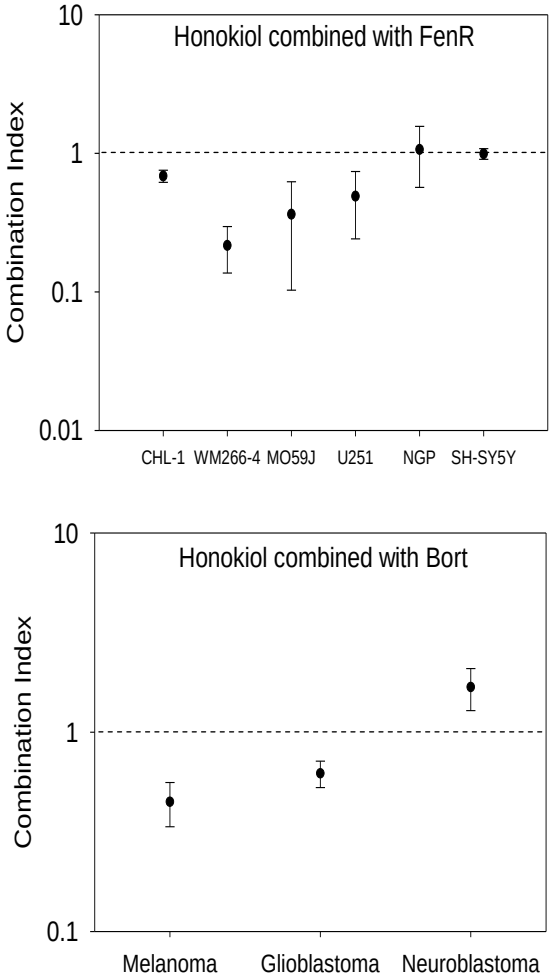

Table 6.5: *Effect of honokiol treatment on ER stress-induced cell death or inhibition of cancer cell viability. Drug interaction review by fixed-dose-ratio analysis for the effect of GRP78 honokiol (HNK) on fenretinide (FenR) or bortezomib (Bort) induced cell death or inhibition of cell viability of melanoma, glioblastoma and neuroblastoma cells. Combination indices (ci) values; < 1 = Synergy (green), ≤ 1 = Additive (black) and > 1 = inhibitory (red). Data are given in Figure 6.12. Alongside the combination indices data are graphs summarising the combination indices obtained for the effect of combining honokiol with either fenretinide or bortezomib for all cell lines individually.*

To investigate the role of the UPR and apoptosis for the enhanced cell death and inhibition of cell viability seen in melanoma and glioblastoma cancer types, western blot analysis for samples treated with fenretinide (For melanoma and glioblastoma: F1 = 5 µM and F2 = 10 µM or neuroblastoma F1 = 2.5 µM and F2 = 5 µM), bortezomib (B1 = 100 nM and B2 = 200 nM or neuroblastoma B1 = 10 nM and B2 = 20 nM) or honokiol (H1 = 50 µM and H2 = 100 µM) alone or in combination (FH1, FH2, BH1 and BH2) were carried out for GRP78 expression, ATF4 induction and caspase 3 cleavage (Figure 6.13).

The effect of honokiol combination with either fenretinide or bortezomib demonstrated cell-line specific and combination indices specific outcomes. Due to the variable outcomes observed when EGCG was combined with either ER stress-inducing agent, with outcomes not correlating with drug dose suggests that the outcome is a consequence of an unstable system. Melanoma cells treated with the fenretinide or bortezomib combinations demonstrated lower induction of GRP78, except WM266-4 cells treated with the BH2 combination (Figure 6.13 A & B ii, BH2, One-Way ANOVA with Bonferroni post hoc corrections, All CHL-1 combinations = $P < 0.0001$, WM266-4; FH1 = $P < 0.05$, FH2, BH1 = $P < 0.0001$ and WM266-4 BH2 = $P < 0.001$).

ATF4 induction in melanoma samples, where fenretinide was combined with honokiol, demonstrated lower induction than agents alone in both melanoma cell lines (Figure 6.13 A & B iii, $P < 0.0001$ for all). For both bortezomib combinations in CHL-1 and the higher combination in WM266-4 cells, an increase in ATF4 induction was observed (CHL-1 BH1 and WM266-4 BH2 = $P < 0.0001$, CHL-1 BH2 = $P < 0.05$). For WM266-4 cells treated with the BH1 combination, a significantly lower induction was observed ($P < 0.05$). Data for caspase 3 cleavage in melanoma cells (Figure 6.13 A & B iv) demonstrated a significant decrease in cleavage in CHL-1 samples treated with both fenretinide combinations and BH2 combination (One-Way ANOVA with Bonferroni post hoc corrections, $P < 0.0001$ for all). CHL-1 cells treated with the BH1 combination and WM266-4 cells with FH2 and BH1 combinations demonstrated significant increases in caspase 3 cleavage (WM266-4 FH1 = $P < 0.05$, all others $P < 0.0001$).

For glioblastoma and neuroblastoma cancer types, the combination of honokiol with either fenretinide or bortezomib significantly reduced the expression of GRP78, ATF4 and cleaved caspase 3 (One-way ANOVA with Bonferroni post hoc corrections, for all combinations $P \leq 0.01$) in all samples except MO59J, U251 (ATF4 and caspase 3) and

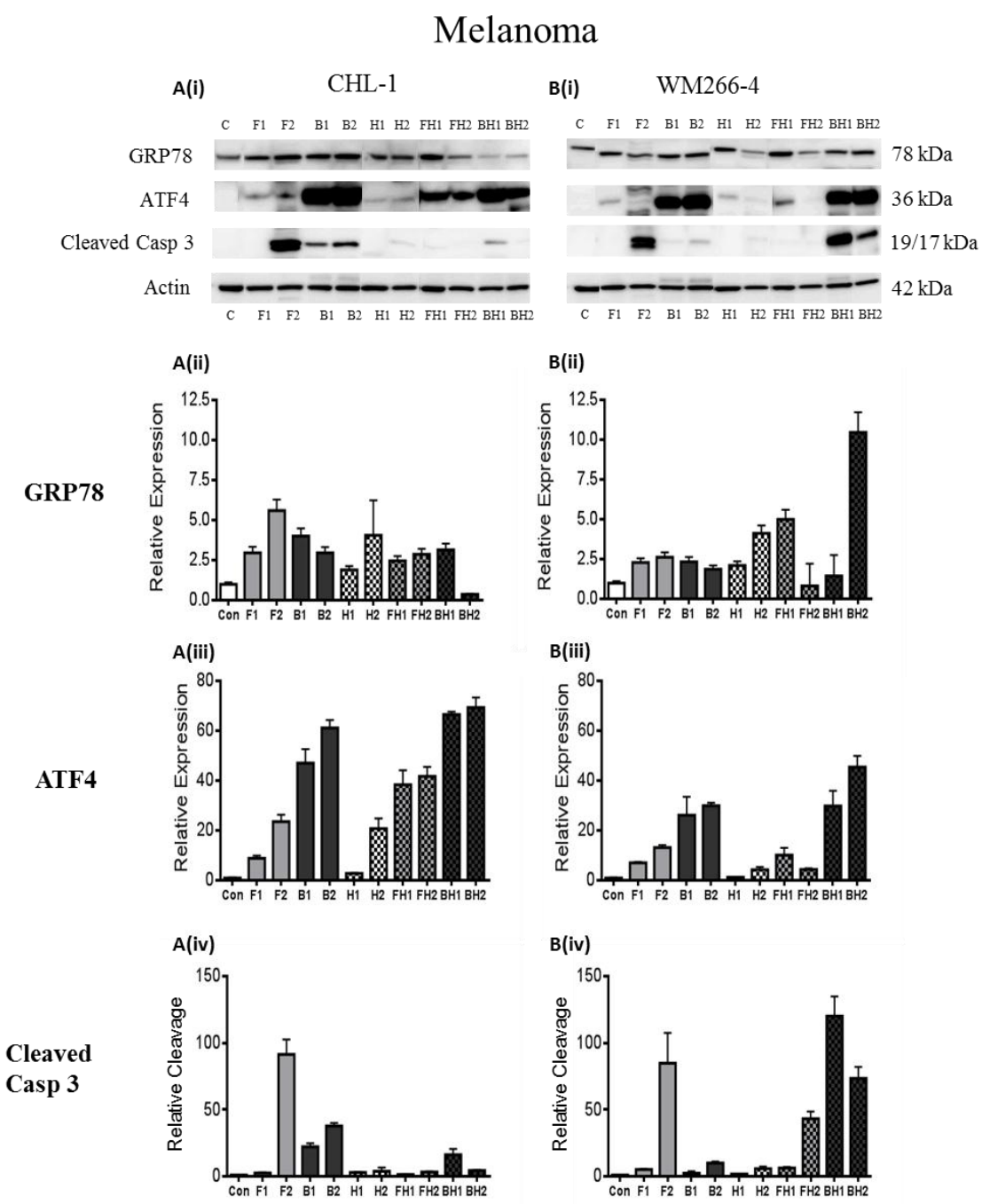
Melanoma
A(i)
CHL-1
B(i)
WM266-4
C F1 F2 B1 B2 H1 H2 FH1 FH2 BH1 BH2
GRP78
ATF4
Cleaved Casp 3
Actin
78 kDa
36 kDa
19/17 kDa
42 kDa
GRP78
ATF4
Cleaved Casp 3
A(ii)
B(ii)
A(iii)
B(iii)
A(iv)
B(iv)
Relative Expression
Relative Cleavage
Con F1 F2 B1 B2 H1 H2 FH1 FH2 BH1 BH2

Glioblastoma

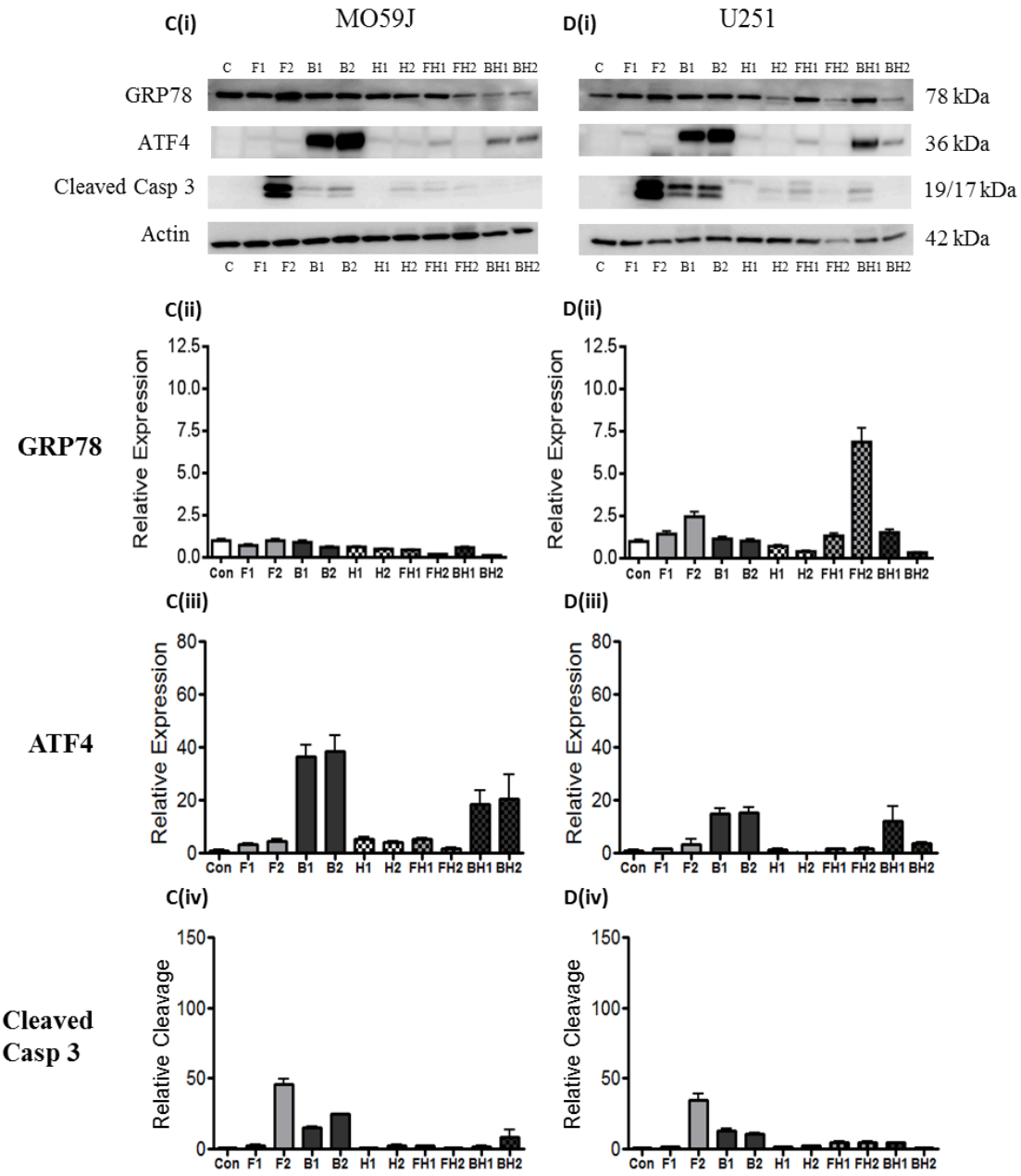

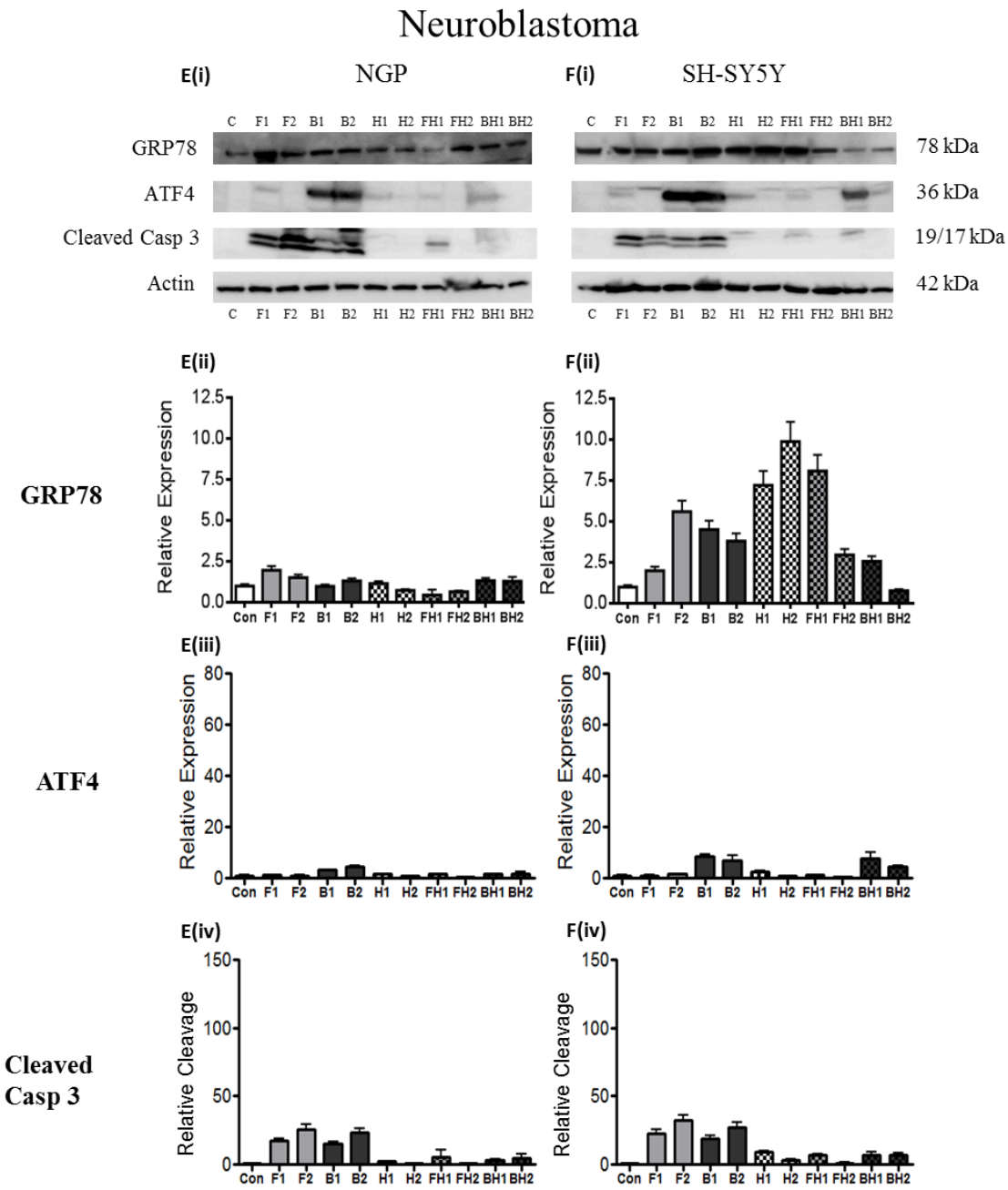
Neuroblastoma
E(i)
NGP
F(i)
SH-SY5Y
C F1 F2 B1 B2 H1 H2 FH1 FH2 BH1 BH2
GRP78
ATF4
Cleaved Casp 3
Actin
78 kDa
36 kDa
19/17 kDa
42 kDa
GRP78
ATF4
Cleaved Casp 3
E(ii)
F(ii)
E(iii)
F(iii)
E(iv)
F(iv)
Relative Expression
Relative Cleavage
Con F1 F2 B1 B2 H1 H2 FH1 FH2 BH1 BH2

Figure 6.13: *The effect of honokiol treatment on fenretinide or bortezomib induced ER stress and induction of apoptosis. Melanoma (A & B), glioblastoma (C & D) and neuroblastoma (E & F) cells were treated with fenretinide (light grey bars, For melanoma and glioblastoma, F1 = 5 µM and F2 = 10 µM or neuroblastoma F1 = 2.5 µM and F2 = 5 µM), bortezomib (Dark grey bars, For melanoma and glioblastoma, B1 = 100 nM and B2 = 200 nM or neuroblastoma B1 = 10 nM and B2 = 20 nM) and honokiol (HNK, Dotted bars, H1 = 50 µM and H2 = 100 µM) alone or in combination for 24 h. Western blot analysis (i) were performed for GRP78 expression, induction of UPR inducible ATF4 and cleavage of caspase 3, using β-Actin as a loading control. Densitometry analysis were performed on GRP78 (ii), ATF4 (iii) and cleaved caspase 3 (iv) and data expressed as mean values, relative to β-Actin as a loading control, of 3 independent experiments ± 95%. Graphs are scaled across cancer types, differing depending on the protein of interest to allow for a visual comparison for the effect of drug combinations.*

N.B. The western blot analysis for the effect of honokiol alone and in combination with ER stress-inducing agents in melanoma cells was carried out in collaboration with Miss Caroline Brady. These blots were loaded in a different order, thus have been cropped to preserve the order for comparison with the other cancer types.

		Combination				
Cell Line	**Protein**	**FH1**	**FH2**		**BH1**	**BH2**
CHL-1	**GRP78**					
WM266-4						
MO59J						
U251						
NGP						
SH-SY5Y						
CHL-1	**ATF4**					
WM266-4						
MO59J						
U251						
NGP						
SH-SY5Y						
CHL-1	**Cleaved Caspase 3**					
WM266-4						
MO59J						
U251						
NGP						
SH-SY5Y						

Table 6.6: *The effect of honokiol on fenretinide or bortezomib induced ER stress and apoptosis of cancer cells. A Summary table for the effect of drug combination in comparison to ER stress-inducing agent (fenretinide = F, Bortezomib = B) or honokiol (H) treatment control. Data are the average of the response of 3 individual experiments and demonstrate an increase (green), decrease (red) or no significant difference (grey) in protein expression.*

SH-SY5Y (GRP78 and ATF4) treated with FH1 ($P > 0.05$) or U251 cells treated with FH2 which demonstrated an increase in GRP78 expression ($P < 0.0001$).

6.2.4: Inhibition of GRP78 increases sensitivity to ER stress-induced melanoma cell death.

To test the hypothesis that the combination of GRP78 inhibitor with ER stress-inducing agent results in cells that undergo cell death at an earlier time point, CHL-1 and WM266-4 melanoma cells were treated with honokiol with either fenretinide or bortezomib, alone or in combination and cells assessed for the induction of cell death (Figure 6.14) and then investigated for the effect of drug combinations at 6, 12 and 24 h by western blot analysis for GRP78 expression, ATF4 induction and caspase 3 cleavage (Figure 6.15). Honokiol, rather than EGCG was used in these experiments as honokiol has been shown to bind to GRP78 stronger and also showed induction of ER stress. CHL-1 and WM266-4 cell death analysis demonstrated that cell death was significantly increased in either of the fenretinide (Figure 6.14 A & C) or bortezomib (Figure 6.14 B & D) combination samples at 6 and 12 h (One-way ANOVA with Bonferroni post hoc corrections, $P < 0.0001$ between combination and related ER stress-inducing agent alone), and as well as the expected 24 h time point ($P < 0.0001$).

Western blot analysis showed that there were significant differences in protein expressions between 6 and 12 h in CHL-1 and WM266-4 metastatic melanoma cells (Figure 6.15). Data demonstrated that in comparison to agents alone, drug combinations significantly increased GRP78 expression by 6 h (Figure 6.15 A & B ii, One-way ANOVA with Bonferroni post hoc corrections, CHL-1 with either fenretinide or bortezomib combined with honokiol or WM266-4 cells with fenretinide and honokiol $P < 0.0001$), however by 12 h demonstrated significantly lower expression than agents alone (CHL-1 and WM266-4 with fenretinide combined with honokiol $P < 0.0001$ or with bortezomib and honokiol $P < 0.01$ or 0.05, respectively). Investigating the effect of drug combination on ATF4 induction (Figure 6.15 A & B iii) highlighted that only CHL-1 treated with the bortezomib combination demonstrated significantly higher expression (One-way ANOVA with Bonferroni post hoc corrections, $P < 0.0001$), with WM266-4 cells treated with fenretinide combination showing significantly less ATF4 induction ($P < 0.0001$). By the 12 h time point CHL-1 cells with bortezomib

combination showed lower levels of ATF4 induction than agents alone (One-way ANOVA with Bonferroni post hoc corrections, $P < 0.001$), however WM266-4 cells treated with bortezomib combination showed significantly higher expression ($P < 0.0001$). Investigating the induction of caspase 3 cleavage at 6 and 12 h (Figure 6.15 A & B iv) demonstrated a significant increase in both CHL-1 and WM266-4 cells with either fenretinide or bortezomib combined with honokiol, in comparison to single agent (One-way ANOVA with Bonferroni post hoc corrections, CHL-1 cells at 6 h with bortezomib combination $P < 0.0001$, 12 h with either fenretinide or bortezomib combined with honokiol $P < 0.0001$ or 0.05 respectively. WM266-4 cells at 6 h with either combination or 12 h with bortezomib $P < 0.0001$ or 12 h with fenretinide $P < 0.01$).

CHL-1 and WM266-4 cells treated for 6 h with fenretinide or bortezomib alone or in combination with honokiol were imaged by light microscopy (Figure 6.16) to give a visual indication of the effect of drug combination on a population of melanoma cells. Images demonstrate that in samples treated with the combined action, fewer cells were left attached.

Time-course experiments suggest that in the drug combination treated cells there was a significant increase in death earlier than agents alone. This resulted in the loss of a cohort of cells from the overall population that were sensitive to death by ER stress-induced death prior to the conventional 24 h time point.

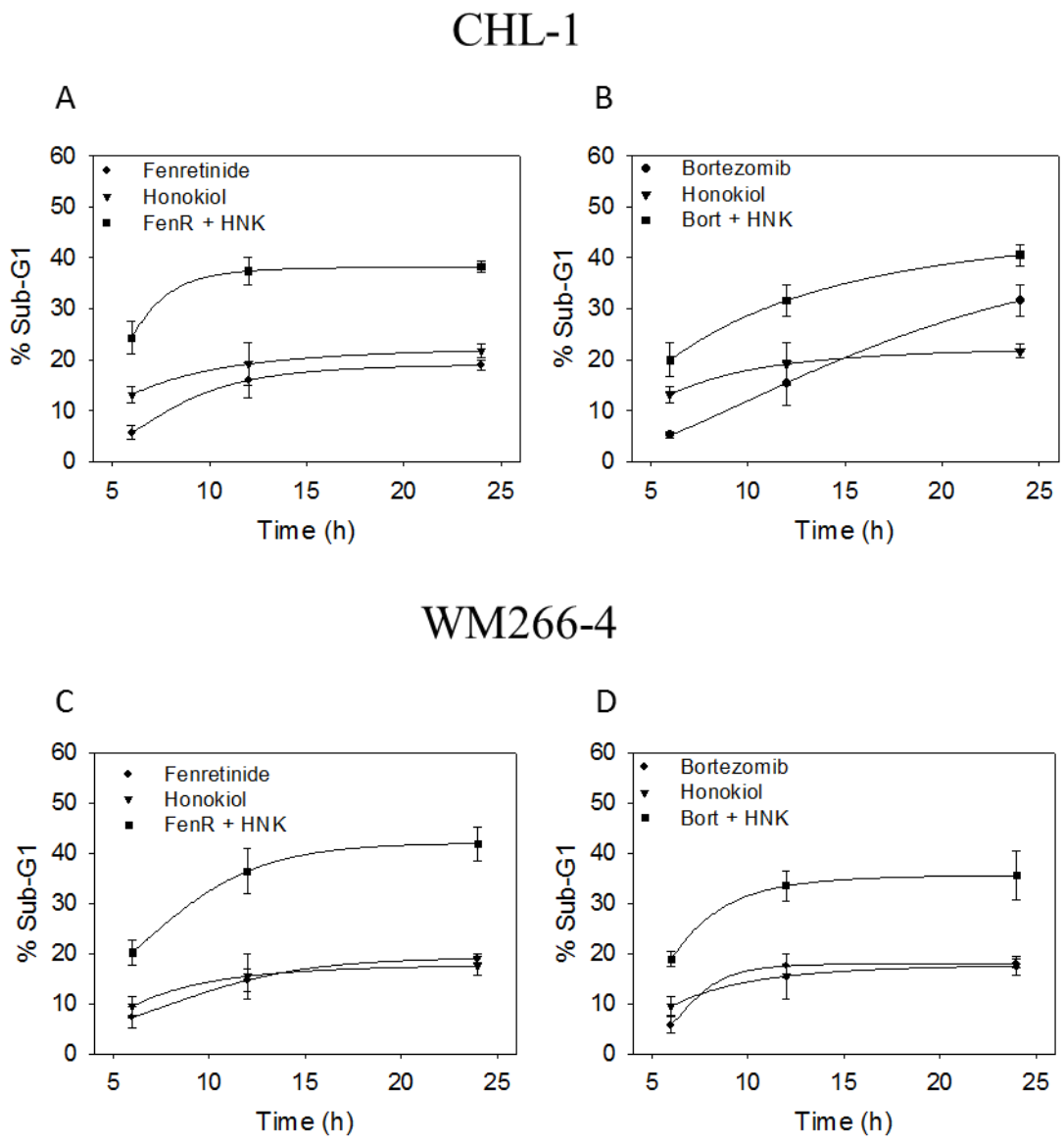

Figure 6.14: *Time-course analysis for the effect of honokiol treatment on ER stress-induced cell death. CHL-1 (A & B) and WM266-4 (C & D) melanoma cells were treated with fenretinide (10 µM, A & C), bortezomib (200 nM, Bort, B & D) or honokiol (50 µM HNK) for 6, 12 or 24 h, alone or in combination (hashed bars) prior to analysis of cell death by flow cytometry of propidium iodide stained cells. Data are the mean of the percentage SubG1 peaks of 3 independent experiments ± 95% CI.*

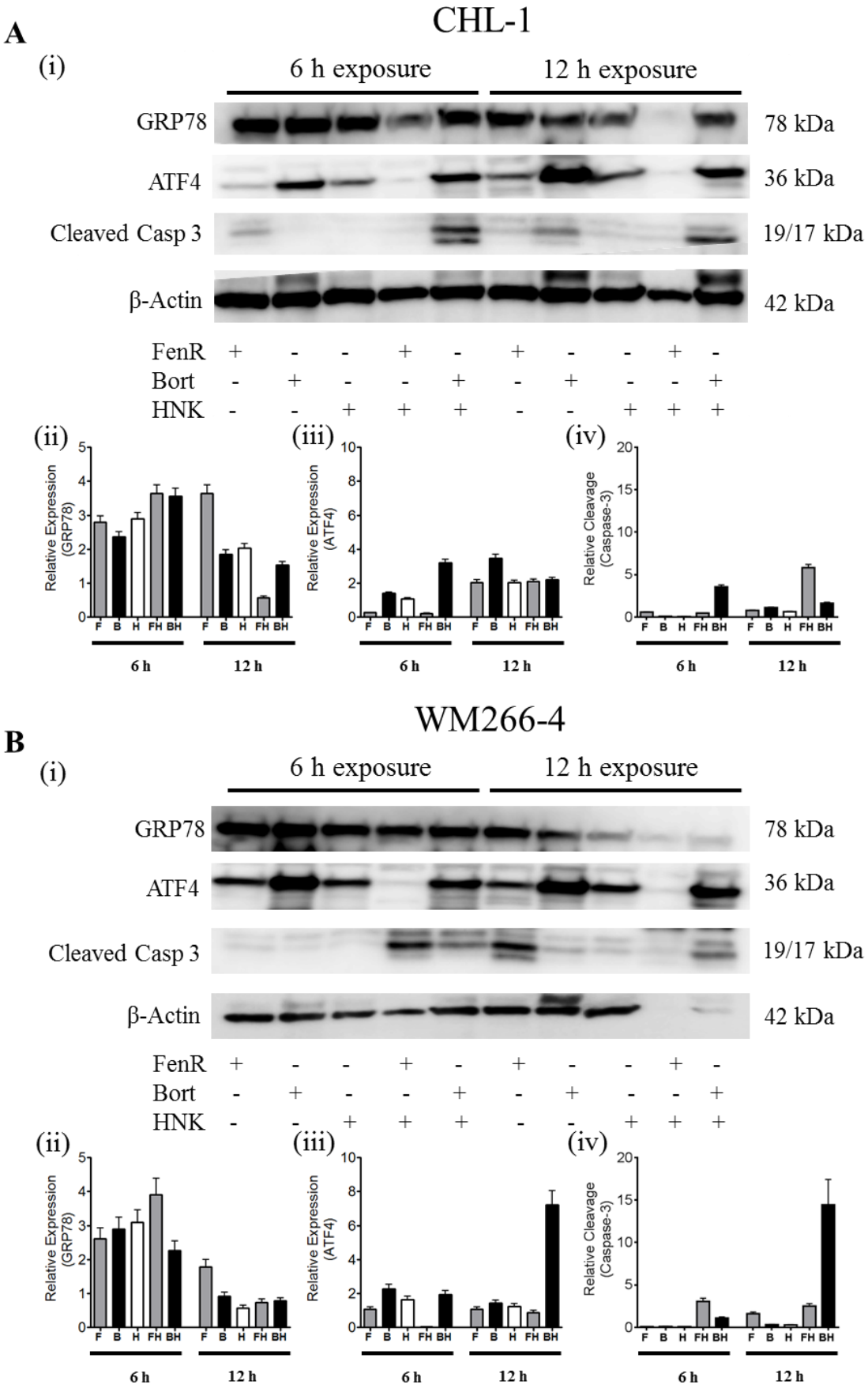
A
CHL-1
(i)
6 h exposure
12 h exposure
GRP78
78 kDa
ATF4
36 kDa
Cleaved Casp 3
19/17 kDa
β-Actin
42 kDa
FenR + - - + - + - - + -
Bort - + - - + - + - - +
HNK - - + + + - - + + +
(ii)
Relative Expression (GRP78)
(iii)
Relative Expression (ATF4)
(iv)
Relative Cleavage (Caspase-3)
F B H FH BH F B H FH BH
6 h
12 h
B
WM266-4
(i)
6 h exposure
12 h exposure
GRP78
78 kDa
ATF4
36 kDa
Cleaved Casp 3
19/17 kDa
β-Actin
42 kDa
FenR + - - + - + - - + -
Bort - + - - + - + - - +
HNK - - + + + - - + + +
(ii)
Relative Expression (GRP78)
(iii)
Relative Expression (ATF4)
(iv)
Relative Cleavage (Caspase-3)
F B H FH BH F B H FH BH
6 h
12 h

Figure 6.15: *Time-course for the effect of GRP78 inhibition by honokiol treatment on ER stress and apoptosis. CHL-1 (A) and WM266-4 (B) melanoma cells were treated with fenretinide (FenR, 10 µM), bortezomib (Bort, 200 nM) or honokiol (HNK, 50 µM) for 6 and 12h. Samples were analysed by western blot for GRP78 and downstream UPR inducible factor ATF4 as a marker of ER stress, as well as the formation of cleaved caspase 3 products to allow investigate differences in pro-apoptotic stimuli between samples treated alone or in combination and between time points. β-Actin was used as a loading control. Densitometry analyses were performed for the effect of fenretinide (grey), Bort (black) or honokiol (white) alone or in combination, on 3 independent experiments for GRP78(ii) , ATF4(iii) and cleaved caspase 3 (iv) expression. Data were expressed relative to loading control ± 95% CI.*

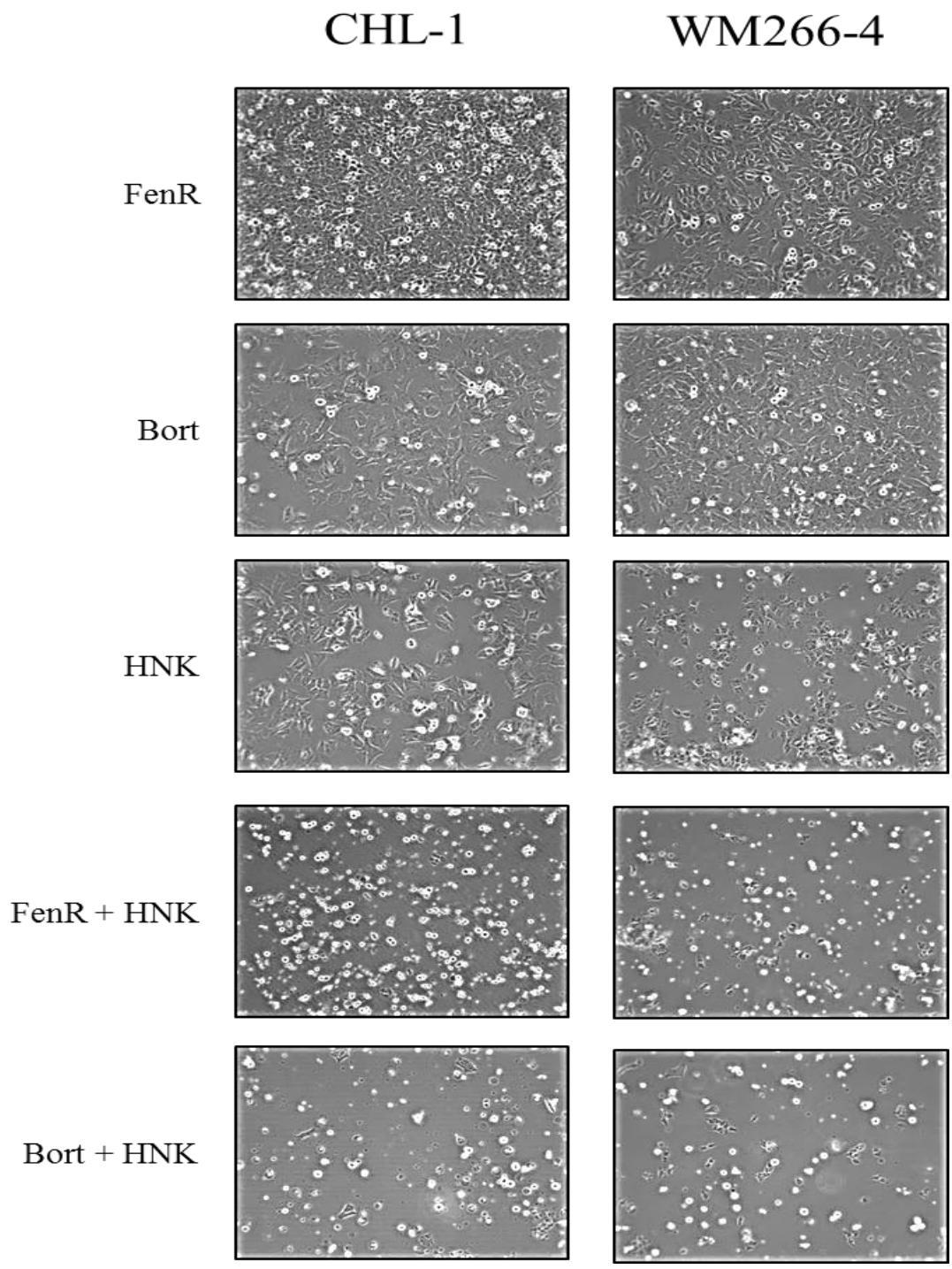

Figure 6.16: *Photo-micrographs for the effect of honokiol treatment on melanoma cell sensitivity to fenretinide or bortezomib induced ER stress and apoptosis over time. CHL-1 and WM266-4 melanoma cells were treated with fenretinide (FenR, 10 µM), bortezomib (Bort, 200 nM) or honokiol (HNK, 50 µM) for 6 h, alone or in combination prior to light microscopy imaging. Images above are representative of 3 individual experiments.*

6.2.5: Comparison of cell death across neural-crest-derived cancer types.

Dose-response data for ER stress-inducing agents fenretinide and bortezomib, as well as GRP78 inhibitors $SubAB_5$, EGCG and honokiol were analysed for the Ec_{50} and maximum achievable level of cell death (upper asymptote, Figure 6.17). The Ec_{50} of all agents (Figure 6.17 A) were ranked in order of potency for all cell lines (Figure 6.17 B). Mean ranks of each cell line (of all agents) were calculated to assess a cell lines overall susceptibility. Data demonstrated that resistance to death was cancer type specific (mean rank, Figure 6.17 B), with melanoma being the most resistant to death, more than glioblastoma and finally neuroblastoma. Data obtained for the ability of cancer types to induce ATF4 during periods of ER stress demonstrated that the magnitude of response was cancer type specific (Chapter 3, Figure 3.7 & 3.8). These data suggest that cells which are capable of inducing high levels of ATF4 (melanoma) require more drug to elicit a response. Comparing these observations to data for the upper asymptotes did not correlate together, with the maximum achievable level of death being dependent on cell line (Figure 6.17 D). Comparing upper asymptotes showed that $SubAB_5$ induced cell death significantly less than all other agents (One-way ANOVA with Tukey post hoc corrections, $P \leq 0.05$, for all agents) and fenretinide induced the highest levels of cell death, consistently across all cell lines ($P \leq 0.05$).

Box plot analysis to compare the effect of drug showed that EGCG and honokiol varied largely across cancer types (Figure 6.17 E), in comparison to bortezomib and $SubAB_5$, and although EGCG and honokiol showed large variation in Ec_{50} they induced death to a similar level in all cell lines (demonstrated by low variation in asymptote, Figure 6.17 F). Interestingly, honokiol had higher achievable levels of death than EGCG (Figure 6.17 F, One-way ANOVA with Tukey post hoc corrections, $P < 0.05$) and has been shown to bind to GRP78 stronger than EGCG (Hawkins unpublished data).

A

Cell line	Ec50				
	FenR	Bort	Tox	EGCG	HNK
CHL-1	38.48	0.12	0.68	10.30	49.10
WM266-4	9.08	0.21	0.11	51.20	51.00
MO59J	13.07	0.22	0.04	4.60	56.20
U251	12.23	2.44	0.08	9.00	37.30
NGP	3.05	0.02	0.05	5.70	15.30
SH-SY5Y	5.24	0.01	0.11	18.60	14.60
median	10.65	0.17	0.09	9.65	43.20
mean	13.53	0.50	0.18	16.57	37.25

B

Cell line	Ec50						
	FenR	Bort	Tox	EGCG	HNK	mean rank	SD rank
CHL-1	6	3	6	4	4	4.6	1.3
WM266-4	3	4	4	6	5	4.4	1.1
MO59J	5	5	1	1	6	3.6	2.4
U251	4	6	3	3	3	3.8	1.3
NGP	1	2	2	2	2	1.8	0.4
SH-SY5Y	2	1	5	5	1	2.8	2.0

C

Cell line	Upper Asymptote				
	FenR	Bort	Tox	EGCG	HNK
CHL-1	90.35	30.37	15.30	24.20	61.30
WM266-4	36.30	31.61	10.90	36.40	51.80
MO59J	81.03	46.94	17.60	21.10	53.10
U251	78.48	100.00	12.50	21.00	40.30
NGP	32.53	34.53	11.40	29.80	49.50
SH-SY5Y	52.82	44.09	20.70	23.40	51.10
median	65.65	39.31	13.90	23.80	51.45
mean	61.92	47.92	14.73	25.98	51.18

D

Cell line	Upper Asymptote						
	FenR	Bort	Tox	EGCG	HNK	mean rank	SD rank
CHL-1	6	1	4	4	6	4.2	2.0
WM266-4	2	2	1	6	4	3	2.0
MO59J	5	5	5	2	5	4.4	1.3
U251	4	6	3	1	1	3	2.1
NGP	1	3	2	5	2	2.6	1.5
SH-SY5Y	3	4	6	3	3	3.8	1.3

E

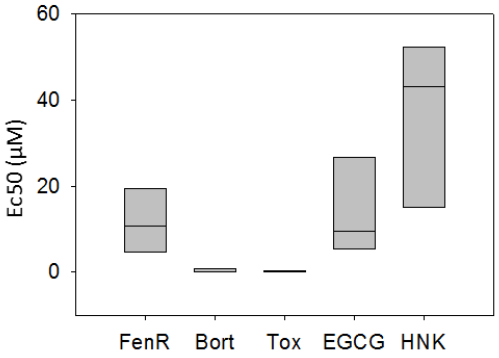

F

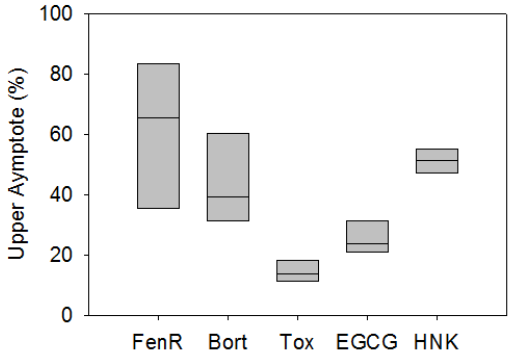

Figure 6.17: *Comparing ER stress-inducing agents and inhibitors of GRP78 for the induction of cell death. The* Ec_{50} *(µM) of fenretinide (FenR), bortezomib (Bort),* $SubAB_5$ *(Tox), epigallocatechin gallate (EGCG) and honokiol (HNK) were compared across cell lines (A) and ranked in order of potency (B) to compared cell line sensitivity (E). Data for the maximum achieved level of cell death (%, upper asymptote) were also calculated (C & F) and ranked in order of drug effect (D).*

6.2.6: Results summary.

- Treatment of neural-crest-derived cell lines with $SubAB_5$, EGCG or honokiol resulted in a dose-dependent increase in cell death or inhibition of cell viability.
- Exposure of neural-crest-derived cancer cells to $SubAB_5$ resulted in a significant reduction in GRP78 expression.
- Over the time scale used, cleavage of GRP78 was not complete, even at high $SubAB_5$ concentrations; nevertheless, cleavage occurred rapidly and the level of cleavage increased over 24 h.
- Combination of $SubAB_5$ with either fenretinide or bortezomib in melanoma and glioblastoma significantly enhanced cell death and inhibited cell viability, in comparison to agents alone.
- EGCG enhanced fenretinide-induced melanoma and glioblastoma cell death. However, EGCG showed an inhibitory effect when combined with bortezomib.
- Honokiol enhanced ER-stress induced cell death of melanoma and glioblastoma cells.
- Combining an ER stress-inducing agent with $SubAB_5$, EGCG or honokiol in neuroblastoma cells resulted in an inhibition in cell death, compared to agents alone
- The combination of honokiol with either fenretinide or bortezomib resulted in the induction of cell death at significantly earlier time points to that of agents alone.
- Comparing Ec_{50} values suggest that sensitivity to death correlates with capacity to induce ATF4.

6.3: Discussion.

Testing the hypothesis that inhibition of GRP78 combined with an ER stress-inducing agent would enhance cell death of melanoma and glioblastoma and neuroblastoma cancer cells, showed that $SubAB_5$ (toxin), honokiol with either ER stress-inducing agent, and EGCG with fenretinide (for melanoma) significantly induced cell death and inhibition of cell viability. In combination with ER stress-inducing agents, data showed a synergistic potentiation of both cell death and inhibition of cell viability in melanoma cells, synergistic to additive outcome for glioblastoma and inhibitory interactions in neuroblastoma. Analysis by western blotting for the effect of GRP78 inhibition on the ability of ER stress-inducing agents to induce the expression of UPR elements GRP78 and ATF4 or the apoptotic marker, cleaved caspase 3, demonstrated that the combination of GRP78 inhibitor with ER stress-inducing agents resulted in a variable response of the UPR and resulted in cells undergoing death at earlier time points than agents alone.

Treating melanoma or glioblastoma cells with $SubAB_5$ synergistically enhanced ER stress-induced cell death or inhibition of cell death of fenretinide or bortezomib [266]. Treatment with $SubAB_5$ cleaves GRP78 and therefore inhibits GRP78 functioning in a non-competitive and irreversible manner [198, 200]. Quantification of cellular concentrations of GRP78 and the UPR activators demonstrated that in these cancer types, GRP78 existed in excess and therefore reduction in expression by cleavage or by siRNA mediated techniques, shifted the dynamic equilibrium and stimulated UPR induced death. Conversely, neuroblastoma cells demonstrated that when GRP78 expression was reduced, cells became more resistant to ER stress. These data confirm the data gathered using siRNA mediated techniques (Figure 4.8 – 4.10) and highlight the importance of understanding the dynamic equilibrium of the UPR as a marker of cellular outcome to GRP78 inhibition. Treatment of all cell lines with $SubAB_5$ resulted in an increase in GRP78 cleaved product and demonstrated induction of cell death in all cancer types compared to mutant toxin ($SubA_{A272}B$). In melanoma and glioblastoma the mutant toxin, at high doses, showed the induction of inhibition of cell viability. This may be due to low-level activity of $SubA_{A272}B$.

The liver and kidney toxicity induced by $SubAB_5$ in mice models [321], and the gastrointestinal disease and haemolytic ureamic syndrome associated with shiga

bacteria [322] may mean that $SubAB_5$ is only useful as a laboratory tool. However, Backer *et al.,* fused SubA to epidermal growth factor (EGF) and demonstrated that EGF-SubA could cleave GRP78 and was synergistic in combination with drugs which up-regulate GRP78 [319]. The EGF receptor (EGFR) is often over-expressed in tumour cells and EGF-$SubAB_5$ has a significantly greater effect in cells over-expressing EGFR [319].

Investigating the effect of natural compounds; EGCG and honokiol, both known to interact with GRP78 [318, 324, 325] demonstrated, with regard to EGCG, that outcome was not only cancer-type specific but dependent on the ER stress-inducing agent it was combined with. Melanoma and glioblastoma cells demonstrated mild synergy when combined with fenretinide, but not bortezomib. Although EGCG has been shown to interact directly with the ATPase domain of GRP78, it can also bind to and inhibit the 26S proteasome [325]. Previous research has demonstrated that combining fenretinide and bortezomib, resulted in a synergistic increase in melanoma cell death; coupled with data demonstrating an inhibitory effect of EGCG on bortezomib induced cell death, these results may suggest that the response seen with EGCG is a consequence of 26S interaction as well as GRP78 inhibition. EGCG may impede bortezomib interaction with the 26S, yet elicit lower inhibition than bortezomib. This was confirmed by western blot analysis for the effect of EGCG treatment on ER stress, which demonstrated no significant induction of ATF4, suggesting that EGCG alone may not activate the UPR.

Honokiol combined with either fenretinide or bortezomib in melanoma and glioblastoma resulted in synergy. Melanoma cells showing greater levels of synergy than that of glioblastoma. Dose-response data demonstrated the induction of the UPR, demonstrating a direct consequence of honokiol treatment on ER stress, suggesting a biologically-significant effect on GRP78. Also, dose-response data for the induction of cell death demonstrated that a significantly-higher concentration of honokiol was required to induce death, in comparison to EGCG. Alastair Hawkins and Heather Lamb demonstrated that honokiol interacts with GRP78 stronger than EGCG, suggesting that honokiol may be a more specific inhibitor of GRP78; however this study shows that honokiol is required at a higher dose to induce cell death than that of EGCG. The data from this study, demonstrating the ability of honokiol to elicit an ER stress response and enhance ER stress-induced death, coupled with the data from Jack Arbiser and Alastair

Hawkins demonstrating a direct interaction between GRP78 and honokiol, suggests that honokiol is an inhibitor of GRP78.

Data comparing the effect of honokiol dose on induction of cell death to the effect on ER stress (GRP78 and ATF4) and apoptosis (caspase 3 cleavage) induction showed that for neuroblastoma, the relative expression of cleaved caspase 3 was higher than that of ATF4. This was the opposite relationship to that observed in melanoma and glioblastoma (Figure 6.11 G). Although all cancer types showed an induction in cell death to honokiol as a single agent, the ability of honokiol to enhance fenretinide and bortezomib induced death was different across cancer types, in the same observed trend. Earlier research demonstrated that neuroblastoma cells treated with either fenretinide or bortezomib induced significantly lower levels of ATF4, than other cancer types (Results chapter, Figure 3.7 & 3.8). These observations suggest that the differences in activity of the PERK cascade of the UPR may be important for cancer outcome during combinational treatment. It is possible that the capacity of neuroblastoma cells to induce ATF4 may reach the maximum during single agent treatment and therefore during combined drug treatment, where both agents require ATF4 signalling for a response, no enhancement of death could be achieved. To evaluate the differences between cancer types for caspase 3 cleavage and ATF4 induction, a tetracyclin repressor system could be optimised for ATF4. This would allow for the importance of ATF4 expression to be confirmed in UPR induced cell death for single and combined treatments. This system would allow for ATF4 expression to be increased in neuroblastoma to confirm if this would enhance sensitivity to combinational treatments.

Western blot analysis for the effect of GRP78 inhibition on fenretinide or bortezomib induced ER stress or activation of apoptosis (Figures: 6.6, 6.9 & 6.13) demonstrated no consistent increase in ER stress or activation of caspase 3 cleavage compared to agents alone; in the majority of cases a decrease in expression in comparison to the accumulative effect of agents alone was observed. Although these data do not marry directly with the cell death and viability data, research into the effect of drug combination over earlier time points demonstrated that in samples exposed to combination of honokiol and ER stress-inducing agents, significantly higher expression of cleaved caspase 3 was present within cells, suggesting that data for the effect of combination for 24 h may have missed the effect of the combination due to the time point analysed and demonstrated inconsistent data due to the later stage of stress that the cells were undergoing.

Data also highlighted that samples treated with honokiol and ER stress-inducing agents underwent significantly more cell death than agents alone at 6 and 12 h, as well as the 24 h time point. If cells were undergoing cell death at earlier time points, analysis of protein expression at 24 h may have resulted in the assessment of expression of a sub-population of cells that were not sufficiently primed to death stimuli and therefore to understand the real effect of honokiol on fenretinide or bortezomib induced stress, analysis at 6 h or earlier may be required. Targeting GRP78 to enhance cellular sensitivity to ER stress-induced cell death is dependent on the relationship that exists within the UPR, with regards to GRP78 and the UPR activator expression. GRP78 expression has been shown to be up-regulated in a number of solid tumours and therefore overcoming this by specific targeted therapy may result in cancer cells more susceptible to chemotherapy as a direct consequence of UPR signalling or due to cells no longer being so efficient at buffering external stressors such as glucose or oxygen deprivation. Targeting cancer cells with an inhibitor of GRP78 may prime cancer cells to death stimuli by shifting the dynamic equilibrium in favour of a more active UPR. The use of the $SubAB_5$ as a possible therapeutic inhibitor is prevented by its high toxicity to the liver and kidneys; however research conjugating the toxin to EGF has shown a reduction in toxicity as well as an increase in cellular up-take in cancer cells over-expressing the EGFR [319].

Further research into the use of honokiol is required to determine maximum achievable doses, as well as to investigate the effect in vivo to establish if this natural inhibitor could be used clinically to enhance cell death of melanoma or glioblastoma, which to date have no reliable therapy.

6.4: Conclusion

In summary, this study showed that inhibiting GRP78, affected cancer cells in the same way predicted by alteration in levels of expression. Honokiol, a novel candidate that has been shown to interact with GRP78 possesses greater potential to enhance ER stress-induced death, than that of EGCG of $SubAB_5$, even though $SubAB_5$ synergistically enhanced ER stress -induced death of melanoma. The effect of the combined treatments resulted in variable outcomes for markers of ER stress and apoptosis and this maybe a consequence of time, as data for the effect of honokiol combined with ER stress-inducing agents fenretinide or bortezomib over time showed increased death and stress at earlier time points for combinations, compared to signal agent treatment.

Chapter 7:

Final Discussion and Future Prospects.

7.1: Dynamic model of the UPR.

Studies of the relationship between GRP78 expression and prognosis of cancer patients have highlighted a difference in patient prognosis between melanoma and glioblastoma to that of neuroblastoma [113, 115, 116]. Increased GRP78 expression in melanoma and glioblastoma has demonstrated a direct correlation with disease state, chemo-resistance and metastasis [113, 256, 326]. However, a study in neuroblastoma has shown the opposite, with a better prognosis in patients presenting with an increased expression of GRP78 [116].

To determine the differential effects of GRP78 on neural-crest-derived tumour survival, the aim of the present study was to investigate potential differences in UPR component expression and function. This study set out to compare the role of GRP78 in a panel of neural-crest-derived cancer cell lines, incorporating melanoma, glioblastoma and neuroblastoma. Cellular concentrations of GRP78, as well as the effect of GRP78 modulation in response to ER stress were determined in all cancer types and the effect of GRP78 modulation had on the UPR activators; PERK, IRE1 and ATF6, as well as the magnitude of response of each arm of the UPR to stress. As such these studies allowed for a direct comparison of the UPR capacity between cancer types and the differences in signalling that may account for the opposing clinical outcomes observed between melanoma, glioblastoma and neuroblastoma patients with respect to GRP78 expression levels.

Current understanding suggests that GRP78 exists within a dynamic equilibrium with the UPR activators, inhibiting their function during periods where there is no ER stress (as described in Figure 4.2). This ensures that a homeostatic response to insults in the ERs ability to function is primed, ready to buffer ER stress efficiently and immediately, when required. GRP78 has a higher affinity to the exposed charged regions of unfolded or misfolded proteins than to the UPR activators and therefore during ER stress, binds to these substrates, releasing the UPR activators and initiating a response. The present study revealed differences in the activity of the UPR and expression levels of UPR components, which as a consequence may alter the dynamic equilibrium between GRP78 and the UPR activators during ER stress, resulting in a sensitization of neuroblastoma to ER stress.

7.1.1: GRP78 expression.

Although research from this study confirmed the sensitivity of all three neural-crest-derived cancer types to ER stress [82, 112, 204, 327]. To gain a more detailed understanding of the signalling of the UPR that may result in differences in disease outcome, depending on GRP78 expression, melanoma, glioblastoma and neuroblastoma cell lines were analysed for their expression of GRP78 (Chapter 3).

Comparing cellular concentrations of GRP78 demonstrated no significant differences in expression between cell lines of the same cancer type. However, overall, GRP78 expression was significantly increased in melanoma compared to glioblastoma or neuroblastoma, with glioblastoma demonstrating higher expression levels than neuroblastoma.

This cancer type-specific expression of GRP78 may reflect a cell type requirement of GRP78. Melanoma cells may require a more active ER or greater abundance in ER machinery, as they may require a higher protein synthesis output, due to the production of melanin [328] and therefore as a direct consequence of ER function have evolved a higher expression of GRP78 than other cell types. Also, due to being an important component of the skin, melanocytes may have higher chaperone concentrations to help buffer any damage as a result of UV-light-induced ROS accumulation on ER integrity [329, 330]. Increased ROS load has been implicated in several pathological states including photo-aging and photo-carcinogenesis of the skin. Large efforts have been made to better define the involvement of ROS in photo-carcinogenesis and photo-aging. Both pathological processes share common features; however, they reveal unique molecular characteristics which finally determine the fate of the cell and its host [330]. As well as causing permanent genetic changes involving proto-oncogenes and tumour suppressor genes, ROS activate cytoplasmic signal transduction pathways that are related to growth differentiation, senescence, transformation and tissue degradation [330]. Therefore, the constant stimulation by UV light could result in chaperone induction or resulted in a cell type that has evolved to express chaperones at a higher basal concentration. To gain a better understanding of the role of chaperones across cancer types, a screen of a number of the more common chaperones, such as GRP78, GRP94, HSP70 calnexin and calreticulin would be useful. This would allow for a

comparison of cellular expressions levels of key chaperones to one another and across cancer types and identify any underlying correlations.

Data comparing the cellular concentration of GRP78 in human metastatic melanoma cells, to that of primary melanocytes confirmed a significant increase in GRP78 expression with disease (chapter 3, Figure 3.2 C). These data highlighted that melanocytes have a similar GRP78 concentration to that of glioblastoma cells, implying that melanocytes may contain higher expression of GRP78 to other cell types, glioblastoma have higher levels of GRP78 expression compared to surrounding non-cancerous tissue [113, 326]. These findings also support the previous immunohistochemical data for the correlation of GRP78 with melanoma disease stage [115], where a significant difference in GRP78 expression was observed between normal melanocytes and that of late stage metastatic disease. Glial cells are the main support for neurons, not only to hold the neurons in place and provide the insulating myelin sheath [331], but also to provide metabolites, replenishment of oxygen and energy to the neurons, ensuring that the neurones are capable of functioning [332]. Due to the importance of glial cells, up-regulation of key cellular proteins and pathways may have occurred to gain a selective advantage, increasing the probability of survival during stress or damage to the brain.

When comparing melanoma, glioblastoma and neuroblastoma cancer types, it must be taken into consideration that although all three are dendritic cell types and derived from the neural-crest, only neuroblastoma is formed as a direct result of deregulation of development, while melanoma and glioblastoma arising post cellular development as a consequence of genetic and/or environmental abnormalities in already-differentiated cells. Therefore, the significantly lower expression in neuroblastoma may be a consequence of the origin of this cancer type [333]. This lower expression in neuroblastoma may be due to cell immaturity, and therefore the lack of regular exposure to changes in environmental conditions. However, to date little is known about the molecular biology behind glioma development and it is possible that it arises from a precursor cell, formed during neural-crest development which lays dormant until stimulated, and furthermore it is this precursor cell that shows a difference in GRP78 expression.

Research into the expression of chaperones, such as GRP78, has demonstrated that expression levels of individual chaperones can fluctuate between cell types, but overall,

cell lines with similar ER capacity and rate of protein synthesis have similar overall expression of chaperones. For example neuroblastoma cells have been shown to over-express GRP94 [230, 334]. This may suggest that in neuroblastoma, other signalling cascades maybe more prevalent and that although increased expression of GRP78 protein has been shown to be prognostically favourable, this in part may be due to the down regulation of another, more vital chaperone or component of the ER, that ultimately leads to the loss of capacity to buffer stress and therefore an enhanced UPR response (including the increase in GRP78 expression observed) [116] and thus the increase in GRP78 is a consequence of stress-induced death, rather than a factor that triggers the induction of death stimuli.

7.1.2: Stoichiometry of the UPR.

Due to the cell-type-specific expression of GRP78, this factor may ultimately influence the signalling ability of the UPR, which could result in differences in response outcome when GRP78 expression was up-regulated. Therefore experiments included in the present study focused on quantifying the expression of the UPR activators to achieve a clearer interpretation of the dynamic equilibrium of the UPR.

Investigation into the expression of GRP78 compared to that of the UPR activators (total UPR activator concentration) highlighted significant differences between the relationship of GRP78 to UPR activator in melanoma and glioblastoma, to that of neuroblastoma. For melanoma 1: 0.65, Glioblastoma 1: 0.7 and neuroblastoma 1: 1.5, for GRP78: UPR activator total (averaged between cell lines of the same cancer type). The assumption inherent within this thesis is that GRP78 is in a dynamic equilibrium with the UPR activators such that in the absence of unfolded protein substrates the pool of free UPR activators is low. An excess of GRP78 would allow unfolded proteins substrates to bind to GRP78 without substantially increasing the pool of free UPR activators. This would be the proposal situation for melanoma and glioblastoma. Conversely, neuroblastoma cells demonstrated an abundance of UPR activators. With regards to the dynamic equilibrium that exists between GRP78, UPR activators and substrate, in melanoma and glioblastoma the equilibrium is in favour of an inactive response, yet neuroblastoma demonstrates a dynamic equilibrium in favour of an active UPR.

Of the individual UPR activators, IRE1 was the most abundant in all cell lines tested. The expression levels of PERK and ATF6 were significantly lower than that of IRE1 and demonstrated no difference to each other. These findings highlight the importance of IRE1 within the UPR. IRE1 is the evolutionary conserved UPR activator that has been well documented to have both pro-death and pro–survival attributes [335, 336]. IRE1 is a bi-functional trans-membrane kinase or endoribonuclease that induces the non-conventional splicing of XBP-1 mRNA to produce the b-ZIP transcription activator, XBP-1s, which is capable of binding to ERSE and UPRE to activate the characteristic responses of the UPR [337]. In addition to the splicing of XBP1 mRNA, IRE1 kinase can also activate pro-survival responses, as well as the induction of pro-death stimuli, via the c-Jun N-terminal kinase (JNK) signalling pathway, through the Mitogen-Activated Protein Kinase Kinase Kinase (MAP3K) cascade and the activation of autophagy through TRAF2 signalling [338, 339].

Studies by Lee *et al.,* demonstrated that treatment of neuronal cells with the ER stress-inducing agents tunicamycin and thapsigargin (Tg), increased the aggregation of mutant huntingtin (mtHTT), as a result of IRE1 activation. The kinase activity, but not the endoribonuclease activity of IRE1 was necessary to stimulate mtHTT aggregation and increased death of neuronal cells, including SH-SY5Y cells [340]. Interestingly, ER stress impaired autophagy flux via the IRE1-TRAF2 pathway enhanced cellular accumulation of mtHTT [340]. These findings, coupled with the data from this study demonstrating the abundance of IRE1 in comparison to the other UPR activators, thus suggest that IRE1 is the key mediator of the UPR. It may also indicate that PERK or ATF6 activity enhances the response of IRE-1 [340], allowing for a more diverse array of responses, in both signal strength and outcome, that is more capable of buffering a variety of stresses encountered by a multi-cellular organism.

7.1.3: Mapping UPR activity during ER stress.

Assessment of the induction of the UPR, in response to ER stress-induced by either fenretinide or bortezomib demonstrated that all cancer types significantly induced all three cascades of the UPR, in response to either agent. These data highlighted a greater induction of ATF4 in melanoma than either glioblastoma or neuroblastoma, and that bortezomib is a more potent inducer of the UPR. When comparing the induction levels of ATF4 to the expression of PERK, melanoma and glioblastoma demonstrated a

correlation, with higher expression of PERK found in the melanoma cells, which were capable of inducing high levels of downstream ATF4. However, NGP and SH-SY5Y neuroblastoma cell lines demonstrated similar levels of ATF4 induction to each other, yet varied significantly in their expressions of PERK. Interestingly, although melanoma and glioblastoma had more GRP78 than UPR activators and therefore should demonstrate a decrease in likelihood of UPR activation in comparison to neuroblastoma, melanoma cells demonstrated a stronger induction of ATF4, indicative of a more active UPR.

Fenretinide and bortezomib induced both ATF6 cleavage and XBP-1 splicing in all cancer types, which eventually resulted in a recovery in expression, back to basal levels, as a down-stream consequence of UPR activation. An inbuilt replenishment in the signalling response exists in the UPR to ensure the system can recover [341]. However, in neuroblastoma cells, treated with either ER stress-inducing agent, a significant expression of XBP-1s was still detected at 24 h, whereas in melanoma and glioblastoma cells XBP-1 had returned to basal levels. These data support the hypothesis that differences in the dynamic equilibrium between GRP78 and the total sum of the UPR activators may affect the signalling outcome of the UPR. Data showed that neuroblastoma possessed a higher proportion of UPR activators to GRP78 molecules that could inhibit them. This would therefore allow for a low level turnover of the UPR, demonstrated in these samples as a persistent expression of XBP-1s. The detection of XBP-1s at 24 h, coupled with the observed dynamic equilibrium in neuroblastoma, suggests that these cells may react to a lower level of ER stress due to the inability of GRP78 to completely inactivate the UPR. This in part may be responsible for neuroblastoma cells being more sensitive to ER stress-inducing agents, in particular bortezomib.

Conversely, in neuroblastoma there was no observable induction of XBP-1s in the control samples, suggesting that the XBP-1s present at 24 h in samples treated with either ER stress-inducing agents was a direct consequence of stress-related UPR induction and not a consequence of the lack of GRP78 to negatively regulate the UPR activators. Therefore, the difference in activity time between neuroblastoma and the other neural-crest-derived cancers may be related to the level of stress achieved within the neuroblastoma cells, the ability of the cell to recover or remove unfolded or miss-folded proteins. For example the low level of ATF4 induction in neuroblastoma would result in a significantly lower induction of chaperones, folding machinery or amino acid

recovery via the PERK arm of the UPR, as well as a smaller effect on global protein synthesis. This lack of ATF4 induction would therefore suggest that neuroblastoma cells rely more on the IRE-1 arm of the UPR to recover from ER stress, more than either melanoma or glioblastoma, and as data for XBP-1 splicing demonstrated that neuroblastoma cells generate similar levels of XBP-1s during stress to that of melanoma and glioblastoma, thus it may take these cells significantly longer to recover.

Comparing the activation of IRE1 of human neural-crest cancer cells, to that of yeast, suggests that co-factors may be important in the activation of the UPR. The yeast form of IRE1 relies not only on release from GRP78 and homo-dimerization, but a direct interaction with unfolded proteins [242, 342]. Although research into the structure of IRE1 has indicated that the mammalian form lacks the relevant sequence for interaction with unfolded proteins [342], research has not yet focused on the hypothesis that processing of XBP-1 mRNA may require a cofactor, itself induced by ER stress. This would confirm the data generated for neuroblastoma, where no significant induction of XBP-1s could be observed at 0 h, but was present at 24 h.

Previous studies have implicated the time of activity of each arm of the UPR, as the crucial factor in the outcome of the UPR [225]. Studies highlight the IRE1 and ATF6 arms of the UPR, as a faster response mechanism to stress, yet demonstrated shorter activity times [225, 341]. The inactivation of UPR stimulation via the IRE1 and ATF6 arms, by GRP78, allowed induction of pro-apoptotic GADD153 via the PERK arm of the UPR to induce death, if stress still persisted. Taking into consideration studies demonstrating that IRE1 can also activate the transcription of Gadd153 mRNA via XBP-1s, along with the data obtained from this study that demonstrated differences in the level of UPR activation, depending on the level of stress, as well as stressor, it is possible to determine that time may contribute to the outcome of ER stress. However, time is not the only factor in determining the response outcome [305, 339].

Research by DuRose *et al.*,, into GRP78 dissociation, demonstrated that the kinetic behaviours for the activation of the UPR sensors could be governed by the affinity of GRP78 for unfolded proteins or the dissociation constants of GRP78 from PERK, IRE1 or ATF6 [273]. Observations suggested a more complicated scenario. Rapid dissociation of GRP78 from both IRE1 and PERK occurred during Tg-induced stress suggesting a high-affinity of GRP78 for unfolded proteins after Tg treatment, however the slower activation of ATF6 by Tg suggests the opposite [273]. Therefore, if the

affinity of GRP78 for UPR activators plays a major role, the kinetic order of IRE1, PERK, and ATF6 should be the same for any type of ER stress and all three UPR activators, however, this was not observed. Interestingly, ATF6 activation was found to be rapid in response to DTT, thus suggesting a stress specific response. DuRose *et al.,* also demonstrated, using immune-precipitation techniques, that the kinetics of GRP78 with either IRE1 or PERK supported the concept an additional control [273], as PERK auto-phosphorylation occuered within 15 min of DTT or Tg treatment, but GRP78 dissociation was only observed from 30 min. This suggests that PERK phosphorylation occurred under GRP78 interaction. Also DuRose *et al.,* showed GRP78-IRE1 re-association at time points when IRE1 was still active [273]. Thus, although GRP78 dissociation clearly occurs during UPR activation, the kinetic behaviour of all three UPR sensors suggests the presence of additional regulatory mechanisms. Therefore, it may be possible that an additional control mechanism exists allowing the UPR activators to be fine-tuned, both in the speed and extent of activation, depending on the type and magnitude of ER stress. Furthermore, Schindler *et al.,* showed that the addition of ATP and DTT synergistically induced the dissociation of ATF6 from GRP78. These findings therefore suggest that the requirement of a co-factor(s), such as PDI, maybe important for protein release [343].

To gain a better understanding of the UPR response to stress, surface plasmon resonance (SPR) analysis for the interaction of GRP78 with the UPR activators could thus be carried out to compare affinities. Also, to determine if neural-crest-derived cancer cells respond differently to stress, with regards to the activation of the UPR, time course studies using a larger array of ER stress-inducing agents could be carried out to determine if the UPR responds in a homogenous way, or differs depending on stress. Finally, this study has assessed the activation of the UPR from a top down approach, focusing on early markers of the UPR cascade. To determine if the presence of XBP-1s in neuroblastoma at 24 h and confirm that the UPR in melanoma or glioblastoma are inactive, investigating the activation of reporter elements (ERSE and UPRE) using a reporter assay approach could be carried out, determining the overall activation of the UPR as a control. This work would also allow for a comparison across cancer types for the ability of fenretinide or bortezomib to induce UPR related genes, allowing for a correlation of transcription factor induction with gene activation. Finally the kinase activity of IRE1 could be assessed to confirm the differences in activity over time between cancer types as well as to compare this component of the UPR.

7.2: The effect of altering GRP78 expression on the outcome of ER stress-induced neural-crest-derived cancer cell death.

To identify the importance of the dynamic equilibrium that exists between GRP78 and the UPR activators, the expression of GRP78 was altered and the effect this had on cell death, in response to ER stress-inducing agents, was observed.

7.2.1: The effect of siRNA mediated knockdown in GRP78 expression.

Using siRNA mediated techniques to reduce GRP78 protein expression transiently demonstrated that in melanoma and glioblastoma cell lines, an increase in sensitivity to ER stress-induced cell death occurred in comparison to control transfected cells. The reduction in GRP78 expression by over 50% in either melanoma or glioblastoma would be expected to shift the dynamic equilibrium of the UPR, decreasing the inhibitory effect that GRP78 has on PERK, IRE1 or ATF6, and priming the UPR to a higher level of activation under basal ER synthesis. Thus, on addition of ER stress-inducing agents, more cell death or inhibition of cell viability was observed. These findings suggests that although the UPR was, in principal, already at a higher activity level and thus more capable to cope with stress, cell death was significantly increased. These data therefore suggest that the possible shift in the dynamic equilibrium resulted in the activation of pro-apoptotic stimuli (Gadd153) and when either fenretinide or bortezomib were added; their perturbation of ER function significantly enhanced the pro-apoptotic stimuli to a greater extent, which was sufficient to overcome any changes in expression of the pro-survival machinery.

To gain a better understanding of the mechanism by which a reduction in GRP78 expression enhances ER stress-induced melanoma and glioblastoma cell death, research would need to be carried out to test the hypothesis that a reduction in GRP78 expression effects cellular outcome to stress. This could be achieved by time course analysis for the induction of Gadd153 in all cells types, with reduced GRP78 expression in comparison to controls.

The reduction in GRP78 may have also affected the capacity to respond, or buffer the ER stress [344] induced by either fenretinide or bortezomib. GRP78 is a known chaperone with holdase activity [345], capable of binding to unfolded or mis-folded

proteins and holding them in a more appropriate orientation for bond addition or removal. Chaperones hold unfolded substrates in an intermediately folded state to prevent irreversible aggregation and to catalyse the refolding of unfolded substrates in an energy- and co-chaperone-dependent reaction [346]. Therefore, a reduction in GRP78 expression would reduce the ability of a cell to bind and modify unfolded protein substrates, resulting in a reduction in capacity to buffer ER stress. This could ultimately result in more cell death, as the time under stress prior to UPR activation would be significantly reduced and allow a greater induction of pro-death stimuli over time. Research to confirm this hypothesis is required and could focus on the over-expression of other key chaperones, such as GRP94, calnexin, calriticulin or HSP70 [347], in cells with reduced GRP78 expression in order to determine if the loss of chaperone activity is the main driver of enhanced death.

Testing the effect of reduced GRP78 expression on the sensitivity of neuroblastoma cells to ER stress-induced death demonstrated no significant difference in sensitivity. These data demonstrated that although GRP78 in neuroblastoma was reduced by more than 50%, this had no effect on the outcome of ER stress. The fact that neuroblastoma contain more UPR activators to GRP78 molecules, may mean that a further reduction in the expression of GRP78, did not have the same effect on shifting the dynamic equilibrium as that seen in melanoma or glioblastoma.

Interestingly, this research suggests that the reduction in GRP78 expression in neuroblastoma had no significant effect on the chaperone-based response to ER stress, as cells under ER stress showed no increase in ER stress-induced death. Previous studies have demonstrated the importance of GRP94 in neuroblastoma [230]. Therefore, to determine if GRP94 is a crucial chaperone in neuroblastoma, vital for ER integrity during stress, future work should test the hypothesis that changes in GRP94 expression alter neuroblastoma cell sensitivity to ER stress.

To gain a better understanding for the relationship that exists between GRP78 and the UPR activators, Stable clones with reduced GRP78 expression would allow for the study of the effect of long term reduction in GRP78 expression on UPR activator concentrations (and the affect this has on the dynamic equilibrium), chaperones and folding machinery expressions (pro-survival attributes) or Gadd153, caspases and BCl-2 family members NOXA or PUMA expressions (Pro-death attributes). In addition, research could be carried out into the effect of a reduction in GRP78 expression on

downstream ERSE and UPRE activation and micro-arrays for the effect of ER stress on protein induction to gather a more comprehensive insight into the effect of GRP78 expression and changes in GRP78 expression over cancer types.

7.2.2: The effect of stable over-expression of GRP78.

Neural-crest-derived cancer cells, stably over-expressing GRP78 demonstrated that in melanoma and glioblastoma, over-expression of GRP78 significantly inhibited ER stress-induced cell death. These data confirm those for the reduction in GRP78 expression and highlight the importance of GRP78 in melanoma and glioblastoma cell survival. Further increasing the expression of GRP78 resulted in a significant decrease in the level of ATF4 induction achieved by ER stress-inducing agents and research into the effect of GRP78 expression on protein ubiquitination, in response to bortezomib treatment, demonstrated that cells over-expressing GRP78 had significantly less proteins tagged by ubiquitin.

These results could be dependent on the increase in GRP78 chaperone expression or due to the inhibition in activation of the UPR. Increasing the chaperone content of a cell would allow for a higher proportion of unfolded or misfolded proteins to be sequestered by a chaperone at any given time, increasing the ability of ER-machinery to mask stress and prevent the induction of the UPR. An increase in GRP78 would also affect the dynamic equilibrium of the UPR, shifting the outcome toward an inactive state. A decrease in UPR activity would reduce ERAD activation and in turn could influence the overall level of proteins tagged with ubiquitin during periods of ER stress. To determine which consequence of GRP78 is vital for melanoma or glioblastoma cell survival, experiments to determine the activity of the other two arms of the UPR should be carried out to allow for a complete assessment of the UPR. In addition, to determine if chaperone activity is the vital component of GRP78, in buffering ER stress in cells with enhanced GRP78, cells over-expressing GRP78 could undergo knockdown of other important chaperones, such as GRP94 or HSP70. Furthermore, cells over-expressing other chaperones could be tested for the effect this has on UPR induction in response to either fenretinide or bortezomib. Neuroblastoma, as for the effect of reduced GRP78 expression, demonstrated a different response to either melanoma or glioblastoma. Data for neuroblastoma cells over-expressing GRP78 showed a significant increase in

sensitivity to ER stress-inducing agents, as well as demonstrating a significantly greater UPR response.

Further dissection of the relationship between GRP78 and the UPR activators in over-expressing cells, in comparison to control, demonstrated that stable over-expression of GRP78 resulted in unexpected changes to the expression of PERK, IRE1 and ATF6. Melanoma demonstrated an increase in IRE1 and decrease in PERK and ATF6, glioblastoma demonstrated a reduction in PERK, and neuroblastoma demonstrated an increase in all three UPR activators. When comparing the effect of over-expression on the ratio of GRP78 to UPR activators (sum of all three sensors), data demonstrated that in melanoma and glioblastoma there was an overall increase in the ratio of GRP78: UPR activators. In contrast, in neuroblastoma there was a significant increase in UPR activators relative to GRP78.

Data for glioblastoma demonstrated a reduction in PERK expression and this could ultimately explain the reduction in ATF4 induction in the GRP78 over-expressing cells. However, this change in PERK expression was not seen in melanoma and therefore data support the hypothesis that GRP78 over-expression is responsible for the decrease in stress achieved by either fenretinide or bortezomib, resulting in the reduced ATF4 induction. However it is unclear if this is due to chaperone activity, altering the stress directly by removing unfolded or misfolded proteins or as a result of the increased inhibition of the UPR. In neuroblastoma however the significant increase in PERK may have contributed to the increase in ATF4 expression.

Over-expression of GRP78 in neuroblastoma cells resulted in a significant induction of cell death, which was not observed in either melanoma or glioblastoma. Testing the effect of GRP78 transfection in neuroblastoma cells highlighted a significant induction of cell death with GRP78. Stable GRP78 over-expressing clones for neuroblastoma demonstrated a mere 1.3 fold increase in GRP78. These findings support the concept that increases in GRP78 expression result in neuroblastoma cell death due to a shift in the dynamic equilibrium in favour of GRP78 and an inactive UPR. Furthermore these observations may suggest a vital role for the UPR in neuroblastoma cell survival, buffering the effect of other pro-death stimuli and changes in neuroblastoma physiology as a consequence of tumour microenvironment, drug treatment, or even cell proliferation rate that relies on an active UPR for survival.

7.3: Implications of targeting GRP78 as a therapeutic strategy in neural-crest-derived cancers.

GRP78 expression has been shown to be up-regulated in a variety of cancer types [113, 115]. Therefore, this study has tested the effect of inhibiting GRP78 across a panel of neural-crest-derived cancer types. The aim of this work was to assess the effect of inhibiting GRP78 activity on the dynamic equilibrium as a test of the hypothesis that melanoma and glioblastoma can be sensitized to ER stress and that in neuroblastoma, responses to GRP78 deregulation would have no therapeutic significance.

Studies using a nucleoside analogue or a GRP78 specific antibody, have suggested that interference in ATP exchange or prevention of cell surface GRP78 – substrate interaction using a targeted antibody [348], can significantly increase ER stress-induced cell death [295, 313, 349]. These possibilities were tested in this study but neither strategy was found to enhance the responses of fenretinide nor bortezomib induced death and, therefore, the data have not been included in this thesis.

7.3.1: The effect of $SubAB_5$ cleavage of GRP78 on ER stress-induced cell death.

Inactivation of GRP78, by $SubAB_5$ specific cleavage, also resulted in a significant enhancement of melanoma and glioblastoma cell death [198, 200]. These findings confirm the data generated form the present study for the effect of altering GRP78 expression on cell line sensitivity. $SubAB_5$ is a specific inhibitor of GRP78 and showed a significant reduction in full length protein, however demonstrated a weaker effect to that of siRNA mediated knockdown. These data suggest that although GRP78 is cleaved, it may still be capable of interacting with a substrate, helping to buffer ER stress, be it to a lesser extent.

Wolfson *et al.,* described the ability of $SubAB_5$ to activate the UPR [320]. Data from the present study did not demonstrate any significant induction of the UPR, with regard to ATF4 induction by $SubAB_5$ treatment [320]. This may be a consequence of concentration, as Wolfson *et al.*, used 1 µg/ml, a 200 fold higher concentration than that used in this present study [320]. Interestingly, Wolfson *et al.*, demonstrated that

$SubAB_5$ induced eIF2α phosphorylation for the first 4 h of treatment; however the reduction in GRP78 expression persisted for 24 h [320]. This therefore may suggest that the induction of the UPR was not as a consequence of GRP78 cleavage. $SubAB_5$ is internalised by clathrin dependent uptake [199] and maybe the inhibition of global protein synthesis was as a consequence of a significant intake of foreign material into the cell, inducing ER stress.

7.3.2: The effect of natural inhibitors of GRP78 on ER stress-induced cell death.

Alastair Hawkins and Jack Arbiser (personal communication) have shown that EGCG and honokiol both interact with GRP78, and more specifically the ATP binding domain (unpublished data, personal communications). These interactions may affect the ability of GRP78 to bind to ATP, thus affecting the function of GRP78 and its dynamic equilibrium with the UPR activators. Affecting the chaperone activity of GRP78 may sensitize cells to react to lower levels of ER stress, as well as possibly hindering the interaction of GRP78 with the UPR activators. Both outcomes would result in earlier activation of the UPR and UPR based pro-apoptotic stimuli (Gadd153), increasing the likelihood that ER stress-inducing agents activate cell death pathways. The present study showed that both EGCG and honokiol had significant effects on ER stress-induced cell death of melanoma and glioblastoma (only honokiol), with honokiol also demonstrating a significantly stronger effect. Interestingly, research comparing the strength of interaction of EGCG or honokiol with GRP78 demonstrated that honokiol binds with significantly higher affinity (Alastair Hawkins, unpublished data, personal communication).

The effect of EGCG in the present study was dependent on the ER stress-inducing agent it was combined with, but demonstrated an inhibitory effect on bortezomib. Previous data had shown EGCG can bind to and inhibit the 26S proteasome [318] and therefore competition for or overlap in 26S proteasome inhibition may have resulted in the observed poor combinational activity. Hill *et al.*, demonstrated that the combination of fenretinide and bortezomib synergistically enhanced melanoma cell death [82] and hence the significant effect seen when EGCG was combined with fenretinide, may have been due to the interaction with the 26S proteasome. However, EGCG unlike

bortezomib showed no activation of the UPR, which may suggest that if EGCG does bind to and inhibit the 26S proteasome; it is significantly weaker than that of bortezomib.

Results from the present study also showed that at high doses, honokiol induced markers of ER stress, as well as synergistically enhancing fenretinide and bortezomib-induced cell death of melanoma and glioblastoma. To confirm honokiol as a candidate GRP78 inhibitor, and test its potential to enhance fenretinide- or bortezomib-induced cell death, *in vivo* toxicity studies are thus required to determine the maximum tolerated dose achievable, and determine if this correlates with the *in vitro* range which demonstrated a synergistic enhancement of cell death. Furthermore, xenograft models for melanoma and glioblastoma for the effect of bortezomib, fenretinide and honokiol, alone and in combination should be carried out. Combination of either EGCG or honokiol with ER stress-inducing agents in neuroblastoma demonstrated no significant enhancement of death. This confirms the expression analysis, suggesting that targeting GRP78 as a therapeutic strategy to enhance ER stress-induced death is not an appropriate approach for neuroblastoma.

Finally, apoptosis is a coordinated and often energy-dependent process that involves the activation of a group of cysteine proteases (caspases) and a complex cascade of events that link the initiating stimuli to the final demise of the cell [81]. Thus, global ATP deregulation may serve to hinder the induction of cell death. Data from this study demonstrated that the combination of a GRP78 inhibitor (that targets the ATP binding domain of GRP78) with an ER stress-inducing agent, resulted in an increase in cell death, This suggests that the interaction of EGCG or honokiol maybe with an area close to the ATP binding domain, rather than directly with it. To gain a better understanding of the impact of EGCG or honokiol on GRP78 function and ATP binding, the ATPase activity of GRP78 should be tested alone and in the presence of inhibitor. The increase in cell death confirms that EGCG or honokiol are appropriate inhibitors for enhancing ER stress-induced cell death. Interestingly, the enhanced induction of cell death for the EGCG combinations in melanoma and glioblastoma and the honokiol combinations in glioblastoma was via a caspase independent route. These findings were suggested from the reduction in cleaved caspase 3.

7.4: ER stress and the activation of autophagy.

To date, the importance of autophagy, activated via the UPR is not completely understood. Knockdown studies of PERK or mutating the phosphorylation site of eIF2α have implicated the importance of p-eIF2α in UPR stimulated autophagy [350]. Interestingly, phosphorylation of eIF2α and the resulting inhibition of global protein synthesis are critical to PERK mediated activation of autophagy [338]. Studies have additionally demonstrated the importance of eIF2α in autophagic signalling as evidenced by observations demonstrating eIF2α can be phosphorylated by PERK, PKR, GCN2 and HRI from a number of contrasting stimuli [91], both ER stress and non-ER stress-inducing stimuli [351]. The resulting shift in protein translation by the phosphorylation of eIF2α leads to an increase in ATG12 expression and UPR stimulated induction of tribbles homologue 3 (TRB3) resulting in the inhibition of the protein kinase B/mammalian target of rapamycin (PKB/mTOR) pathway, and the induction of autophagy [352].

In addition, the interaction of active IRE1 with TRAF-2 leads to the activation of JNK, which in turn results in the phosphorylation of BCL-2 [338], and dysregulation beclin-1 activity [338]. This loss of Beclin-1 inhibition, in this context, resulted in the induction of autophagy [353]. However, a decrease in XBP-1 expression has also been shown to induce autophagy, that protects cells against superoxide dismutase 1 (SOD1) aggregate toxicity [354], suggesting that activation of autophagy by IRE1 can result in opposing outcomes, depending on the route of induction [338].

The present study highlighted differences in UPR signalling between melanoma and glioblastoma to that of neuroblastoma. Melanoma and glioblastoma demonstrated stronger induction of ATF4, downstream consequence of p-eIF2α, than that of neuroblastoma. This outcome may result in differences in the magnitude of response to which autophagy can contribute to the outcome of ER stress. Interestingly, differences in the activity of the IRE1 arm were also observed, with neuroblastoma demonstrating XBP-1 splicing for a significantly longer period of time to that of either melanoma or glioblastoma. These observations suggest that autophagy may contribute to the differences in neural-crest-derived cancer cells response to ER stress and that further research into the dynamics of autophagy, with regards to the contribution it plays in the balance between survival or death.

ATF6 (-/-) knockout mice are highly susceptible to bacterial infections, as a result of the loss of autophagic function. ATF6 has been shown to regulate interferon gamma (IFNG) induced death associated protein kinase 1 (Dapk1) expression via the CRE/ATF promoter site, in association with CCAAT/enhancer-binding protein beta (CEBPB). IFNG induced cleavage of ATF6 and MAPK 1/3 dependant phosphorylation of CEBPB control Dapk1. When either ATF6 or CEBPB are removed, IFNG fails to activate autophagy [355, 356]. However, research from the present study demonstrated no significant difference between cancer types in ER stress-induced ATF6 cleavage and therefore the contribution of this arm of the UPR, with regard to homeostatic or autophagic responses and is unlikely to contribute to the differences in disease outcome.

To determine if neural-crest-derived cancer cells differ in their capacity to mediate/activate UPR induced autophagy, further research comparing cancer types for the induction of autophagy should be carried out. Also, the present study focused on the endoribonuclease activity of IRE1 and to gain a complete understanding, the IRE1 kinase domain activity should be investigated to determine the contribution of the JNK pathway for the induction of autophagy and death by either fenretinide or bortezomib.

Fenretinide induced ROS and bortezomib induced 26S proteasome inhibition, the mechanisms by which these agents have been reported to induce ER stress; however they may also induce an autophagic response in an ER stress independent manner. Bortezomib induced 26S proteasome inhibition triggers death via UPR induced Gadd153 induction as well as IRE-TRAF2 induced autophagy, via JNK1 activation. However, inhibition of the 26S proteasome results in deregulation of p62 expression. It has been hypothesised that p62 interacts with ubiquitin tails of other tagged proteins, and undergoes degradation. However, the resulting accumulation of tagged proteins by 26S proteasome inhibition prevents p62 degradation and stimulates p62 to interact with LC3, activating autophagy. Fenretinide induces ROS by interfering with ceramide synthesis. Ceramide is maintained in dynamic equilibrium with sphingosine and S1P. These proteins are known to have opposing effects on survival and death. Therefore interfering in this dynamic equilibrium by reducing ceramide hinders phosphoinositide 3-kinase (PI3K) regulated suppression of autophagy. The increase in ROS as a consequence of fenretinide increases ataxia-telangiectasia mutated (ATM) activity, ultimately resulting in the inhibition of the mTORC1 complex, activating autophagy [357].

Due to the close interaction between ER stress-induced UPR and autophagy pathways, ER stress-induced cell death remains a viable target to induce death in cancer types resistant to traditional chemotherapeutics. Combining ER stress-inducing agents with inhibitors of the UPR enhances cell death by causing an imbalance between pro-survival and –death stimuli of homeostatic response mechanisms. Therefore, further research into ER stress would allow for a more comprehensive understanding of the role of the UPR and autophagy in cancer cell survival and allow for specific target(s), such as GRP78, to be identified to synergise the response of current chemotherapeutics capable of perturbing ER function.

7.5: Conclusions.

This study, investigating the UPR in neural-crest-derived cancer types showed that melanoma and glioblastoma display increased sensitivity to ER stress-induced cell death in response to fenretinide and bortezomib when GRP78 expression is reduced. Also, when the expression of GRP78 was increased, melanoma and glioblastoma demonstrated enhanced resistance in comparison to control cells. However, GRP78 expression in neuroblastoma does not demonstrate any biological significance on ER stress-induced death. The dependence of a cancer cell on GRP78 to buffer ER stress and increase resistance to ER stress-induced cell death can be better understood by the relationship that exists between GRP78 and the UPR activators. Cancer types, such as melanoma and glioblastoma, with more GRP78 to that of UPR activators become more sensitive to ER stress when GRP78 is reduced. This was confirmed when GRP78 inhibitor honokiol, enhanced melanoma and glioblastoma cell death when combined with either fenretinide or bortezomib. Therefore, honokiol represents a novel candidate agent for in vivo analysis as a therapeutic strategy for the treatment of melanoma or glioblastoma.

This study is unique in its comparison of three neural-crest-derived cancer types and confirms that differences do exist between cancer types, with regard to their outcome to enhanced GRP78 expression. This study also discovered that this is a consequence of the dynamic equilibrium that GRP78 has with the UPR activators; PERK, IRE1 and ATF6. This study highlighted that a cancer type with more GRP78 to UPR activators became more resistant to ER stress-induced cell death and therefore clinical observation of GRP78 as a biomarker for disease outcome could be strengthened by investigating the relationship between GRP78 and the UPR activators. To date, cancer research is moving toward specific targeted therapies, not only dependent on the type of cancer but also on the disease stage and the expression levels of specific protein markers that have been shown to alter response to therapy. This study using quantifiable techniques to understand relationships which underlie the sensitivity of a homeostatic response mechanism sets a benchmark for the level of interpretation that can be gained into the characteristics of a signalling cascade to allow for the observation of abnormalities.

Chapter 8:

References.

1. Gilbert, S.F., *Early vertebrate development, neurulation and the ectoderm.* In Developmental Biology1994, Massachusetts: Sinauer Associates inc.
2. Newgreen, D.F., et al., *Changes in cell adhesion and extracellular matrix molecules in spontaneous spinal neural tube defects in avian embryos.* Teratology, 1997. **55**(3): p. 195-207.
3. Zhang, S.C., et al., *In vitro differentiation of transplantable neural precursors from human embryonic stem cells.* Nat Biotechnol, 2001. **19**(12): p. 1129-33.
4. Raible, D.W. and J.S. Eisen, *Restriction of neural crest cell fate in the trunk of the embryonic zebrafish.* Development, 1994. **120**(3): p. 495-503.
5. Baker, C.V., et al., *Early- and late-migrating cranial neural crest cell populations have equivalent developmental potential in vivo.* Development, 1997. **124**(16): p. 3077-87.
6. Gilbert S F, *Developmental Biology*. 4 ed1994: Sinauer Associates. 244-294.
7. Selleck, M.A. and M. Bronner-Fraser, *Origins of the avian neural crest: the role of neural plate-epidermal interactions.* Development, 1995. **121**(2): p. 525-38.
8. Baroffio, A., E. Dupin, and N.M. Le Douarin, *Common precursors for neural and mesectodermal derivatives in the cephalic neural crest.* Development, 1991. **112**(1): p. 301-5.
9. Jiang, X., et al., *Fate of the mammalian cardiac neural crest.* Development, 2000. **127**(8): p. 1607-16.
10. Trainor, P.A., *Making headway: the roles of Hox genes and neural crest cells in craniofacial development.* ScientificWorldJournal, 2003. **3**: p. 240-64.
11. Levine M and Hoey T, *Homeobox proteins as sequence specific transcription factors.* Cell, 1988. **55**: p. 537-40.
12. Gilchrest, B.A., *Sun exposure and vitamin D sufficiency.* Am J Clin Nutr, 2008. **88**(2): p. 570S-577S.
13. Lin J Y and Fisher D E, *melanocyte biology and skin pigmentation.* Nature, 2007. **445**(7130): p. 843-50.
14. Metcalf, J.S., *Melanoma: criteria for histological diagnosis and its reporting.* Semin Oncol, 1996. **23**(6): p. 688-92.
15. Hirobe, T., *Structure and function of melanocytes: microscopic morphology and cell biology of mouse melanocytes in the epidermis and hair follicle.* Histol Histopathol, 1995. **10**(1): p. 223-37.
16. Wilkie, A.L., S.A. Jordan, and I.J. Jackson, *Neural crest progenitors of the melanocyte lineage: coat colour patterns revisited.* Development, 2002. **129**(14): p. 3349-57.
17. Costin G E and Hearing V J, *Human skin pigmentation: melanocytes modulate skin colour in response to stress.* Feseb J, 2007. **21**(4): p. 976-94.

18. Costin, G.E. and V.J. Hearing, *Human skin pigmentation: melanocytes modulate skin color in response to stress.* FASEB J, 2007. **21**(4): p. 976-94.
19. E, B.R., *Melanosome transfer to and translocation in the keratinocyte.* Exp Dermatol, 2003. **12**(Suppl 2): p. 5-12.
20. Hirobe T, *Role of keratinocyte derived factors involved in regulating the proliferation and differentiation of mammalioan epidermal melanocytes.* Pigment Cell Res, 2005. **18**(1): p. 2-12.
21. Herraiz, C., et al., *Signaling from the human melanocortin 1 receptor to ERK1 and ERK2 mitogen-activated protein kinases involves transactivation of cKIT.* Mol Endocrinol, 2011. **25**(1): p. 138-56.
22. Yasumoto, K., et al., *Functional analysis of microphthalmia-associated transcription factor in pigment cell-specific transcription of the human tyrosinase family genes.* J Biol Chem, 1997. **272**(1): p. 503-9.
23. Healy E and Jordan S A, *Functional variation of the MCR1 alleles from red haired individuals.* Hum Mol Gen, 2001. **10**(21): p. 2397-402.
24. Strum R A and Box N F, *Human pigmentation genetics: the difference is only skin deep.* Bioessays, 1998. **20**(9): p. 712-21.
25. Kollias N and Sayre R M, *Photoprotection by melanin.* J Photochem Photobiol B, 1991. **9**(2): p. 135-60.
26. Kollias, N. and R.M. Sayre, *Photoprotection by melanin.* J Photochem Photobiol B, 1991. **9**(2): p. 135-60.
27. Lucas, R., *Global Burden of Disease of Solar Ultraviolet Radiation, Environmental Burden of Disease Series,.* News Release, World Health Organisation, 2006. **2006**(13).
28. Erika, L. and M.D. Rager, *Cutaneous Melanoma: Update on Prevention, Screening, Diagnosis, and Treatment.* American Family Physician, 2005. **72**(2): p. 269-276.
29. *Cancer Research U.K*. 2007 19/02/2007]; Available from: http://info.cancerresearchuk.org/cancerstats/types/melanoma/.
30. *Melanoma of the skin*. 2007 21/02/2007]; Available from: http://seer.cancer.gov/statfacts/html/melan.html.
31. Hussein, M.R., A.K. Haemel, and G.S. Wood, *Apoptosis and melanoma: molecular mechanisms.[see comment].* Journal of Pathology, 2003. **199**(3): p. 275-88.
32. Garnett, M.J. and R. Marais, *Guilty as charged: B-RAF is a human oncogene.* Cancer Cell, 2004. **6**: p. 313-319.
33. Casula, M., et al., *BRAF gene is somatically mutated but does not make a major contribution to malignant melanoma susceptibility: the Italian Melanoma Intergroup Study.* J Clin Oncol, 2004. **22**(2): p. 286-92.

34. Thompson, J.F. and R.A. Scolyer, *Cutaneous Melanoma.* Lancet, 2005. **365**: p. 687-701.
35. Thompson, J.F., R.A. Scolyer, and R.F. Kefford, *Cutaneous melanoma.* Lancet, 2005. **365**(9460): p. 687-701.
36. Pashankar, F.D., M.S. O'Dorisio, and Y. Menda, *MIBG and somatostatin receptor analogs in children: current concepts on diagnostic and therapeutic use.* J Nucl Med, 2005. **46 Suppl 1**: p. 55S-61S.
37. *Neuroblastoma in children*. 2008 05.01.2009]; Available from: http://www.cancerbackup.org.uk/cancertype/childrenscancers/typesofchildrenscancers/neuroblastoma#9216.
38. *Pediatric Cancers*. 2008 05.01.2009]; Available from: http://www.merck.com/mmpe/sec19/ch285/ch285b.html.
39. *Wikipedia - Neuroblastoma*. 2008 22.12.2008.]; Available from: http://en.wikipedia.org/wiki/Neuroblastoma.
40. Brodeur G M, *Neuroblastoma: biological insights into a clinical enigma.* Nature Reviews, 2003. **3**(3): p. 203-16.
41. Schulte, J.H., S. Horn, and T. Otto, *MYCN regulates oncogenic MicroRNAs in neuroblastoma.* Int J Cancer, 2008. **122**(3): p. 699–704.
42. Schulte J H, Horn S, and Otto T, *MYCN regulates oncogenic MicroRNAs in neuroblastoma.* Int J Cancer, 2008. **122**(3): p. 699–704.
43. Institute, N.C. *Neuroblastoma Treatment* 2008 27.12.2008]; Available from: http://www.cancer.gov/cancertopics/pdq/treatment/neuroblastoma/HealthProfessional/page3#Section_17.
44. He, F. and Y.E. Sun, *Glial cells more than support cells?* Int J Biochem Cell Biol, 2007. **39**(4): p. 661-5.
45. Jabs, R., et al., *Synaptic transmission onto hippocampal glial cells with hGFAP promoter activity.* J Cell Sci, 2005. **118**(Pt 16): p. 3791-803.
46. Newman, E.A., *Glial cell inhibition of neurons by release of ATP.* J Neurosci, 2003. **23**(5): p. 1659-66.
47. Angulo, M.C., et al., *Glutamate released from glial cells synchronizes neuronal activity in the hippocampus.* J Neurosci, 2004. **24**(31): p. 6920-7.
48. Konishi, Y. and A. Bonni, *The E2F-Cdc2 cell-cycle pathway specifically mediates activity deprivation-induced apoptosis of postmitotic neurons.* J Neurosci, 2003. **23**(5): p. 1649-58.
49. Allen, N.J. and B.A. Barres, *Signaling between glia and neurons: focus on synaptic plasticity.* Curr Opin Neurobiol, 2005. **15**(5): p. 542-8.
50. Kornblum, H.I., *Introduction to neural stem cells.* Stroke, 2007. **38**(2 Suppl): p. 810-6.

51. Hu, J., et al., *Schwann cells promote neurite outgrowth of dorsal root ganglion neurons through secretion of nerve growth factor.* Indian J Exp Biol, 2011. **49**(3): p. 177-82.
52. Shoshan, Y., et al., *Expression of oligodendrocyte progenitor cell antigens by gliomas: implications for the histogenesis of brain tumors.* Proc Natl Acad Sci U S A, 1999. **96**(18): p. 10361-6.
53. Taylor, L.P., *Diagnosis, treatment, and prognosis of glioma: five new things.* Neurology, 2010. **75**(18 Suppl 1): p. S28-32.
54. Agarwala, S.S. and J.M. Kirkwood, *Temozolomide, a novel alkylating agent with activity in the central nervous system, may improve the treatment of advanced metastatic melanoma.* Oncologist, 2000. **5**(2): p. 144-51.
55. Friedman, H.S., T. Kerby, and H. Calvert, *Temozolomide and treatment of malignant glioma.* Clinical Cancer Research, 2000. **6**(7): p. 2585-97.
56. Lawson, M.D., *Choices in Adjuvant Therapy of Melanoma.* Cancer Control, 2005. **12**(4): p. 236-241.
57. Friedman, H.S., T. Kerby, and H. Calvert, *Temozolomide and treatment of malignant glioma.* Clin Cancer Res, 2000. **6**(7): p. 2585-97.
58. Torres, S., et al., *A combined preclinical therapy of cannabinoids and temozolomide against glioma.* Mol Cancer Ther, 2011. **10**(1): p. 90-103.
59. Fulda, S. and K.M. Debatin, *Extrinsic versus intrinsic apoptosis pathways in anticancer chemotherapy.* Oncogene, 2006. **25**(34): p. 4798-811.
60. Lavrik, I., A. Golks, and P.H. Krammer, *Death receptor signaling.* J Cell Sci, 2005. **118**(Pt 2): p. 265-7.
61. Herr, I. and K.M. Debatin, *Cellular stress response and apoptosis in cancer therapy.* Blood, 2001. **98**(9): p. 2603-14.
62. Kulczycka, K., M. Dlugosz, and J. Trylska, *Molecular dynamics of ribosomal elongation factors G and Tu.* Eur Biophys J, 2011. **40**(3): p. 289-303.
63. Nagata, S., *Fas ligand-induced apoptosis.* Annu Rev Genet, 1999. **33**: p. 29-55.
64. Kruidering, M. and G.I. Evan, *Caspase-8 in apoptosis: the beginning of "the end"?* IUBMB Life, 2000. **50**(2): p. 85-90.
65. Budihardjo I, et al., *Biochemical pathways of caspase activation during apoptosis.* Annu. Rev. Cell Dev. Biol., 1999. **15**: p. 269-90.
66. Irmler M, et al., *Inhibition of death receptor signals b y cellular FLIP.* Nature, 1997. **388**: p. 190-95.
67. Marsters S A, et al., *A novel receptor for Apo2L/TRAIL contains a truncated death domain.* Curr. Biol., 1997. **7**: p. 1003-6.

68. Jiang, Y., et al., *Prevention of constitutive TNF receptor 1 signaling by silencer of death domains.* Science, 1999. **283**(5401): p. 543-6.

69. Drew, B. and C. Leeuwenburgh, *Method for measuring ATP production in isolated mitochondria: ATP production in brain and liver mitochondria of Fischer-344 rats with age and caloric restriction.* Am J Physiol Regul Integr Comp Physiol, 2003. **285**(5): p. R1259-67.

70. *Wikipedia - Mitochondria*. 2008 02.12.2008]; Available from: http://en.wikipedia.org/wiki/Mitochondria.

71. Youle, R.J. and A. Strasser, *The BCL-2 protein family: opposing activities that mediate cell death.* Nat Rev Mol Cell Biol, 2008. **9**(1): p. 47-59.

72. Martinou J and Green D R, *Breaking the mitochondrial barrier.* Nature Reviews, 2001. **2**: p. 63-7.

73. Zamzami N and Kroemer G, *The mitochondrion in apoptosis: how pandora's box opens.* Nature Reviews, 2001. **2**: p. 67-71.

74. Fesik S W, *Insights into programmed cell death through structural biology.* Cell, 2000. **103**: p. 273-82.

75. Youle R J and Strasser A, *The BCL-2 protein family: opposing activities that mediate cell death.* nature Reviews, 2008. **9**: p. 47-59.

76. Galluzzi L and Kroemer G, *Mitochondrial apoptosis without VDAC.* Nature Cell Biology, 2007. **9**(5): p. 487-89.

77. Liu X, et al., *Induction of apoptotic program in cell-free extracts: requirement for dATP and cytochrome c.* Cell, 1996. **86**: p. 147-57.

78. Wei M C, Lindsten T, and Mootha V K, *tBID, a membrane targeted death ligand, oligomerizes BAK to release cytochrome c.* Genes and Development, 2000. **14**: p. 2060-71.

79. Adams j. M, *Ways of dying: multiple pathways to apoptosis.* Genes and Development, 2003. **17**: p. 2481-95.

80. Sancar, A., et al., *Molecular mechanisms of mammalian DNA repair and the DNA damage checkpoints.* Annu Rev Biochem, 2004. **73**: p. 39-85.

81. Elmore, S., *Apoptosis: a review of programmed cell death.* Toxicol Pathol, 2007. **35**(4): p. 495-516.

82. Hill, D.S., et al., *Combining the Endoplasmic Reticulum Stress-Inducing Agents Bortezomib and Fenretinide as a Novel Therapeutic Strategy for Metastatic Melanoma.* Clinical Cancer Research, 2009. **15**(4): p. 1192-1198.

83. Corazzari, M., et al., *Targeting homeostatic mechanisms of endoplasmic reticulum stress to increase susceptibility of cancer cells to fenretinide-induced apoptosis: The*

role of stress proteins ERdj5 and ERp57. British Journal of Cancer, 2007. **96**(7): p. 1062-1071.

84. Weinmann, M., C. Belka, and L. Plasswilm, *Tumour hypoxia: impact on biology, prognosis and treatment of solid malignant tumours.* Onkologie, 2004. **27**(1): p. 83-90.

85. Cairns, R.A., I.S. Harris, and T.W. Mak, *Regulation of cancer cell metabolism.* Nat Rev Cancer, 2011. **11**(2): p. 85-95.

86. Field-Smith, A., G.J. Morgan, and F.E. Davies, *Bortezomib (Velcadetrade mark) in the Treatment of Multiple Myeloma.* Ther Clin Risk Manag, 2006. **2**(3): p. 271-9.

87. Szegezdi E, Fitzgerald U, and Samali A, *Caspase-12 and ER-stress-mediated apoptosis.* Ann. N.Y.Acad. Sci., 2003. **1010**: p. 186-94.

88. Voeltz, G.K., M.M. Rolls, and T.A. Rapoport, *Structural organization of the endoplasmic reticulum.* EMBO Rep, 2002. **3**(10): p. 944-50.

89. *Wikipedia - Endoplasmic Reticulum*. 2008 02.12.2008.]; Available from: http://en.wikipedia.org/wiki/Endoplasmic_reticulum.

90. Adesnik M, et al., *Retention of mRNA on the endoplasmic reticulum membranes after in vivo disassembly of polysomes by an inhibitor of initiation.* J Cell Biol, 1976. **71**: p. 307-13.

91. Schroder, M., *The mammalian unfolded protein response.* Annual Review of Biochemistry, 2005. **74**: p. 739-789.

92. Gallie, D.R., *Protein-protein interactions required during translation.* Plant Mol Biol, 2002. **50**(6): p. 949-70.

93. Kaufman, R.J., *Regulation of mRNA translation by protein folding in the endoplasmic reticulum.* Trends Biochem Sci, 2004. **29**(3): p. 152-8.

94. Lu, P.D., et al., *Cytoprotection by pre-emptive conditional phosphorylation of translation initiation factor 2.* EMBO J, 2004. **23**(1): p. 169-79.

95. Dantley, K.A., H.K. Dannelly, and V. Burdett, *Binding interaction between Tet(M) and the ribosome: requirements for binding.* J Bacteriol, 1998. **180**(16): p. 4089-92.

96. Gingras, A.C., B. Raught, and N. Sonenberg, *eIF4 initiation factors: effectors of mRNA recruitment to ribosomes and regulators of translation.* Annu Rev Biochem, 1999. **68**: p. 913-63.

97. Lopez-Lastra, M., A. Rivas, and M.I. Barria, *Protein synthesis in eukaryotes: the growing biological relevance of cap-independent translation initiation.* Biol Res, 2005. **38**(2-3): p. 121-46.

98. Gross, J.D., et al., *Ribosome loading onto the mRNA cap is driven by conformational coupling between eIF4G and eIF4E.* Cell, 2003. **115**(6): p. 739-50.

99. Jang, S.K., et al., *A segment of the 5' nontranslated region of encephalomyocarditis virus RNA directs internal entry of ribosomes during in vitro translation.* J Virol, 1988. **62**(8): p. 2636-43.

100. Le, S.Y. and J.V. Maizel, Jr., *A common RNA structural motif involved in the internal initiation of translation of cellular mRNAs.* Nucleic Acids Res, 1997. **25**(2): p. 362-69.

101. Kurzchalia D, et al., *The signal sequence of nascent preprolactin interacts with the 54K polypeptide of the signal recognition particle.* Nature, 1986. **320**: p. 634-6.

102. Dobson C M, *Principles of protein folding, misfolding and aggregation.* Semin Cell Dev Biol, 2004. **15**: p. 3-16.

103. Dobson, C.M., *Principles of protein folding, misfolding and aggregation.* Semin Cell Dev Biol, 2004. **15**: p. 3-16.

104. Creighton, T.E., *Protein folding.* Biochem J, 1990. **270**(1): p. 1-16.

105. Hartl, F.U. and M. Hayer-Hartl, *Converging concepts of protein folding in vitro and in vivo.* Nat Struct Mol Biol, 2009. **16**(6): p. 574-81.

106. Moreno-Gonzalez, I. and C. Soto, *Misfolded protein aggregates: mechanisms, structures and potential for disease transmission.* Semin Cell Dev Biol, 2011. **22**(5): p. 482-7.

107. Vabulas, R.M., et al., *Protein folding in the cytoplasm and the heat shock response.* Cold Spring Harb Perspect Biol, 2010. **2**(12): p. a004390.

108. Chen, Y., et al., *Oxygen consumption can regulate the growth of tumors, a new perspective on the Warburg effect.* PLoS One, 2009. **4**(9): p. e7033.

109. Kultz, D., *Molecular and evolutionary basis of the cellular stress response.* Annu Rev Physiol, 2005. **67**: p. 225-57.

110. Fink, A.L., *Chaperone-mediated protein folding.* Physiol Rev, 1999. **79**(2): p. 425-49.

111. Schroder, M., *The unfolded protein response.* Molecular Biotechnology, 2006. **34**(2): p. 279-290.

112. Armstrong, J.L., et al., *Regulation of endoplasmic reticulum stress-induced cell death by ATF4 in neuroectodermal tumor cells.* J Biol Chem, 2010. **285**(9): p. 6091-100.

113. Lee, H.K., et al., *GRP78 is overexpressed in glioblastomas and regulates glioma cell growth and apoptosis.* Neuro-Oncology, 2008. **10**(3): p. 236-243.

114. Hersey, P. and X.D. Zhang, *Adaptation to ER stress as a driver of malignancy and resistance to therapy in human melanoma.* Pigment Cell & Melanoma Research, 2008. **21**(3): p. 358-367.

115. Zhuang, L., et al., *Expression of glucose-regulated stress protein GRP78 is related to progression of melanoma.* Histopathology, 2009. **54**(4): p. 462-70.

116. Hsu, W.M., et al., *GRP78 expression correlates with histologic differentiation and favorable prognosis in neuroblastic tumors.* International journal of Cancer, 2005. **113**(6): p. 920-7.

117. Brewer J W and D.J. A, *PERK mediates cell-cycle exit during mammalian unfolded protein response.* Proc.Natl. Acad.Sci.USA, 2000. **97**: p. 12625-30.

118. Kozutsumi Y, *The presence of malfolded proteins in the endoplasmic reticulum signals the induction of glucose regulatory proteins.* Nature, 1988. **332**: p. 462-4.

119. Schonthal A H, *Endoplasmic reticulum stress and autophagy as targets for cancer therapy.* Cancer Letters, 2008. **Article in press**.

120. Szegezdi E, et al., *Mediators of endoplasmic reticulum stress induced apoptosis.* EMBO reports, 2006. **7**(9): p. 880-5.

121. Stankiewicz A R, et al., *hsp70 inhibits heat-induced apoptosis upstream of mitochondria by preventing Bax translocation.* Journal of biological chemistry, 2005. **280**(46): p. 38729-39.

122. Munro S and Pelham H R B, *An hsp 70 like protein in the ER: Identity with the 78 kd glucose-regulated protein and immunoglobulin heavy chain binding protein.* Cell, 1986. **46**: p. 291-300.

123. Schroder M and Kaufman R J, *ER stress and the unfolded protein response.* Mutation research, 2004. **569**: p. 29-63.

124. Laitusis A L, Brostrum M A, and Brostrum C O, *The dynamic role of GRP78/BiP in the coordination of mRNA Translation with protein processing.* The Journal of Biological Chemistry, 1999. **274**(1): p. 486-93.

125. Ni, M., Y. Zhang, and A.S. Lee, *Beyond the endoplasmic reticulum: atypical GRP78 in cell viability, signalling and therapeutic targeting.* Biochem J, 2011. **434**(2): p. 181-8.

126. Berger, C.L., et al., *A lymphocyte cell surface heat shock protein homologous to the endoplasmic reticulum chaperone, immunoglobulin heavy chain binding protein BIP.* Int J Cancer, 1997. **71**(6): p. 1077-85.

127. Misra, U.K., et al., *The role of Grp 78 in alpha 2-macroglobulin-induced signal transduction. Evidence from RNA interference that the low density lipoprotein receptor-related protein is associated with, but not necessary for, GRP 78-mediated signal transduction.* Journal of Biological Chemistry, 2002. **277**(44): p. 42082-7.

128. Schroder H C, Hassanein M A, and Muller W E G, *Induction of DNA strand breaks and expression of HSP70 and GRP78 homolog by Cadmium in the marine sponge Suberites domuncula.* Arch. Environ.Contam.Toxicol., 1998. **36**: p. 47-55.

129. Barnes J A and S.I. W, *Glucose-regulated protein 78 (GRP78) is elavated in embryonic mouse heart and induced following hypoglycemic stress.* Anat Embryol, 2000. **2002**: p. 67-74.

130. Kim K S, Kim Y K, and Lee A S, *Expression of the glucose regulated proteins (GRP78 and GRP94) in differentiated and undifferentiated mouse embryonic cells and the use of the GRP78 promoter as an expression system in embryonic cells.* Differentiation, 1990. **42**: p. 153-59.

131. Lee A S, *GRP78 induction in cancer: Therapeutic and prognostic implications.* Cancer Res, 2007. **67**(8): p. 3496-9.

132. Mao C, et al., *In vivo regulation of Grp78/BiP transcription in the embryonic heart:role of the endoplasmic reticulum stress response element and GATA-4.* Journal of biological chemistry, 2006. **281**: p. 8877-87.

133. Barnes J A, Smoak I W, and Branch S, *Expression of glucose regulated proteins (GRP78 and GRP94) in hearts and forelimb buds of mouse embyros exposed to hypoglycemia in vitro.* Cell Stress Chaperones, 1999. **4**: p. 250-8.

134. Chevalier, M., et al., *Substrate binding induces depolymerization of the C-terminal peptide binding domain of murine GRP78/BiP.* J Biol Chem, 1998. **273**(41): p. 26827-35.

135. Gething M-J, *Role and regulation of the ER chaperone BiP.* Cell and Developmental Biology., 1999. **10**: p. 465-72.

136. Dejeans, N., et al., *Endoplasmic reticulum calcium release potentiates the ER stress and cell death caused by an oxidative stress in MCF-7 cells.* Biochem Pharmacol, 2010. **79**(9): p. 1221-30.

137. Murphy T C, Woods N R, and Dickson A J, *Expression of the transcription factor GADD153 is an indicator of apoptosis for recombinant chinease hamster ovary (CHO) cells.* Biotechnology and Bioengineering, 2001. **75**(6): p. 621-9.

138. Pyrko P, et al., *The unfolded protein response regulator GRP78/BiP as a novel target for increasing chemosensitivity in malignant gliomas.* Cancer Res, 2007. **67**(20): p. 9809-16.

139. Rao R V, et al., *Coupling endoplasmic reticulum stress to the cell death program: role of the ER chaperone GRP78.* FEBS Letters, 2002. **514**: p. 122-8.

140. Reddy R K, Mao C, and Lee A S, *Endoplasmic reticulum chaperone protein GRP78 protects cells from apoptosis induced by topoisomerase inhibitors.* the Journal of Biological Chemistry, 2003. **278**(23): p. 20915-24.

141. Satoh, M., et al., *Modulation of the phosphorylation of glucose-regulated protein, GRP78, by transformation and inhibition of glycosylation.* Exp Cell Res, 1993. **205**(1): p. 76-83.

142. Yamaguchi Y, et al., *Endoplasmic reticulum (ER) chaperone regulation and survival of cells compensatory for deficiency in the ER stress response kinase, PERK.* The Journal of Biological Chemistry, 2008. **283**(25): p. 17020-9.

143. Harding H P, Zhang Y, and Ron D, *Protein translation and folding are coupled by an endoplasmic-reticulum-resident kinase.* Nature, 1999. **379**: p. 271-4.

144. Bertolotti A, et al., *Dynamic interaction of BiP and ER stress transducers in the unfolded-protein response.* Nature Cell Biology, 2000. **2**(6): p. 326-32.

145. Harding HP, et al., *Regulated translation initiation controls stress-induced gene expression in mammalian cells.* Mol Cell. , 2000. **6**(5): p. 1099-108.

146. Brewer J W, et al., *Mammalian unfolded protein response inhibits cyclin D1 translation and cell cycle progression.* Proc.Natl. Acad.Sci.USA, 1999. **96**: p. 8505-10.

147. Cullinan S B, et al., *Nrf2 is a direct PERK substrate and effector of PERK-dependant cell survival.* Mol Cell Biol, 2003. **23**: p. 7198-209.

148. Hinnebusch A G, *The eIF-2 alpha kinases: regulators of protein synthesis in starvation and stress.* Semin Cell Biol, 1994. **5**(6): p. 417-26.

149. Harding H P, et al., *An intergrated stress response regulates amino acid metabolism and resistance to oxidative stress.* Mol Cell., 2003. **11**: p. 619-33.

150. Vattem K M and Wek R C, *Reinitiation involving upstream ORFs regulates ATF4 mRNA translation in mammalian cells.* Proc.Natl. Acad.Sci.USA, 2004. **101**: p. 11269-74.

151. Fels D R, *The PERK/eIF2alpha/ATF4 module of the UPR in hypoxia resistance and tumour growth.* Cancer Biology and Therapy, 2006. **5**(7): p. 723-8.

152. Wing X, et al., *Signals from the stressed endoplasmic reticulum induce C/EBP-homologous protein (CHOP/GADD153).* Mol Cell Biol, 1996. **16**: p. 4273-80.

153. He C H, et al., *Identification of activating transcrition factor 4 (ATF4) as an Nrf2-interacting protein. Implications of heme oxygenase-1 gene regulation.* Journal of biological chemistry, 2001. **276**: p. 20858-65.

154. Van Huizen R, et al., *P58^{IPK}, a novel endoplasmic reticulum stress inducible protein and potential negative regulator of eIFalpha signaling.* Journal of biological chemistry, 2003. **278**: p. 15558-64.

155. Kebache S, Cardin E, and Larose L, *Nck-1 antagonizes the endoplasmic reticulum stress induced inhibition of translation.* Journal of biological chemistry, 2004. **279**: p. 9662-9671.

156. Nikawa J and Yamashita S, *IRE1 encodes a putative protein kinase containing a membrane scanning domain and is required for inositol phototrophy in Saccharomyces cerevisiae.* Mol Microbiol, 1992. **6**: p. 1441-46.

157. Promlek, T., et al., *Membrane aberrancy and unfolded proteins activate the endoplasmic reticulum stress sensor Ire1 in different ways.* Mol Biol Cell, 2011. **22**(18): p. 3520-32.

158. Bertolotti A, et al., *Increased sensitivity to dextran sodium sulphate colitis in IRE1 beta-deficient mice.* J.clin.invest, 2001. **107**: p. 585-93.

159. Urano, F., et al., *Coupling of stress in the ER to activation of JNK protein kinases by transmembrane protein kinase IRE1.* Science, 2000. **287**(5453): p. 664-6.

160. Papa F R, et al., *Bypassing a kinase activity with an ATP-competitive drug.* Science, 2003. **302**: p. 1533-7.

161. Lee K, et al., *IRE-1 mediated unconventional mRNA splicing and S2P-mediated ATF6 cleavage merge to regulate XBP1 in signaling the unfolded protein response.* Genes and Development, 2002. **16**: p. 452-466.

162. Merksamer, P.I. and F.R. Papa, *The UPR and cell fate at a glance.* J Cell Sci, 2010. **123**(Pt 7): p. 1003-6.

163. Arch, R.H., R.W. Gedrich, and C.B. Thompson, *Translocation of TRAF proteins regulates apoptotic threshold of cells.* Biochem Biophys Res Commun, 2000. **272**(3): p. 936-45.

164. Dupoux, A., et al., *cIAP1-dependent TRAF2 degradation regulates the differentiation of monocytes into macrophages and their response to CD40 ligand.* Blood, 2009. **113**(1): p. 175-85.

165. Kroemer, G., L. Galluzzi, and C. Brenner, *Mitochondrial membrane permeabilization in cell death.* Physiol Rev, 2007. **87**(1): p. 99-163.

166. Deng, Y., et al., *A JNK-dependent pathway is required for TNFalpha-induced apoptosis.* Cell, 2003. **115**(1): p. 61-70.

167. Liang, Q., et al., *c-Jun N-terminal kinases (JNK) antagonize cardiac growth through cross-talk with calcineurin-NFAT signaling.* EMBO J, 2003. **22**(19): p. 5079-89.

168. Shen, J.S., et al., *Stable binding of ATF6 to BiP in the endoplasmic reticulum stress response.* Molecular and Cellular Biology, 2005. **25**(3): p. 921-932.

169. Haze K, et al., *Mammalian transcription factor ATF6 is synthesized as a transmembrane protein and activated by proteolysis in response to endoplasmic reticulum stress.* Mol Cell Biol, 1999. **10**: p. 3787-99.

170. Yoshida H, et al., *ATF6 activated by proteolysis binds in the presence of NF-Y (CBF) directly to the cis-acting element responsible for mammalian unfolded protein response.* Mol Cell Biol, 2000. **20**: p. 6755-67.

171. Zeng L, et al., *ATF6 mediates SREBP2-mediated lipogenesis.* EMBO, 2004. **23**: p. 950-58.

172. Van Huizen, R., et al., *P58^{IPK}, a novel endoplasmic reticulum stress inducible protein and potential negative regulator of eIFalpha signaling.* Journal of biological chemistry, 2003. **278**: p. 15558-64.

173. Blais, J.D., et al., *Activating transcription factor 4 is translationally regulated by hypoxic stress.* Mol Cell Biol, 2004. **24**(17): p. 7469-82.

174. Nakatsukasa, K. and J.L. Brodsky, *The recognition and retrotranslocation of misfolded proteins from the endoplasmic reticulum.* Traffic, 2008. **9**(6): p. 861-70.

175. Ruddock, L.W. and M. Molinari, *N-glycan processing in ER quality control.* J Cell Sci, 2006. **119**(Pt 21): p. 4373-80.

176. Pearse, B.R. and D.N. Hebert, *Lectin chaperones help direct the maturation of glycoproteins in the endoplasmic reticulum.* Biochim Biophys Acta, 2010. **1803**(6): p. 684-93.

177. Molinari, M., et al., *Role of EDEM in the release of misfolded glycoproteins from the calnexin cycle.* Science, 2003. **299**(5611): p. 1397-400.

178. *Wikipedia - ERAD*. 2008 14.12.2008]; Available from: http://en.wikipedia.org/wiki/ERAD.

179. *Wikipedia - Sec61*. 2008 14.12.2008]; Available from: http://en.wikipedia.org/wiki/Sec61.

180. Bays, N.W. and R.Y. Hampton, *Cdc48-Ufd1-Npl4: stuck in the middle with Ub.* Curr Biol, 2002. **12**(10): p. R366-71.

181. Bernassola, F., A. Ciechanover, and G. Melino, *The ubiquitin proteasome system and its involvement in cell death pathways.* Cell Death Differ, 2010. **17**(1): p. 1-3.

182. Marciniak S J and Ron D, *Endoplasmic Reticulum stress signaling in disease.* The American Physiological Society, 2006. **86**: p. 1133-49.

183. Jimbo, A., et al., *ER stress induces caspase-8 activation, stimulating cytochrome c release and caspase-9 activation.* Exp Cell Res, 2003. **283**(2): p. 156-66.

184. Armstrong, J.L., et al., *Role of Noxa in p53-independent fenretinide-induced apoptosis of neuroectodermal tumours.* Apoptosis, 2007. **12**(3): p. 613-622.

185. Morishima N, et al., *translocation of Bim to the ER mediates ER stress signaling for activation of caspase 12 during ER stress induced apoptosis.* The Journal of Biological Chemistry, 2004. **279**(48): p. 50375-81.

186. Armstrong J L, et al., *Role of Noxa in p53-independant fenretinide-induced apoptosis of neuroblastoma tumours.* Apoptosis, 2007. **12**: p. 613-22.

187. Guilbault, C., et al., *Fenretinide corrects newly found ceramide deficiency in cystic fibrosis.* Am J Respir Cell Mol Biol, 2008. **38**(1): p. 47-56.

188. Veronesi, U., et al., *Fifteen-year results of a randomized phase III trial of fenretinide to prevent second breast cancer.* Ann Oncol, 2006. **17**(7): p. 1065-71.

189. Reynolds, C.P., et al., *Retinoid therapy of high-risk neuroblastoma.* Cancer Lett, 2003. **197**(1-2): p. 185-92.

190. Dmitrovsky, E., *Fenretinide activates a distinct apoptotic pathway.* J Natl Cancer Inst, 2004. **96**(17): p. 1264-5.

191. Milo, L.J., Jr., et al., *Chemical and biological evaluation of dipeptidyl boronic acid proteasome inhibitors for use in prodrugs and pro-soft drugs targeting solid tumors.* J Med Chem, 2011. **54**(13): p. 4365-77.

192. Lee, E.C., et al., *Antitumor activity of the investigational proteasome inhibitor MLN9708 in mouse models of B-cell and plasma cell malignancies.* Clin Cancer Res, 2011. **17**(23): p. 7313-23.

193. Jia, H., et al., *Proteomics of apoptosis of multiple myeloma cells induced by proteasome inhibitor PS-341.* Zhong Nan Da Xue Xue Bao Yi Xue Ban, 2010. **35**(8): p. 784-91.

194. Li, C., et al., *Proteasome inhibitor PS-341 (bortezomib) induces calpain-dependent IkappaB(alpha) degradation.* J Biol Chem, 2010. **285**(21): p. 16096-104.

195. Li, T., et al., *Phase II study of the proteasome inhibitor bortezomib (PS-341, Velcade) in chemotherapy-naive patients with advanced stage non-small cell lung cancer (NSCLC).* Lung Cancer, 2010. **68**(1): p. 89-93.

196. Formelli, F. and L. Cleris, *Synthetic Retinoid Fenretinide Is Effective against a Human Ovarian-Carcinoma Xenograft and Potentiates Cisplatin Activity.* Cancer Research, 1993. **53**(22): p. 5374-5376.

197. Ahmad, S., et al., *Lung epithelial cells release ATP during ozone exposure: signaling for cell survival.* Free Radic Biol Med, 2005. **39**(2): p. 213-26.

198. Paton, A.W., et al., *AB(5) subtilase cytotoxin inactivates the endoplasmic reticulum chaperone BiP.* Nature, 2006. **443**(7111): p. 548-552.

199. Paton, A.W. and J.C. Paton, *Escherichia coli Subtilase Cytotoxin.* Toxins (Basel), 2010. **2**(2): p. 215-228.

200. Paton, A.W., et al., *A new family of potent AB(5) cytotoxins produced by Shiga toxigenic Escherichia coli.* Journal of Experimental Medicine, 2004. **200**(1): p. 35-46.

201. Lovat, P.E., et al., *Effector mechanisms of fenretinide-induced apoptosis in neuroblastoma.* Experimental Cell Research, 2000. **260**(1): p. 50-60.

202. Lovat, P.E., et al., *Increasing melanoma cell death using inhibitors of protein disulfide isomerases to abrogate survival responses to endoplasmic reticulum stress.* Cancer Res, 2008. **68**(13): p. 5363-9.

203. Lovat, P.E., et al., *Molecular mechanisms of fenretinide-induced apoptosis of neuroblastoma cells.* Signal Transduction and Communication in Cancer Cells, 2004. **1028**: p. 81-89.

204. Corazzari, M., et al., *Growth and DNA damage-inducible transcription factor 153 mediates apoptosis in response to fenretinide but not synergy between fenretinide and chemotherapeutic drugs in neuroblastoma.* Mol Pharmacol, 2003. **64**(6): p. 1370-8.

205. Hornik, K. *The (R)*. 2012; Available from: {http://CRAN.R-project.org/doc/FAQ/R-FAQ.html}.

206. Hebert, D.N. and M. Molinari, *In and out of the ER: protein folding, quality control, degradation, and related human diseases.* Physiol Rev, 2007. **87**(4): p. 1377-408.

207. Hetz, C. and L.H. Glimcher, *Fine-tuning of the unfolded protein response: Assembling the IRE1alpha interactome.* Mol Cell, 2009. **35**(5): p. 551-61.

208. Ma, Y. and L.M. Hendershot, *The role of the unfolded protein response in tumour development: friend or foe?* Nat Rev Cancer, 2004. **4**(12): p. 966-77.

209. Bertolotti, A., et al., *Dynamic interaction of BiP and ER stress transducers in the unfolded-protein response.* Nature Cell Biology, 2000. **2**(6): p. 326-32.

210. Shen, J.S., et al., *ER stress regulation of ATF6 localization by dissociation of BiP/GRP78 binding and unmasking of golgi localization signals.* Developmental Cell, 2002. **3**(1): p. 99-111.

211. de Silva, A.M., W.E. Balch, and A. Helenius, *Quality Control in the Endoplasmic Reticulum: Folding and Misfolding of Vesicular Stomatitis Virus G Protein in Cells and In Vitro.* The Journal of Cell Biology, 1990. **111**: p. 857-866.

212. Schroder, M. and R.J. Kaufman, *ER stress and the unfolded protein response.* Mutat Res, 2005. **569**(1-2): p. 29-63.

213. Szegezdi, E., et al., *Mediators of endoplasmic reticulum stress-induced apoptosis.* Embo Reports, 2006. **7**(9): p. 880-885.

214. Harding, H.P., Y. Zhang, and D. Ron, *Protein translation and folding are coupled by an endoplasmic-reticulum-resident kinase.* Nature, 1999. **397**(6716): p. 271-274.

215. Muaddi, H., et al., *Phosphorylation of eIF2alpha at serine 51 is an important determinant of cell survival and adaptation to glucose deficiency.* Mol Biol Cell, 2010. **21**(18): p. 3220-31.

216. Cullinan, S.B., et al., *Nrf2 is a direct PERK substrate and effector of PERK-dependant cell survival.* Mol Cell Biol, 2003. **23**: p. 7198-209.

217. He, C.H., et al., *Identification of activating transcrition factor 4 (ATF4) as an Nrf2-interacting protein. Implications of heme oxygenase-1 gene regulation.* Journal of biological chemistry, 2001. **276**: p. 20858-65.

218. Cox, J.S., C.E. Shamu, and P. Walter, *Transcriptional induction of genes encoding endoplasmic reticulum resident proteins requires a transmembrane protein kinase.* Cell, 1993. **73**(6): p. 1197-206.

219. Mori, K., et al., *A transmembrane protein with a cdc2+/CDC28-related kinase activity is required for signaling from the ER to the nucleus.* Cell, 1993. **74**(4): p. 743-56.

220. Eymin, B., et al., *Increased gadd153 messenger RNA level is associated with apoptosis in human leukemic cells treated with etoposide.* Cancer res, 1997. **57**(4): p. 686-95.

221. Ryan, H.E., J. Lo, and R.S. Johnson, *HIF-1 alpha is required for solid tumor formation and embryonic vascularization.* EMBO J, 1998. **17**(11): p. 3005-15.

222. Thews, O., et al., *Impact of extracellular acidity on the activity of P-glycoprotein and the cytotoxicity of chemotherapeutic drugs.* Neoplasia, 2006. **8**(2): p. 143-52.

223. Kerbel, R.S., *Tumor angiogenesis: past, present and the near future.* Carcinogenesis, 2000. **21**(3): p. 505-15.

224. Liquing, Z., et al., *Expression of glucose-regulated stress protein GRP78 is related to progression of melanoma.* Histopathology, 2009. **54**(4): p. 462-470.

225. Lin, J.H., et al., *IRE1 signaling affects cell fate during the unfolded protein response.* Science, 2007. **318**(5852): p. 944-949.

226. Hetz, C., *The unfolded protein response: controlling cell fate decisions under ER stress and beyond.* Nat Rev Mol Cell Biol, 2012. **13**(2): p. 89-102.

227. DuRose, J.B., A.B. Tam, and M. Niwa, *Intrinsic capacities of molecular sensors of the unfolded protein response to sense alternate forms of endoplasmic reticulum stress.* Molecular Biology of the Cell, 2006. **17**(7): p. 3095-3107.

228. Schuck, S., et al., *Membrane expansion alleviates endoplasmic reticulum stress independently of the unfolded protein response.* J Cell Biol, 2009. **187**(4): p. 525-36.

229. Tse, J., et al., *Reduction of GRP78 increases expression of ATF4, GRP94, GADD153 in mIMCD3 cells. .* The FASEB Journal, 2009. **23**: p. 970-1.

230. Bando, Y., et al., *GRP94 reduces cell death in SH-SY5Y cells perturbated calcium homeostasis.* Apoptosis, 2004. **9**(4): p. 501-8.

231. Zhou, J., et al., *The crystal structure of human IRE1 luminal domain reveals a conserved dimerization interface required for activation of the unfolded protein response.* Proc Natl Acad Sci U S A, 2006. **103**(39): p. 14343-8.

232. Hail, N., H.J. Kim, and R. Lotan, *Mechanisms of fenretinide-induced apoptosis.* Apoptosis, 2006. **11**(10): p. 1677-1694.

233. Wu, J.M., A.M. DiPietrantonio, and T.C. Hsieh, *Mechanism of fenretinide (4-HPR)-induced cell death.* Apoptosis. , 2001 **Oct;6:**(5): p. 377-88.

234. Bold, R., *"Development of the proteasome inhibitor Velcade (TM) (Bortezomib)" by Julian Adams, Ph.D., and Michael Kauffman, MD, Ph.D.* Cancer Investigation, 2004. **22**(2): p. 328-329.

235. Brignole, C., et al., *Effect of bortezomib on human neuroblastoma cell growth, apoptosis, and angiogenesis.* Journal of the National Cancer Institute, 2006. **98**(16): p. 1142-57.

236. Jackson, G., et al., *Bortezomib, a novel proteasome inhibitor, in the treatment of hematologic malignancies.* Cancer Treat Rev, 2005. **31**(8): p. 591-602.

237. Nawrocki, S.T., et al., *Bortezomib inhibits PKR-like endoplasmic reticulum (ER) kinase and induces apoptosis via ER stress in human pancreatic cancer cells.* Cancer Research, 2005. **65**(24): p. 11510-11519.

238. O'Connor, O.A., et al., *The combination of the proteasome inhibitor bortezomib and the bcl-2 antisense molecule oblimersen sensitizes human B-cell lymphomas to cyclophosphamide.* Clinical Cancer Research, 2006. **12**(9): p. 2902-2911.

239. Poulaki, V., et al., *The proteasome inhibitor bortezomib induces apoptosis in human retinoblastoma cell lines in vitro.* Invest Ophthalmol Vis Sci. , 2007 **Oct;48**(10): p. 4706-19.

240. Unterkircher, T., et al., *Bortezomib primes glioblastoma, including glioblastoma stem cells, for TRAIL by increasing tBid stability and mitochondrial apoptosis.* Clin Cancer Res, 2011. **17**(12): p. 4019-30.

241. Wang, X.Z., et al., *Signals from the stressed endoplasmic reticulum induce C/EBP-homologous protein (CHOP/GADD153).* Molecular and Cellular Biology, 1996. **16**(8): p. 4273-4280.

242. Oikawa, D., Y. Kimata, and K. Kohno, *Self-association and BiP dissociation are not sufficient for activation of the ER stress sensor Ire1.* J Cell Sci, 2007. **120**(Pt 9): p. 1681-8.

243. Yoshida, H., et al., *ATF6 activated by proteolysis binds in the presence of NF-Y (CBF) directly to the cis-acting element responsible for mammalian unfolded protein response.* Mol Cell Biol, 2000. **20**: p. 6755-67.

244. Shen, J. and R. Prywes, *ER stress signaling by regulated proteolysis of ATF6.* Methods, 2005. **35**(4): p. 382-9.

245. Shen, J., et al., *Stable binding of ATF6 to BiP in the endoplasmic reticulum stress response.* Mol Cell Biol, 2005. **25**(3): p. 921-32.

246. Shen, J., et al., *ER stress regulation of ATF6 localization by dissociation of BiP/GRP78 binding and unmasking of Golgi localization signals.* Dev Cell, 2002. **3**(1): p. 99-111.

247. Okamura, K., et al., *Dissociation of Kar2p/BiP from an ER Sensory Molecule, Ire1p, Triggers the Unfolded Protein Response in Yeast.* Biochemical and Biophysical Research Communications, 2000. **279**(2): p. 445-450.

248. Kimata, Y., et al., *Genetic evidence for a role of BiP/Kar2 that regulates Ire1 in response to accumulation of unfolded proteins.* Mol Biol Cell, 2003. **14**(6): p. 2559-69.

249. Okamura, K., et al., *Dissociation of Kar2p/BiP from an ER sensory molecule, Ire1p, triggers the unfolded protein response in yeast.* Biochem Biophys Res Commun, 2000. **279**(2): p. 445-50.

250. Li, J., et al., *The unfolded protein response regulator GRP78/BiP is required for endoplasmic reticulum integrity and stress-induced autophagy in mammalian cells.* Cell Death and Differentiation, 2008. **15**(9): p. 1460-1471.

251. Suzuki, T., et al., *Reduction of GRP78 expression with siRNA activates unfolded protein response leading to apoptosis in HeLa cells.* Arch Biochem Biophys, 2007. **468**(1): p. 1-14.

252. Scriven, P., et al., *Activation and clinical significance of the unfolded protein response in breast cancer.* Br J Cancer, 2009. **101**(10): p. 1692-8.

253. Ramsay, R.G., et al., *Expression of stress response protein glucose regulated protein-78 mediated by c-Myb.* Int J Biochem Cell Biol, 2005. **37**(6): p. 1254-68.

254. Luk, J.M., et al., *Proteomic profiling of hepatocellular carcinoma in Chinese cohort reveals heat-shock proteins (Hsp27, Hsp70, GRP78) up-regulation and their associated prognostic values.* Proteomics, 2006. **6**(3): p. 1049-57.

255. Uramoto, H., et al., *Expression of endoplasmic reticulum molecular chaperone Grp78 in human lung cancer and its clinical significance.* Lung Cancer, 2005. **49**(1): p. 55-62.

256. Zhang, J., et al., *Association of elevated GRP78 expression with increased lymph node metastasis and poor prognosis in patients with gastric cancer.* Clin Exp Metastasis, 2006. **23**(7-8): p. 401-10.

257. Xing, X., et al., *Glucose regulated protein 78 (GRP78) is overexpressed in colorectal carcinoma and regulates colorectal carcinoma cell growth and apoptosis.* Acta Histochem, 2011. **113**(8): p. 777-82.

258. Dong, D., et al., *A critical role for GRP78/BiP in the tumor microenvironment for neovascularization during tumor growth and metastasis.* Cancer Res, 2011. **71**(8): p. 2848-57.

259. Schroder, M., *Endoplasmic reticulum stress responses.* Cell Mol Life Sci, 2008. **65**(6): p. 862-94.

260. Markovic, S.N., S.M. Geyer, and F. Dawkins, *A phase II study of bortezomib in the treatment of metastatic malignant melanoma.* Cancer Research, 2005. **103**(12): p. 2584-9.

261. Montaldo, P.G., et al., *N-(4-hydroxyphenyl) retinamide is cytotoxic to melanoma cells in vitro through induction of programmed cell death.* International Journal of Cancer, 1999. **81**(2): p. 262-267.

262. Puduvalli, V.K., et al., *Fenretinide activates caspases and induces apoptosis in gliomas.* Clin Cancer Res, 1999. **5**(8): p. 2230-5.

263. Bilecova-Rabajdova, M., et al., *Analysis of changes in pro (Gadd153) and anti apoptotic (Grp78) gene expression after ischemic-reperfusion injury of the small intestine.* Prague Med Rep, 2010. **111**(4): p. 249-56.

264. Fernandez, J., et al., *Translation mediated by the internal ribosome entry site of the cat-1 mRNA is regulated by glucose availability in a PERK kinase-dependent manner.* J Biol Chem, 2002. **277**(14): p. 11780-7.

265. Futami, T., M. Miyagishi, and K. Taira, *Identification of a network involved in thapsigargin-induced apoptosis using a library of small interfering RNA expression vectors.* J Biol Chem, 2005. **280**(1): p. 826-31.

266. Martin, S., et al., *Targeting GRP78 to enhance melanoma cell death.* Pigment Cell Melanoma Res, 2010. **23**(5): p. 675-82.

267. Saitoh, Y., et al., *Induction of apoptosis by N-(4-hydroxyphenyl)retinamide in glioma cells.* Int J Oncol, 1999. **15**(3): p. 499-504.

268. Adams, J. and M. Kauffman, *Development of the proteasome inhibitor Velcade (Bortezomib).* Cancer Invest, 2004. **22**(2): p. 304-11.

269. Adams, J., *The development of proteasome inhibitors as anticancer drugs.* Cancer Cell, 2004. **5**(5): p. 417-21.

270. Zhuang, L., et al., *Mcl-1, Bcl-XL and Stat3 expression are associated with progression of melanoma whereas Bcl-2, AP-2 and MITF levels decrease during progression of melanoma.* Mod Pathol, 2007. **20**(4): p. 416-26.

271. Flockhart, R.J., et al., *NFAT signalling is a novel target of oncogenic BRAF in metastatic melanoma.* Br J Cancer, 2009. **101**(8): p. 1448-55.

272. Gamble, L.D., et al., *MYCN sensitizes neuroblastoma to the MDM2-p53 antagonists Nutlin-3 and MI-63.* Oncogene, 2012. **31**(6): p. 752-63.

273. DuRose, J.B., A.B. Tam, and M. Niwa, *Intrinsic capacities of molecular sensors of the unfolded protein response to sense alternate forms of endoplasmic reticulum stress.* Mol Biol Cell, 2006. **17**(7): p. 3095-107.

274. McAllister, S.S. and R.A. Weinberg, *Tumor-host interactions: a far-reaching relationship.* J Clin Oncol, 2010. **28**(26): p. 4022-8.

275. Kaplan, R.N., B. Psaila, and D. Lyden, *Niche-to-niche migration of bone-marrow-derived cells.* Trends Mol Med, 2007. **13**(2): p. 72-81.

276. Karnoub, A.E., et al., *Mesenchymal stem cells within tumour stroma promote breast cancer metastasis.* Nature, 2007. **449**(7162): p. 557-63.

277. Mantovani, A., et al., *Cancer-related inflammation.* Nature, 2008. **454**(7203): p. 436-44.

278. Kaplan, R.N., et al., *VEGFR1-positive haematopoietic bone marrow progenitors initiate the pre-metastatic niche.* Nature, 2005. **438**(7069): p. 820-7.

279. Orimo, A., et al., *Stromal fibroblasts present in invasive human breast carcinomas promote tumor growth and angiogenesis through elevated SDF-1/CXCL12 secretion.* Cell, 2005. **121**(3): p. 335-48.

280. Vermeulen, L., et al., *Wnt activity defines colon cancer stem cells and is regulated by the microenvironment.* Nat Cell Biol, 2010. **12**(5): p. 468-76.

281. Yauch, R.L., et al., *A paracrine requirement for hedgehog signalling in cancer.* Nature, 2008. **455**(7211): p. 406-10.

282. Mahadevan, N.R. and M. Zanetti, *Tumor stress inside out: cell-extrinsic effects of the unfolded protein response in tumor cells modulate the immunological landscape of the tumor microenvironment.* J Immunol, 2011. **187**(9): p. 4403-9.

283. Dong, D., et al., *Critical role of the stress chaperone GRP78/BiP in tumor proliferation, survival, and tumor angiogenesis in transgene-induced mammary tumor development.* Cancer Res, 2008. **68**(2): p. 498-505.

284. Romero-Ramirez, L., et al., *XBP1 is essential for survival under hypoxic conditions and is required for tumor growth.* Cancer Res, 2004. **64**(17): p. 5943-7.

285. Romero-Ramirez, L., et al., *X box-binding protein 1 regulates angiogenesis in human pancreatic adenocarcinomas.* Transl Oncol, 2009. **2**(1): p. 31-8.

286. Bi, M., et al., *ER stress-regulated translation increases tolerance to extreme hypoxia and promotes tumor growth.* EMBO J, 2005. **24**(19): p. 3470-81.

287. Blais, J.D., et al., *Perk-dependent translational regulation promotes tumor cell adaptation and angiogenesis in response to hypoxic stress.* Mol Cell Biol, 2006. **26**(24): p. 9517-32.

288. Virrey, J.J., et al., *Stress Chaperone GRP78/BiP Confers Chemoresistance to Tumor-Associated Endothelial Cells.* Molecular Cancer Research, 2008. **6**(8): p. 1268-1275.

289. Dorner, A.J., L.C. Wasley, and R.J. Kaufman, *Overexpression of Grp78 Mitigates Stress Induction of Glucose Regulated Proteins and Blocks Secretion of Selective Proteins in Chinese-Hamster Ovary Cells.* Embo Journal, 1992. **11**(4): p. 1563-1571.

290. Munro, S. and H.R. Pelham, *An Hsp70-like protein in the ER: identity with the 78 kd glucose-regulated protein and immunoglobulin heavy chain binding protein.* Cell, 1986. **46**(2): p. 291-300.

291. Matsumoto, A. and P.C. Hanawalt, *Histone H3 and heat shock protein GRP78 are selectively cross-linked to DNA by photoactivated gilvocarcin V in human fibroblasts.* Cancer Res, 2000. **60**(14): p. 3921-6.

292. Shin, B.K., et al., *Global profiling of the cell surface proteome of cancer cells uncovers an abundance of proteins with chaperone function.* J Biol Chem, 2003. **278**(9): p. 7607-16.

293. McFarland, B.C., et al., *Plasminogen kringle 5 induces apoptosis of brain microvessel endothelial cells: sensitization by radiation and requirement for GRP78 and LRP1.* Cancer Res, 2009. **69**(13): p. 5537-45.

294. Davidson, D.J., et al., *Kringle 5 of human plasminogen induces apoptosis of endothelial and tumor cells through surface-expressed glucose-regulated protein 78.* Cancer Res, 2005. **65**(11): p. 4663-72.

295. Reddy, R.K., et al., *Endoplasmic reticulum chaperone protein GRP78 protects cells from apoptosis induced by topoisomerase inhibitors: role of ATP binding site in suppression of caspase-7 activation.* Journal of Biological Chemistry, 2003. **278**(23): p. 20915-24.

296. Su, R., et al., *Grp78 promotes the invasion of hepatocellular carcinoma.* BMC Cancer, 2010. **10**: p. 20.

297. Watson, L.M., et al., *Overexpression of the 78-kDa glucose-regulated protein/immunoglobulin-binding protein (GRP78/BiP) inhibits tissue factor procoagulant activity.* J Biol Chem, 2003. **278**(19): p. 17438-47.

298. Yeung, B.H., et al., *Glucose-regulated protein 78 as a novel effector of BRCA1 for inhibiting stress-induced apoptosis.* Oncogene, 2008. **27**(53): p. 6782-9.

299. Ben, J., et al., *Glucose-regulated protein 78 inhibits scavenger receptor A-mediated internalization of acetylated low density lipoprotein.* J Mol Cell Cardiol, 2009. **47**(5): p. 646-55.

300. Dorner, A.J., L.C. Wasley, and R.J. Kaufman, *Overexpression of GRP78 mitigates stress induction of glucose regulated proteins and blocks secretion of selective proteins in Chinese hamster ovary cells.* EMBO J, 1992. **11**(4): p. 1563-71.

301. Virrey, J.J., et al., *Stress chaperone GRP78/BiP confers chemoresistance to tumor-associated endothelial cells.* Mol Cancer Res, 2008. **6**(8): p. 1268-75.

302. Huang, S.P., et al., *Capsaicin-induced apoptosis in human hepatoma HepG2 cells.* Anticancer Res, 2009. **29**(1): p. 165-74.

303. Zhai, L., et al., *Decreased cell survival and DNA repair capacity after UVC irradiation in association with down-regulation of GRP78/BiP in human RSa cells.* Exp Cell Res, 2005. **305**(2): p. 244-52.

304. Michallet, A.S., et al., *Compromising the unfolded protein response induces autophagy-mediated cell death in multiple myeloma cells.* PLoS One, 2011. **6**(10): p. e25820.

305. Lin, J.H., et al., *Divergent effects of PERK and IRE1 signaling on cell viability.* PLoS One, 2009. **4**(1): p. e4170.

306. Hong, S.J., T.M. Dawson, and V.L. Dawson, *Nuclear and mitochondrial conversations in cell death: PARP-1 and AIF signaling.* Trends Pharmacol Sci, 2004. **25**(5): p. 259-64.

307. Joza, N., et al., *Essential role of the mitochondrial apoptosis-inducing factor in programmed cell death.* Nature, 2001. **410**(6828): p. 549-54.

308. Rab, A., et al., *Endoplasmic reticulum stress and the unfolded protein response regulate genomic cystic fibrosis transmembrane conductance regulator expression.* Am J Physiol Cell Physiol, 2007. **292**(2): p. C756-66.

309. Martin, S., et al., *Targeting GRP78 to enhance melanoma cell death.* Pigment Cell Melanoma Res. **23**(5): p. 675-82.

310. Schmidt, B.Z. and D.H. Perlmutter, *Grp78, Grp94, and Grp170 interact with alpha1-antitrypsin mutants that are retained in the endoplasmic reticulum.* Am J Physiol Gastrointest Liver Physiol, 2005. **289**(3): p. G444-55.

311. Sou, S.N., K.M. Ilieva, and K.M. Polizzi, *Binding of human BiP to the ER stress transducers IRE1 and PERK requires ATP.* Biochem Biophys Res Commun, 2012. **420**(2): p. 473-8.

312. Palleros, D.R., et al., *ATP-induced protein-Hsp70 complex dissociation requires K+ but not ATP hydrolysis.* Nature, 1993. **365**(6447): p. 664-6.

313. Rao, R.V., et al., *Coupling endoplasmic reticulum stress to the cell death program: role of the ER chaperone GRP78.* Febs Letters, 2002. **514**(2-3): p. 122-128.

314. Macias, A.T., et al., *Adenosine-derived inhibitors of 78 kDa glucose regulated protein (Grp78) ATPase: insights into isoform selectivity.* J Med Chem. **54**(12): p. 4034-41.

315. Williamson, D.S., et al., *Novel Adenosine-Derived Inhibitors of 70 kDa Heat Shock Protein, Discovered Through Structure-Based Design.* Journal of Medicinal Chemistry, 2009. **52**(6): p. 1510-1513.

316. Macias, A.T., et al., *Adenosine-derived inhibitors of 78 kDa glucose regulated protein (Grp78) ATPase: insights into isoform selectivity.* J Med Chem, 2011. **54**(12): p. 4034-41.

317. Ermakova, S.P., et al., *(-)-Epigallocatechin gallate overcomes resistance to etoposide-induced cell death by targeting the molecular chaperone glucose-regulated protein 78.* Cancer Res, 2006. **66**(18): p. 9260-9.

318. Nam, S., D.M. Smith, and Q.P. Dou, *Ester bond-containing tea polyphenols potently inhibit proteasome activity in vitro and in vivo.* J Biol Chem, 2001. **276**(16): p. 13322-30.

319. Backer, J.M., et al., *Chaperone-targeting cytotoxin and endoplasmic reticulum stress-inducing drug synergize to kill cancer cells.* Neoplasia, 2009. **11**(11): p. 1165-73.

320. Wolfson, J.J., et al., *Subtilase cytotoxin activates PERK, IRE1 and ATF6 endoplasmic reticulum stress-signalling pathways.* Cellular Microbiology, 2008. **10**(9): p. 1775-1786.

321. Furukawa, T., et al., *Fatal hemorrhage induced by subtilase cytotoxin from Shiga-toxigenic Escherichia coli.* Microb Pathog, 2011. **50**(3-4): p. 159-67.

322. Proulx, F., E.G. Seidman, and D. Karpman, *Pathogenesis of Shiga toxin-associated hemolytic uremic syndrome.* Pediatr Res, 2001. **50**(2): p. 163-71.

323. Bai, X., et al., *Honokiol, a small molecular weight natural product, inhibits angiogenesis in vitro and tumor growth in vivo.* J Biol Chem, 2003. **278**(37): p. 35501-7.

324. Chen, Y.J., et al., *Honokiol induces cell apoptosis in human chondrosarcoma cells through mitochondrial dysfunction and endoplasmic reticulum stress.* Cancer Lett. **291**(1): p. 20-30.

325. Golden, E.B., et al., *Green tea polyphenols block the anticancer effects of bortezomib and other boronic acid-based proteasome inhibitors.* Blood, 2009. **113**(23): p. 5927-37.

326. Pyrko, P., et al., *The unfolded protein response regulator GRP78/BiP as a novel target for increasing chemosensitivity in malignant gliomas.* Cancer Research, 2007. **67**(20): p. 9809-9816.

327. Kardosh, A., et al., *Aggravated endoplasmic reticulum stress as a basis for enhanced glioblastoma cell killing by bortezomib in combination with celecoxib or its non-coxib analogue, 2,5-dimethyl-celecoxib.* Cancer Res, 2008. **68**(3): p. 843-51.

328. Goding, C.R., *Melanocytes: the new Black.* Int J Biochem Cell Biol, 2007. **39**(2): p. 275-9.

329. Slominski, A., et al., *Melanin pigmentation in mammalian skin and its hormonal regulation.* Physiol Rev, 2004. **84**(4): p. 1155-228.

330. Scharffetter-Kochanek, K., et al., *UV-induced reactive oxygen species in photocarcinogenesis and photoaging.* Biol Chem, 1997. **378**(11): p. 1247-57.

331. Soldan, M.M. and I. Pirko, *Biogenesis and significance of central nervous system myelin.* Semin Neurol, 2012. **32**(1): p. 9-14.

332. Tsacopoulos, M. and P.J. Magistretti, *Metabolic coupling between glia and neurons.* J Neurosci, 1996. **16**(3): p. 877-85.

333. Nakagawara, A. and M. Ohira, *Comprehensive genomics linking between neural development and cancer: neuroblastoma as a model.* Cancer Lett, 2004. **204**(2): p. 213-24.

334. Little, E., et al., *The glucose-regulated proteins (GRP78 and GRP94): functions, gene regulation, and applications.* Critical Reviews in Eukaryotic Gene Expression, 1994. **4**(1): p. 1-18.

335. Ron, D. and P. Walter, *Signal integration in the endoplasmic reticulum unfolded protein response.* Nat Rev Mol Cell Biol, 2007. **8**(7): p. 519-29.

336. Rutkowski, D.T., et al., *Adaptation to ER stress is mediated by differential stabilities of pro-survival and pro-apoptotic mRNAs and proteins.* PLoS Biol, 2006. **4**(11): p. e374.

337. Yamamoto, K., et al., *Differential contributions of ATF6 and XBP1 to the activation of endoplasmic reticulum stress-responsive cis-acting elements ERSE, UPRE and ERSE-II.* J Biochem, 2004. **136**(3): p. 343-50.

338. Verfaillie, T., et al., *Linking ER Stress to Autophagy: Potential Implications for Cancer Therapy.* Int J Cell Biol, 2010. **2010**: p. 930509.

339. Kim, I., W. Xu, and J.C. Reed, *Cell death and endoplasmic reticulum stress: disease relevance and therapeutic opportunities.* Nat Rev Drug Discov, 2008. **7**(12): p. 1013-30.

340. Lee, H., et al., *IRE1 plays an essential role in ER stress-mediated aggregation of mutant huntingtin via the inhibition of autophagy flux.* Hum Mol Genet, 2012. **21**(1): p. 101-14.

341. Haze, K., et al., *Mammalian transcription factor ATF6 is synthesized as a transmembrane protein and activated by proteolysis in response to endoplasmic reticulum stress.* Mol Biol Cell, 1999. **10**(11): p. 3787-99.

342. Kimata, Y., et al., *Two regulatory steps of ER-stress sensor Ire1 involving its cluster formation and interaction with unfolded proteins.* J Cell Biol, 2007. **179**(1): p. 75-86.

343. Schindler, A.J. and R. Schekman, *In vitro reconstitution of ER-stress induced ATF6 transport in COPII vesicles.* Proc Natl Acad Sci U S A, 2009. **106**(42): p. 17775-80.

344. Liu, H., et al., *Endoplasmic reticulum chaperones GRP78 and calreticulin prevent oxidative stress, Ca2+ disturbances, and cell death in renal epithelial cells.* J Biol Chem, 1997. **272**(35): p. 21751-9.

345. Schroder, M., *Engineering eukaryotic protein factories.* Biotechnol Lett, 2008. **30**(2): p. 187-96.

346. Nollen, E.A. and R.I. Morimoto, *Chaperoning signaling pathways: molecular chaperones as stress-sensing 'heat shock' proteins.* J Cell Sci, 2002. **115**(Pt 14): p. 2809-16.

347. Ni, M. and A.S. Lee, *ER chaperones in mammalian development and human diseases.* FEBS Lett, 2007. **581**(19): p. 3641-51.

348. Misra, U.K., et al., *Ligation of cancer cell surface GRP78 with antibodies directed against its COOH-terminal domain up-regulates p53 activity and promotes apoptosis.* Molecular Cancer Therapeutics, 2009. **8**(5): p. 1350-1362.

349. Pizzo, P. and T. Pozzan, *Mitochondria-endoplasmic reticulum choreography: structure and signaling dynamics.* Trends in Cell Biology, 2007. **17**(10): p. 511-517.

350. Kouroku, Y., et al., *ER stress (PERK/eIF2alpha phosphorylation) mediates the polyglutamine-induced LC3 conversion, an essential step for autophagy formation.* Cell Death Differ, 2007. **14**(2): p. 230-9.

351. Talloczy, Z., et al., *Regulation of starvation- and virus-induced autophagy by the eIF2alpha kinase signaling pathway.* Proc Natl Acad Sci U S A, 2002. **99**(1): p. 190-5.

352. Salazar, M., et al., *Cannabinoid action induces autophagy-mediated cell death through stimulation of ER stress in human glioma cells.* J Clin Invest, 2009. **119**(5): p. 1359-72.

353. Wang, J., *Beclin 1 bridges autophagy, apoptosis and differentiation.* Autophagy, 2008. **4**(7): p. 947-8.

354. Hetz, C., et al., *XBP-1 deficiency in the nervous system protects against amyotrophic lateral sclerosis by increasing autophagy.* Genes Dev, 2009. **23**(19): p. 2294-306.

355. Kalvakolanu, D.V. and P. Gade, *IFNG and autophagy: A critical role for the ER-stress mediator ATF6 in controlling bacterial infections.* Autophagy, 2012. **8**(11).

356. Gade, P., et al., *An IFN-gamma-stimulated ATF6-C/EBP-beta-signaling pathway critical for the expression of Death Associated Protein Kinase 1 and induction of autophagy.* Proc Natl Acad Sci U S A, 2012. **109**(26): p. 10316-21.

357. Ravikumar, B., et al., *Regulation of mammalian autophagy in physiology and pathophysiology.* Physiol Rev, 2010. **90**(4): p. 1383-435.

List of published manuscripts arising from this thesis

S. Martin, D.S. Hill, J.C. Paton, M.A. Birch-Machin, P.E. Lovat, C.P.F. Redfern.
Targeting GRP78 to enhance melanoma cell death
Pigment cell and melanoma research: 2010 Oct; 23 (5): 675-82.
http://www.ncbi.nlm.nih.gov/pubmed/20546536

J.L. Armstrong, **S. Martin**, N.A. Illingworth, D. Jamieson, A. Neilson, P.E. Lovat, C.P.F. Redfern & G.J. Veal.
The impact of retinoic acid treatment on the sensitivity of neuroblastoma cells to fenretinide
Oncology Reports: 27: 293-298, 2012
http://www.ncbi.nlm.nih.gov/pubmed/21964808

List of abstracts arising from this thesis

Martin S, Loeher M, Armstrong J. L, Lovat P. E, Redfern C. P. F. (2012)
Expression of Glucose Regulated Protein 78 effects Fenretinide and Bortezomib induced tumour cell death in vitro.
European Cell Death Organisation (ECDO), Rome, Italy.
(*poster presentation*)

Martin S, Hawkins AR, Lovat PE and Redfern CPF. (2012)
Stoichiometric analysis of the unfolded protein response during stress
European Association for Cancer Research: Cell Death and Cancer, Amsterdam, The Netherlands.
(poster presentation).

Martin S, Lovat PE and Redfern CPF. (2011)
The role of GRP78 in melanoma cell survival
North East Postgraduate Conference, Newcastle upon Tyne, UK
(oral presentation)

DS Hill, Hiscutt EL, **Martin S,** Kerr R, Flockhart R, Armstrong JL, Fulda S and Lovat PE. (2009)
Targeting XIAP to increase endoplasmic reticulum (ER) stress-induced apoptosis of malignant melanoma
International Society for Melanoma Research, Boston, USA
(poster presentation).
Pigment Cell and Melanoma Res 2009, 22:860

Lovat PE, Armstrong JL, **Martin S,** Hill D, Pagliarini, Piacentini M, Redfern CPF, Birch-Machin MA. (2009)
Increasing melanoma cell death using inhibitors of protein disulphide isomerases to abrogate survival responses to endoplasmic reticulum stress
European Society for Dermatological Research meeting, Zurich, Switzerland *(oral presentation)*
J. Invest Dermatol 2009, 129: S744

Armstrong JL, Corazzari M, **Martin S**, Flasaca L, Pagliarini V, Piacentini M, Lovat PE. (2009)

Influence of B-RAF signalling on autophagic cell death of cutaneous metastatic melanoma

European Society for Dermatological Research meeting, Zurich, Switzerland *(poster presentation)*

J. Invest Dermatol 2009, 129: S75